University of California, Santa Barbara

Cleaved-Facet Group-III Nitride Lasers

Ph.D. Dissertation

R. Kehl Sink

This dissertation is submitted in partial satisfaction of the requirements for the degree of Doctor of Philosophy in Electrical and Computer Engineering.

Committee:

Professor John E. Bowers, Chair

Professor Larry A. Coldren

Professor Steve P. DenBaars

Professor Umesh Mishra

December, 2000

The dissertation of R. Kehl Sink
is approved

_____
Professor Larry A. Coldren

_____
Professor Steve P. DenBaars

_____
Professor Umesh K. Mishra

_____
Professor John E. Bowers, Committee Chair

December, 2000

Cleaved-Facet Group-III Nitride Lasers

Electrical and Computer Engineering Department
University of California, Santa Barbara
Santa Barbara, CA 93106

Acknowledgements

Most experimental Ph.D. dissertations represent the work of more than one researcher. This dissertation is no exception. Without the support and help from my family, friends, and colleagues, this dissertation would not have been possible.

Laser diodes would not have been possible without high quality MOCVD laser material. For this reason, I am indebted to Amber Abare, Monica Hansen, Patrick Abraham, Archie Holmes, Tal Margalit, Stacia Keller, and Mike Mack who have helped me by growing GaN- or InP-based material for my work on laser diodes.

Numerous people provided processing suggestions and help over the years. In particular, Thomas Liljeberg, Sheng Zhang, Gerry Robinson, and Dubravko Babiç were extremely helpful. Amber Abare, Pat Corvini, Dan Cohen, Peter Kozodoy, Holger Schmidt, Phil Tavernier, Youli Li, June Hu, Monica Hansen, Mike Mack, Yijen Chiu, Tom Reynolds, and Martin Vandenbroek also deserve recognition. Thanks to the entire UCSB faculty for generating a supportive and collaborative environment.

Other conversations have proved helpful with modeling or enhancing my understanding of nitride laser diodes. In this respect, I would like to thank Shiro Uchida, Shigefusa (Fred) Chichibu, Hughes Marchan, Oded Buchinsky, Paul Fini, and Alexis Black. Joachim Piprek has been a great teacher for the software modeling packages ANSYS, ATLAS, and Lastip and for helping me develop the models included in this dissertation. In the development of the ModeSolver program (Chapter 3 and Appendix C), Radha Nagarajan provided some code for the matrix solver (which provides the initial guess for the transmission matrix solver).

Acknowledgements

Without conversations with graduate students, visitors, post-doctoral researchers, and faculty, my education at UCSB would not have been complete. In this regard, I would like to thank Thomas Liljeberg, Alan Mar, Radha Nagarajan, Dan Tauber, Near Margalit, Mark Topinka, Pat Corvini, Evelyn Hu, Siegfried Fleischer, Ali Shakouri, Rajeev Ram, Jim Speck, Gadi Bahir, Claudio Naddeo, Adrian Keating, Peter Blixt, Jack Whaley, and Dubravko Babiç.

I would also like to thank my committee—John Bowers, Larry Coldren, Steve DenBaars, and Umesh Mishra—for reviewing this dissertation. For help with the layout of the dissertation, I would like to thank my mom, Ann Sink.

I would also like to thank the funding agencies for their support of my work at UCSB. In particular, the support of the NSF Graduate Student Fellowship Program was greatly appreciated.

Dr. Lynne Molter from Swarthmore College and Mrs. Peck from Jordan High School took me under their wing and helped me to develop my engineering and mathematics skills. To them, I am grateful.

I reserve this last paragraph for those people who helped beyond the call of duty. I will always admire Maryanne Becerra's strength and understanding. Amber Abare has grown about 80% of the material that I used for the experiments described in this dissertation. Her positive outlook and unwavering willingness to help are appreciated. Thomas Liljeberg has been a great friend, who has always been willing to help with processing questions and to provide moral support.

Acknowledgements

Dedicated to my parents for their love and encouragement and for the opportunities that they have allowed me in the last 30 years.

Vita

March 21, 1970	Born in Charlotte, NC
June, 1993	B.S., Engineering (High Honors), Swarthmore College B.A., Mathematics, Swarthmore College minor, Education, Swarthmore College
April, 1995	M.S., Electrical Engineering, UC Santa Barbara
December, 2000	Ph.D., Electrical Engineering, UC Santa Barbara

Publications

Patent Application

Patent Pending: Application filed for U.S. Patent April 12, 1996: “A method for making cleaved facets for lasers fabricated with gallium nitride and other non-cubic materials, reduced resistance contacts, and increased p-type dopant activation in p-type metallic nitride.”

Published Papers

“Cleaved and Etched Facet Nitride Laser Diodes.” A. C. Abare, M. P. Mack, M. Hansen, R. K. Sink, P. Kozodoy, S. Keller, J. S. Speck, J. E. Bowers, U. K. Mishra, L. A. Coldren, and S. P. DenBaars. IEEE Journal of Selected Topics in Quantum Electronics, May/June 1998, Vol. 4, No. 3, pp. 505-509.

“Cleaved GaN Facets by Wafer Fusion of GaN to InP.” R. K. Sink, S. Keller, B. P. Keller, D. I. Babiç, A. L. Holmes, D. Kapolnek, S. P. DenBaars, J. E. Bowers, X. H. Wu, and J. S. Speck. Applied Physics Letters, April 8, 1996, Vol. 68, No. 15, pp. 2147-9.

Solutions Manual for Diode Lasers and Photonics Integrated Circuits. R. Kehl Sink, Larry A. Coldren, and Scott W. Corzine. John Wiley & Sons, Inc., New York, 1997, ISBN # 0-471-17865-9.

“A simple fiber-optic multiplexer with wide bit-rate range.” Erik Bodtker, Peter Blixt, Kehl Sink, John E. Bowers. Journal of Optical Communications, October, 1996, Vol. 17, No. 5, pp. 169-171.

Published Conference Proceedings Papers

“Simulation and Optimization of 420 nm InGaN/GaN Laser Diodes.” J. Piprek, R. K. Sink, M. A. Hansen, J. E. Bowers, and S. P. DenBaars. Presented at Physics and Simulation of Optoelectronic Devices VIII, 2000.

"Pulsed Operation of Cleaved-Facet InGaN Laser Diodes." R. K. Sink, A. C. Abare, P. Kozodoy, M. P. Mack, S. Keller, L. A. Coldren, S. P. DenBaars, and J. E. Bowers. Materials Research Society Symposium Proceedings Series, Vol. 482 (ISBN 1-55899 387-8), Nitride Semiconductors; F. A. Ponce, S. P. DenBaars, B. K. Meyer, S. Nakamura, and S. Strite, editors.

"MOCVD Growth of High Output Power InGaN Multiple Quantum Well Light Emitting Diode." P. Kozodoy, A. Abare, R. K. Sink, M. Mack, S. Keller, S. P. DenBaars, U. K. Mishra, and D. Steigerwald. Materials Research Society Symposium Proceedings Series, Vol. 468, Gallium Nitride and Related Materials II. C. R. Abernathy, H. Amano, J. C. Zolper, editors, 1997, pp. 481-486.

"Cleaved Facets in GaN by Wafer Fusion of GaN to InP." R. K. Sink, S. Keller, B. P. Keller, D. I. Babiç, A. L. Holmes, D. Kapolnek, X. H. Wu, J. S. Speck, S. P. DenBaars, and J. E. Bowers. Materials Research Society Symposium Proceedings Series, Vol. 421, Compound Semiconductor Electronics and Photonics, R. J. Shul, S. J. Pearton, F. Ren, C.-S. Wu, editors, October 14, 1996, pp. 165-170.

Conference Presentations

"First Demonstration of a GaAs/GaN Fused p-N Heterojunction." Lee S. McCarthy, James G. Champlain, Peter Kozodoy, Giacinta Parish, R. Kehl Sink, and Umesh K. Mishra. 1998 Electronic Materials Conference, Paper AA2, June 24-26, 1998, Charlottesville, VA.

"Pulsed operation of (Al, Ga, In) N blue laser diodes." A.C. Abare, M.P. Mack, M. Hansen, R.K. Sink, P. Kozodoy, S. Keller, E.L Hu, J.S. Speck, J.E. Bowers, U.K. Mishra, L.A. Coldren, and S.P. DenBaars. Photonics West 1998.

"Pulsed Operation of Cleaved-Facet InGaN Laser Diodes." R. K. Sink, A. C. Abare, P. Kozodoy, M. P. Mack, S. Keller, L. A. Coldren, S. P. DenBaars, and J. E. Bowers. Materials Research Society Fall Meeting 1997, paper D22.1 (postdeadline), December 1-5, 1997, Boston, MA.

"Intersubband Absorption Measured in AlGaN/InGaN MQW." R. Kehl Sink, Gad Bahir, Amber C. Abare, Holger Schmidt, Steven P. DenBaars, and John E. Bowers. 1997 Electronic Materials Conference, Paper Z9 (postdeadline), June 25-27, 1997, Colorado State University, Fort Collins, CO.

"MOCVD Growth and Fabrication Issues of Group-III Nitrides for High Efficiency MQW LEDs and Optically Pumped Laser Structures." S. P. DenBaars, P. Kozodoy, S. Keller, A. Abare, M. Minsky, M. Mack, K. Sink, E. Hu, J. E. Bowers, L. Coldren, U. K. Mishra, S. Imagin, J. Muth, R. Kolbas. CLEO 1997, Paper CTuO4 (Invited), May 18-23, 1997, Baltimore, MD.

"MOCVD Growth of High Output Power InGaN Multiple Quantum Well Light Emitting Diode." P. Kozodoy, A. Abare, R. K. Sink, M. Mack, S. Keller, S. P. DenBaars, U. K. Mishra, and D. Steigerwald. Materials Research Society Spring Meeting 1997, April 1-4, 1997, San Francisco, CA.

"Dynamic Beam Propagation Method for Modeling Pulse Propagation in Flared Semiconductor Laser Amplifiers." S. Balsamo, F. Sartori, G. Perrone, C. Naddeo, I. Montrosset, C. Giuliano, R. K. Sink, P. Blixt, and J. E. Bowers. Integrated Photonics Research Conference, April 29 - May 3, 1996, Boston, MA.

"Cleaved Facets in GaN by Wafer Fusion of GaN to InP." R. K. Sink, S. Keller, B. P. Keller, D. I. Babiç, A. L. Holmes, D. Kapolnek, X.H. Wu, J. S. Speck, S. P. DenBaars, and J. E. Bowers. Materials Research Society Spring Meeting 1996, paper C4.2, April 8-12, 1996, San Francisco, CA.

Abstract

Cleaved-Facet Group-III Nitride Lasers

R. Kehl Sink

Cleaved-facet semiconductor lasers are preferred to etched-facet lasers due to the ease with which they can be manufactured, the flatness of the resultant facet, and the freedom from processing tolerances. Unfortunately, the most promising epitaxial layer/substrate pairing for blue-emitting semiconductor lasers is (0001) InGaN-based QWs grown on (0001) sapphire substrates. In this thesis, I detail the fabrication of cleaved facets for InGaN-based QW lasers by three methods: 1) wafer bonding the InGaN QWs to GaAs or InP and use the cleave planes of the cubic material to force the break of the GaN along desired planes, 2) growing InGaN QWs on (11$\underline{2}$0) sapphire and thin the substrate to <50 μm before cleaving, and 3) using gold bonding to join InGaN QWs to GaAs and use laser ablation to remove sapphire substrate before cleaving. Lasers have been successfully fabricated by the second method. LEDs have been fabricated by the third method, but degradation of the active region by the laser ablation process prohibits lasing in these devices. Device design improvements from optical, electrical, and thermal models are presented. Comparisons of device structures and geometries are made on the basis of these models.

Table of contents

Abbreviations and symbols

AFM	atomic force microscopy
CAIBE	chemically assisted ion beam etching
CL	cathodoluminescence
CVD	chemical vapor deposition
CW	continuous-wave
ECR	electron cyclotron resonance
ELO	epitaxial laterally overgrown (Nakamura) or epitaxial lateral overgrowth (Xerox PARC)
ELOG	epitaxial laterally overgrown GaN (Nakamura) or epitaxial lateral over-growth (Xerox PARC)
FWHM	full width at half maximum
IR	infrared (λ>0.7 or 0.8 μm)
I-V curve	plot of injected current as a function of bias voltage
HVPE	hydride vapor phase epitaxy
III-V material	material, typically crystalline, composed of roughly equal parts of elements from group-III of the periodic table and elements from group-V of the periodic table
LD	laser diode
LEEBI	low-energy electron-beam irradiation
L-I curve	plot of laser light output as a function of injected current
MBE	molecular beam epitaxy
MOCVD	metalorganic chemical vapor deposition
MOVPE (OMVPE)	metalorganic vapor phase epitaxy (equivalent to MOCVD)
MQW	multi-quantum well
PEC etching	photoelectrochemical etching
QW	quantum well
RBS	Rutherford backscattering spectroscopy
RIE	reactive ion etch
SCH	separate confinement heterostructure

SEM	scanning electron microscopy
SLS	strained layer superlattice (equivalent to SSL)
SRH recombination	Shockley-Read-Hall recombination
SSL	strained superlattice
TEM	transmission electron microscopy
UCSB	University of California, Santa Barbara
UV	ultraviolet ($\lambda < 0.4$ μm)
XRD	x-ray diffraction

Variables

a	optical loss - typically specified for a mode in a waveguide structure (units of cm^{-1})
E_c	semiconductor conduction band energy
ΔE_c	band offset in the conduction band at a heterointerface
E_F	Fermi level
E_g	semiconductor band gap (energy gap)
E_v	semiconductor valence band energy
ΔE_v	band offset in the valence band at a heterointerface
$E_{v,LH}$	semiconductor light-hole valence band energy
$E_{v,HH}$	semiconductor heavy-hole valence band energy
λ	wavelength
n	electron carrier density
p	hole density
q	electrostatic charge for an electron

Chapter 1

Introduction to nitride laser diodes

In 1989, there was almost no research being performed in the group-III nitride material system (AlGaInN). The main reason for this lack of interest is that GaN could not be made to be p-type and the n-type GaN crystals that had been grown were highly defected. Blue LEDs, blue lasers, and UV detectors could not be fabricated without p-type material. In 1989, researchers working with Prof. Amano at Nagoya University developed the first p-type GaN material and fabricated the first pn junction group-III nitride LED [1]. This started the boom for GaN research in the 1990's. Blue LEDs and laser diodes were quickly designed and fabricated. Subsequent improvements in group-III nitride growth and processing have brought the field rapidly into production.

The time between the development of the first pn junction and the production of the first commercial CW lasers was less than ten years. The large — and therefore competitive — market for blue semiconductor lasers in high density CDs, laser printers, and medical surgery has given researchers the incentive to rapidly develop group-III nitride materials. There is still much work to be done in understanding this material system, but the large amount of interest in these materials has increased understanding significantly in the last decade.

This chapter introduces many of the common applications for group-III nitride LEDs and lasers and describes some of the major issues confronting device designers. A survey of the nitride laser field is given and is compared with the laser development work performed at UCSB. The remainder of this dissertation describes in more detail the experimental and theoretical work that has been done at UCSB in order to improve group-III nitride laser diodes.[1]

[1] For the remainder of this dissertation, nitride will be used to refer to the AlGaInN material system. This is common in this field. Where SiN is mentioned, it will be described as SiN or silicon nitride in order to avoid confusion.

1.1. Applications

Blue lasers and LEDs have a large number of commercial applications. The largest markets for nitride devices are lighting (replacements for incandescent and fluorescent light bulbs), displays (LED based billboards and projection TVs), and data storage (47 Gb DVD-HD). This section describes the primary applications that have been forecast for group-III nitride light-emitting devices.

1.1.1. Light emitting diodes (LEDs)

The largest market for nitride devices will likely be in the production of blue, green, and white light emitting diodes (LEDs) for large area displays, for stoplights, and for household lighting. Nichia Chemical Company in Japan has been marketing blue LEDs for use in outdoor displays since 1995. These LEDs are used with green CdZnSe or AlGaInP LEDs and red AlGaAs or AlGaInP LEDs to form the complete spectrum of colors.

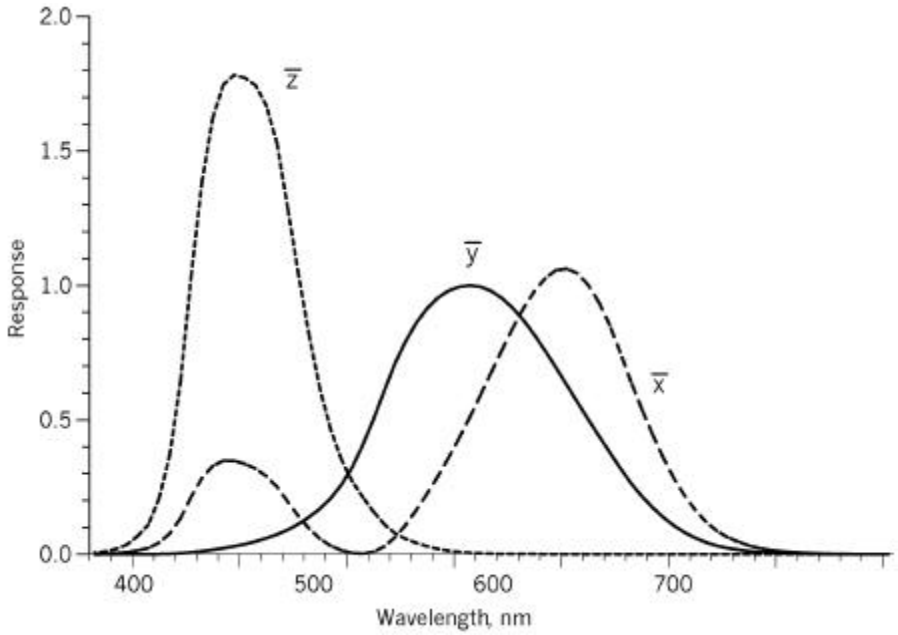

Figure 1. Spectral response of the three different types of receptor cones in the human eye. [2]

These three colors of LEDs are chosen to match the response of the human eye. There are three types of receptor cones in the human retina. These cones act as detectors for color and each cone has a different spectral response as shown in Figure 1. Values x, y, and z are calculated by calculating the normalized overlap between the spectral response of each cone and the spectral density of the incident power. The values of x, y, and z are used to produce the CIE color chart shown in Figure 2. Single wavelength sources lie along the upper perimeter of the curve. Blends of colors are shown in the interior of the gray region. For example, the range of purple hues forms a line between the red and blue positions on the chart. The CIE color chart (the gray region of Figure 2) describes the colors that can be distinguished by the human eye. The red, green, and blue colors used in most monitors and televisions are represented as the corners of the triangle in Figure 2. All colors that are outside the triangle are distinguishable to

the human eye, but cannot be displayed accurately on televisions that are made using current technology [2].

By using LEDs or lasers, color rendition on projection TVs and other displays can be significantly improved. One example of this is a large billboard of LEDs has become a popular form of advertisement in Japan in the last few years. This has been facilitated by the introduction of cheap blue InGaN based LEDs. For LEDs or laser sources to accurately reproduce the colors that the human eye can see, they must produce light as close to the corners of the CIE color chart as possible. This expands the triangle shown in Figure 2 to make a larger range of colors available.

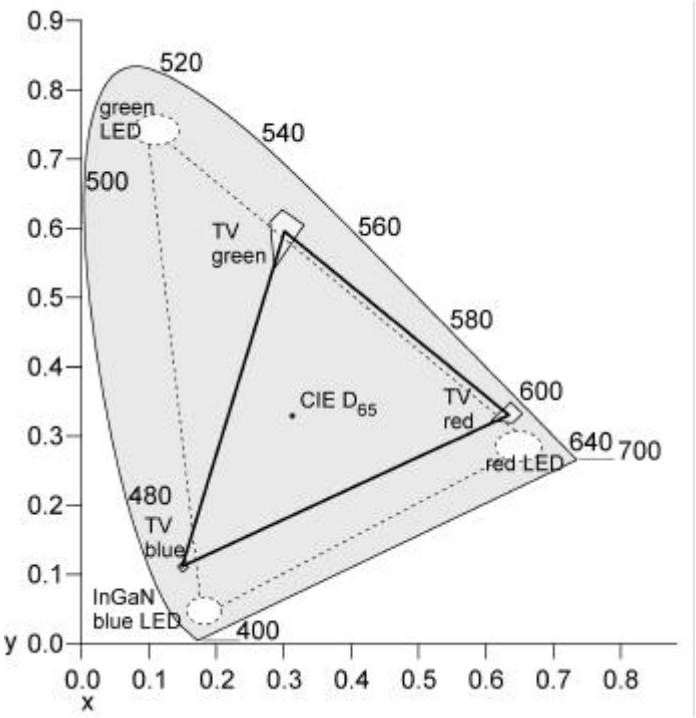

Figure 2. Black and white representation of the CIE Color chart adapted from reference [2]. Only colors inside the triangle can be accurately represented on most TV sets. The human eye can distinguish colors in the gray region. The dashed triangle indicates the colors that can be created using the three LEDs described in the text. An InGaN LED is shown in the lower left corner of the chart.

Red and yellow LEDs have replaced incandescent light bulbs in many traffic lights. These LEDs offer lower electric costs than light bulbs because of their higher wallplug efficiency. The LEDs also reduce maintenance costs due to their significantly longer lifetimes. In the last few years, blue-green or green group-III nitride LEDs have begun to replace the incandescent light bulb in the green portion of many traffic lights.

1.1.2. White light replacement LEDs (cure for the common light bulb)

Another application of blue LEDs is to replace inefficient incandescent and fluorescent light bulbs in home and business lighting. Fluorescent lighting, while

more efficient than incandescent lighting is still unpopular in many homes due to its flickering emission and its harsh tones. Using a combination of red, green, and blue LEDs, incandescent bulbs can be replaced with more pleasing and efficient LED based light sources. Other alternative light sources being explored use a phosphorescent material that absorbs some of the light emitted from blue LEDs. The phosphor then emits the absorbed energy at longer wavelengths. Using this technology, efficiencies as high as 12 lumen/watt have been achieved, which is comparable to the efficiency of an incandescent light bulb. These white LEDs are currently in production by Nichia. Three other large commercial alliances are also developing them.

1.1.3. Laser diodes

While LEDs may form the bulk of the group-III nitride market, many applications require special device characteristics such as high wallplug efficiency, coherent light output, high output power, or narrow emission spectrum. For these applications, laser diodes are required. Laser diodes are more expensive than LEDs to develop and to produce. Therefore, these devices are reserved for applications where their higher cost is offset by the advantage of the laser's specific features. These applications include medical applications, advanced DVD players, gene splicing, projection displays, laser printers, and biochemical reagent sensing and activation.

For each application, the wavelength and output power requirements for the laser diodes are slightly different. Projection displays require high output powers at particular colors that are visible to the eye; specifically lasers with wavelengths of 450 nm emitting 200 mW of power are desired. Biochemical reagent sensing applications require lasers with wavelengths from 470-490 nm. Lasers with these relatively long wavelengths have not been produced with nitrides grown by MOCVD. This limitation in wavelength is due to indium segregation in InGaN

QW laser structures. This topic will be discussed later in this chapter. Methods for achieving such wavelengths are being pursued. Medical applications such as photosensitive medicines allow more precise positioning of treatment because light can be focused to small spots with high intensity. Wavelength is also important for these applications because each particular medicine has a characteristic frequency where the response is maximized.

Another potential market for blue lasers is for medical applications where specific wavelengths are necessary for removal of a particular substance. Red lasers are already used for the removal of tattoos. Infrared lasers are used to remove wrinkles. Green lasers are used to remove so called spider veins. Blue lasers will add to the arsenal of lasers available for use in surgical and medical procedures.

1.1.4. Laser printers and DVD-HD

The two largest markets for group-III nitride lasers are likely to be high quality laser printers and the next generation of DVD players, which have been designated DVD-HD. Both of these applications require that the light be coherent so that the light can be focused down to a diffraction-limited spot. The diffraction limit for the laser spot size is proportional to the square of the wavelength. CD players contain AlGaInAs QW based lasers with wavelengths of 860 nm. DVD players use red lasers at 650 nm, which is a reduction of 1.3 times the wavelength. This means that the spot size is reduced in area by approximately 1.3^2 (=1.7) times. By moving to 410 nm InGaN based lasers, the laser wavelength is reduced by 2.1 times for a spot size reduction of 4.4 times in comparison with CD lasers. The diffraction limited spot size for the 410 nm DVD-HD laser is 2.5 times smaller area than that of the 650 nm DVD laser. With these reductions in spot size, more information can be stored on the same size optical disc. Current DVD technology has incorporated additional improvements

in optics and error correction that have allowed CD storage capacity to increase by an additional factor of four. Further improvements such as recording two levels on each side of a disc are expected to increase the storage capacity of a disc an additional four-fold. This comparison is highlighted in `1.

Technology/ laser material	Wave-length (nm)	Improvement due to wavelength	Improvement due to other factors	Improvements over CDs	Storage capacity
CD (1983) AlGaInAs	860	1	1	——	0.64 Gb
DVD-5 (1996) AlGaInP	650	1.8	4.1	tighter tracks error correction	4.7 Gb
DVD-18 (2000) AlGaInP	650	1.8	14.8	tighter tracks error correction two levels two sides	17 Gb
DVD-HD (2003) AlGaInN	410	4.4	16.7	tighter tracks error correction two levels two sides	47 Gb

Table 1. Storage technologies and improvements [3-5].

Since CDs first were introduced in the early 1980s, improvements in optics, mechanics, and error correction technologies have allowed DVD discs to have higher capacity even without the benefit of the new laser. "The increase in capacity from CD-ROM is due to: 1) smaller pit length (~2.08x increase), 2) tighter tracks (~2.16x), 3) slightly larger data area (~1.02x), 4) more efficient channel bit modulation (~1.06x), 5) more efficient error correction (~1.32x), [and] 6) less sector overhead (~1.06x)."[5] If CD standards were redesigned today, similar improvements could be realized without the improved laser. However, the red laser used in DVD players allows almost double the storage

density and the blue laser used in DVD-HD will allow more than four times as much storage.

If reducing the wavelength for DVD to 410 nm improves the storage density so drastically, it might be argued that moving to even shorter wavelengths would be advantageous. This is not true. As the wavelength gets shorter, it becomes more difficult to find plastics and polymers that are not absorbing. The plastics and polymers that are used in the manufacture of the optical discs have strong absorption for photons with wavelengths below 400 nm. This creates a practical limit for how small the wavelength can be made. Materials do exist that do not absorb shorter wavelengths, but they are currently much more expensive than the plastics currently used. Fortunately, InGaN QW laser structures are easiest to grow with wavelengths from 400 to 420 nm. For longer wavelengths, indium segregation is a problem and for shorter wavelengths the higher aluminum composition in the AlGaN cladding that is required for photon and carrier confinement causes cracking and reduces p-type doping efficiency.

This same reduction in spot size can be taken advantage of in laser printing where a reduction in spot size has a similar effect on the maximum resolution that can be obtained.

1.2. Issues for the development of group-III nitride laser diodes

This section describes issues that are important to the development of nitride optoelectronic devices. Among these issues are heat dissipation, p-type contact resistance, p-type dopant activation, and non-radiative recombination at defect sites. This section reviews discussions in the literature and describes the relevance of these issues to nitride laser development. Related work done at UCSB is described in later sections and in the remainder of this dissertation.

1.2.1. Nakamura's laser diodes

The undisputed leader in nitride laser development is Nichia Chemical Company in Japan. The Nichia research group, led by Shuji Nakamura, was the first to achieve a number of important milestones in nitride optoelectronics including 1) the first thermal activation of p-type dopants [6], 2) the second pn junction [7], 3) the first electrically-pumped pulsed laser diode [8, 9], 4) the first commercially available blue InGaN LED, 5) the first growth of low defect material by epitaxial lateral overgrowth in GaN [10], 6) the first demonstration of strained AlGaN/GaN superlattices allowing thicker cladding layer in laser structure [11], 7) the first CW laser [12, 13], 8) the first CW laser with 10,000 hour lifetime [11, 14, 15], and 9) the first commercially available CW laser.

The fact that Nichia has been able to remain so far ahead of the rest of the researchers in this field is due to the fact that the growth conditions are very sensitive to a number of parameters affected by reactor design. These include gas pressure, precursor adduct formation, and reactor temperature uniformity. Slight differences in reactor design result in major differences in film thickness uniformity, alloy composition, dopant incorporation, and repeatability. For example, a reactor with a slightly different gas intake flow will have a slightly different temperature and flow profile for the source gases, which will cause a change in the reaction rate for the chemical precursors even before they reach the growth surface. Small changes in flow rate or flow direction influence the rates of these adduct reactions significantly and thus cause the problems mentioned above. Other researchers have worked out many of the problems with their reactor designs and are catching up to Nichia, but the optimization of reactor design has been time consuming and has not been well documented in the literature.

1.2.2. P-type material

One of the first problems to be solved for the nitrides was the development of p-type GaN material. Three factors prevented early researchers from obtaining significant p-type conduction: hydrogen passivation of acceptors, low p-type carrier mobility, and high background n-type carrier concentrations.

Hydrogen passivation of p-type dopants in the nitrides was the most significant problem for early researchers. Molecular hydrogen is used as the carrier gas for ammonia during growth of GaN. During growth, the bonds of the molecular hydrogen are broken by thermal energy to yield atomic hydrogen, which incorporates in the GaN lattice. The hydrogen incorporates between the Mg dopant and a nitrogen lattice atom as shown in Figure 3. This hydrogen atom passivates the Mg acceptor meaning that the Mg acceptor will no longer produce a p-type carrier (hole).

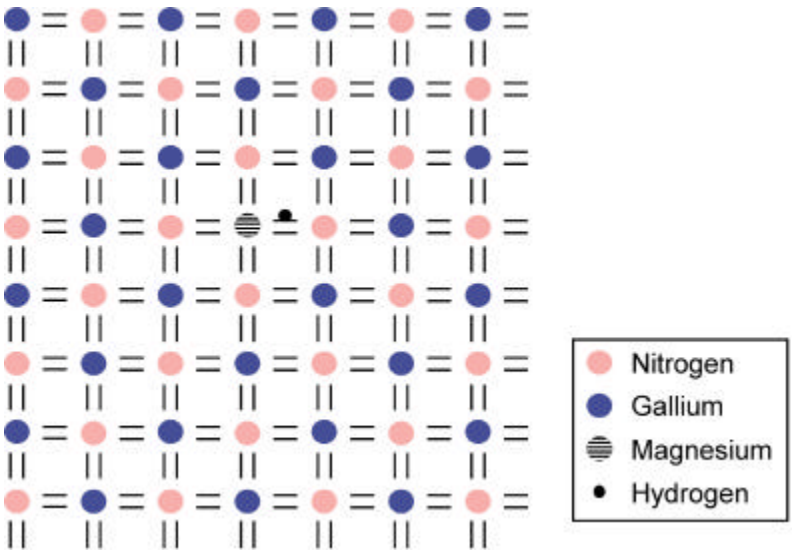

Figure 3. Hydrogen passivation of p-type dopants occurs in group-III nitrides. Low-energy electron-beam irradiation (LEEBI) or thermal activation of the dopants is often used to remove the hydrogen.

In addition to the problem created by hydrogen passivation, the high defect density in GaN is also a problem because defects act as n-type dopants. For

example, the nitrogen vacancy defects (V_N) produce a dopant level approximately 30 meV below the conduction band in GaN. Since GaN is heavily defected (it has a typical defect density of 10^8-10^{10} defects/cm^2), undoped GaN typically has a very high background carrier concentration of approximately n=5*10^{16} cm^{-3}. These n-type carriers will interact with p-type carriers and will compensate them. This makes p-type dopant activation even more important because the p-type dopants must first create carriers to overcome the n-type background carrier density before they can produce net p-type conduction.

This problem is made worse when the relative mobilities are considered. The old electron mobility is much less than the new electron mobility. This means that even if there are more free holes than free electrons, the net material conductivity can be n-type. Even if a large number of p-type carriers are generated, the material conductivity is still not very high due to the low carrier mobility. Hole mobility in nitrides is extremely low in comparison to other semiconductors. Typical estimates of hole mobility range from 2 to 10 cm^2/V s. This mobility compares poorly with that of p-type GaAs and InP, which typically have mobilities of 400 cm^2/V s and 150 cm^2/V s, respectively [16]. Since the mobility is so low, activation of as many acceptors as possible is important to achieving high p-type conductivity.

For much of the early research in the 1970s, all nitride material that was doped with p-type dopants had dopant levels that were too deep, dopants that were passivated by hydrogen atoms, or too few dopants to achieve net p-type conduction. In 1989, the first reports of p-type GaN [1] excited many researchers, who saw it as the breakthrough that would make nitride epitaxy a viable alternative to ZnSe. ZnSe devices were producing higher power and were further developed at the time, but these devices suffered from extremely short device lifetimes.

The first solution for activating the p-type carriers was discovered by the groups of Amano and Akasaki at Nagoya University. They used low-energy electron-beam irradiation (LEEBI) in nitrogen ambient to activate the acceptors. LEEBI activated the acceptors by breaking the bond between the Mg acceptor and the passivating hydrogen atom. The first pn junction in GaN was produced with this method in 1989 [1]. With this method, p-type carrier concentrations of $4*10^{16}$ cm^{-3} were achieved in GaN:Mg; p-type AlGaN:Mg was also achieved [17-20]. While this result was still not good enough for many devices, it gave the first hint that useful p-type GaN could be achieved.

The mechanism for activating the p-type dopants was explored more thoroughly and it was soon discovered that the p-type carriers could be thermally activated, which is a much simpler, cheaper, and reproducible process than LEEBI. Heating Mg-doped GaN to 700ºC produced p-type carrier concentrations of $3*10^{17}$ cm^{-3} [6]. However, there is one problem with this approach: When GaN is heated above 700ºC, nitrogen desorbs from the surface. The remaining nitrogen vacancies act as n-type dopants. For this reason, an optimal activation temperature of approximately 700ºC was initially reported [21].

However, this limit was not fundamental and it was found that by capping the GaN with SiO_2, the activation temperature could be raised even higher without detrimental effects. The typical p-type activation at UCSB is 950ºC for 3 minutes in a nitrogen atmosphere. Above this temperature, device performance is degraded due to diffusion of dopants into (or out of) the active region, indium segregation in the active region, and by diffusion of Si (an n-type dopant in GaN) from the SiO_2 cap into the p-doped GaN. With the 950ºC activation, net p-type carrier concentrations of approximately $6*10^{17}$ cm^{-3} are typical.

Even with the SiO_2 cap, there is evidence that the 950ºC anneal used for p-type dopant activation degrades the quantum wells slightly if the activation anneal is done for too long. McCluskey et al. at Xerox PARC reported that the

InGaN quantum wells suffered significant indium segregation after a 40-hour anneal at 950ºC [22]. In this study, indium-rich precipitates approximately 10 nm high and 25 nm long were formed in the QW region from an initial InGaN 10 well MQW structure with 2 nm wells and 4 nm barriers. Phase separation was first visible after 8 hours of annealing under these conditions. For the short annealing times that are used at UCSB, indium segregation is minimal.

1.2.3. Heat dissipation

Low p-type carrier concentrations and low hole mobilities mean that p-type GaN is highly resistive, even under optimized conditions. This high resistance causes significant heat generation in nitride light emitting devices particularly those that are used for high power applications. High power operation with a high resistance p-type layer leads to significant device heating. In these cases, optimized heat sinking can improve device performance significantly.

A simple calculation illustrates the magnitude of this problem. Consider the first edge emitting lasers, which had a threshold current of approximately 1.7 A and a threshold voltage of 36 V [8, 9]. Therefore, heat dissipation of approximately 60 W is required if the device could be operated in continuous-wave (CW) mode. The heat flow from this type of gain-guided laser approximates two-dimensional flow of a strip heater on an infinite plane. Using this type of model, we can calculate the temperature rise using Equation 1 [23].

Thus, for p-side up mounting on a perfect thermal reservoir at room temperature, the temperature in the active region for a device fabricated on a 100 μm sapphire substrate would be over 700ºC. Alternate designs have used ridge-waveguide lasers to induce a small amount of lateral index guiding. This structure is even worse for heat flow. Assuming a purely 1-dimensional heat flow in the transverse direction, the temperature for such a device could reach 3000ºC (Equation 2) [23].

$$\Delta T = \frac{P \ln(4h/w)}{\pi \xi L} = \frac{(60\ W) \ln(4*(100\ \mu m)/(30\ \mu m))}{\pi (0.45 \frac{W}{cm\ ^oC})(0.15\ cm)} = 730^oC \quad (1)$$

$$\Delta T = \frac{P h}{\xi L w} = \frac{(60\ W)\ (100\ \mu m)}{(0.45 \frac{W}{cm\ ^oC})(0.15\ cm)(30\ \mu m)} = 3000^oC \quad (2)$$

In Equations 1 and 2, ΔT is the difference in temperature between the heat sink and the active region, P is the dissipated power, h is the substrate thickness, ξ is the thermal conductivity of the substrate, L is the length of the laser, and w is the width of the laser stripe.

By mounting p-side down or by choosing another substrate with better thermal conductivity, the heat can be spread over a larger area and dissipated more effectively. Thus, the laser can operate at a much cooler temperature. The solution proposed in this dissertation addresses both of these solutions to the heat flow problem by mounting the device p-side down and by using a thermally conductive substrate instead of sapphire. This method will be described in more detail in Chapters 3 (modeling) and 6 (metal-bonded laser diodes). Since this method helps to solve many of the problems of heat dissipation in GaN, it is potentially very valuable for application to other high power nitride devices, such as RF amplifiers.

1.2.4. Defect density

For such high operating temperatures, defect migration and defect generation would be significant problems in most semiconductor systems. The large defect density in group-III nitrides exacerbates these problems. Despite the large defect density, 10,000 hour CW operation of nitride laser diodes has been demonstrated and these laser diodes are now being commercially produced. One reason for this success is that the high bond strength of the nitrides makes the material very resistant to chemical and thermal degradation. This makes them ideal for many

high temperature and high power electronic applications. Another factor that slows the degradation of nitride devices is the slow motion of dislocations in the nitrides. Sugiura found that the dislocation velocity (propagation of defects) was 10^{10}-10^{20} times lower in GaN than in GaAs at room temperature [24, 25].

While defects may not be as bad in group-III nitride laser diodes as in GaAs, InP, and GaP laser diodes, the large defect densities do affect the lifetime of commercial laser diodes. So defect reduction is still important. In order to extend CW device lifetime, reduction of defect density was necessary. Nakamura has reduced the defect density in Nichia's laser diodes through the use of epitaxial lateral overgrowth in order to achieve 10,000-hour CW operation [15, 26]. (This technique will be discussed in a later section of this chapter.)

Reducing material defects is still one of the best ways to improve device performance and reliability for most light emitting nitride devices. Fortunately the large defect density does not seem to prevent the operation of nitride laser diodes as much as in other material systems. For example, in the nitrides, even a defect density of 10^{8} cm^{-2} does not significantly reduce the gain in the medium. It has been estimated that the gain is not affected until the defect density reaches 10^{10} cm^{-2}. Assuming a short minority carrier diffusion length of 10 nm for n-GaN and a dislocation density of 10^{-10} cm^{-2}, the radiative efficiency can still be as high as 95% [27]. However, there are some indications that the defects do act as sources of dark current in photodiodes (unpublished work by the author). In addition, the defects act as scattering centers for the light in the laser cavity and thus increase the lasing threshold for nitride laser diodes.

The large defect density in the nitrides is caused by the large lattice mismatch between the sapphire substrate and the epitaxial GaN. The mismatch is too large to be accommodated pseudomorphically. Instead, a highly defected buffer layer is grown on the sapphire substrate at low temperature (800ºC). The buffer layer is

then crystallized at 1080ºC. This technique will be described in more detail in the next section.

1.2.5. Substrates for epitaxial nitride growth

Since the large defect density in nitride films is due primarily to the lattice mismatch between the epitaxial film and the sapphire substrate, other choices for substrate material have been considered. Sapphire has been the choice substrate for nitride growth primarily because 1) it is relatively cheap and 2) it is stable at the high growth temperatures required for MOCVD of GaN. For specific applications, its chemical inertness and strong bond strength make it attractive as well. Sapphire is not the perfect substrate, however. It has a very large 13% lattice mismatch with GaN, which prevents pseudomorphic growth of GaN on sapphire and makes an AlN or GaN buffer layer necessary for good quality growth. The buffer layer is deposited as an amorphous film. This film is transformed into a single crystal as the temperature of the substrate is raised to 1080ºC. The resulting GaN buffer layer is highly defected. The edge dislocations terminate in the first 2 μm of GaN growth as edge dislocations grow together and are annihilated. Growing GaN thicker, however, does not eliminate screw dislocations. This means that the first 2 μm of GaN has a large concentration of both screw and edge dislocations. GaN grown on top of this layer will have fewer edge dislocations, but will still have a large number of screw dislocations. This first 2 μm of GaN has been named the template layer because its crystal structure and relatively low defect density serve as the template for epitaxial nitride device structures.

To reduce the defect density (screw and edge dislocations) in the GaN template layer, several methods have been employed. The most effective method has been the use of epitaxial lateral overgrowth (ELO) technology. This method is similar to selective area epitaxy used in other semiconductor systems. In this

method, a SiO_2 mask is deposited on a thin GaN layer. Stripes are patterned in the SiO_2 to expose long channels of GaN. GaN is then regrown by MOCVD. Ga does not stick well to the SiO_2 mask. So the Ga that arrives close to the surface is swept toward the opening in the mask where it sticks to the GaN. The result is that the GaN film grows up through the stripes in the mask and then grows laterally along the top of the SiO_2 mask. The material in the GaN wings is effectively free from the strain that is caused by the lattice mismatch between sapphire and GaN. Therefore, screw dislocations continue to propagate vertically, but the area in the wings is almost free of defects. It is also believed that ELO GaN helps to relieve the strain associated with differences in thermal expansion between GaN and sapphire. This strain relief allows thicker AlGaN cladding regions to be grown. Using ELO GaN, Nakamura has been able to demonstrate 10,000-hour lifetimes for laser diodes running in continuous-wave mode with 2 mW output power [14, 15, 28-30].

Other groups have tried defect reduction using other substrates to see if a reduction in lattice mismatch would help. Growth has been attempted on many substrates and buffer layers including GaAs (100), Si (111), compliant SOI (silicon on insulator), NaCl, quartz, GaP, InP, W, Ga_2O_3, TiO_2, SiC, ZnO, spinel ($MgAl_2O_4$), and MgO [31-35]. Unfortunately, the lattice mismatch in each of these systems is still very large. So, buffer layers are still needed for growth on most of these substrates. Many of these substrates are also poor quality, very expensive, or thermally unstable. There are some exceptions. The special case of growth on SiC is one of these exceptions and it will be discussed toward the end of this chapter.

	Vertical cleave planes?	**GaN lattice mismatch [31]**
c-sapphire (0001)	yes, but cleaving is very difficult	-13%
6H-SiC (0001)	yes	-3.5%
GaN (0001)	yes	0
Si (111)	yes	+16.9%
a-sapphire (11$\underline{2}$0)	yes	NA
$MgAl_2O_4$ spinel (111)	yes	-9%
MgO (111)	yes	-6.4%
ZnO (wurtzite)	yes	+2.3%
$ScAlMgO_4$	yes	+1.8%

Table 2. Comparison of substrate lattice constants for GaN epitaxial MOCVD growth.

Table 2 lists the lattice constants for some of the more promising substrates. Even the smallest of the lattice mismatches is still very large (1.8%). A small negative strain (<2.1%) can be grown lattice matched to AlGaN. InGaN can be used to compensate for positive strain although the indium compositions of greater than 20-30% are difficult to grow without significant indium segregation. The ideal substrate for nitride growth would be bulk GaN crystals. These have been successfully fabricated, but the crystals are very expensive to grow [36, 37]. High quality substrates have been produced with defect densities less than 10^6 cm^{-2} [38]. At this time, even using these relatively low defect substrates, high defect densities of 10^8 cm^{-2} are reported [38]. If large quantities of GaN substrates were produced, however, good quality material would likely be developed.

As shown in Table 2, there are several oxides that have a slightly larger lattice constant than GaN. If high indium content InGaN could be grown without indium segregation, the films could be lattice matched. However, many of these oxides have other problems that preclude their adoption. One choice, ZnO, is not

thermally stable at the high growth temperatures required for GaN. Another choice is the (111) plane of MgO; the (111) plane of MgO is a high-energy plane, which means that it is difficult to produce a high quality substrate by cleaving or polishing. A third choice, spinel, is a closer lattice match to GaN than is sapphire, but the strain for this system (9%) is still not close enough to make growth pseudomorphic.

For certain applications or processes, these oxide substrates may prove useful, however. Laser diodes have been demonstrated on spinel [39]. One of the primary advantages for spinel over sapphire is that it has vertical cleave planes that are parallel to the cleave planes of the epitaxial GaN. The {1120} cleave planes in GaN are parallel to {110} in (111) spinel [40]. This allows lasers to be fabricated using cleaved facets [41] or polished facets [39].

In another application of oxide substrates, Nagoya University/Meijo University published growth of GaN on a ZnO buffer layer on sapphire [42, 43]. They later demonstrated thick growth of GaN using HVPE and subsequent liftoff of these thick GaN layers to form GaN substrates by wet etching the ZnO [44, 45]. Having the ability to remove the sapphire substrate gives the device designer much more flexibility. More recently, a group at Stanford has demonstrated VPE grown GaN on ZnO. However, the growth shows a very broad (0002) GaN x-ray rocking curve indicating that the material is not of high quality [46].

Another important substrate material parameter is the thermal expansion coefficient. The growth of GaN occurs at 1080ºC. At this temperature, the GaN film that is grown reaches equilibrium with the material below it. When the sample is cooled back to room temperature, there is some motion of the atoms to relieve stress, but considerable stress remains in the material after cooling. The differences in thermal expansion cause substantial amounts of stress to build up causing bending of the layers. In the case of GaN grown on sapphire, the bowing of the substrate is quite severe and can even be seen with simple profilometry

measurements. If the stress is large enough, the film relaxes (cracks). Substrates must be chosen which closely match the thermal expansion coefficient of the epitaxial layers.

Other nitride device applications require a substrate to have good thermal conductivity, good electrical conductivity, or vertical cleaved facets. For many of these applications, 6H-SiC is the preferred substrate. Cleaved-facet laser diodes and high power electronic devices have been demonstrated on 6H-SiC. Nitride laser diodes based on 6H-SiC substrates will be described in more detail toward the end of this chapter and in Chapter 6.

1.2.6. Indium segregation and indium phase separation

As mentioned in the previous two sections, even with the proper choice of substrate and growth conditions, nitride epitaxial films still have a large defect density. As discussed, this large defect density occurs primarily due to differences in lattice constant and thermal expansion. These defects increase laser thresholds by providing non-radiative recombination sites and by scattering light. Defects in InGaN also act as seeds for indium segregation (compositional inhomogeneity) [47, 48]. In many ternary and quaternary alloys, compositional fluctuations occur around material defects [47]. This means that there is spatial variation in the chemical make up of the alloy. The InGaN alloy suffers from this problem. In addition, there is InGaN phase separation around certain types of growth defects in the material.

In particular, occurrence of high indium content InGaN has been observed around screw dislocations [47, 48]. It is believed that the screw dislocations act as seeds for spiral growth, which, in turn, produces favorable conditions for InGaN segregation [47]. At the screw dislocation, the growth rate of InGaN is similar to that in the defect free region. However, the evaporation rate of indium from the surface is less in the defected regions due to the additional dangling

bonds at these sites [48]. The defects have been correlated one-to-one with the indium-rich regions by measuring wavelength dependent cathodoluminescence (CL) in InGaN QW samples [47, 48]. Sato, et al. notice that the CL intensity is much brighter in regions with high indium concentrations due to the migration of carriers into these regions [49]. This carrier migration occurs due to the relatively smaller bandgaps of regions with high indium content.

Indium segregation increases laser thresholds for several reasons. These regions have a smaller bandgap due to the large indium concentration, which results in carrier drift to these regions. Unfortunately, because of their smaller bandgap, these regions do not provide much gain at the lasing wavelength since the lasing wavelength is a higher energy wavelength. In addition, it is believed that the defects associated with the high indium concentration regions also act as non-radiative recombination sites for carriers. Fortunately, however, the diffusion length in InGaN is small, which means that the effect of these non-radiative recombination sites is reduced significantly.

The other compositional variation that occurs in InGaN is indium segregation. Typically, InGaN with indium concentrations above x=0.3 will have noticeable indium segregation. This occurs because InN and GaN are expected to have a miscibility gap at the InGaN growth temperature, which is approximately 800ºC [50]. Singh, et al. apply Stringfellow's DLP (delta lattice parameter model) formula and calculate that InN and GaN are not miscible below 2457 K for the zincblende crystal structure [51]. Wurtzite structures of InN and GaN are expected to have a similar temperature range for miscibility. However, it is possible to grow high quality InGaN films with high indium content. High indium content (x=0.81) wurtzite InGaN has been grown in a GaN/InGaN/GaN heterostructure by ECR-MBE (electron cyclotron resonance-assisted molecular beam epitaxy) without phase separation [51]. In this case, the authors grew very thin layers (<50 nm) of InGaN. The strain field from the InGaN/GaN interface is

believed to aid in making InN and GaN miscible for high indium compositions [51].

1.2.7. Facet fabrication techniques

After achieving high quality InGaN growth by minimizing indium segregation, device fabrication is relatively straightforward and will be described in more detail in Chapters 2, 4, and 5. There is one final major problem to be solved: formation of high reflectivity facets. Facets can be formed by cleaving or by etching. This section compares the results that have been achieved by these two methods and the issues involved with each process.

GaN based structures are relatively low index semiconductors due to their large band gaps. A nitride laser structure, for example, typically has a modal index of 2.5, which implies that the uncoated semiconductor/air interface has a theoretical reflectivity of only 18% for a perfectly smooth facet. Facet roughness of less than 20 nm can reduce the reflection of the laser mode by an order of magnitude. For this reason, surface roughness is very important. The surface roughness for facets formed in GaN based laser structures on sapphire have been comparable for facets formed by each of three methods: cleaving, etching, and polishing (see Figure 4). None of these methods produces high quality facets, however. Cleaving GaN that has been grown on other substrates, such as SiC and spinel produces significantly smoother facets in comparison to GaN/sapphire facets.

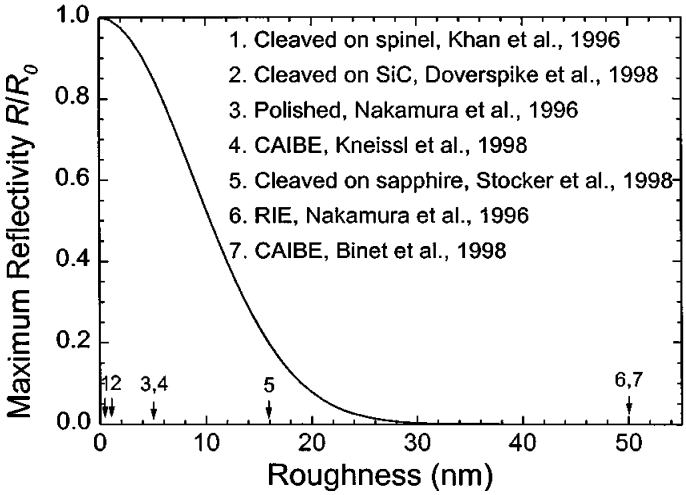

Figure 4. Normalized mirror reflectivity achieved using different methods and substrates for GaN facet formation [52]. $R_0 \approx 18\%$ for group-III nitride laser facets.

The preferred method for facet formation in most semiconductor systems is cleaving because it is a robust method for forming smooth, vertical facets. This method has not been widely adopted for nitride laser diodes grown on basal plane (0001) sapphire, however. The reason for this is that cleaving basal plane sapphire is very difficult because sapphire has many cleave planes that have approximately equal cleave strength. These planes are within a small angular distance. Therefore, it is very easy for a fracture to be redirected from one cleave plane to another by a small amount of surface roughness or a slight misalignment of the applied pressure. This redirection of the cleave is more likely to occur for thick substrates. For this reason, it is important to thin the sapphire. Sapphire is unfortunately very rigid, making it difficult to thin. In addition, it cracks easily when it is lapped thinner than approximately 80 μm. These issues will be discussed further in Chapter 4 and in Appendix D. In summary, cleaving basal plane sapphire is difficult. The payoff for cleaved facets, however, is that the facets that are produced are flat, vertical, and smooth.

Etched facets can be made to have these characteristics as well. For this reason and due to the difficulties with forming cleaved facets, many groups have used etched facets to fabricate laser diodes. However, it is difficult to develop robust recipes for producing high quality facets in this manner. Typical facets produced at UCSB with Cl_2 or Cl_2/Ar based RIE have a slope of 5º-7º and are not as smooth as those produced by cleaving or polishing. Other etching techniques, such as ECR and CAIBE, yield much better results due to the higher level of control over etch conditions. Researchers at Xerox PARC, for example, have used CAIBE to produce facets that are significantly smoother than those made by RIE. The CAIBE facets can be made within 1º-2º of vertical, but this process requires that each facet be masked and etched separately [53-55]. The primary criticism of etched facets is that they are still too rough [52].

Other methods for producing facets are mechanical polishing and focused ion beam (FIB) polishing [39, 56]. Facets made in this way can be made smooth and close to vertical. However, both methods are labor intensive and cannot easily be scaled to production.

Stocker, et al. have reported a cleaving method based on a process used to fabricate GaAs lasers [52]. They report cleaving basal plane sapphire along both the m-planes {1$\underline{1}$00} and the a-planes {11$\underline{2}$0} with this method [52]. Their method is to first thin and polish the sapphire wafer. Then the wafer is attached to a thin metal plate with wax. The wafer is scribed and the metal plate is bent over a round surface. This fractures the sapphire along its crystal planes, thus cleaving the laser bars. This method can be made to work, but it has not been widely implemented due to the difficulty of breaking the sapphire along the proper cleave planes.

Other researchers have avoided the difficulty of cleaving sapphire by using other substrates with more forgiving crystal structures. SiC and spinel both have vertical cleave planes that cleave easily. Researchers at Cree, Inc. and Fujitsu

have grown lasers on SiC and Nichia has grown lasers on spinel (see Table 3). Nichia and UCSB have both produced cleaved-facet lasers on a-plane sapphire [57-59]. This orientation of sapphire cleaves more easily than basal plane sapphire.

In summary, cleaved facets are preferred because their quality is superior to that of etched facets and because they are not subject to etch process variations. Basal plane sapphire, however, is very difficult to cleave. Therefore, etched facets and alternative substrates have been researched significantly. Researchers at Nichia have gone so far as to polish away all of the sapphire in a laser structure so that they can cleave facets in a thick GaN "substrate" [21]. The issue of facet formation will be discussed in more detail in Chapters 2, 4, 5, and 6.

1.3. The competition

The history of group-III nitride epitaxy on sapphire would not be complete without a look at the competing technologies. Blue-emitting semiconductor lasers can be fabricated using nitride epitaxy on sapphire or by at least three other methods: 1) ZnMgSSe on GaAs substrates (also, on ZnSe substrates), and 2) polymers on glass substrates, and 3) nitride epitaxy on SiC substrates.

Before p-type GaN had been achieved, the most promising technology for blue-emitting semiconductor lasers was ZnSe epitaxy. A claim of CW (continuous-wave mode) operation at 515 nm with a lifetime of 101.5 hours was reported in 1996 [60]. In 1998, the device lifetimes had only been extended to 300-400 hours for an output power of 1 mW and a threshold voltage of 4 V [61, 62]. For the same two-year period, Nakamura extended the lifetime of his lasers from 27 hours in 1996 [12, 13] to 10,000 hours in 1998 [21]. This comparison shows the incredible potential for nitride lasers over the ZnSe based competition. The reason for this dramatic difference in device lifetime is that ZnSe and other

II-VI lasers suffer from extremely short lifetimes due to the rapid propagation of dark line defects in these material systems. Within a few years of the first pn junction in GaN, much of the research in ZnSe was terminated or was switched to focus on nitride structures instead.

The second alternative for blue emitting devices is polymers. Polymer gain is still very low and therefore polymers have not yet been used to fabricate a laser diode. However, the ease and low cost with which these types of devices can be fabricated make them excellent candidates to replace semiconductor laser diodes in the long term. Polymer laser structures are much cheaper to produce because the deposition methods for the epitaxial layers are less complex. In addition, since polymers are amorphous or polycrystalline, instead of monocrystalline, lattice mismatch with the substrate is not as important and there is more freedom to choose substrates based on other characteristics.

The other competing technology is nitride lasers on SiC (silicon carbide) substrates. Many of the issues for laser development of group-III nitrides on SiC are the same as they are on sapphire: large lattice mismatch between epitaxy and substrate, poor p-type contacts, and poor p-type dopant activation are problems in both systems. However, SiC has many advantages over sapphire as a substrate for nitride lasers. First, SiC is electrically conductive, which makes processing and packaging of devices easier because devices can be made to have one top side contact and one bottom side contact. Initially, this advantage could not be realized because the AlN buffer layer, which was required for growth of high quality GaN was insulating. More recent papers have indicated that high quality nitride laser structures can be grown on a conductive buffer layer [63]. A second advantage of SiC over sapphire is that SiC is a much better thermal conductor than sapphire at room temperature. As described above, many of the uses for group-III nitride devices require high power or high temperature operation of the devices. In these cases, optimized heat sinking can improve device performance

significantly. A third advantage of SiC over sapphire is that SiC has vertical cleave planes. In basal-plane (c-plane) sapphire, the {11$\underline{2}$0} planes (a-planes) can be used as vertical cleave planes. However, these cleave plane are not the planes with the weakest bond strength. The {1$\underline{1}$02} planes (r-planes) are the preferred cleavage planes for sapphire. These planes are not perpendicular to the substrate surface and therefore do not form good mirrors. The sapphire can be forced to break along the a-planes, but these planes are close in angular position to the r-planes. This means that it is very easy to couple from one cleave plane to another, and thus form a jagged facet. SiC does not have this problem, however, because it has vertical cleave planes that have very different fracture (shear) strength than other competing planes. That means that cleaving SiC is similar to cleaving cubic semiconductors such as GaAs and InP. This is desirable in the formation of cleaved-facet lasers and should improve the yield over comparable sapphire-based cleaved-facet devices.

SiC laser diodes have had trouble getting enough momentum to develop to their full potential, however, because of the high costs of SiC substrates. ELO GaN is based on cheap sapphire substrates and has eliminated many of the problems associated with the lattice mismatch between sapphire and GaN. This has allowed the development of high quality GaN films and has prevented many researchers from switching to SiC substrates. Therefore, sapphire has remained the most popular substrate for laser diodes, despite its apparent disadvantages.

This is evident by the number of institutions reporting sapphire based electrically pumped nitride laser diodes in the last 5 years. These are listed in Table 3.

Organization	First author	Year	Lasing	Substrate	Mirrors	Reference
Nichia Chem.	Nakamura, S.	1995	pulsed	c-sapphire	etched	[8, 9]
Nichia Chem.	Nakamura, S.	1996	pulsed	a-sapphire	cleaved	[57]
Nichia Chem.	Nakamura, S.	1996	pulsed	spinel	polished	[39]
Meijo Univ.	Akasaki, I.	1996	pulsed	c-sapphire	etched	[64]
Nichia Chem.	Nakamura, S.	1996	CW	c-sapphire	etched	[12, 13]
Toshiba	Itaya, K.	1996	pulsed	c-sapphire	cleaved	[65]
Nichia Chem.	Nakamura, S.	1996	CW	ELO GaN c-sapphire	etched	[10]
UCSB	Mack, M.	1997	pulsed	c-sapphire	etched	[66]
UCSB	Sink, R.K.	1997	pulsed	a-sapphire	cleaved	[58, 59]
Fujitsu	Domen, K.	1997	pulsed	SiC	cleaved	[67-69]
Cree, Inc.	Bulman, G.E.	1997	pulsed	6H-SiC	cleaved	[70]
Cree, Inc.	Edmond, J.	1997	CW	6H-SiC	cleaved	[71]
Sony	Nakamura, F.	1997	pulsed	c-sapphire	cleaved	[72]
HP Labs/ HP Labs Japan	Yamada, N.	1997	pulsed	a-sapphire	cleaved	[73]
Xerox PARC	Kneissl, M.	1998	pulsed	c-sapphire	Etched (CAIBE)	[74]
Nichia Chem.	Nakamura, S.	1998	CW	GaN	cleaved	[21]
Pioneer	Kimura, Y.	1998	pulsed	a-sapphire	cleaved	[75]
UCSB	Mack, M.P.	1998	pulsed	c-sapphire	etched then FIB polish	[56]
Sony	Kobayashi, T.	1998	CW	c-sapphire	cleaved	[76]
Fujitsu	Soejima, R.	1998	CW 250K	6H-SiC	cleaved	[77]
Xerox PARC	Hofstetter, D.	1998	pulsed	c-sapphire	DFB 3^{rd} order	[78]
UCSB	Abare, A.C.	1999	pulsed	c-sapphire	DFB 3^{rd} order	[79]

Table 3. Universities and corporations that have developed electrically pumped nitride lasers since 1995.

1.4. Outline of dissertation

At UCSB, I have worked on three generations of nitride lasers. The first generation laser is a broad area laser that was designed to maximize heat dissipation. The second-generation laser is a ridge-waveguide laser that integrates reduction of electron overflow, improvements in device geometry, reduction of current spreading, and optimized optical waveguiding. The third generation builds on the improvements of the second generation and adds p-side down mounting (for better heat dissipation) and improved facet quality. The improvements from one generation to the next are derived from experimental measurements and theoretical models, which helped to optimize the electrical, thermal, and optical properties of the lasers. This dissertation describes my experimental work and theoretical modeling of an in-plane cleaved-facet nitride laser as part of the effort at UCSB to improve nitride laser diode performance.

Chapter 2 describes the work done to obtain cleaved facets in nitride laser diodes. Chapter 3 describes the modeling work that I have performed to improve the quality and understanding of nitride laser diodes at UCSB. Each of the three generations is described in this chapter. Chapter 4 recounts the fabrication of nitride laser diodes on A-plane sapphire and discusses in detail the issues involved in the process steps. Chapter 5 introduces a novel method for fabrication of cleaved-facet nitride laser diodes. This method uses gold bonding technology and laser ablation to transfer the nitride epitaxial layers to a GaAs substrate. Chapter 6 details future directions for this project and explains the advantages and limitations of the methods described in other parts of the dissertation. It also explores the advantages presented by using SiC as a substrate for nitride laser diodes.

Many material parameters are not well known, and many electrical and optical processes are not understood. Therefore, many questions remain unanswered. Despite this limitation, I hope that this dissertation provides a clear

description of the field of blue-emitting laser diodes and inspires a continuation of this work at UCSB.

1.5. References

[1] H. Amano, M. Kito, K. Hiramatsu, and I. Akasaki, "P-type conduction in Mg-doped GaN treated with low-energy electron beam irradiation (LEEBI)," *Japanese Journal of Applied Physics, Part 2 (Letters)*, vol. 28, pp. L2112-2114, 1989.

[2] C. Poynton, "A Guided Tour of Color Space," presented at SMPTE Advanced Television and Electronic Imaging Conference, San Francisco, CA, 1995.

[3] http://www.ee.washington.edu/conselec/CE/kuhn/cdmulti/chap1/history.htm. Accessed June 15, 1999.

[4] C. Crotty, "DVD: Now Playing," *Mac World*, pp. 71, 1998.

[5] http://www.videodiscovery.com/vdyweb/dvd/dvdfaq.html. Accessed May 2, 1999.

[6] S. Nakamura, T. Mukai, M. Senoh, and N. Iwasa, "Thermal annealing effects on p-type Mg-doped GaN films," *Japanese Journal of Applied Physics, Part 2 (Letters)*, vol. 31, pp. L139-142, 1992.

[7] S. Nakamura, M. Senoh, and T. Mukai, "Highly P-typed Mg-doped GaN films grown with GaN buffer layers," *Japanese Journal of Applied Physics, Part 2 (Letters)*, vol. 30, pp. L1708-1711, 1991.

[8] S. Nakamura, M. Senoh, S. Nagahama, N. Iwasa, T. Yamada, T. Matsushita, H. Kiyoku, and Y. Sugimoto, "InGaN-Based Multi-Quantum-Well-Structure Laser Diodes," *Japanese Journal of Applied Physics (Part 2)*, vol. 35, pp. L74-L76, 1996.

[9] "Nichia Demonstrates the First Nitride Laser," *Compound Semiconductor*, vol. Jan/Feb, pp. 7-8, 1996.

[10] S. Nakamura, M. Senoh, S. I. Nagahama, N. Iwasa, T. Yamada, T. Matsushita, H. Kiyoku, Y. Sugimoto, T. Kozaki, H. Umemoto, M. Sano, and K. Chocho, "Present status of InGaN/GaN/AlGaN-based laser diodes," presented at Second International Conference on Nitride Semiconductors, Tokushima, Japan, 1998.

[11] S. Nakamura, M. Senoh, S. I. Nagahama, N. Iwasa, T. Yamada, T. Matsushita, H. Kiyoku, Y. Sugimoto, T. Kozaki, H. Umemoto, M. Sano, and K. Chocho, "InGaN/GaN/AlGaN-based laser diodes with modulation-doped strained-layer superlattices," *Japanese Journal of Applied Physics, Part 2 (Letters)*, vol. 36, pp. 1568-1571, 1997.

[12] S. Nakamura, M. Senoh, S. Nagahama, N. Iwasa, T. Yamada, T. Matsushita, Y. Sugimoto, and H. Kiyoku, "Room temperature continuous-wave operation of

InGaN multi-quantum-well structure laser diodes," *Applied Physics Letters*, vol. 69, pp. 4056-4058, 1996.

[13] S. Nakamura, M. Senoh, S. Nagahama, N. Iwasa, T. Yamada, T. Matsushita, Y. Sugimoto, and H. Kiyoku, "First room-temperature continuous-wave operation of InGaN multi-quantum-well-structure laser diodes," presented at LEOS Annual Meeting, Boston, MA, 1996.

[14] S. Nakamura, "InGaN/GaN/AlGaN-based laser diodes with an estimated lifetime of longer than 10000 hours," presented at Material Research Society Fall '97 Meeting, Boston, MA, 1997.

[15] S. Nakamura, "InGaN-based laser diodes with an estimated lifetime of longer than 10,000 hours," presented at Physics and Simulation of Optoelectronic Devices VI, San Jose, CA, USA, 1998.

[16] S. M. Sze, *Physics of Semiconductor Devices*, 2nd ed. New York: John Wiley & Sons, 1981.

[17] I. Akasaki, H. Amano, N. Koide, M. Kotaki, and K. Manabe, "Conductivity control of GaN and fabrication of UV/blue GaN light emitting devices," *Physica B*, vol. 185, pp. 428-432, 1993.

[18] I. Akasaki, H. Amano, M. Kito, and K. Hiramatsu, "Photoluminescence of Mg-doped p-type GaN and electroluminescence of GaN p-n junction LED," *Journal of Luminescence*, vol. 48-49, part 2, pp. 666-670, 1991.

[19] I. Akasaki and H. Amano, "Room temperature ultraviolet/blue light emitting devices based on AlGaN/GaN multi-layered structure," *Extended Abstracts of the 1992 International Conference on Solid State Devices and Materials*, pp. 327-329, 1992.

[20] I. Akasaki and H. Amano, "Conductivity control of AlGaN, fabrication of AlGaN/GaN multi-heterostructure and their application to UV/blue light emitting devices," presented at Wide Band Gap Semiconductors Symposium, Boston, MA, USA, 1991.

[21] S. Nakamura, M. Senoh, S. Nagahama, N. Iwasa, T. Yamada, T. Matsushita, H. Kiyoku, Y. Sugimoto, T. Kozaki, H. Umemoto, M. Sano, and K. Chocho, "InGaN/GaN/AlGaN-based laser diodes with cleaved facets grown on GaN substrates," *Applied Physics Letters*, vol. 73, pp. 832-834, 1998.

[22] M. D. McCluskey, L. T. Romano, B. S. Krusor, D. P. Bour, N. M. Johnson, and S. Brennan, "Phase separation in InGaN/GaN multiple quantum wells," *Applied Physics Letters*, vol. 72, pp. 1730-1732, 1998.

[23] L. A. Coldren and S. W. Corzine, *Diode Lasers and Photonic Integrated Circuits*. New York, NY: John Wiley & Sons, 1995.

[24] L. Sugiura, "Dislocation motion in GaN light-emitting devices and its effect on device lifetime," *Journal of Applied Physics*, vol. 81, pp. 1633-1638, 1997.

[25] L. Sugiura, "Comparison of degradation caused by dislocation motion in compound semiconductor light-emitting devices," *Applied Physics Letters*, vol. 70, pp. 1317-1319, 1997.

[26] S. Nakamura, "InGaN multiquantum-well-structure laser diodes with GaN-AlGaN modulation-doped strained-layer superlattices," *IEEE Journal of Selected Topics in Quantum Electronics*, vol. 4, pp. 483-489, 1998.

[27] T. Sugahara, H. Sato, M. Hao, Y. Naoi, S. Kurai, S. Tottori, K. Yamashita, K. Nishino, L. T. Romano, and S. Sakai, "Direct evidence that dislocations are non-radiative recombination centers," *Japanese Journal of Applied Physics, Part 2 Letters*, vol. 37, pp. L398-400, 1998.

[28] S. Nakamura, M. Senoh, S. Nagahama, N. Iwasa, T. Yamada, T. Matsushita, H. Kiyoku, Y. Sugimoto, T. Kozaki, H. Uimemoto, M. Sang, and K. Chocho, "High-power, long-lifetime InGaN/GaN/AlGaN-based laser diodes grown on pure GaN substrates," *Japanese Journal of Applied Physics, Part 2 (Letters)*, vol. 37, pp. L309-312, 1998.

[29] S. Nakamura, "Blue lasers meet commercial requirements," *Photonics Spectra*, vol. 32, pp. 130-132, 134-135, 1998.

[30] S. Nakamura, "High-power InGaN-based laser diodes with a long lifetime," presented at Metalorganic Vapour Phase Epitaxy 1998. Ninth International Conference, La Jolla, CA, 1998.

[31] E. S. Hellman, C. D. Brandle, L. F. Schneemeyer, D. Wiesmann, I. Brener, T. Siegrist, G. W. Berkstresser, D. N. E. Buchanan, and J. E.H. Hartford, "$ScAlMgO_4$: an oxide substrate for GaN epitaxy," *MRS Internet Journal of Nitride Semiconductor Research*, vol. 1, pp. 1, 1996.

[32] N. P. Kobayashi, J. T. Kobayashi, P. D. Dapkus, W. J. Choi, A. E. Bond, X. Zhang, and D. H. Rich, "GaN growth on Si(111) substrate using oxidized AlAs as an intermediate layer," *Applied Physics Letters*, vol. 71, pp. 3569-3571, 1997.

[33] Y. Kobayashi, F. Scholz, and N. Kobayashi, "Surface morphology and carbon incorporation for hexagonal GaN/(111)B GaAs metalorganic vapor phase epitaxy using dimethylhydrazine and trimethylgallium," *Japanese Journal of Applied Physics, Part 1 (Regular Papers, Short Notes & Review Papers)*, vol. 36, pp. 2592-2595, 1997.

[34] N. P. Kobayashi, J. T. Kobayashi, C. Won-Jin, and P. D. Dapkus, "Single-crystal α-GaN grown on a α-Ga_2O_3 template layer," *Applied Physics Letters*, vol. 73, pp. 1553-1555, 1998.

[35] J. Cao, D. Pavlidis, Y. Park, J. Singh, and A. Eisenbach, "Improved quality GaN by growth on compliant silicon-on-insulator substrates using metalorganic chemical vapor deposition," *Journal of Applied Physics*, vol. 83, pp. 3829-3834, 1998.

[36] K. Pakula, A. Wysmolek, K. P. Korona, J. M. Baranowski, R. Stepniewski, I. Grzegory, M. Bockowski, J. Jun, S. Krukowski, M. Wroblewski, and S. Porowski, "Luminescence and reflectivity in the exciton region of homoepitaxial GaN layers grown on GaN substrates," *Solid State Communications*, vol. 97, pp. 919-922, 1996.

[37] K. Pakula, J. M. Baranowski, R. Stepniewski, A. Wysmolek, I. Grzegory, J. Jun, S. Porowski, M. Sawicki, and K. Starowieyski, "Growth of GaN metalorganic chemical vapour deposition layers on GaN single crystals," presented at 24th International School of Physics of Semiconducting Compounds, Jaszowiec, Poland, 1995.

[38] F. A. Ponce, D. P. Bour, W. Gotz, N. M. Johnson, H. I. Helava, I. Grzegory, J. Jun, and S. Porowski, "Homoepitaxy of GaN on polished bulk single crystals by metalorganic chemical vapor deposition," *Applied Physics Letters*, vol. 68, pp. 917-919, 1996.

[39] S. Nakamura, M. Senoh, S. Nagahama, N. Iwasa, I. Yamada, T. Matsushita, H. Kiyoku, and Y. Sugimoto, "Characteristics of InGaN multi-quantum-well-structure laser diodes," *Applied Physics Letters*, vol. 68, pp. 3269-3271, 1996.

[40] C. J. Sun, J. W. Yang, Q. Chen, M. A. Khan, T. George, P. Chang-Chien, and S. Mahajan, "Deposition of high quality wurtzite GaN films over cubic (111) $MgAl_2O_4$ substrates using low pressure metalorganic chemical vapor deposition," *Applied Physics Letters*, vol. 68, pp. 1129-1131, 1996.

[41] M. Asif Khan, C. J. Sun, J. W. Yang, Q. Chen, B. W. Lim, M. Zubair Anwar, A. Osinsky, and H. Temkin, "Cleaved cavity optically pumped InGaN-GaN laser grown on spinel substrates," *Applied Physics Letters*, vol. 69, pp. 2418-2420, 1996.

[42] T. Detchprohm, K. Hiramatsu, H. Amano, and I. Akasaki, "Hydride vapor phase epitaxial growth of a high quality GaN film using a ZnO buffer layer," *Applied Physics Letters*, vol. 61, pp. 2688-2690, 1992.

[43] T. Detchprohm, H. Amano, K. Hiramatsu, and I. Akasaki, "The growth of thick GaN film on sapphire substrate by using ZnO buffer layer," *Journal of Crystal Growth*, vol. 128, pp. 384-390, 1993.

[44] T. Detchprohm, K. Hiramatsu, N. Sawaki, and I. Akasaki, "Metalorganic vapor phase epitaxy growth and characteristics of Mg-doped GaN using GaN substrates," *Journal of Crystal Growth*, vol. 145, pp. 192-196, 1994.

[45] T. Detchprohm, K. Hiramatsu, N. Sawaki, and I. Akasaki, "The homoepitaxy of GaN by metalorganic vapor phase epitaxy using GaN substrates," *Journal of Crystal Growth*, vol. 137, pp. 170-174, 1994.

[46] T. Ueda, T. F. Huang, S. Spruytte, H. Lee, M. Yuri, K. Itoh, T. Baba, and J. S. Harris, Jr., "Vapor phase epitaxy growth of GaN on pulsed laser deposited ZnO buffer layer," *Journal of Crystal Growth*, vol. 187, pp. 340-346, 1998.

[47] T. Sugahara, H. Maosheng, W. Tao, D. Nakagawa, Y. Naoi, K. Nishino, and S. Sakaj, "Role of dislocation in InGaN phase separation," *Japanese Journal of Applied Physics, Part 2 Letters*, vol. 37, pp. L1195-1198, 1998.

[48] H. Sato, T. Sugahara, Y. Naoi, and S. Sakai, "Compositional inhomogeneity of InGaN grown on sapphire and bulk GaN substrates by metalorganic chemical vapor deposition," *Japanese Journal of Applied Physics, Part 1 Regular Papers, Short Notes & Review Papers*, vol. 37, pp. 2013-2015, 1998.

[49] H. Sato, T. Sugahara, Y. Naoi, and S. Sakai, "Compositional inhomogeneity of InGaN grown on sapphire and bulk GaN substrates by metalorganic chemical vapor deposition," *Japanese Journal of Applied Physics, Part 1 (Regular Papers, Short Notes & Review Papers)*, vol. 37, pp. 2013-2015, 1998.

[50] I. Ho and G. B. Stringfellow, *Applied Physics Letters*, vol. 69, pp. 2701, 1996.

[51] R. Singh, D. Doppalapudi, T. D. Moustakas, and L. T. Romano, "Phase separation in InGaN thick films and formation of InGaN/GaN double heterostructures in the entire alloy composition," *Applied Physics Letters*, vol. 70, pp. 1089-1091, 1997.

[52] D. A. Stocker, E. F. Schubert, W. Grieshaber, K. S. Boutros, and J. M. Redwing, "Facet roughness analysis for InGaN/GaN lasers with cleaved facets," *Applied Physics Letters*, vol. 73, pp. 1925-1927, 1998.

[53] F. Binet, J. Y. Duboz, N. Laurent, C. Bonnat, P. Collot, F. Hanauer, O. Briot, B. Gil, F. Scholz, J. Off, and A. Sohmer, "Optical pumping in nitride cavities with etched mirror facets," presented at EMRS 1997 Spring Meeting, Symposium L: III-V Nitrides Semiconductors and Ceramics: from Material Growth to Device Applications, Strasbourg, France, 1997.

[54] A. T. Ping, I. Adesida, and M. A. Khan, "Study of chemically assisted ion beam etching of GaN using HCl gas," *Applied Physics Letters*, vol. 67, pp. 1250-1252, 1995.

[55] I. Adesida, A. T. Ping, C. Youtsey, T. Dow, M. Asif Khan, D. T. Olson, and J. N. Kuznia, "Characteristics of chemically assisted ion beam etching of gallium nitride," *Applied Physics Letters*, vol. 65, pp. 889-891, 1994.

[56] M. P. Mack, G. D. Via, A. C. Abare, M. Hansen, P. K. Kozodoy, S. Keller, J. S. Speck, U. K. Mishra, L. A. Coldren, and S. P. DenBaars, "Improvement of GaN-based laser diode facets by FIB polishing," *Electronics Letters*, vol. 34, pp. 1315-1316, 1998.

[57] S. Nakamura, M. Senoh, S. Nagahama, N. Iwasa, T. Yamada, T. Matsushita, H. Kiyoku, and Y. Sugimoto, "InGaN multi-quantum-well-structure laser diodes with cleaved mirror cavity facets," *Japanese Journal of Applied Physics*, vol. 35, pp. L217-L220, 1996.

[58] R. K. Sink, A. C. Abare, P. Kozodoy, M. P. Mack, S. Keller, L. A. Coldren, S. P. DenBaars, and J. E. Bowers, "Pulsed Operation of Cleaved-Facet InGaN Laser

Diodes," presented at Materials Research Society Fall Meeting 1997, Boston, MA, 1997.

[59] A. C. Abare, M. P. Mack, M. Hansen, R. K. Sink, P. Kozodoy, S. Keller, J. S. Speck, J. E. Bowers, U. K. Mishra, L. A. Coldren, and S. P. DenBaars, "Cleaved and Etched Facet Nitride Laser Diodes," *IEEE Journal of Selected Topics in Quantum Electronics*, vol. 4, pp. 505-509, 1998.

[60] H. Okuyama and A. Ishibashi, "Present status and future of ZnSe type light emitting devices," *Applied Physics*, vol. 65, pp. 687-696, 1996.

[61] E. Kato, H. Noguchi, M. Nagai, and H. Okuyama, "Significant progress in II-IV blue-green laser diode lifetime," *Electronics Letters*, vol. 34, pp. 282-284, 1998.

[62] Y. Sanaka, H. Okuyama, S. Kijima, and E. Kato, "II-VI laser diode with low operating voltage and long device lifetime," *Electronics Letters*, vol. 34, pp. 1891-1892, 1998.

[63] K. Doverspike, G. E. Bulman, S. T. Sheppard, H. S. Kong, M. T. Leonard, H. Dieringer, J. A. Edmond, K. L. More, Y. K. Song, M. Kuball, and A. V. Nurmikko, "InGaN/GaN lasers grown on SiC," presented at In-Plane Semiconductor Lasers: from Ultraviolet to Mid-Infrared II, San Jose, CA, 1998.

[64] I. Akasaki, S. Sota, H. Sakai, T. Tanka, M. Koike, and H. Amano, "Shortest Wavelength Semiconductor Laser Diode," *Electronics Letters*, vol. 32, pp. 1105, 1996.

[65] K. Itaya, M. Onomura, J. Nishio, L. Sugiura, S. Saito, M. Suzuki, J. Rennie, S. Nunoue, M. Yamamoto, H. Fujimoto, Y. Kokubun, Y. Ohba, G. Hatakoshi, and M. Ishaikawa, "Room temperature pulsed operation of nitride based multi-quantum-well laser diodes with cleaved facets on conventional C-face sapphire substrates," *Japanese Journal of Applied Physics*, vol. 35, pp. L1315-L1317, 1996.

[66] M. P. Mack, A. Abare, M. Aizcorbe, P. Kozodoy, S. Keller, U. K. Mishra, L. Coldren, and S. DenBaars, "Characteristics of Indium-Gallium-Nitride Multiple-Quantum-Well Blue Laser Diodes Grown by MOCVD," *MRS Internet Journal of Nitride Research*, vol. 2, pp. 41, 1997.

[67] K. Domen, A. Kuramata, R. Soejima, K. Horino, S. Kubota, and T. Tanahashi, "Lasing mechanism of InGaN-GaN-AlGaN MQW laser diode grown on SiC by low-pressure metal-organic vapor phase epitaxy," presented at Second International Conference on Nitride Semiconductors, Tokushima, Japan, 1997.

[68] K. Domen, A. Kuramata, R. Soejima, K. Horino, S. Kubota, and T. Tanahashi, "Lasing mechanism of InGaN-GaN-AlGaN MQW laser diode grown on SiC by low-pressure metal-organic vapor phase epitaxy," *IEEE Journal of Selected Topics in Quantum Electronics*, vol. 4, pp. 490-497, 1998.

[69] K. Domen, A. Kuramata, and T. Tanahashi, "Lasing mechanism of InGaN/GaN/AlGaN multiquantum well laser diode," *Applied Physics Letters*, vol. 72, pp. 1359-1361, 1998.

[70] G. E. Bulman, K. Doverspike, S. T. Sheppard, T. W. Weeks, H. S. Kong, H. M. Dieringer, J. A. Edmond, J. D. Brown, J. T. Swindell, and J. F. Schetzina, "Pulsed operation lasing in a cleaved-facet InGaN/GaN MQW SCH laser grown on 6H-SiC," *Electronics Letters*, vol. 33, pp. 1556-1557, 1997.

[71] J. A. Edmond, H. Kong, M. T. Leonard, K. Doverspike, G. E. Bulman, W. Weeks, K. G. Irvine, and V. A. Dmitriev, "Nitride-based emitters on SiC substrates," presented at Second International Conference on Nitride Semiconductors, Tokushima, Japan, 1997.

[72] F. Nakamura, "Room temperature pulsed operation of a GaInN MQW laser diode with an optimized well number," presented at Second International Conference on Nitride Semiconductors, Tokushima, Japan, 1997.

[73] N. Yamada, Y. Kaneko, S. Watanabe, Y. Yamaoka, T. Hidaka, S. Nakagawa, and E. Marenger, "Room temperature pulsed operation of nitride-based ridge-waveguide laser diode with cleaved facets," presented at IEEE LEOS '97 Annual Meeting, San Francisco, CA, 1997.

[74] M. Kneissl, D. P. Bour, N. M. Johnson, L. T. Romano, B. S. Krusor, R. Donaldson, J. Walker, and C. Dunnrowicz, "Characterization of AlGaInN diode lasers with mirrors from chemically assisted ion beam etching," *Applied Physics Letters*, vol. 72, pp. 1539-1541, 1998.

[75] Y. Kimura, M. Miyachi, H. Takahashi, T. Tanaka, M. Nishitsuka, A. Watanabe, H. Ota, and K. Chikuma, "Room-temperature pulsed operation of GaN-based laser diodes on a-face sapphire substrate grown by low-pressure metalorganic chemical vapor deposition," *Japanese Journal of Applied Physics, Part 2 (Letters)*, vol. 37, pp. L1231-1233, 1998.

[76] T. Kobayashi, F. Nakamura, K. Naganuma, T. Tojyo, H. Nakajima, T. Asatsuma, H. Kawai, and M. Ikeda, "Room-temperature continuous-wave operation of GaInN/GaN multiquantum well laser diode," *Electronics Letters*, vol. 34, pp. 1494-1495, 1998.

[77] R. Soejima, A. Kuramata, S. Kubota, K. Domen, K. Horino, and T. Tanahashi, "Continuous-Wave Operation at 250K of InGaN Multiple Quantum Well Laser Diodes Grown on 6H-SiC with Vertical Conducting Structure," *Japanese Journal of Applied Physics, part 2*, vol. 37, pp. L1205-1207, 1998.

[78] D. Hofstetter, R. L. Thornton, L. T. Romano, D. P. Bour, M. Kneissl, and R. M. Donaldson, "Room-temperature pulsed operation of an electrically injected InGaN/GaN multi-quantum well distributed feedback laser," *Applied Physics Letters*, vol. 73, pp. 2158-2160, 1998.

[79] A. C. Abare, M. Hansen, J. S. Speck, L. A. Coldren, and S. P. DenBaars, "Demonstration of electrically pumped nitride distributed feedback lasers employing dielectric gratings," presented at Device Research Conference, Santa Barbara, CA, 1999.

Chapter 2

Cleaved facets for nitride laser diodes

2.1. Motivation

Basal plane sapphire — also known as (0001) α-Al_2O_3 or c-plane sapphire — is a common substrate for the heteroepitaxy of GaN. This presents a challenge for fabrication of cleaved-facet nitride lasers: in basal plane sapphire the cleave planes with the lowest shear strength are not perpendicular to the wafer surface (vertical). Because of this difficulty, etched facets have been popular for nitride lasers. Cleaved facets are the preferred mirror choice, however. Cleaved facets are easier to manufacture than etched facets because they are less affected by processing variations such as temperature, gas composition, plasma density, acceleration voltage, and pressure. In addition, etching often leaves the surface rough and slightly angled (see Figure 1). Both of these facet characteristics reduce the useful reflection of the laser mode. With the application of high reflectivity (HR) coatings, however, both cleaved-facet and etched-facet mirrors can offer suitable reflectivity for CW operation. As described in Table 3 of Chapter 1, cleaved-facet lasers have been fabricated for GaN grown on a number of substrates including SiC, a-plane sapphire, c-plane sapphire, and spinel. This chapter describes several methods for achieving vertical cleaved facets in nitride laser diodes.

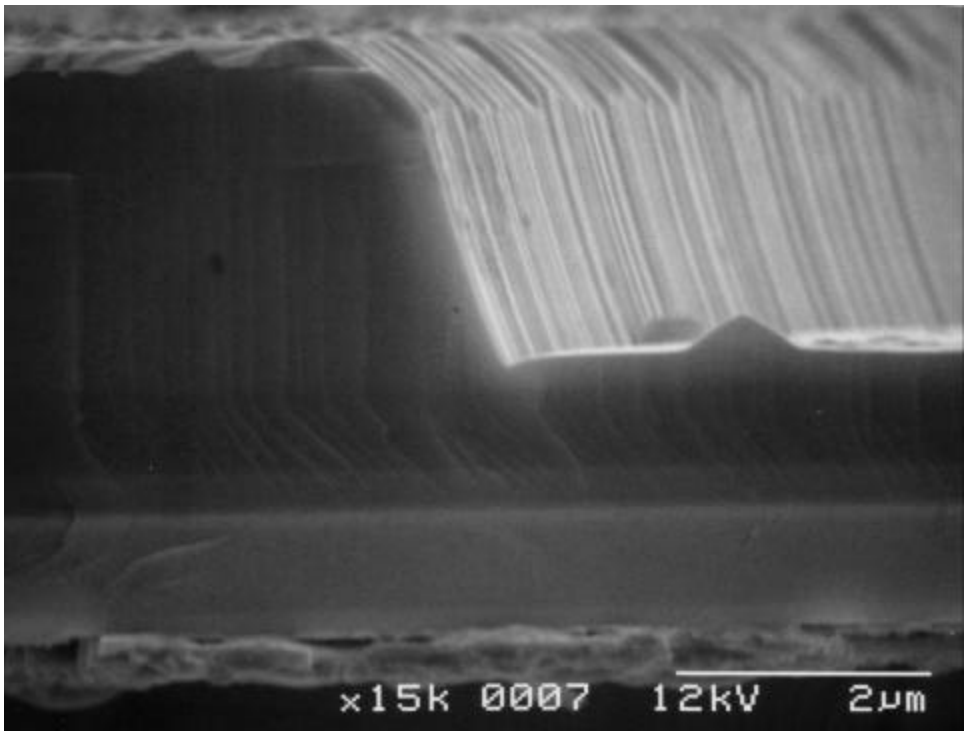

Figure 1. An RIE-etched facet is angled by 4-5º from vertical after optimizing process parameters. In addition, etched facets are subject to process variations and are rougher than cleaved facets. For these reasons, cleaved facets are preferred over etched facets.

The rest of this section describes the crystal symmetry of sapphire and of wurtzite GaN. A pictorial representation is presented of the cleave planes and describes how these planes are oriented within the crystal structure.

The second section describes cleaving of a-plane sapphire. Vertical cleave planes of sapphire are used to fracture the GaN to form the mirror facet for the group-III nitride laser. The facet produced is jagged due to the misorientation of the GaN and sapphire cleave planes, but the facet quality is suitable for creating laser diodes.

The third section describes the growth of group-III nitride lasers on GaN or SiC substrates. Both GaN and SiC substrates cleave well and have cleave planes that are parallel to those of the epitaxial GaN. Both processes have been

demonstrated and offer many advantages over other methods. These advantages include vertical and smooth cleave planes, vertical conduction, and improved thermal conductivity. These substrates provide very good cleaved facets that are potentially much easier to produce than those on sapphire.

The fourth section describes a novel method—based on wafer fusion—for fabricating cleaved facets. A successful demonstration of the fusion of hexagonal (wurtzite) GaN (α-GaN/α-Al_2O_3) to a (100) InP substrate is presented. This fusion occurs without voids or oxide at the interface. Optically flat, vertical, cleaved facets in the GaN are then fabricated parallel to the crystallographic planes of the host InP. I-V measurements have been performed across the n-N fused interface. These results show that the fused interface exhibits a barrier for electrons passing from the InP to the GaN and ohmic conduction of electrons moving in the opposite direction.

A comparison of these cleaving technologies is given in the last section.

2.1.1. Crystal symmetry for sapphire and GaN

The crystals of GaN and sapphire have much less symmetry than those in other III-V material systems. α-GaN (also called h-GaN) has wurtzite crystal structure, which means that it falls into the C_{6v} (C6mc) symmetry group [1]. Sapphire (α-Al_2O_3) has a corundum crystal structure, which puts it in the D_{3d} (R$\underline{3}$c) symmetry group [1]. Both of these structures are 6-fold rotational symmetry around the c-axis. The crystal structures for sapphire and GaN are diagrammed in Figures 2 and 3. Both crystals are pictured in the (0001) orientation.

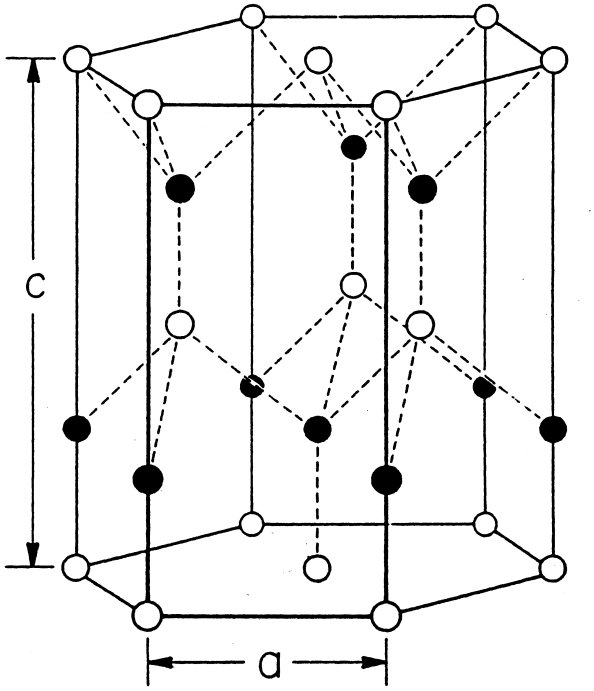

Figure 2. Wurtzite crystal structure for GaN [2].

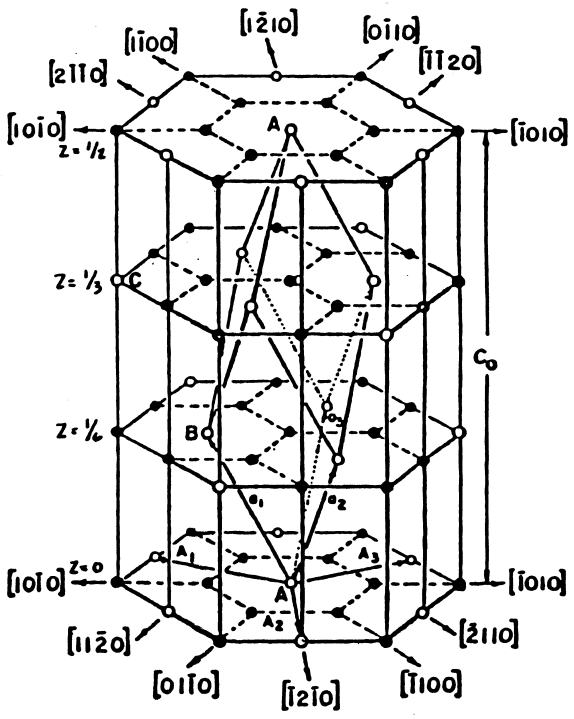

Figure 3. Corundum crystal structure for sapphire [2].

For forming cleaved facets in laser diodes, smooth and vertical cleave planes are required in the region where the optical mode is contained. This region is usually limited to the epitaxial layers. To form facets that are both smooth and vertical across the epitaxial layers, the crystal structure of the substrate and the epitaxy must first have vertical cleave planes. Additionally, the vertical cleave planes of the two materials must lie in the same plane. In the case of GaN grown on basal plane sapphire, both sapphire and GaN will cleave along vertical planes: the a-planes, {11$\underline{2}$0}. Due to the way the atoms line up during the epitaxial growth, however, each of the sapphire a-planes is 30º from the GaN a-planes. Since this is true, either the m-plane {1$\underline{1}$00} of sapphire or the m-plane of GaN must be used as one of the cleave planes. Forcing the cleave along the m-plane of sapphire can be done, but this plane has a slightly higher bond strength than the

a-plane. It is therefore easier to make a good cleaved facet using the sapphire a-plane. Researchers at Meijo University [3] and HP Labs Japan [4] have demonstrated using the a-plane of sapphire to cleave vertical facets in GaN.

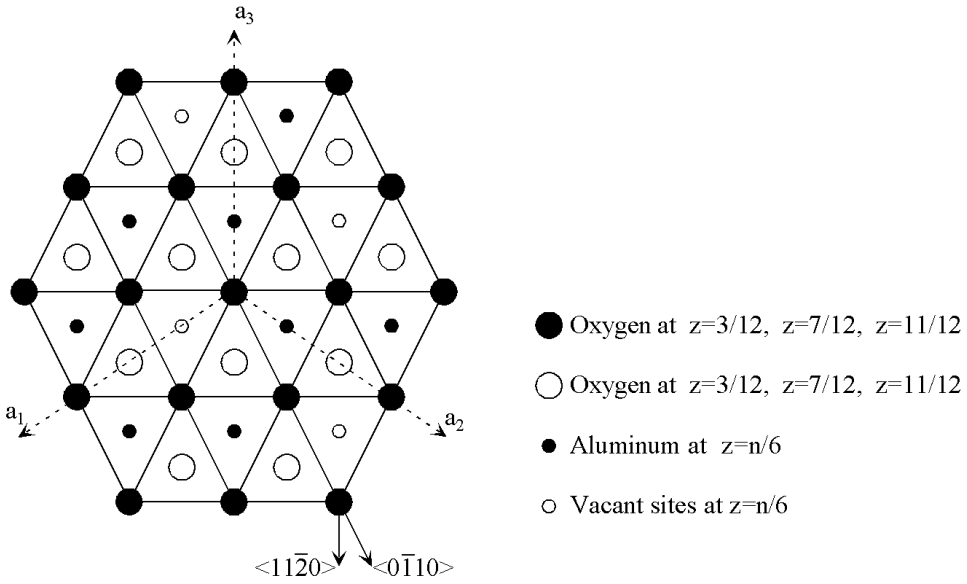

Figure 4. A diagram of the atomic structure for sapphire. Z is in the direction perpendicular to the plane of the paper. The numerical values for z-coordinates are normalized to one lattice period in the z-direction [2].

The crystal structure shown in Figure 4 was used to calculate the relative orientations of the crystal planes of sapphire. These orientations are shown in Figure 5, which gives the stereographic projection diagram for the planes of c-plane sapphire. Stereographic projections are typically used for describing Laue x-ray diffraction data. The diagram is constructed by assuming that the c-axis of sapphire points out of the plane of the paper and the a-axis points to the right. The normal vectors to the crystal planes are then drawn and the points where the normal vectors intersect the unit sphere are noted. A straight line is drawn between these points on unit sphere and the south pole of the unit sphere. The projection onto the paper is formed where these lines intersect the plane of the paper. (The plane of the paper is typically drawn coplanar with the equator of the

unit sphere, but this location does not affect the final projection.) Thus, vertical cleave planes will be located along the circumference of the circle and all inclined planes will be located in the interior of the circle. The center of the circle represents the normal to the substrate. The distance from the center of the circle describes the inclination angle for the plane relative to the substrate surface [5].

The sapphire {1$\underline{1}$00} m-planes are parallel to the GaN {11$\underline{2}$0} planes and both are vertical. However, there are a number of problems with using these planes as mirror planes. First, cleaving is difficult because these cleave planes are very close in angle to other cleave planes of sapphire. In addition, the m-plane is not one of the preferred cleave planes of sapphire. Sapphire cleaves most easily along the inclined r-planes (1$\underline{1}$02) and the r-planes lie very close to the a-planes and m-planes. For comparison, in (100) GaAs and InP, the cleave planes are separated by 90º. In (100) Si, the cleave planes are separated by 60º. Each of these material systems cleaves relatively easily along a chosen cleave plane. In (0001) sapphire, only 30º separate the r-planes and a-planes and it is the r-plane that cleaves preferentially. Mechanically, this makes it very easy for a cleave to couple from the a-plane to the r-plane, resulting in a jagged edge. This mechanical coupling can occur through a small amount of surface roughness, a slight misalignment of the cleaving forces, an intentional patterning of the surface, or a large defect in the crystal structure.

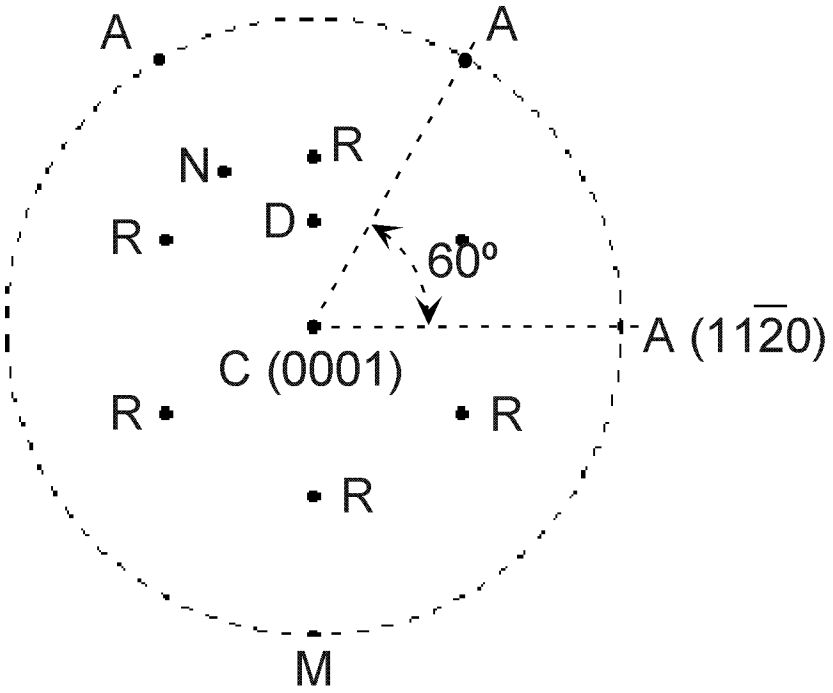

Figure 5. Stereographic projection for basal plane sapphire.

To prevent this coupling between planes, sapphire must be lapped very thin before it is cleaved. In the case of laser diodes fabricated at Meijo University, the sapphire was polished to a thickness of 50 μm before being cleaved. For soft materials such as GaAs and InP, polishing to these thicknesses can be achieved without observing any cracking. However, polishing sapphire is more difficult because the rigidity of sapphire makes it prone to cracking when it is thinned below 80-100 μm. In addition, the high bond strength of sapphire means that polishing without the aid of a polishing machine is very time consuming.

Even after polishing it successfully, sapphire is very difficult to cleave. Stocker, et al. claim to have cleaved basal plane sapphire along both the a-plane and the m-planes [6]. Other methods such as using scribe and break to form cleaved facets have also been described by Stocker, et al. [6]

2.2. Cleaving a-plane sapphire

Another method for forming cleaved facets is to use a-plane sapphire substrates. The crystal projection diagram for a-plane sapphire is shown in Figure 6. In this crystal orientation, several of the r-planes are vertical planes and can therefore be used for laser mirrors.

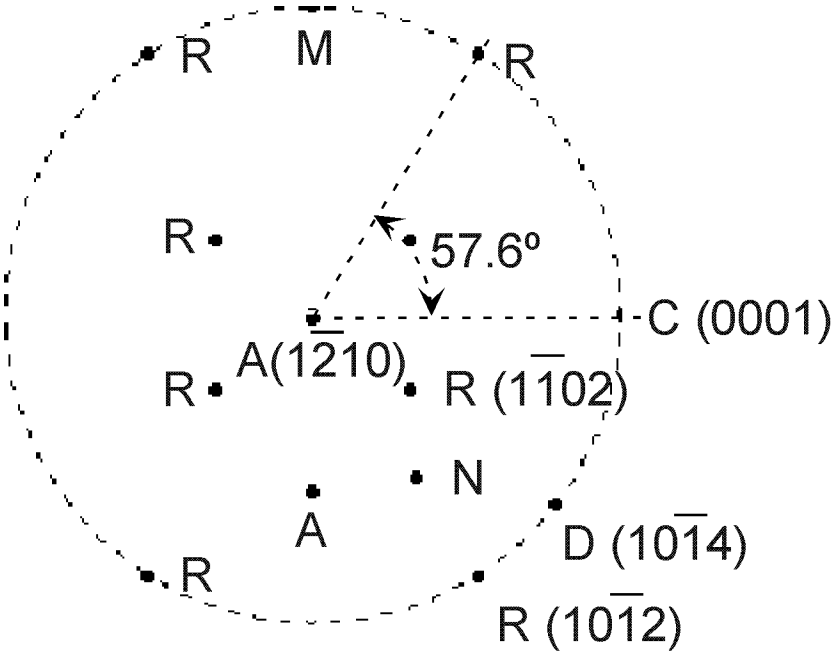

Figure 6. Stereographic crystal projection for a-plane sapphire.

As described in the previous section, the r-planes are the most natural cleave planes for sapphire because they have the weakest bond strength. For this reason, cleaving the r-planes of a-plane sapphire is much easier than cleaving the a-plane or m-plane of c-plane sapphire. This means that a-plane sapphire does not have to be thinned quite as much as c-plane sapphire in order to be cleaved. Thinning a-plane sapphire to 70-100 μm is sufficient for reliable cleaving. Since sapphire does not have to be thinned as much, many of the problems with the cracking of sapphire are reduced.

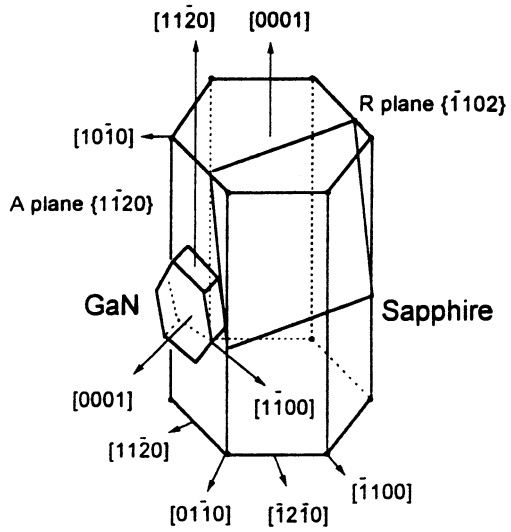

Figure 7. In this crystal plane diagram, the growth direction is to the left of the figure as illustrated by the arrow on the GaN surface [7]. The hexagonal shapes indicate the symmetry of the crystals.

Unfortunately, a-plane sapphire is not a panacea for cleaving problems. The main problem for GaN facets formed on a-plane sapphire is the misorientation of the GaN and sapphire cleave planes. During growth, the a-plane of the GaN lines up with the c-plane of sapphire as shown in Figure 7. Unfortunately, the c-plane of sapphire is polar and is therefore not a useful cleave plane. The r-planes in sapphire are located 57.6º to either side of the c-plane in sapphire. The six-fold symmetry of the GaN means that the a-planes are distributed every 60º. Thus, the a-plane of the GaN is misoriented by 2.4º from the vertical r-plane of sapphire as shown in Figures 6 and 7. For a cleave that starts in the sapphire, this angular misalignment is small enough that the fracture does propagate along the a-plane of the GaN. Lasers can be fabricated using these facets if the striations do not significantly intersect the area of the optical mode. However, due to these striations, laser yield is very low with this process. The misalignment does, however, cause problems. The GaN and sapphire cleave planes remain roughly parallel along the entire length of the cleaved facet. In order for this to happen

despite the crystal misorientations of the cleave planes requires a periodic adjustment of the crystal planes. This adjustment is manifest as periodic striations along the optical facet of the laser diode. Figure 8 shows an SEM micrograph of such a cleaved facet.

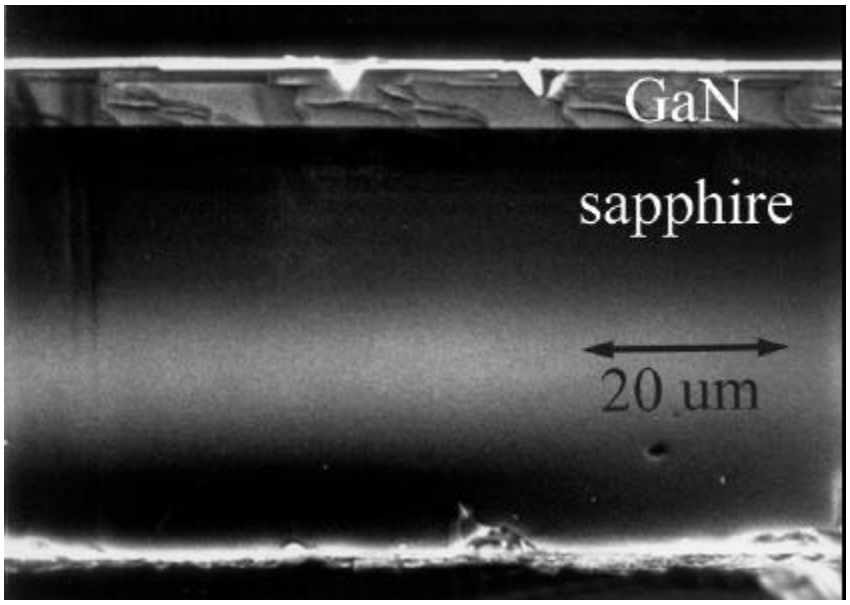

Figure 8. An SEM micrograph of a cleaved GaN/a-plane sapphire facet. The striations in the GaN are visible in the epitaxial layers. These striations are due to the 2.4º rotational misalignment between the GaN and sapphire cleave planes.

2.3. Cleaved facets for GaN/SiC or GaN/GaN

A better process is to use a substrate that has cleave planes that are parallel to those of the nitride epitaxial layers. One method that has not been explored in detail at UCSB is the fabrication of nitride laser diodes on SiC substrates. As mentioned in the first chapter, SiC has a number of properties that make it better than sapphire for the fabrication of nitride laser diodes. One of these is the ability to form vertical cleaved facets easily. 6H-SiC has vertical cleave planes which line up with the cleave planes of the GaN. Atomically smooth cleave planes can

therefore be formed. Unlike sapphire, there are only a few cleave planes in SiC that break easily. This means that coupling from one cleave plane to another during cleaving occurs much less frequently than it does in sapphire. Reliable cleaving can thus be performed with this process. The one negative to this method is that high quality SiC is not readily available. Cree, Inc. has been the dominant manufacturer of SiC wafers and is beginning to sell high quality SiC substrates. SiC does, however, remain very expensive relative to the cost of sapphire.

A final method for forming cleaved facets is based on growing very thick GaN on sapphire and removing the sapphire substrate by polishing, liftoff, or laser ablation. Nakamura has used this method in his most recent laser diodes to create high quality facets, to allow vertical conduction of carriers, and to provide better thermal dissipation. The growth of a thick, high-quality GaN layer is difficult, however, and few other researchers have been able to achieve the same results. Nakamura reports that this growth can be performed in approximately 4 hours using hydride vapor phase epitaxy (HVPE) [8].

2.4. Cleaved facets by wafer fusion of GaN to InP

This section describes the successful fabrication of cleaved facets by a novel method that requires wafer fusion of InP to epitaxial GaN. Wafer fusion was first performed over a large area by Liau and Mull in 1991 [9]. Since that time, wafer fusion has been used for many applications because it is a simple method that allows layer structures to be fabricated that cannot be achieved by traditional growth methods. For example, researchers at Hewlett Packard use wafer fusion in the production of transparent-substrate AlGaInP/GaP LEDs [10]. Using a double-fused structure, Babiç, et al. demonstrated the first long-wavelength vertical-cavity surface-emitting lasers (VCSELs) to operate in continuous-wave

(CW) mode at room temperature [11]. Resonant cavity photodetectors and heterojunction avalanche photodetectors based on fusion have also been reported [12, 13]. As illustrated by these examples, the restrictions of material choices due to thermal expansion and lattice mismatch are less stringent for fused interfaces than for heterojunctions grown by MOCVD or MBE [14]. While thermal expansion differences can still have a dramatic effect on the quality of the fused interface, proper control of the temperature cycle can yield good quality fusion. For both nitride VCSELs and nitride in-plane lasers, these relaxed restrictions will give device designers increased flexibility to choose materials based on optimal thermal or electrical characteristics. Therefore, wafer fusion will potentially solve many of the problems that occur in nitride lasers that result from the choice of sapphire as the substrate material.

2.4.1. Wafer fusion of GaN to InP

The GaN films used for wafer fusion are grown by atmospheric pressure metal-organic chemical vapor deposition (MOCVD) using TMGa and NH_3 sources in a Thomas Swan Ltd. reactor. A 19 nm GaN nucleation layer is grown at 600ºC on basal plane sapphire substrates before growing a thicker GaN film at 1080ºC. The GaN film thickness for the samples varies from 1.5 to 2.5 μm with a root mean square (rms) surface roughness of approximately 2 nm as measured by atomic force microscopy (AFM). Additional details of the growth process are reported in reference [15] and in Chapters 1 and 4. The InP samples are (100) n-type substrates with no epitaxially grown layers. The InP sample used for electrical characterization of the interface did have epitaxially grown layers, which will be described in more detail below.

GaN to InP fusion is accomplished by a simple method: The GaN and InP samples, each 8 x 8 mm, are cleaned with solvents. Channels 10 μm wide with a period of 150 μm are etched into the InP sample to allow gas and liquid to escape

from the interface during fusion [16] and to relieve strain in the structure that is introduced during the cooling process. This strain results from the differences in thermal expansion between the InP and the GaN/sapphire. The oxide layers from both samples are removed with a 49% HF solution. While both surfaces are wet with HF, the GaN and InP are pressed together using the fixture shown in Figure 9. These samples are then heated (under pressure) to 750ºC and held at this temperature for 60 minutes.

The fusion fixture used to hold the samples together is illustrated in Figure 9. The fixture is made from DFP-3-2 graphite, which is stable at high temperature and has a relatively low coefficient of thermal expansion. The pressure dome that rests on top of the samples is designed to press uniformly on the samples even if the graphite plate that is pushing on it is slightly inclined relative to the base of the fixture. Reasonably uniform pressure can be applied as long as the wafers are centered under the domed pressure piece. It has been found experimentally that optimal fusion occurs when the rectangular top graphite piece is kept as level as possible.

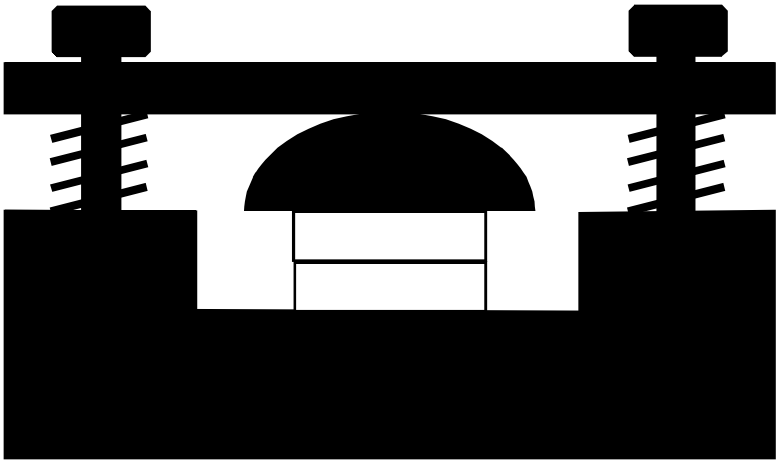

Figure 9. The fusion fixture that is used to hold the InP and GaN samples together during fusion is designed to apply uniform pressure over the entire wafer surface. The rounded dome of the top pressure piece allows for uniform pressure to be applied even when the screws are not tightened uniformly or when bowing occurs in the top plate. If this piece were rectangular instead of rounded, non-uniform tightening of the screws would result in non-uniform pressure on the sample [9].

The high temperature used for wafer fusion allows for active mass transport of the indium at the InP/GaN interface. This mass transport effectively levels the surface of the moderately rough GaN to allow a better matching of the InP and GaN surfaces. This surface mobility is approximately 20 times higher than bulk material mobility and allows a relatively rapid migration of the carriers. As the samples move into close proximity, the interface mobility slows slightly to 10-15 times the bulk mobility as atoms move along atomic channels between the two materials. Once the samples are in atomic contact over the entire surface, the bonds at the surface rearrange themselves to achieve a lower energy state. A surface with many dangling bonds is in a relatively high-energy state in comparison to the state in which these dangling bonds from opposing surfaces bond together across the interface. Therefore, it is energetically favorable for the two wafers to fuse together to form a single semiconductor crystal. As the sample is cooled, it is important to cool very slowly to prevent cracking of the semiconductors due to differences in thermal expansion between the two

materials. The build up of strain is reduced primarily by two methods: 1) bulk mobility of atoms and 2) relaxation. The first method is the most desirable. If the sample is cooled slowly, bulk mobility of atoms can occur to compensate for differences in thermal expansion. If the sample is cooled rapidly, the atoms do not have time to migrate to reduce the strain and the sample relaxes (cracks) to release the strain [17]. The channels that are etched into the InP also provide some strain relief.

Thus, with slow cooling and etched channels, the build-up of strain during fusion can be reduced. High quality fusion results from this procedure as shown by the cross-section transmission electron microscopy (TEM) in Figures 10 and 11. The InP/GaN fused interface is free of voids and has no oxide layer, which indicate that the two samples are well fused. In addition, the defects formed by the fusion process are contained within a few monolayers of the fused interface, which demonstrates that the wafer fusion preserves the structural integrity of the InP and GaN.

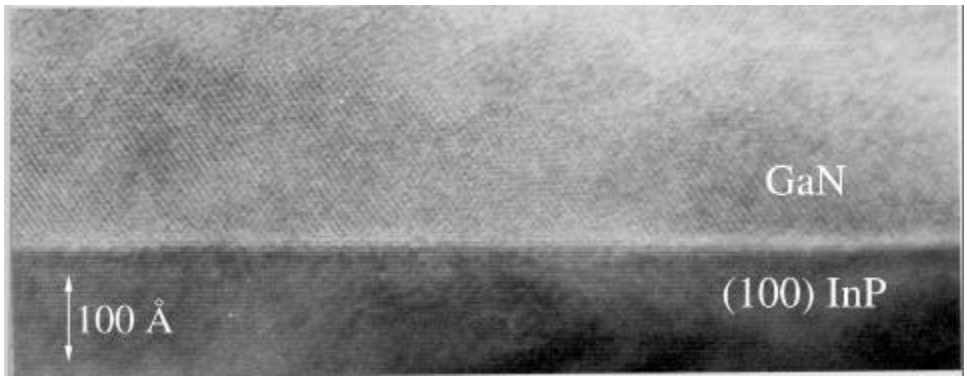

Figure 10. A TEM micrograph of an InP/GaN fused interface is shown. Fusion was performed at 750ºC for 60 minutes.

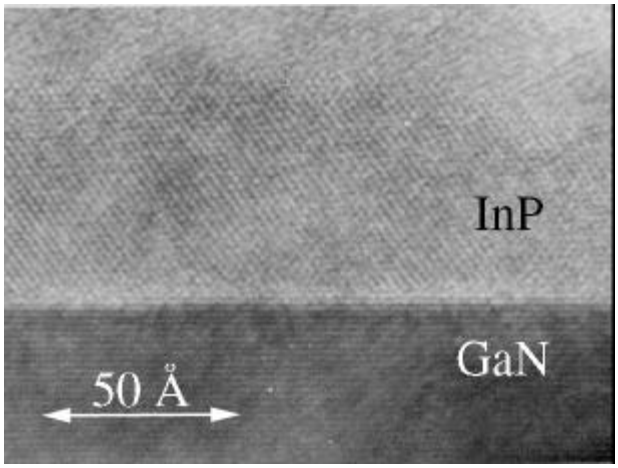

Figure 11. An enlargement of TEM micrograph of an InP/GaN fused interface is shown. Fusion was performed at 750ºC for 60 minutes. The (001) plane of InP and (11$\underline{2}$0) plane of GaN in this sample are unintentionally misoriented by 4º for this sample.

2.4.2. Formation of cleaved facets in fused structure

After fusion, the sapphire substrate can be lapped using 15-μm diamond slurry to make it thin enough for cleaving (<150 μm). By making a scribe mark on the InP host substrate, turning the fused samples over, and pressing on the sapphire, the GaN and thinned sapphire are forced to cleave parallel to the {110} crystal planes of the InP. A scanning electron microscope (SEM) micrograph of the cleaved facet (Figure 12) provides further evidence that the interface is free of

voids and therefore well fused. Facets produced in this manner appear to be optically flat when examined by bright-field, dark-field, and Nomarski interference contrast microscopy and by SEM.

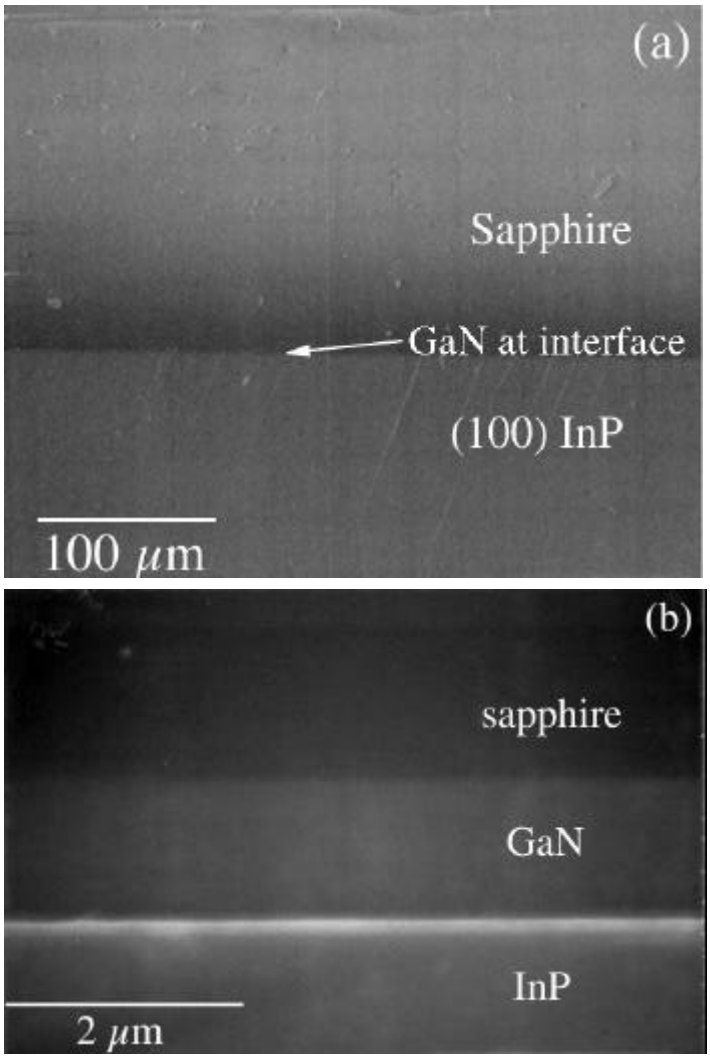

Figure 12 (a) An SEM micrograph of a cleave through an InP/GaN fused interface. This sample was cleaved without lapping the sapphire substrate at all. The cleave plane from the InP propagates through the GaN and sapphire to produce a smooth cleave plane that can be used as a mirror facet in an in-plane laser or other optoelectronic device. The interface is free of voids, which indicates that the junction is well fused. (b) A higher magnification SEM micrograph of an InP/GaN fused junction shows the epitaxial layer structure of the fused samples. The sapphire substrate of this sample was lapped before cleaving.

2.4.3. Electrical characterization of the fused interface

Many optoelectronic devices are possible with this technology. Current injection across the fused interface is critically important for most of these devices. To measure the electrical characteristics of the junction, the InP substrate used for the cleaving demonstration is replaced with an epitaxially grown structure, InP/$In_{.53}Ga_{.47}As$/InP. This is done in order to provide an etch stop layer for removing the InP substrate. The epitaxial InP and InGaAs layers are 500 nm and 200 nm thick, respectively, with n-type Si doping of approximately 10^{18} cm^{-3} and 10^{19} cm^{-3}. The InP and GaN epitaxial layers are fused using the same process described above. After fusion, the InP substrate is etched away, stopping on the InGaAs etch stop layer. Selected areas of the InGaAs and InP epitaxial layers are then etched away to make contact to the GaN as shown in Figure 13(a). 200 nm thick aluminum contacts are evaporated onto the GaN and annealed at 500ºC. Ni/AuGe/Ni/Au contacts are evaporated onto the InP and a second anneal at 430ºC is performed. For the InP contact, the first Ni barrier layer is designed to prevent diffusion of the Ge to the fused junction, thereby preserving the electrical characteristics of the fused junction.

The electrical characteristics of the fused interface are measured using a four-point probe measurement (Figure 13(a)) that is designed to reduce the effects of contact resistance. The pads are nominally 200 µm wide (in the direction perpendicular to current flow) and 170 µm long and are spaced by 20 µm. The resistance along this 20-µm separation has not been subtracted from the electrical measurements. Figure 13(b) shows the current-voltage (I-V) characteristic of the fused interface. Electrons moving from the GaN to the InP encounter almost no detectable barrier. Electrons moving from the InP to the GaN encounter a potential barrier of several electron volts.

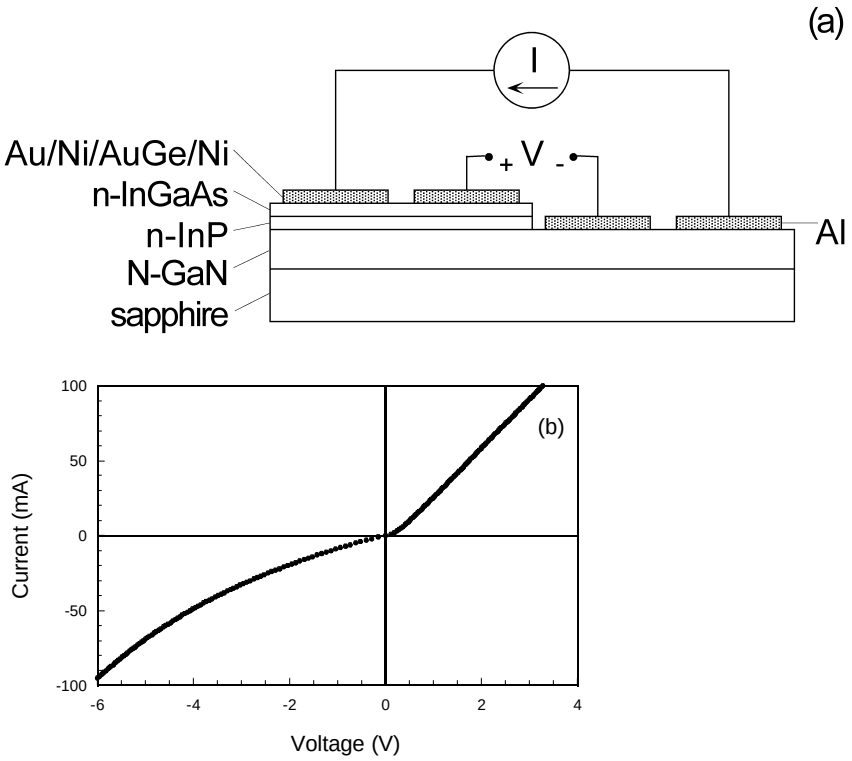

Figure 13(a). The electrical characteristics of the n-InP/N-GaN fused junction are measured using a four-point probe structure with 200 μm wide pads separated by 20 μm gaps. (b) The measured current voltage curve shows that electrons can be injected through the interface for small voltage levels. The direction of positive current across the junction is from InP to GaN (i.e. electrons passing from GaN to InP).

The barrier for electrons that is observed in this experiment is not necessarily present in all GaN/InP fused samples. The density of dangling bonds can be changed drastically by rotating the two crystals before bonding so that the crystals bond in a slightly different orientation. Changing the rotation angle by only a few degrees can produce a barrier due to interface states created by these dangling bonds [18]. Optimization of the rotation angle between GaN and InP was not performed in this set of experiments.

The I-V curve measured across fused interfaces is not well understood even in well-characterized material pairs such as InP/GaAs [19]. Due to these

complexities, calculation of a band diagram from known parameters is difficult. We can make a basic estimate as to what the band diagram is based on the electron affinities of the two fused materials: Based on the differences in electron affinities between GaN and InP, the heterointerface is expected to be a broken gap interface. The band discontinuities based on these differences are given by Equations 1 and 2. It should be recognized, however, that this method for calculation often does not give accurate band offsets.

$$\Delta E_C = E_C(\text{InP}) - E_C(\text{GaN}) = 1.9 \text{ eV} \quad (1)$$

$$\Delta E_V = E_V(\text{InP}) - E_V(\text{GaN}) = 4.2 \text{ eV} \quad (2)$$

If these band offsets are used, we can model the fused interface as a typical broken gap interface, like that of InAs/GaSb. This band structure is shown in Figure 14. At such an interface with no bias applied, electrons accumulate on one side (in this case, the GaN side) and holes accumulate on the other side (InP). As a bias is applied, the electrons and holes mix across the interface, which causes a Fermi level gradient. Electron and hole recombination produces current. This explanation of current flow predicts ohmic current flow in both directions. The slight nonlinearity in the negative voltage regime of Figure 13(b) is not well understood. One possible explanation is that this nonlinearity is due to surface states resulting from dangling bonds at the InGaAs/InP heterointerface.

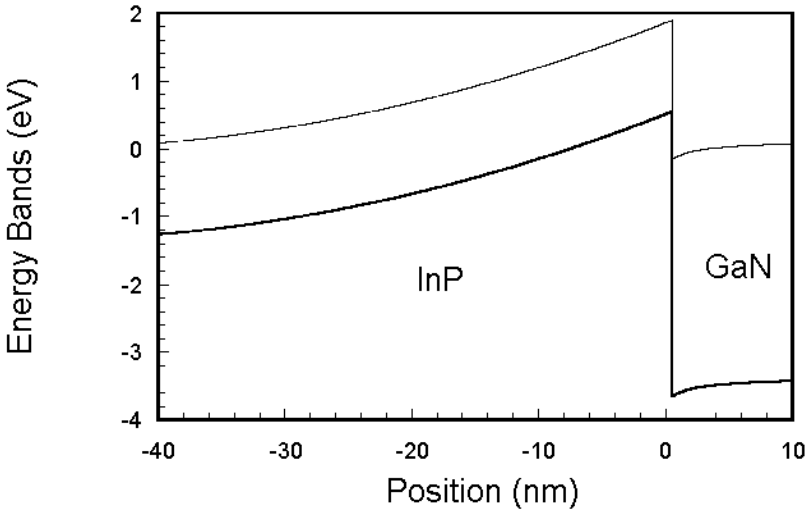

Figure 14. Possible band diagram of fused interface. Band offsets are given by the difference in electron affinities. This model neglects carrier injection, surface states, strain, piezoelectric effects, and interface impurities.

For fusion of p-InP to p-GaN, hole injection is not predicted to occur in this manner. The large valence band discontinuity is expected to give a barrier that prevents hole injection for low voltages. Therefore, near ohmic injection of holes from p-InP to p-GaN across a fused junction should not occur. A voltage drop of several volts is expected for hole injection.

2.4.4. Transfer of GaN to conductive substrates

Although fusion is not likely to significantly improve p-type contacts for GaN, fusion will possibly ease the fabrication of devices by allowing the transfer of device layers to conductive substrates. By growing a sacrificial liftoff layer on the sapphire substrate, the sapphire substrate can be removed completely from the GaN device layers after fusion. The InP substrate now functions as the substrate for the device. This procedure is shown in Figure 15. This procedure is expected to have two primary advantages: 1) it is expected to make cleaving

easier because the thick sapphire substrate will be removed and 2) backside contacts can be made to the InP substrate, which makes fabrication of many devices, such as in-plane lasers, much simpler.

Figure 15. Removal of sapphire substrate by etching a sacrificial layer grown on the sapphire. This will allow easier cleaving and simpler device designs for in-plane optoelectronic devices. One possible choice for the sacrificial layer is ZnO [20-24].

The InP/InGaAs/InP epitaxial layer structure used for the electrical characterization provided a good measure for the fusion uniformity. After etch removal of the InP substrate, only a thin layer of epitaxial InP/InGaAs remained. In areas that were not well fused, this thin layer cracked and broke away. After etching the substrate, we were therefore able to determine the proportion of sample area that was well fused. For a typical processing run, fusion was achieved over 60-70% of the sample area. The lack of fusion over the other 30-40% of the sample is attributed to increased surface roughness of the GaN in those regions. InGaN samples with an indium mole fraction of 10-20% were also fused to InP with the idea that the extra indium would facilitate mass transport at the interface. The proportion of area fused was not noticeably improved over the GaN samples, however. We believe that the indium content of the InGaN samples was too low to compensate for the increased roughness of the InGaN samples over the GaN samples.

In summary, optically flat, cleaved facets have been achieved in GaN epitaxial layers after bonding the GaN to InP. No indications of interface voids or oxide formation were found, which reveals that the samples were well fused. In

addition, current injection has been demonstrated across the fused interface at low voltages. Both of these experiments indicate that this method provides a viable technique for the fabrication of facets in GaN in-plane laser diodes. Fusion uniformity has not yet been satisfactory for laser production, however. Using smoother GaN epitaxial layers can alleviate this problem.

2.5. Conclusion

There are a number of technologies that have been demonstrated for fabricating GaN facets on sapphire substrates: 1) the method that has been the most popular is etching facets with RIE or CAIBE. While the quality of these facets has improved, they still suffer from roughness and slight off-vertical angles. 2) Another method is using cleaved facets on a-plane sapphire. GaN facets made on a-plane sapphire are not smooth due to the misalignment of the sapphire and GaN cleave planes. 3) GaN facets made on c-plane sapphire using the a-plane of sapphire as the cleave plane are smoother, but are very difficult to make because the cleave planes used in this case are not the primary cleave planes of sapphire. So the sapphire must be thinned to less than 50 μm in order to get reliable cleaves.

There are two methods that can easily produce atomically flat cleave planes in GaN: The first is using SiC (or GaN) substrates. The SiC cleave planes are vertical and the substrate breaks easily along these planes. In addition, the GaN cleave planes line up with the cleave planes of SiC. Thus, atomically flat cleave planes can be created in this material system. The other method for creating atomically flat cleave planes is by using the fusion bonded InP to cleave the GaN crystal along desired crystal planes. Unfortunately, GaN devices made by wafer fusion suffer from poor electrical characteristics at the fused interface, although better matching of the crystal planes during bonding may solve this problem. In

addition, it is very difficult to remove the sapphire substrate because there is no sacrificial wet etch that can liftoff the sapphire substrate. This makes processing devices with such facets very difficult. These two problems with wafer-fused facets have been addressed 1) by using gold bonding at the interface to improve the electrical characteristics of the interface and 2) by using laser ablation to remove the sapphire substrate. These methods will be described in more detail in Chapter 5.

2.6. References

[1] R. W. G. Wyckoff, *Crystal Structures*, vol. 1, 2nd ed. New York, NY: John Wiley & Sons, 1963.

[2] S. P. DenBaars, "Wide Bandgap Semiconductors," presented at UCSB (Class Notes), 1998.

[3] I. Akasaki, S. Sota, H. Sakai, T. Tanka, M. Koike, and H. Amano, "Shortest Wavelength Semiconductor Laser Diode," *Electronics Letters*, vol. 32, pp. 1105, 1996.

[4] N. Yamada and e. al., "Room Temperature Pulsed Operation of Nitride-Based Ridge-Waveguide Laser Diode with Cleaved Facets," presented at IEEE-LEOS Meeting, San Francisco, CA, 1997.

[5] R. F. Bunshah, *Techniques for the Direct Observation of Structure and Imperfections, Part 2* in *Techniques of Metals Research* vol. 2. New York: John, Wiley, & Sons, 1969.

[6] D. A. Stocker, E. F. Schubert, W. Grieshaber, K. S. Boutros, and J. M. Redwing, "Facet roughness analysis for InGaN/GaN lasers with cleaved facets," *Applied Physics Letters*, vol. 73, pp. 1925-1927, 1998.

[7] A. Alemu, B. Gil, M. Julier, and S. Nakamura, "Optical properties of wurtzite GaN epilayers grown on A-plane sapphire," *Physical Review B (Condensed Matter)*, vol. 57, pp. 3761-3764, 1998.

[8] S. Nakamura, M. Senoh, S. I. Nagahama, N. Iwasa, T. Yamada, T. Matsushita, H. Kiyoku, Y. Sugimoto, T. Kozaki, I. Umemoto, M. Sano, and K. Chocho, "InGaN/GaN/AlGaN-based laser diodes grown on GaN substrates with a fundamental transverse mode," *Japanese Journal of Applied Physics, Part 2 (Letters)*, vol. 37, pp. L1020-1022, 1998.

[9] Z. L. Liau and D. E. Mull, "Wafer fusion: A novel technique for optoelectronic device fabrication and monolithic integration," *Applied Physics Letters*, vol. 56, pp. 737-739, 1991.

[10] F. A. Kish, D. A. Defevere, D. A. Vanderwater, and G. R. Trott, *Electronics Letters*, vol. 30, pp. 1790, 1994.

[11] D. I. Babic, K. Streubel, R. P. Mirin, N. M. Margarlit, J. E. Bowers, E. L. Hu, D. E. Mars, L. Yang, and K. Carey, *IEEE Photonic Technology Letters*, vol. 7, pp. 1225, 1995.

[12] I. H. Tan, J. J. Dudley, D. I. Babic, D. A. Cohen, B. D. Young, E. L. Hu, J. E. Bowers, B. I. Miller, U. Koren, and M. G. Young, *IEEE Photonic Technology Letters*, vol. 6, pp. 811, 1994.

[13] A. Hawkins, T. Reynolds, D. England, D. Babic, M. Mondry, and J. Bowers, presented at LEOS 8th Annual Meeting, San Francisco, CA, 1995.

[14] R. J. Ram, J. J. Dudley, J. E. Bowers, L. Yang, K.Carey, S. J. Rosner, and K. Nauka, *Journal of Applied Physics*, vol. 78, pp. 4227, 1995.

[15] B. P. Keller, S. Keller, D. Kapolnek, M. Kato, H. Masui, S. Imagi, U. K. Mishra, and S. P. DenBaars, *Electronics Letters*, vol. 31, pp. 1102, 1995.

[16] D. I. Babic, K. Streubel, R. P. Mirin, N. M. Margalit, M. G. Peters, E. L. Hu, and J. E. Bowers, *to be published in Optical and Quantum Electronics, Special Issue "Optoelectronics based on Indium Phosphide and Related Materials" (May 1996).*, 1996.

[17] J. Höfler, April 20, 1999, personal communication.

[18] Y. Okuno, "Investigation on direct bonding of III-V semiconductor wafers with lattice mismatch and orientation mismatch," *Applied Physics Letters*, vol. 68, pp. 2855-2857, 1996.

[19] K. A. Black, A. R. Hawkins, N. M. Margalit, D. I. Babic, A. L. H. Jr., Y.-L. Chang, P. Abraham, J. E. Bowers, and E. L. Hu, "Fusion Bonding: Hetero-interfacial Materials Analysis and Device Application," in *Heterogeneous Integration: Systems on a Chip*, vol. CR70, A. Husain and M. Fallahi, Eds. Bellingham, WA: SPIE, pp. 30-55, 1998.

[20] T. Detchprohm, K. Hiramatsu, H. Amano, and I. Akasaki, "Hydride vapor phase epitaxial growth of a high quality GaN film using a ZnO buffer layer," *Applied Physics Letters*, vol. 61, pp. 2688-2690, 1992.

[21] T. Detchprohm, H. Amano, K. Hiramatsu, and I. Akasaki, "The growth of thick GaN film on sapphire substrate by using ZnO buffer layer," *Journal of Crystal Growth*, vol. 128, pp. 384-390, 1993.

[22] T. Detchprohm, K. Hiramatsu, N. Sawaki, and I. Akasaki, "Metalorganic vapor phase epitaxy growth and characteristics of Mg-doped GaN using GaN substrates," *Journal of Crystal Growth*, vol. 145, pp. 192-196, 1994.

[23] T. Detchprohm, K. Hiramatsu, N. Sawaki, and I. Akasaki, “The homoepitaxy of GaN by metalorganic vapor phase epitaxy using GaN substrates,” *Journal of Crystal Growth*, vol. 137, pp. 170-174, 1994.

[24] T. Ueda, T. F. Huang, S. Spruytte, H. Lee, M. Yuri, K. Itoh, T. Baba, and J. S. Harris, Jr., “Vapor phase epitaxy growth of GaN on pulsed laser deposited ZnO buffer layer,” *Journal of Crystal Growth*, vol. 187, pp. 340-346, 1998.

Chapter 3

Laser optimization

This chapter describes the design of a GaN laser. Optical, electrical, and thermal modeling will be presented with the goal of emphasizing some of the ways in which these devices have been or can be improved.

In the first section, the epitaxial layer structure will be described. The basic design for the laser structure and laser geometry is similar to those for broad area lasers in other material systems. The differences between the nitride lasers and other III-V lasers will be highlighted in the modeling sections that follow.

The optical waveguide modeling has led to improvements in the epitaxial layer structure by increasing the mode confinement and reducing modal loss for the laser diode. Optimization of the cladding region thicknesses and the separate confinement heterostructure (SCH) regions are described.

The first electrical model presented in this chapter is based on the commercial program ATLAS. Due to a number of limitations in ATLAS, the models presented are suitable only for observing broad trends. The most severe limitations is that ATLAS does not incorporate piezo-electric or quantum confinement effects into the energy bands. This makes carrier flow and recombination through the quantum wells inaccurate. However, the results are accurate enough to be able to analyze current spreading. Despite their crudeness, these models do give us important information about the operation of nitride laser diodes.

A second electrical model is presented. This model is based on LASTIP simulations, which provide a more accurate and more complete description of both the electrical band structure and the optical performance of the laser. Three particular aspects of the LASTIP model will be discussed in detail: current spreading, non-uniform pumping of the wells (in both the lateral and transverse directions), and electron overflow from the QWs. A detailed comparison of L-I curves and band structures for different laser structures is used to analyze trends and optimize the laser design.

The final section gives a calculation of the thermal impedance of the laser diode. This is useful for describing why the choice of substrate is so important in laser diodes that operate p-side up.

Despite all of the modeling, progress has been slow because these lasers are still primarily growth limited, which means that many of the suggested improvements cannot be implemented at this time. The material has improved dramatically in the last five years, however, and there is no reason to believe that CW lasing will not be achieved soon. Toward this end, more extensive measurements will be done to more precisely isolate the cause of the high laser thresholds and device failures. A description of some of these measurements will be described throughout this chapter and will be reviewed at the end of the chapter.

3.1. Layer and device structure

3.1.1. Device geometry

Along with dramatic changes in laser structure that have been made by the growers in our group, there have been three distinct generations of fabrication and epitaxy. The differences between these three generations are derived from improvements in the electrical, thermal, and optical properties of the lasers.

The first generation nitride laser structure is shown in Figure 1. It will be referred to as Design A throughout this dissertation. This is a top-contacted gain-guided cleaved-facet laser [1-3]. The purpose for each layer in this laser is similar to that for each layer of a typical GaAs or InP laser. An a-plane sapphire substrate is used as a substrate for a 19-nm low temperature i-GaN nucleation layer. The nucleation layer is deposited as an amorphous film, which changes into island pyramids as it is heated. These pyramids serve as seed crystals for the GaN crystal that will be grown subsequently at high temperature. (This process is

believed to be similar to the process of epitaxial lateral overgrowth, in which a small window of GaN is exposed through a SiO_2 mask and thus acts as a seed crystal for the lateral growth of GaN.) The next layer is 2-3 μm GaN:Si. This GaN layer allows the threading dislocations to be reduced because as GaN is grown thicker, many of the threading dislocations grow together and thus terminate. This GaN:Si template layer effectively serves as the substrate for the laser structure. A soft compressively strained $In_{.05}Ga_{.95}N$ layer is grown 0.1 μm thick to act as a compliance layer to prevent cracking in the AlGaN cladding layer. A 0.4-μm $Al_{.06}Ga_{.94}N$:Si cladding is used for optical confinement of the laser mode. The separate confinement heterostructure (SCH) layer is composed of 30 nm of unintentionally doped GaN. The multi-quantum well (MQW) active region is 10 quantum wells of 3 nm $In_{.18}Ga_{.82}N$ separated by 6 nm $In_{.06}Ga_{.94}N$ barriers. Doping on the n-side is approximately $5 * 10^{18}$ cm^{-3}. These layers are mirrored on the p-type side with p-type carrier concentrations approximately $2 * 10^{17}$ cm^{-3}. More detailed descriptions of these layers are given in Chapter 3.

The device geometry was designed to maximize heat dissipation. Therefore, the mesa is very wide (125 μm) so that the heat spreads and is thus dissipated more efficiently. This has the added benefit of allowing devices to be probed easily because of the large area available for top contacts. While the wide mesas probably help heat dissipation, they also require the current to travel along a narrow and long lateral path, which created a large series resistance.

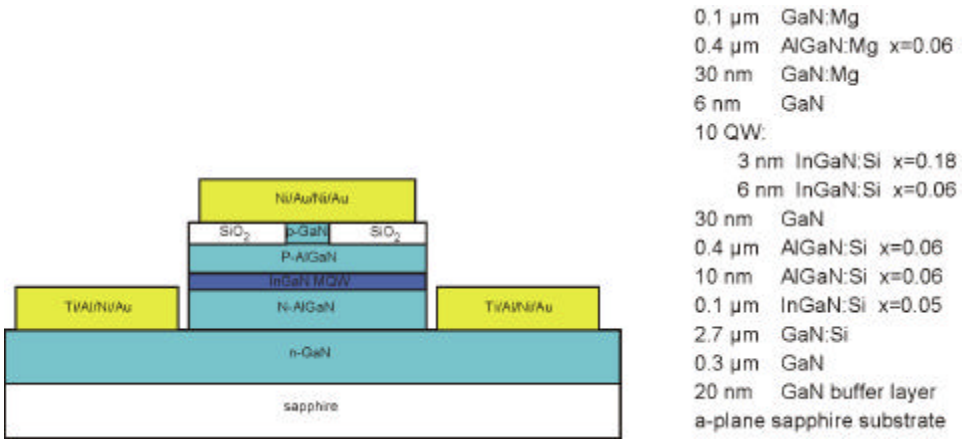

Figure 1. The first generation laser diode was designed for good heat dissipation. (This geometry will be referred to as 'Design A' in the remainder of this dissertation.)

The second- and third-generation laser diodes incorporated several improvements in both layer structure and device design as shown in Figures 2 and 3. These improvements include a thicker AlGaN cladding region for better optical confinement, a strained layer superlattice for a slight reduction in strain, an AlGaN cap to reduce electron overflow from the QWs, a narrower ridge for better lateral optical confinement, and fewer quantum wells to reduce asymmetric pumping of the wells. In Design B, the contacts are much closer than in Design A. This has the advantage of reducing heat generation due to lateral resistance. Design C has a vertical contact structure, which reduces heating even more. Design C uses the same epitaxial layer structure as Design B, but is mounted p-side down using a gold bonding process. There are other differences that will be described extensively later in this chapter and in Chapter 5.

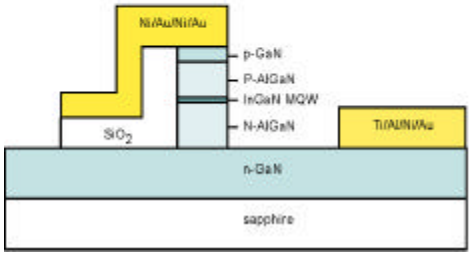

0.1 µm GaN:Mg
0.5 µm SLS (AlGaN:Mg x=0.20 and GaN:Mg)
0.1 µm GaN:Mg
20 nm AlGaN:Mg x=0.20
10 nm GaN
5 QW:
4 nm InGaN:Si x=0.12
10 nm InGaN:Si x=0.05
0.1 µm GaN
0.5 µm SLS (AlGaN:Si x=0.20 and GaN:Si)
0.1 µm InGaN:Si x=0.05
3.0 µm GaN:Si
0.6 µm GaN
20 nm GaN buffer layer
c-plane sapphire substrate

Figure 2. The second generation laser diode was optimized for optical and electrical performance at the expense of reduced heat dissipation. (This geometry will be referred to as 'Design B' in the remainder of this dissertation.)

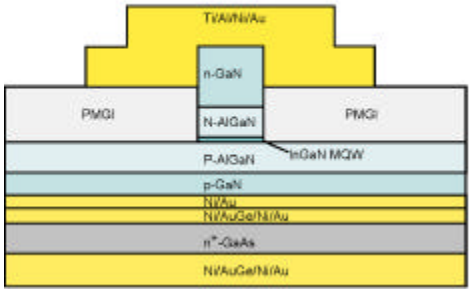

0.6 µm GaN
3.0 µm GaN:Si
0.1 µm InGaN:Si x=0.05
0.5 µm SLS (AlGaN:Si x=0.20 and GaN:Si)
0.1 µm GaN
5 QW:
10 nm InGaN:Si x=0.05
4 nm InGaN:Si x=0.12
10 nm GaN
20 nm AlGaN:Mg x=0.20
0.1 µm GaN:Mg
0.5 µm SLS (AlGaN:Mg x=0.20 and GaN:Mg)
0.1 µm GaN:Mg

Figure 3. The third generation laser diode optimizes optical, electrical, and thermal performance, but is more difficult to fabricate than Designs A and B. Advantages in mirror facet quality are also obtained with this design. (This geometry will be referred to as Design C in the remainder of this dissertation.)

3.1.2. Epitaxial layers

This section will describe the epitaxial layer structure and the lateral device geometry for UCSB nitride laser diodes. The layer structure and device geometry will then be used as the basis for the models presented in subsequent sections of this chapter.

Laser Designs B and C were described briefly at the end of the previous section. The epitaxial layers of these structures are listed in Table 1 and will be

discussed in more detail below. On the sapphire substrate, a thin GaN buffer layer is grown. As described for Design A, this ~20 nm layer of GaN is deposited at low temperature as an amorphous film. The buffer layer is subsequently heated to form a crystalline foundation upon which the rest of the epitaxial layer structure will be built. Even after the crystallization is finished, the GaN film remains highly defected. As GaN is grown on top of this buffer layer, many of the edge and threading dislocations terminate by growing together. Most of this defect reduction occurs within the first 0.5-1.0 μm, but high quality films are only grown by depositing more than 2 μm of GaN. This first 2-4 μm of GaN has been named (at UCSB) the template layer. The top portion of this template layer also serves as the n-type contact layer. Since the sapphire substrate is insulating, all devices made on sapphire are top contacted.

Following the GaN template layer, an InGaN layer is deposited to help prevent cracking of the AlGaN cladding layers. This InGaN layer is believed to help in two ways. First, the InGaN is compressively strained when grown on GaN, while AlGaN is grown with tensile strain [4]. Therefore, a layer of InGaN offers strain compensation for the AlGaN cladding regions. Second, InGaN is softer than the GaN template region and is believed to act as a compliance layer to reduce the propagation and initiation of defects.

Once the InGaN strain relief layer has been deposited, relatively thick $Al_{0.06}Ga_{0.94}N$ cladding layers can be grown, with a maximum thickness of approximately 0.4 μm. For thicknesses greater than 0.4 μm, a high density of cracks is frequently observed. These cracks are due to thermal expansion differences and lattice mismatches between the GaN and AlGaN layers [5]. To grow thicker layers without cracks, strained superlattices (SSL) are used. These layers do not crack as easily because the thin AlGaN layers that make up the SSL require a larger strain before the material will relax (crack) [5-7]. Thus, the cladding layers can be grown thicker or the aluminum composition in the

cladding can be increased without an increase in the crack density. There is still an upper limit on the cladding layer thickness, but the thickness limit is increase when AlGaN SSL layers are used in place of a thick single layer of AlGaN.

Following the n-type cladding layer, the separate confinement heterostructure (SCH) layer is grown. This layer acts as a light guiding layer as found in double heterojunction laser diodes in many other material systems [8].

The rest of the laser structure is similar to lasers in other III-V material systems. The multi-quantum well (MQW) active region is grown between the n-type and the p-type SCH regions. An AlGaN electron barrier layer is inserted between the active region and the p-type SCH to prevent electron overflow from the QWs. The electron barrier layer is followed by a p-type SCH, a p-type cladding, and a p-type contact layer.

Layer	Material composition	Thickness (nm)		Doping density (10^{18} cm^{-3})	
contact layer	p-GaN	100		50	Mg
p-type cladding	p-$Al_{0.2}Ga_{0.8}N$/p-GaN SL	500		100/50	Mg
light guiding region (graded to GaN)	p-GaN	100		50	Mg
electron barrier	p-$Al_{0.2}Ga_{0.8}N$	20		100	Mg
QW growth cap	i-GaN+Zn	10		0.1	UID
quantum barrier	i-$In_{0.05}Ga_{0.95}N$+Zn	10		0.1	UID
quantum wells	i-$In_{0.12}Ga_{0.88}N$+Zn	4	5x repetition	0.1	UID
quantum barriers	n-$In_{0.05}Ga_{0.95}N$+Zn	10		6.5	Si
waveguide	i-GaN	100		0.1	UID
n-type cladding	n-GaN/n-$Al_{0.2}Ga_{0.8}N$ SL	500		1.1/2.2	Si
compliance/strain compensation layer	n-$In_{0.04}Ga_{0.96}N$	100		2.4	Si
standard template/ contact layer	n-GaN	3000		3.0	Si
part of standard template	i-GaN	600		0.1	UID
low temperature buffer layer	i-GaN	<2		0.1	UID
substrate	c-sapphire			insulating	

Table 1. Typical epitaxial layers for nitride laser diodes with approximate thicknesses, doping levels, and alloy compositions. UID (unintentionally doped) refers to the background n-type carrier concentration for nominally intrinsic material. Note that the carrier density for Mg doped material is approximately two orders of magnitude lower than the doping density due to the large activation energy for Mg.

3.2. Optical modeling

The indexes of refraction for these layers are calculated in Appendix B.

Optical modeling of the mode profile has been used to optimize the overlap of the laser mode with the gain profile and to calculate loss and gain for modes as

layer thicknesses are changed. I have written a program—called ModeSolver—that allows the user to vary the width of layers or pairs of layers in a structure and output these results to a file. The mathematical basis for this program is described in Appendix C.

In this section, I will describe the modeling that I have done for the nitride laser structure. As mentioned above, gain measurements have been done for InGaN quantum well structures, but no consensus has been reached on a value for gain. Similarly for loss, measurements of modal loss have been reported, but no values of loss for individual layers have been reported. This makes it nearly impossible to produce an accurate model, but modeling can be used to help recognize general trends. For example, the modal gain is plotted as a function of the lower cladding layer thickness in Figure 6 to show the improvement in modal gain as the cladding layer thickness is improved. As improved numbers for loss and gain in GaN are reported, the ModeSolver program can be used to produce more accurate and refined predictions. All of the results presented in this section were calculated with ModeSolver using the transfer matrix method.

The gain and index for the regions with multiple layers are calculated as average values. For example, in the MQW region the gain is calculated as an average of the gain for the QWs and the loss for the barriers. The average material gain for the quantum wells is given in Equation 1.

$$\text{gain} = \frac{(2600\ \text{cm}^{-1}) * 4\ \text{nm} + (-50\ \text{cm}^{-1}) * 10\ \text{nm}}{14\ \text{nm}} = 707\ \text{cm}^{-1} \quad (1)$$

The values used for the optical modeling are listed in Table 2.

Layer	Thickness	Material	Index	Gain (cm^{-1})
p-contact	0.5 μm	Au	1.626	$-5.83*10^5$
p-contact	0.02 μm	Ni	1.615	$-7.42*10^5$
contact layer	0.1 μm	GaN	2.5067	-50
p-cladding region SSL	0.50 μm	$Al_{.2}Ga_{.8}N$/GaN	2.4599	-50
light guiding region	0.1 μm	GaN	2.5067	-50
electron barrier layer	0.020 μm	$Al_{.2}Ga_{.8}N$	2.4131	-50
MQW stack (4 nm well/10 nm barrier)	0.070 μm	$In_{.12}Ga_{.88}N$/ $In_{.05}Ga_{.95}N$	2.5729	707
light guiding region	0.10 μm	GaN	2.5067	-45
n-cladding region SSL	0.50 μm	$Al_{.2}Ga_{.8}N$/GaN	2.4599	-45
compliance/strain compensation layer	0.1 μm	$In_{.04}Ga_{.96}N$	2.5444	-45
template (average number of defects)	2.1 μm	GaN	2.5067	-50
template (many defects)	1.0 μm	GaN	2.5067	-1000
template (many, many defects)	0.5 μm	GaN	2.5067	-5000
substrate		c-sapphire	1.766	0

Table 2. Gain and loss values are estimates based on typical laser structures lasing at 420 nm. Material thicknesses are given for Designs B and C.

Values for loss and gain in the group-III nitrides are chosen to give a modal loss of approximately 50 cm^{-1} to fit in the range of values reported (43 cm^{-1} and 200 cm^{-1}) by Nakamura and Xerox PARC for their laser diodes [9, 10].

3.2.1. Cladding layer thickness

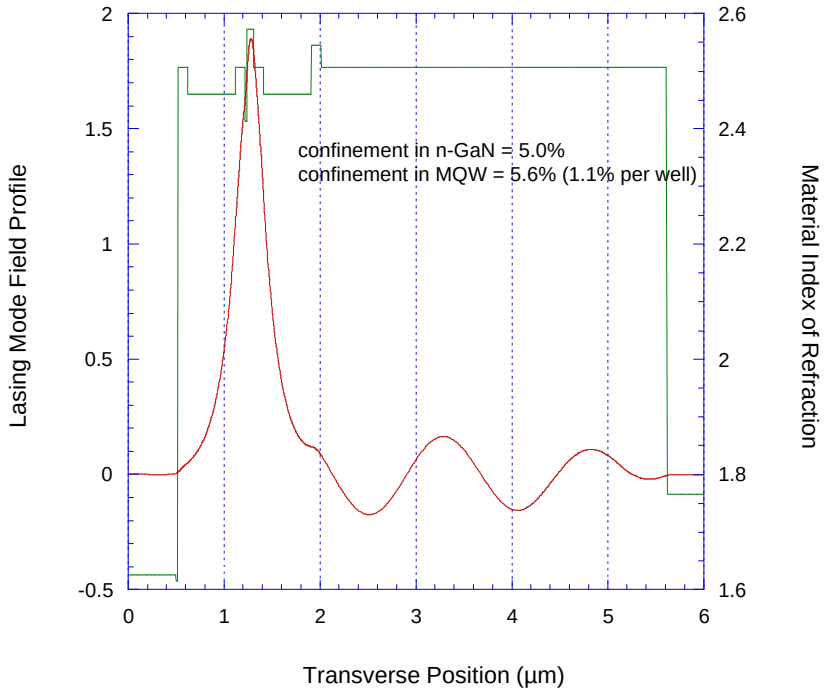

Figure 4. Mode profile for lasers made with Designs B and C. A 10 nm SCH region on either side of the active region serves as the light confining layer. The cladding on each side is 0.5 µm. Significant power leaks into the lower n-GaN template region.

ModeSolver calculates the mode profile for the laser structure. For the device described in Table 2, the dominant laser mode is shown in Figure 4. This laser mode shows a reasonable confinement factor for the active region (1.1% per well). Unfortunately, the modal gain for this mode is significantly reduced because a large percentage of the optical power from the lasing mode is confined within the GaN template region (5%). The top part of this region is comparable in defect density to that of the QW and cladding regions. However, the GaN region adjacent to the sapphire has a significantly higher defect density and therefore has a significantly higher loss. These defects affect modal loss primarily as scattering sites: They increase the modal loss by coupling light to other modes or by reflecting it out of the cavity.

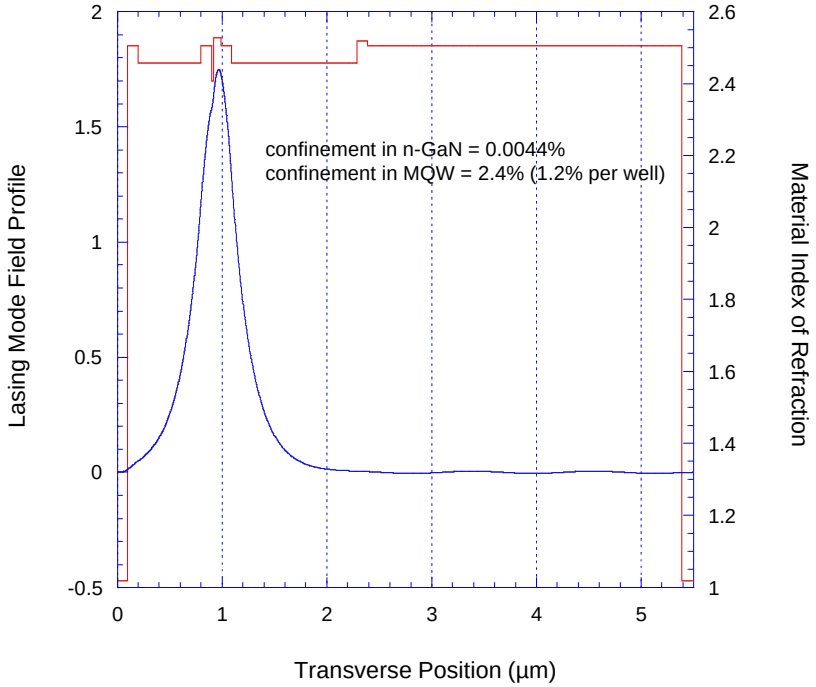

Figure 5. Mode profile for Nakamura laser [11]. Nakamura uses a much thicker cladding region, but with slightly lower aluminum composition (7% average aluminum composition) in the SSL. In this way, Nakamura is able to reduce the power in the GaN template region to almost zero.

An improved structure has been demonstrated by Nakamura, who increased the n-type cladding thickness from 0.5 μm to 1.2 μm by reducing the aluminum composition slightly [11]. The improvement from such a change is shown in Figures 5 and 6. In this case, the confinement in the quantum wells (1.2% per well) is slightly improved over the structure with a thinner cladding region (1.1% per well). More importantly, the amount of power in the GaN template region is reduced to a negligible level (0.004%). In this case, the defect scattering is reduced significantly.

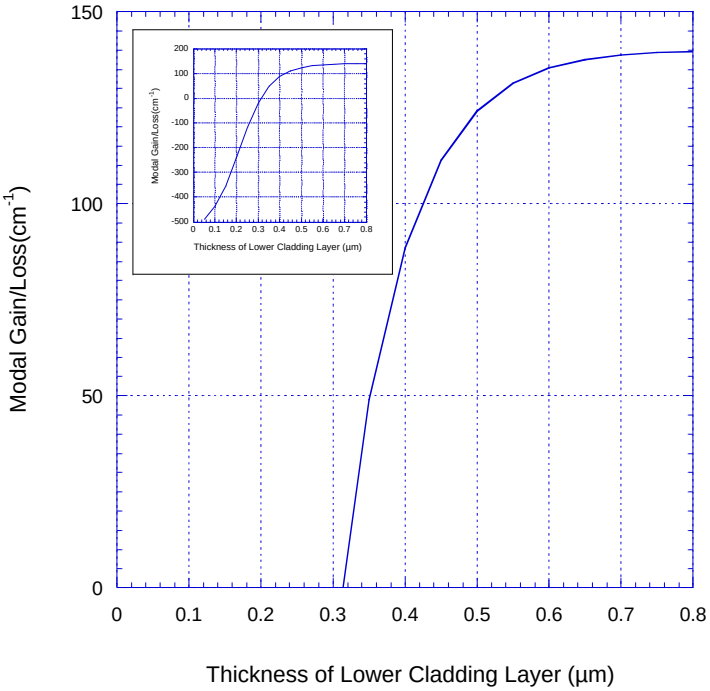

Figure 6. Modal gain as a function of lower cladding region thickness. Upper (p-type) cladding thickness was fixed at 0.5 μm.

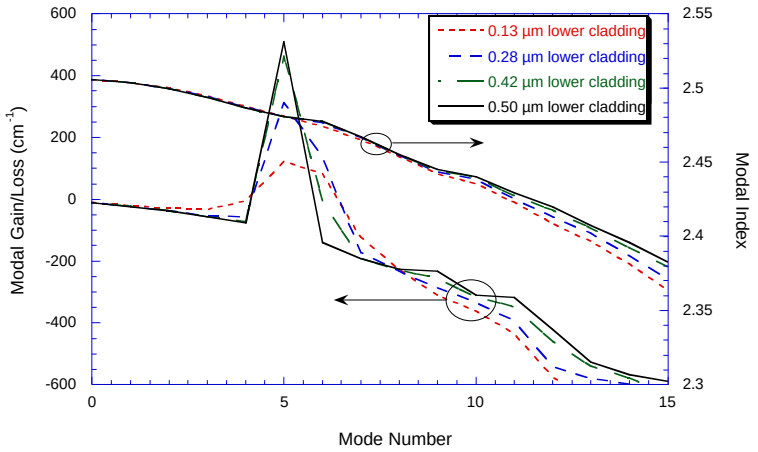

Figure 7. Mode competition in laser diodes is shown with the lower cladding thickness used as a parameter. In each case, the upper cladding thickness is 0.5 µm. By increasing the cladding region thickness, confinement is increased and loss due to free carrier absorption and defect scattering is reduced. This effect is most pronounced as the cladding is increased to 0.4 µm. Beyond this point, the device is still improved by increasing the cladding thickness, but the effect is not as dramatic.

Another important factor in the design of lasers is the side mode suppression between adjacent modes. In early versions of laser design A, we used a thin cladding layer. The small cladding thickness resulted in modes 5 and 6 having similar modal gain. This increases the lasing threshold because any carriers that are stimulated to recombine by non-lasing modes are not contributing to the lasing action, but are nonetheless part of the threshold current. If more than one mode has significant overlap with the gain region, then this mode is pumped with carriers that would otherwise contribute to gain of the lasing mode. Figure 7 compares the gain or loss for the lasing mode as the thickness of the lower cladding region is changed. As can be seen from this model, increasing the cladding layer thickness has a profound effect for thicknesses less than 0.4 µm. Smaller improvements are noticed for thicker layers.

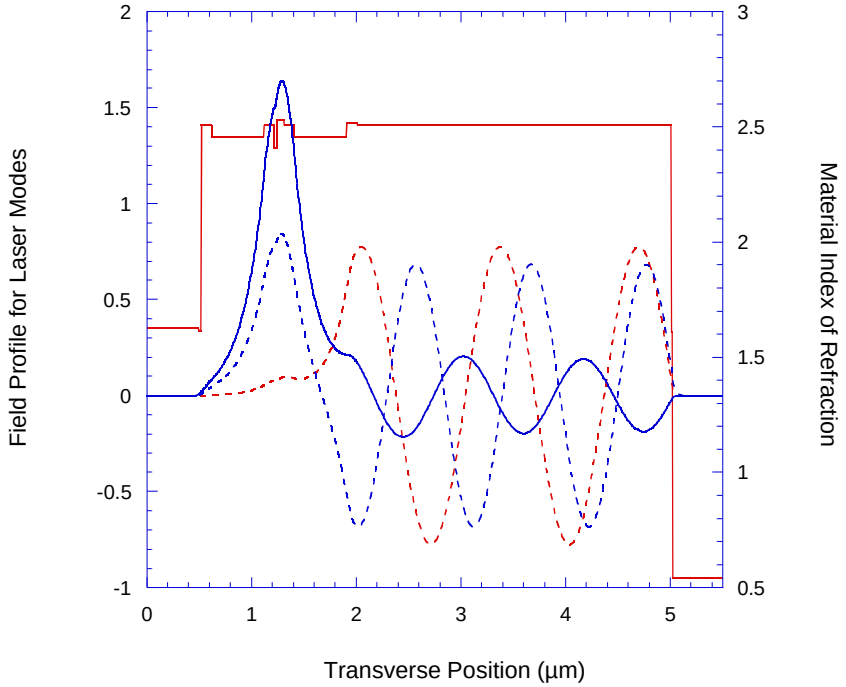

Figure 8. Laser mode competition for 0.5 μm upper and lower cladding regions of UCSB laser structure.

Changing the upper cladding region also has an effect, but the metal in the contacts, while it is high loss, also acts as a reflector. For this reason, increasing the upper cladding region is less important. In addition, making the upper cladding thicker means that more heat will be generated due to the poor electrical conductivity of p-type AlGaN. This means that making the upper cladding region thicker will probably not reduce the lasing threshold.

3.2.2. Experimental verification for optical model

Nearfield scanning optical microscopy (NSOM) has been performed on a laser at UCSB with a polished facet [12]. The optical profile from this device did not match that of the model shown by the modeling. This discrepancy is believed to be due to scattering from defects or to interference from other modes. The

calculated far field pattern for our laser at UCSB is given in Figure 5. This field pattern is strongly influenced by the amount of loss in the structure since the loss values affect the symmetry of the mode.

Measured results for similar lasers at Xerox PARC show a good match to the theory developed here. The measured profile from the Xerox laser showed the predicted number of oscillations in the far field pattern, indicating that it was lasing in the predicted (7^{th} order) mode [10].

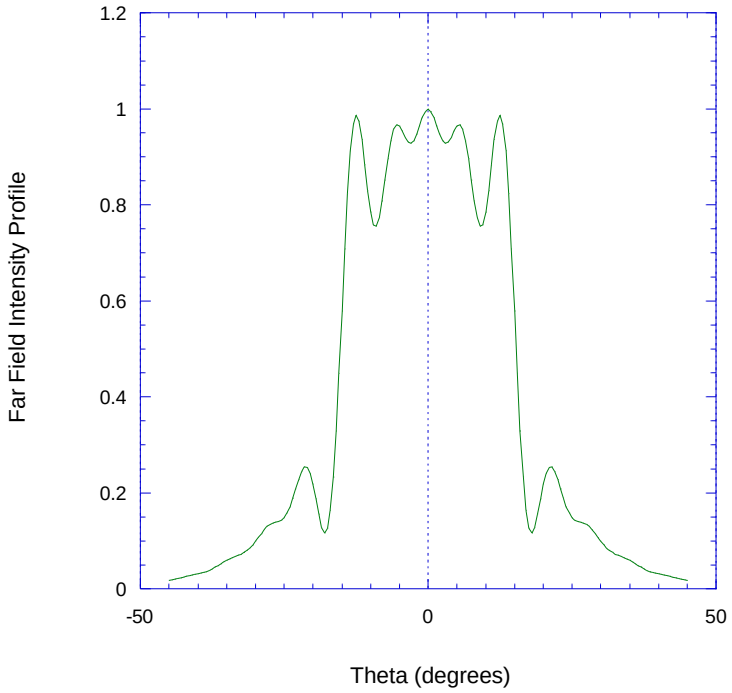

Figure 9. Transverse far field pattern predicted by optical modeling for UCSB laser. Loss and gain have a strong influence on the shape of the far field pattern.

3.2.3. Separate confinement heterostructure (SCH) layer thickness

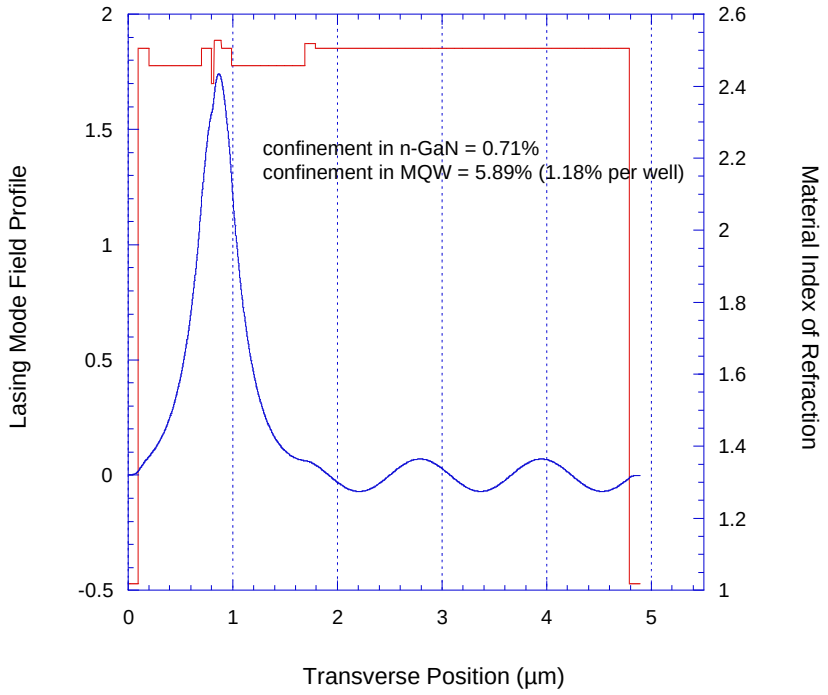

Figure 10. Cladding regions 0.5 µm and 0.7 µm and SCH = 100 nm on either side of active region.

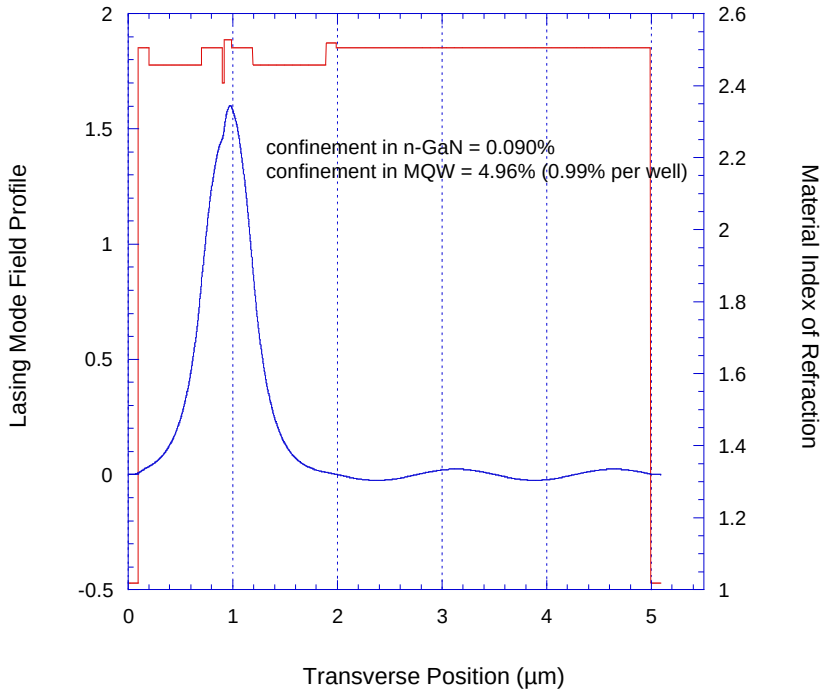

Figure 11. Cladding regions 0.5 μm and 0.7 μm and SCH = 200 nm on either side of active region.

By increasing the cladding region thickness, as shown in Nakamura's laser above (see Figure 5), the laser can be described as operating in the fundamental mode (zeroth order mode) since almost no power is observed in the GaN template region [11, 13]. If a thinner cladding is desired, however, the lower cladding can be extended to 0.7 μm and approximate fundamental mode operation can be obtained by extending the width of the SCH region slightly. This comes at the expense, however, of a reduction in confinement factor for the wells due to a broadening of the laser mode in the wider SCH waveguide. Therefore, if low threshold operation is desired, a 0.1 μm SCH region and a thick cladding is the best choice (Figure 10). However, if fundamental mode operation is necessary and thick cladding layers cannot be grown, then increasing the SCH waveguide region to 0.2 μm would be helpful (Figure 11).

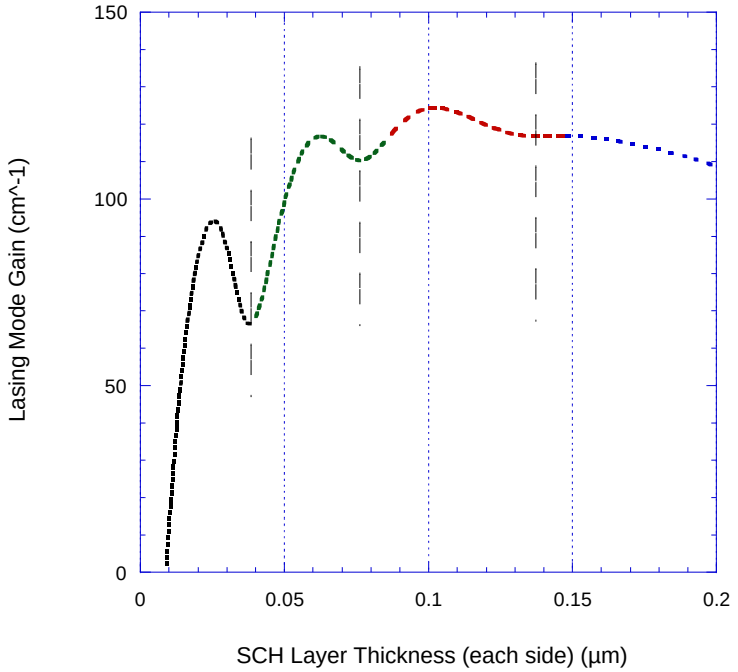

Figure 12. The modal gain for the lasing mode as the SCH region thickness is varied. The upper and lower cladding thicknesses are both 0.5 µm. Four distinct regions are shown. Each represents a different lasing mode for the superstructure.

As seen in Figure 12, varying the SCH region thickness has only a slight effect on lasing threshold after the waveguide is thick enough to confine the mode well. The major effect after this thickness is reached is the oscillation in modal gain due to coupling of the lasing mode into the template region.

As can be seen in this figure, the SCH region and the GaN template region act as a pair of coupled QWs. When the modal index of the top guide is matched to the modal index of the lower guide, maximum coupling occurs between the two guides. Since the coupling of power into the template region increases the loss seen by the mode, the lasing threshold is increased when the modal indexes of the two waveguides are not matched. Optimal laser design will keep the modal index of the two waveguides as far separated as possible to reduce the waveguide coupling.

3.3. Electrical modeling

After the epitaxial layer structure are designed and optimized using the optical model, the device geometry can be refined by modeling the current flow in the device. This section presents a model of the current flow in the device as modeled by the program ATLAS (produced by Silvaco, Inc.). Electrical modeling of the laser devices has demonstrated that the current spreading in the p-type material is small, but current spreading in the active region cannot be neglected for the gain guided device geometry. Issues such as non-uniform pumping of the wells and the high lateral resistance for the gain-guided structure will also be discussed.

3.3.1. Limitations of the model

As in the optical modeling, the ATLAS electrical model lacks several parameters that are needed for accurate modeling. These parameters include doping levels, mobilities, carrier effective masses, strain, piezo-electric constants, and band offsets. Additional inaccuracies result from the non-reproducibility and non-uniformity of layer structures. This makes it difficult to actually test new designs against experiment and makes it difficult to design experiments to measure accurate parameter values. Doping levels and mobilities, for example, are easily measured for isolated structures, but the variation from wafer to wafer is large. In addition, the fabrication of more complicated structures (such as strained superlattice claddings) introduces large strain fields and increases piezo-electric effects that change the electrical band structure, and thus change the current flow.

In addition to the inaccuracies due to the material parameters, the ATLAS models presented in this section suffer from the limitations of the program itself. ATLAS is a very simple program that is not designed to handle MQW lasers, which have very high carrier levels. However, ATLAS gives useful graphical

output that is helpful for examining current spreading in devices. In short, the simple models presented in this section can provide information and can be used to diagnose problems such as current spreading and problems with carrier overflow. These models cannot be used to match experimental IV curves or to precisely understand current flow within the MQW regions. With these caveats, the models produced by ATLAS can provide some insight into how the laser diodes will operate and how they can be improved.

Lastip by Crosslight is much better suited to handle this material system and should be used if more accurate modeling is needed. Lastip has material parameter files that include many of the necessary parameters for the nitride system and it provides a more sophisticated physical model of the laser physics. Lastip simulations will be described later in this chapter.

3.3.2. Gain guided laser diode

Figure 13 shows the current flow in one half of the symmetric laser bar. Almost no current spreading occurs in the p-type material. There is a slight amount of current spreading just above the active region, where the AlGaN barrier encourages lateral hole flow. However, most of the current spreading occurs within the active region itself. This current spreading means that there will be a non-negligible fraction of the carriers that are pumping material outside of the lasing mode. Also, the likelihood of shorting due to defected material is increased by the presence of large amounts of current spreading. This is a significant concern due to the high defect density in the nitrides.

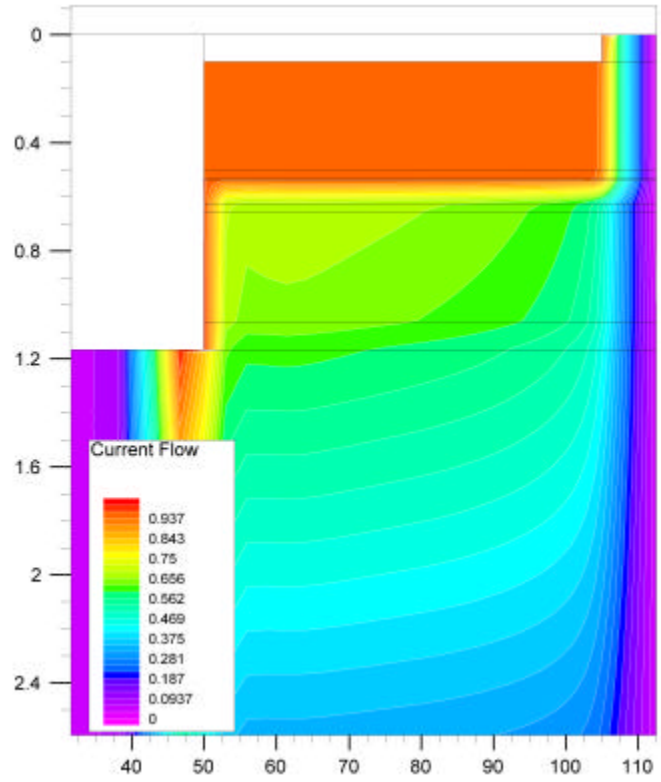

Figure 13. Current flow in gain-guided nitride MQW laser (Design A). Only half of the structure is presented. The other half can be inferred by symmetry. The units of the graph axes are μm. The MQW region is located between 0.536 and 0.626 μm in this diagram.

Another problem with the structures of Design A is electron overflow from the active region into the p-type SCH region. Due to the low p-type carrier mobility and the low p-type carrier concentrations in GaN and AlGaN, electrons are able to drift far into the p-type region before encountering a hole and recombining. This electron overflow increases the threshold current density by preventing holes from reaching quantum wells [14]. Thus, electron overflow effectively creates a substantial amount of hole leakage current for these devices. An electron barrier layer has been included in most recent devices (Designs B and C), but was not included in the early devices that are discussed in Chapter 4. This electron overflow is seen from our models to be significantly reduced by the

inclusion of a 20 nm $Al_{.2}Ga_{.8}N$ electron barrier layer between the MQW active region and the p-type SCH region. This will be discussed in more detail in the next section.

One additional problem with this design is clear from the ATLAS model. This is the problem of large lateral resistance. The n-type GaN template region, through which most of the current flows, is relatively conductive, but the distance that the current has to traverse is 40-50 μm and the template region is relatively thin. This creates a large lateral resistance, which increases the voltage drop for the laser and generates heat. This suggests the need to increase the thickness of the template region in order to reduce the heat generated by the large lateral resistance.

3.3.3. Ridge-waveguide laser diode

Ridge-waveguide lasers (Design B) have been used more frequently recently due to their reduced current spreading and the increased optical confinement. These devices are also theoretically predicted to be less prone to shorting and generate less heat than the gain guided structure described in Figure 13 (Design A). The reduced current spreading is shown in Figure 14, where the edge of the ridge forces a more uniform current injection of the laser diode. These ridges are still relatively wide in comparison to the optical wavelength; so the advantages due to increased optical confinement are relatively small.

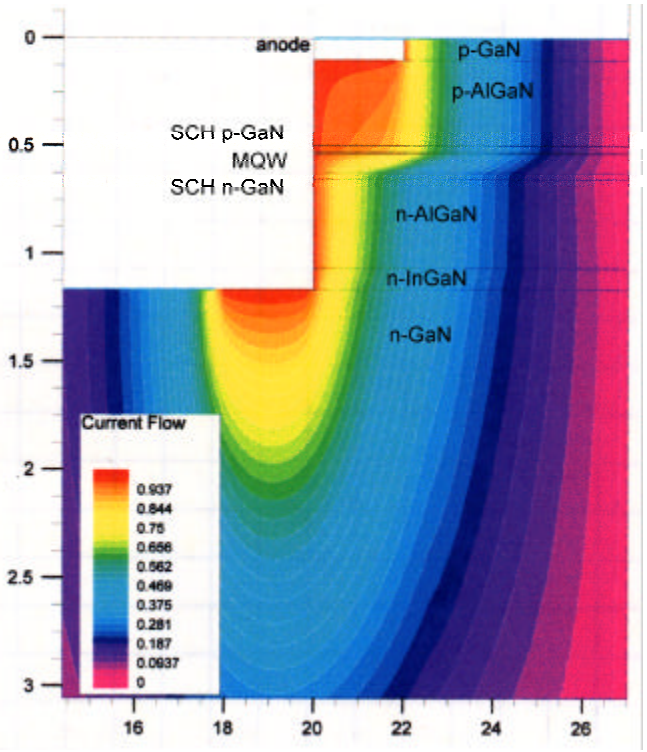

Figure 14. Current flow in ridge waveguide GaN MQW laser (Design B). The ridge is 14 μm wide. The contacts for current injection are 10 μm wide.

3.3.4. Metal-bonded laser diode

For comparison, current flow in the flip chip bonded structure (Design C) is also presented. This geometry will be discussed in more detail in Chapter 5. Design C is expected to have a more uniform current injection than either Design A or B. This is due to the vertical pumping that is allowed by the backside contact for this geometry.

In this structure the current spreading is limited by patterning of the n-type material. Since the n-type material is much more conductive than the p-type material, care must be taken to make sure the ridge etch is made within approximately 0.5 μm of the active region to reduce current spreading in the n-

GaN template layer. This is because the n-type AlGaN is less conductive than the n-type GaN. Therefore, the etch must pass through the n-type GaN to reduce current spreading. Ideally, the etch will stop just below the active region. This etch will be discussed further in Chapters 5 and 6.

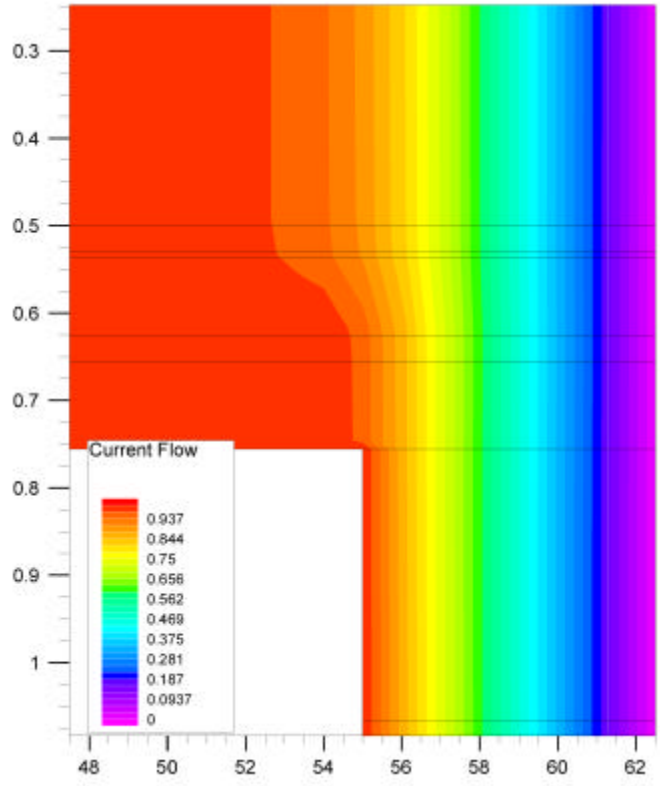

Figure 15. Current flow in a metal bonded GaN MQW laser (Design C). Current spreading is more significant in this structure because the lateral current confinement is done in the n-type material instead of in the p-type material. By keeping the current spreading region limited to the n-AlGaN, current spreading can be kept low. The MQW region is located between 0.536 and 0.626 μm in this diagram. Note that this device is depicted p-side up for easier comparison with Designs A and B (Figures 13 and 14).

3.3.5. Conclusions

This section has discussed two limitations for the gain-guided laser geometry (Design A): 1) current spreading and 2) high lateral resistance. Current spreading can be made reasonably small for each structure presented, but it is worst for the

gain-guided structure in which the current spreads significantly as it crosses the active region. This current spreading causes carrier injection non-uniformity. The ridge-waveguide laser and the metal-bonded laser both show significant reductions in current spreading because etched mesas physically limit the path of current flow for the electrons. The second problem with the gain-guided structure is the large lateral resistance associated with the current flow from the center of the mesa to the edge, where the n-type contact is located. To reduce the lateral resistance for this structure (and to reduce the heat generation associated with that resistance) the n-type doping must be high. Unfortunately, increasing the n-type doping is believed to increase free carrier absorption in the material and thus to increase the optical loss. The most improvement for both of these problems is expected from using the metal bonded structure (Design C), which uniformly injects current from the backside contact of the structure.

3.4. Quantum well and gain modeling

One of the severe limitations of the ATLAS program is that it does not allow the inclusion of quantum wells in a meaningful way. This makes electrical current calculations less accurate. The program Lastip [16] by Crosslight, Inc. performs more accurate calculations for quantum confinement and recombination in the quantum wells.

The gain model used by Lastip numerically calculates the effects of strain, line broadening, and valence band mixing. The results presented in our paper are the first results that describe a fully self-consistent simulation of the GaN laser using a gain model specifically optimized to handle the InGaN wurtzite crystal (hexagonal symmetry) [17]. This gain model is based on the Hamiltonian for wurtzite crystals that is presented by Chuang, et. al [18]. All previous models, such as the self-consistent model presented by Domen, et. al., have approximated

the wurtzite gain curves using models based on zincblende crystal structures [14, 15]. Using the wurtzite crystal bands makes gain and band-edge dispersion calculations more accurate than numerical calculations made with cubic approximations [19]. The self-consistent numerical solution presented in this section accurately considers the effects of carrier drift, diffusion, thermionic emission, index guiding of the optical mode, wavelength dependent gain, current spreading, defect recombination, stimulated recombination, and Auger recombination. Thermal effects are neglected. Six lateral modes are considered in each of the simulations. This is enough modes to smooth the carrier profiles in the lateral direction and to make a relatively accurate approximation of spatial hole burning effects.

Because this model includes a relatively accurate and self-consistent description of both optical and electrical performance, it is useful for analyzing trends regarding the optimum number of quantum wells for this laser system. In addition, the model is used to roughly estimate the effects of current spreading, Shockley-Read-Hall recombination, electron overflow, and non-uniform injection into the quantum wells.

3.4.1. Lastip parameters for nitride laser

The laser modeled as the reference laser design for this section is a 5-QW laser as depicted in Figure 2 (Design B) with the layers described in more detail in Table 1. The material parameters that are specific to the Lastip model are described in Table 3. For simplicity, the lowest 0.6 μm of GaN and the sapphire substrate are not included in the model. This does not affect the result. The other difference between the reference laser and the layer description given in Table 1 is that p-type GaN light guiding region is not graded for the reference case. Instead it is made of a single material composition. One example described below discusses the effects of the graded region and shows that this change has little effect. All

other lasers described in this chapter will be compared to the reference laser design.

Parameter	$In_xGa_{1-x}N$	GaN	$Al_xGa_{1-x}N$
laser stripe width	5 µm		
facet reflectivity calculated using modal index of n=2.49	18%		
cavity length for laser	1000 µm		
calculated effective mirror loss [20]	17 cm^{-1}		
modal loss	42 cm^{-1} [21]		
lattice constant [35, 36]	(0.3189 + 0.0359x) nm	0.3189 nm	(0.3189 - 0.0077x) nm
index of refraction for l=420 nm (see Appendix B)	2.5067+0.91x	2.5067	2.5067-0.43x
dielectric constant value	9.5+5.5x	9.5	9.5-1.0x
Shockley-Read-Hall (SRH) recombination lifetime	0.5 ns for 5 QWs [30] 1.5 ns for 10 QWs [30] 1 ns for bulk [16]	1 ns [16]	0.1 ns [16]
spontaneous emission parameter for passive layers only	$2\ 10^{-10}$ cm^3/s [31, 32]		
Auger recombination coefficient	$2\ 10^{-31}$ cm^6/s [22][2]		
band bending (strained)	3.2 eV [23]	—	0.25 eV [23]
band bending (unstrained)	3.8 eV [23]	—	—
GaN band offset ratio ($\Delta E_c/\Delta E_v$)	3/7 [15]	—	2/1 [24]
energy gap (E_g) at 300 K	1.89 eV (InN)	3.42 eV	6.28 eV (AlN)
electron affinity	use ($\Delta E_c/\Delta E_v$)* ΔE_g	4.07 eV	use ($\Delta E_c/\Delta E_v$)* ΔE_g
Mg activation energy	170 meV [24]	170 meV [24]	170+300x [25]

[2] The value for the Auger recombination coefficient is given because it is the one used for the models presented in this section. This value is believed to be several orders of magnitude too high. However, this is the only published value that is currently available in the literature. Using this high value will increase the lasing thresholds presented here, but should not change the observed trends.

Si activation energy	20 meV [29]		
longitudinal conduction band effective mass (G well)	$(0.20-0.09x)m_0$ [36]	$(0.20)m_0$ [20]	$(0.20+0.13x)m_0$ [20]
transverse conduction band effective mass (G well)	$(0.18-0.09x)m_0$ [36]	$(0.18)m_0$ [20]	$(0.18+0.07x)m_0$ [20]
hole mobility	2 cm^2/V s [28]		
electron mobility	100 cm^2/V s [26]	200 cm^2/V s [26]	30 cm^2/V s [26]
hole saturation velocity	2 10^7 cm/s	2 10^7 cm/s	1 10^7 cm/s
electron saturation velocity	2 10^7 cm/s		
Elastic constants note: 1 Gpa = 10^{10} dyn/cm^2	[34] C_{13}=114-20x C_{33}=381-181x	[34] C_{13}=114 Gpa C_{33}=381 GPa	[20] [34] C_{13}=114+20x C_{33}=381+3x
spin orbit coupling energy (D_{so})	12 meV [35]		
crystal field split energy (D_1)	16 meV [35]		16-74.5x meV [35]
spin-orbit split energy (D_2, D_3)	4 meV [35]		4+2.8x meV [35]
valence band effective mass (Luttinger-like) parameters:	[19]	[19]	[19]
A_1	-7.24-2.04x	-7.24	-7.24+2.61x
A_2	-0.51-0.09x	-0.51	-0.51+0.64x
A_3	6.73+1.95x	6.73	6.73-1.97x
A_4	-3.36-0.98x	-3.36	-3.36+0.99x
A_5	-3.35-0.97x	-3.35	-3.35+1.18x
A_6	-4.72-1.36x	-4.72	-4.72+1.95x
a (hydrostatic deformation potential)	-8.16 eV [27]		
a_c (conduction band part of hydrostatic deformation potential)	-4.08 eV [27]		
valence band shear deformation potentials [27]:			
D_1	0.7 eV		
D_2	2.1 eV		
D_3	1.4 eV		

D_4	-0.7 eV
longitudinal optical phonon energy	90 meV [28]
effective intraband carrier relaxation time	15 fs calculated by model (consistent with [29, 30])
renormalization parameter (bandgap shrinkage coefficient)	$\xi = 4.5\ 10^{-8}$ eV cm for 4 nm InGaN QW [31] $dE_g = -\xi N^{1/3}$ [20]

Table 3. Device parameters used in Lastip model.

The parameters given in Table 3 are used to model the laser band structure and recombination mechanisms inside the MQW active region. As mentioned earlier, many of these parameters have not been well determined or are still in dispute.

One example of the problems with the parameters is the conduction band offsets. For large band offsets, two-dimensional electron gases are created at the heterojunctions. These two dimensional electron gases have significantly higher conductivity than bulk material. The magnitude of this conductivity difference depends on the magnitude of the band offset. So an accurate modeling of the conduction and valence band offsets is important. Several published reports for band offsets for the AlGaN alloys describe a large range of values for the percentage of the band offset that occurs in the conduction band: 40%-80% [32, 33]. The band offsets for InGaN are even less well characterized and also have a large range of values. For InGaN an estimated value of 30% of the energy gap change is believed to occur in the conduction band [33].

The band offset measurements performed on laser material thus far have been performed by XPS. While this method is relatively precise, the resulting values may not accurately reflect the band offsets of actual laser material. Since XPS is a surface technique, only heterojunctions with thin top layers can be measured. Since these thin layers are capable of maintaining a higher strain than actual laser material, the interface potential may be affected through the piezo-electric effect.

This leads to measurements not reflecting the band offsets that are actually occuring in the device. Therefore, more accurate measurements need to be performed on material that is similar to the device structure in question.

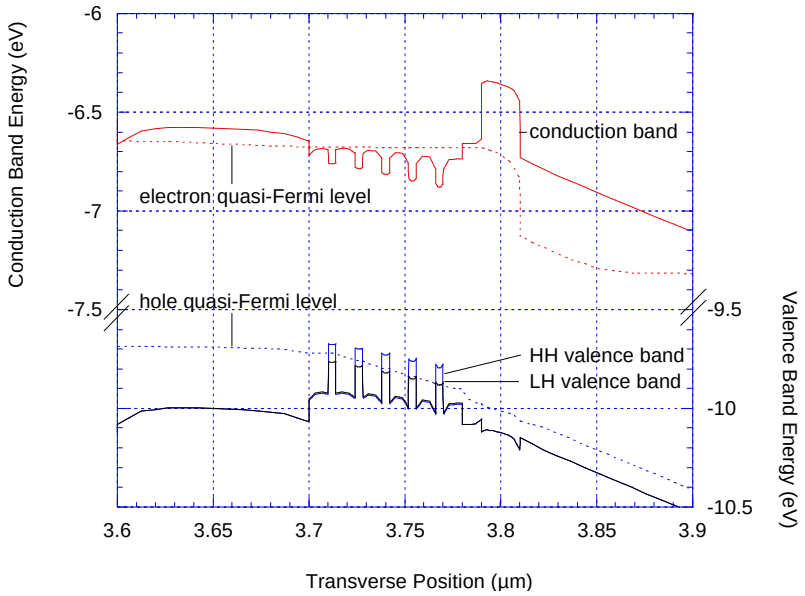

Figure 16. Band diagram at threshold (I=940 mA) for the reference laser. (P-type material will be on the right side of graphs in this subsection.)

The Lastip model calculates the band diagram at equilibrium (no applied voltage) and then increases the voltage and current in steps until lasing threshold is reached. At each step, a 2-dimensional self-consistent calculation of the band diagram, carrier concentration profile, and photon concentration profile is performed. For the reference laser, the lasing threshold occurs at 940 mA. The band diagram at threshold is given in Figure 16. In this diagram, the electron quasi-Fermi level is well above conduction band in the MQW region and well below the conduction band in other regions. This implies that electrons are well confined to the MQW region, as desired. Similarly, holes are well confined within the quantum wells.

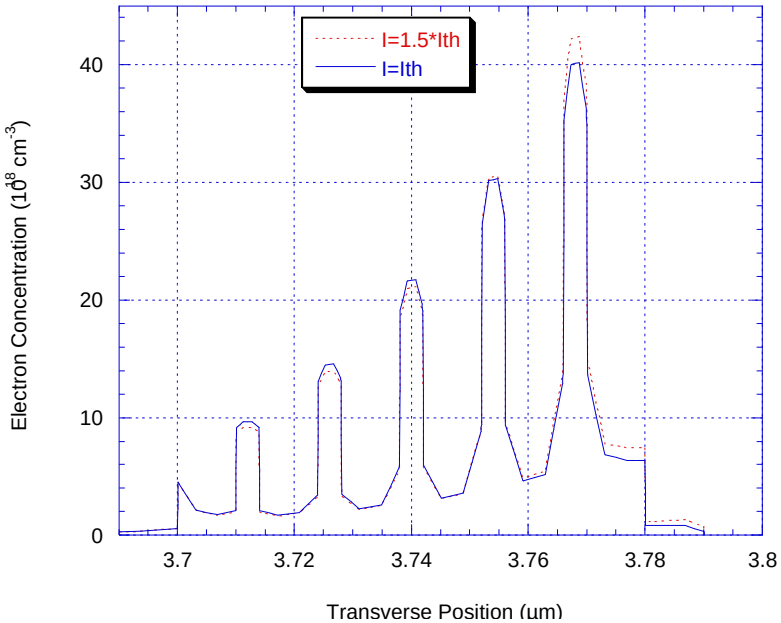

Figure 17. Transverse carrier density for GaN MQW laser diode for two bias points: (a) just above threshold (solid) and (b) far above threshold (dashed). For both cases, there are 10-20% more holes in the QWs than electrons.

Using the band diagram for the laser, the carrier density in the active region can be calculated. A plot of the carrier density is made along the central axis of the laser in the transverse direction (Figure 17). This indicates that there is significant inhomogeneity in the quantum well carrier concentrations and this inhomogeneity becomes increasingly more significant as the current level is increased. This has also been seen in other material systems and is explained in more detail by Piprek, et al. [34]. K. Domen has predicted this effect in nitride lasers [15]. This change with increasing current occurs because for higher current levels there is an increased voltage drop across the MQW region. Since the quasi-Fermi levels vary with voltage, the carrier density will drop across the quantum well. Thus, for increased current levels, the carrier density becomes increasingly non-uniform.

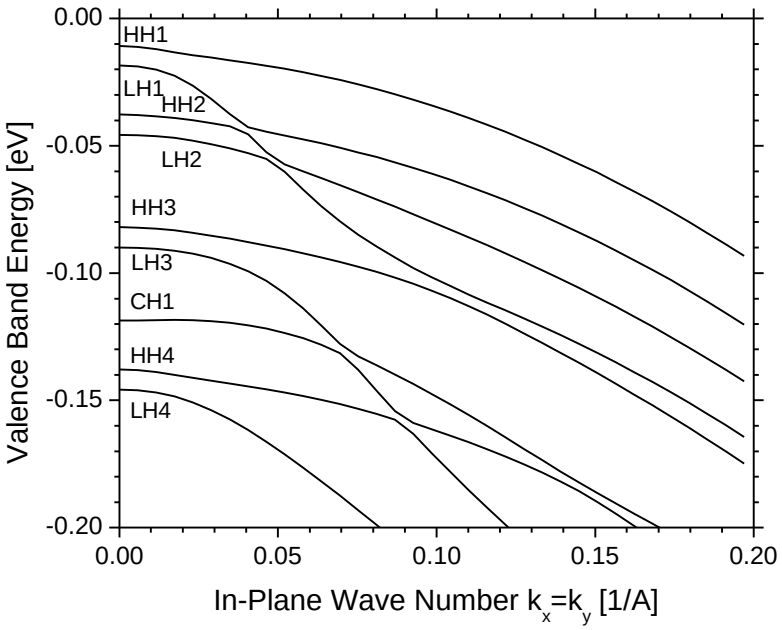

Figure 18. Dispersion of valence subbands in the plane of the quantum well.

Once the carrier density has been calculated, the gain can be determined using the MQW conduction and valence band dispersion diagrams. The conduction band and the out-of-plane (perpendicular or z-directed) valence band dispersion are described using the effective mass parameters. The interaction for the in-plane valence bands is calculated self-consistently. The in-plane dispersion curves for the valence bands are shown in Figure 18. The relatively small separation of less than 10 meV between the LH_1 and HH_1 valence bands means that both of these bands contribute significantly to gain at threshold and both must be considered when calculating carrier density and gain.

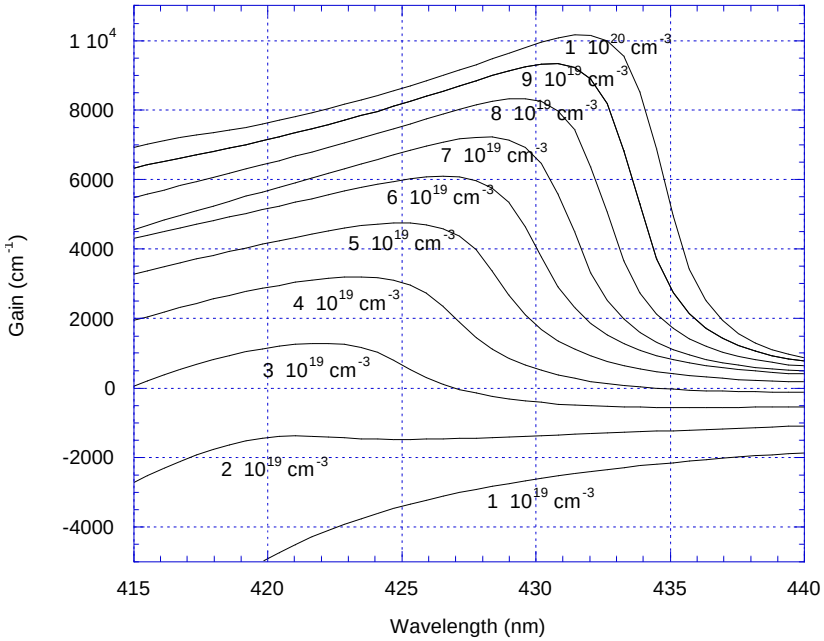

Figure 19. The gain spectrum for reference laser structure. As the carrier density is increased, the gain peak shifts to longer wavelengths due to carrier-to-carrier interaction, which causes bandgap shrinkage (also called bandgap renormalization).

Using the calculated band dispersion curves from Figure 18 and the electron and hole effective masses from Table 3, the gain spectrum can be calculated. In addition to this, the intraband scattering time is computed and contributes to the band shrinkage as the carrier density increases. Figure 19 shows that as the carrier density increases, the bandgap shrinks slightly. This is explained by the scattering model. When this model is removed, the increase in wavelength with carrier density is not seen [17, 35].

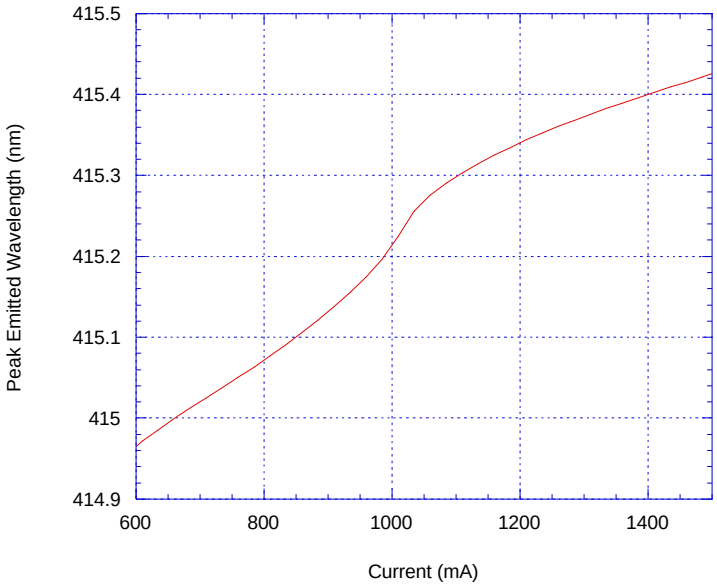

Figure 20. Peak emitted wavelength for the 5 QW reference laser as a function of current. Threshold for this laser occurs at 940 mA.

The gain spectrum presented in Figure 19 assumes that the number of electrons and holes in the quantum wells is equal. This is not true in the nitride system. In the nitrides, the hole concentration in the MQW region is calculated to be 10-25% higher than the electron concentration. Due to this difference in carrier concentrations, the wavelength shifts to longer wavelengths as shown in Figure 20.

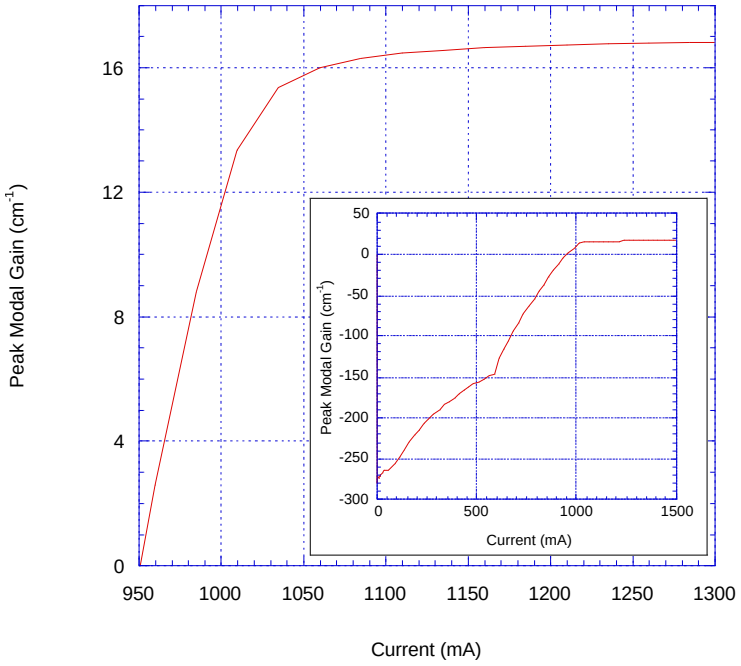

Figure 21. Peak gain as a function of current. The kink in the plot (at 600 mA) is due to two different modes being dominant for different current levels.

Once the dispersion curves for the valence and conduction bands are known, the calculated carrier density for the MQW can be used to calculate the modal gain for each of the six lateral modes considered in this model. The peak modal gain is shown in Figure 21. This plot includes the 42 cm^{-1} background modal loss attributed to scattering in the passive waveguide regions (see Table 3). The peak modal gain is calculated to be 17 cm^{-1} for a laser with facet reflectivity of 0.18 and a length of 1 mm. (This is the point at which modal gain equals mirror loss [20].)

The kink in the inset plot at approximately 600 mA occurs when a different laser mode becomes dominant. As expected, the gain is clamped above threshold and does not show a significant increase even when the current is increased 50% above threshold.

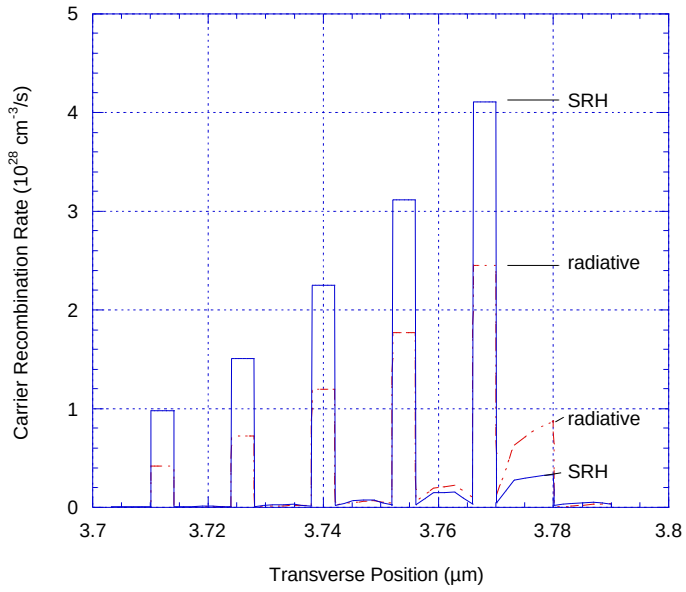

Figure 22. The current lost to Shockley-Read-Hall defect recombination and to spontaneous recombination contribute significantly to the threshold current. These curves are for threshold carrier densities.[3]

Within the laser, the carrier concentrations can also be used to analyze how much of the threshold current is due to certain mechanisms. As shown in Figure 22, the amount of threshold current that is due to defect recombination (Shockley-Read-Hall recombination) is significant. The dimension of the MQW region is approximately (5 * 4 nm) * (5 μm) * (1 mm) = 10^{-10} cm^3, which means that an average MQW recombination rate of $2.4x10^{28}$ cm^{-3} for SRH recombination in the MQW corresponds to a current of approximately 400 mA. Reducing defect recombination in the MQW region would significantly reduce the lasing threshold for nitride lasers.

[3] Auger recombination is expected to be negligible in this laser due to the large bandgap in the nitride material system, but it is incorrectly calculated in this model. Auger recombination has been omitted from this graph.

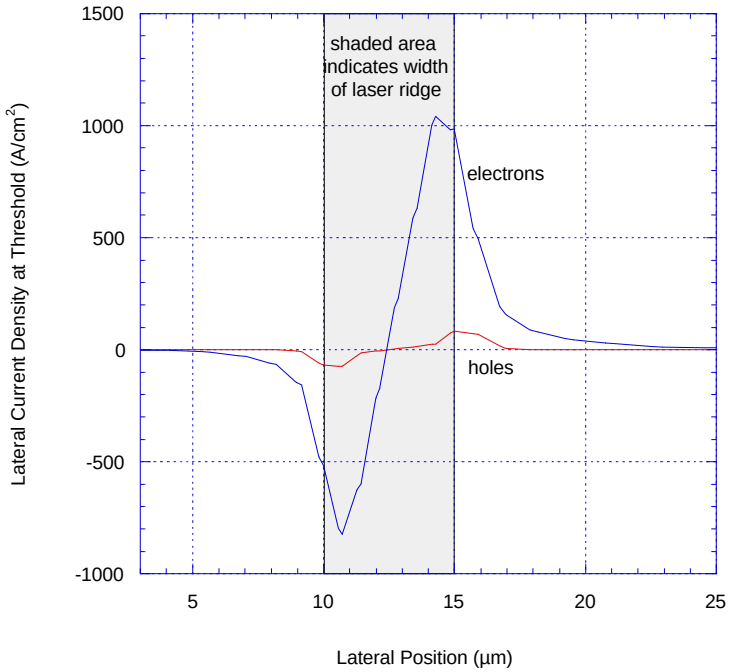

Figure 23. Lateral current density along the lateral direction along the top quantum well. There is a significant shift in electrons to the left side of the ridge and holes to the right side of the ridge.

Another effect that should be minimized in the nitride laser diodes is the lateral current in the MQW region. This lateral current allows carriers to escape the waveguiding region and thus to pump regions outside of the optical waveguiding region. The energy in the carriers that do escape outside the lateral waveguide region is effectively wasted and can be considered as leakage current in laser calculations. Figures 23 and 24 show that the lateral current is similar to that in other material systems. It is important to reduce this lateral current as much as possible.

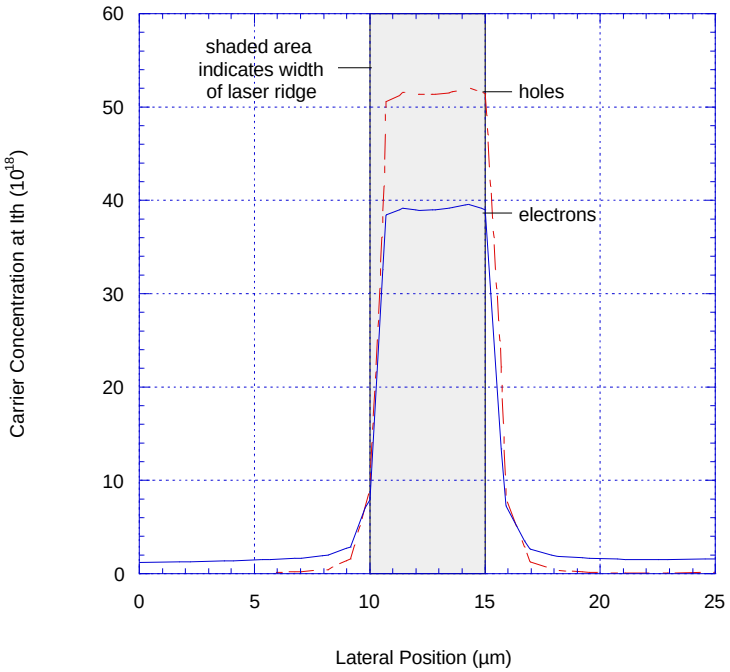

Figure 24. Lateral carrier profile at threshold along the top QW. Both the electrons and holes are shifted noticeably to the right side of the ridge. The n-type contact pad is on the right side of the laser ridge, which explains this asymmetry.

Moving the n-type contact to the lower side of 3 µm n-GaN template region and locating it directly underneath the p-type contact can be done to analyze the effect of current spreading. An improved estimate is achieved by removing all semiconductor material that is not directly between the two contacts. This effectively produces a 1-dimensional simulation. The resulting light output curve is shown in Figure 25. From this graph, it is deduced that removing lateral current flow reduces the threshold current by 54%!

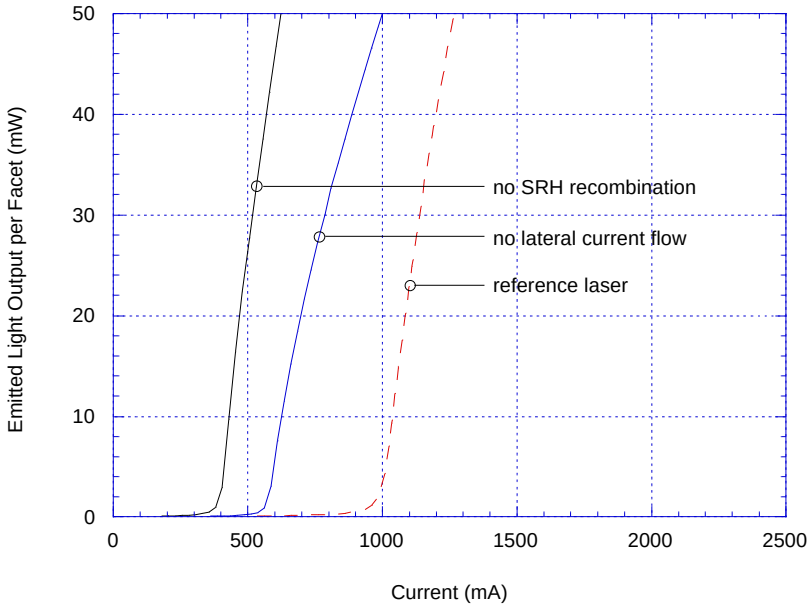

Figure 25. Lasing threshold can be substantially reduced if either defect recombination or lateral current flow is removed from the model. This indicates that these two effects are important to laser design and laser geometries should be designed to reduce these effects.

Similarly, other effects can be analyzed by turning on or off various aspects of the design. For example, if the Shockley-Read-Hall carrier recombination times are increased to 1 μs, this effectively eliminates current due to defect recombination in the model. As shown in Figure 25, the threshold current drops by 62% when this is done. This provides a better estimate of how much the threshold current could be reduced if defect recombination were reduced.

3.4.2. AlGaN electron barrier layer

As seen in the last subsection, the Lastip model is very useful for quickly describing trends. In this subsection, the model is used to analyze the effects of the AlGaN electron barrier and to determine the optimum thickness for this layer.

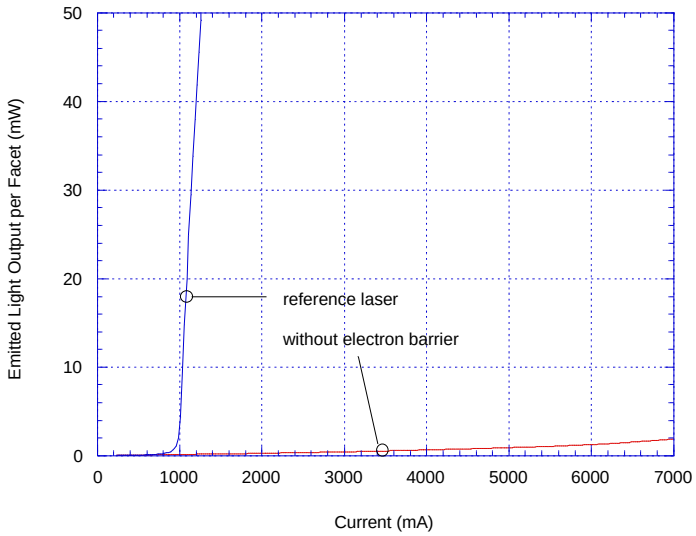

Figure 26. Laser light output for a laser without a p-type AlGaN electron barrier layer is compared to the reference laser. The electron barrier layer dramatically reduces lasing threshold by allowing increased carrier densities to accumulate in the MQW active region.

Figure 26 demonstrates the effect of removing the 10 nm $Al_{0.2}Ga_{0.8}N$ electron barrier layer. By removing the AlGaN barrier layer, the threshold increases from 940 mA to over 7000 mA. The simulation was stopped at 7000 mA. At this point, the peak modal gain is -16 cm^{-1} (i.e. loss). A peak modal gain of +17 cm^{-1} is needed for lasing for this particular laser (see Figure 21).

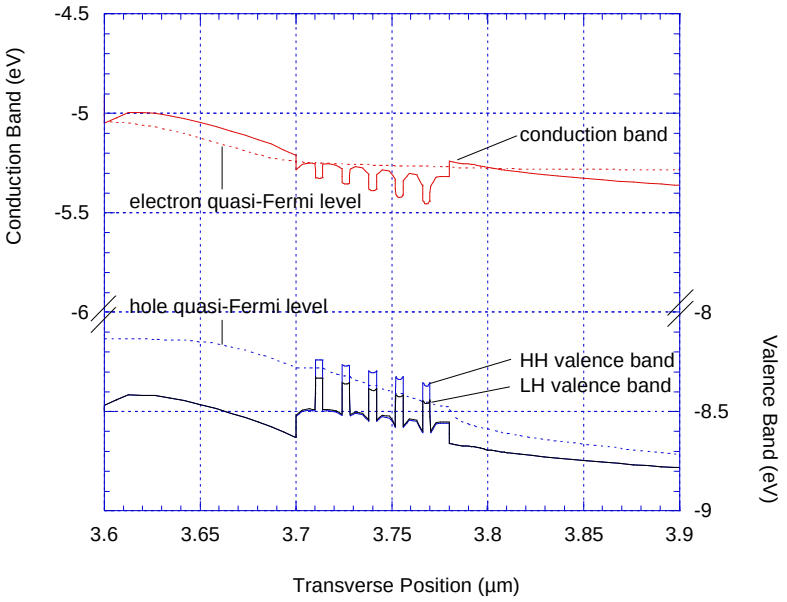

Figure 27. Band diagram below threshold (I=7A) for laser with electron barrier layer removed.

The cause for this drastic increase in threshold can be seen by comparing the band diagrams of the laser diodes with and without the barrier layer (Figures 16 and 27): Without the barrier layer, electrons flow into the p-type region where they recombine without increasing the laser gain. When the barrier layer is present, these electrons are stopped and are confined to the MQW active region.

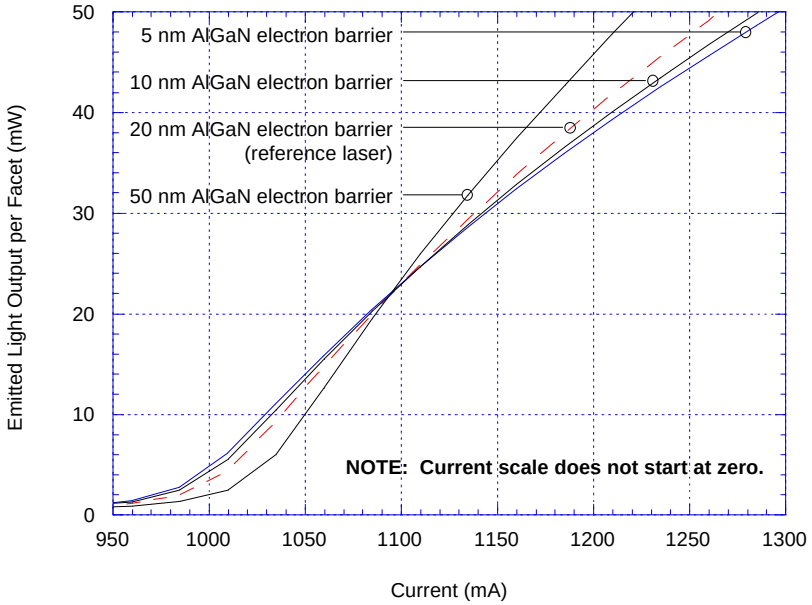

Figure 28. As the electron barrier layer thickness is changed, the laser light output changes very little. Even a small 5-10 nm AlGaN barrier layer will be sufficient to trap electrons in the QW region.

There is an optimum thickness for this barrier layer. Making the layer too thin means that the layer will allow electrons to tunnel through it. Making the electron barrier layer too thick may provide a barrier for hole transport. Making the electron barrier thicker will also reduce the optical confinement of the laser mode, which increases the material gain needed for lasing. In Figure 28, the width of the p-type $Al_{0.2}Ga_{0.8}N$ electron barrier layer is varied from 5 nm to 50 nm. The effect of this variation is minimal, which indicates that this is not a critical parameter. Thicker barrier layers produce a slight increase in threshold current, which is most likely due to the reduced optical confinement. The thicker barrier layers also produce slightly more efficient lasers. To achieve the lowest threshold, a relatively thin barrier of 10 nm is recommended. The Lastip model shows that the threshold current can be reduced further by using even thinner barrier layers (5 nm). However, the Lastip model that we use does not include

tunneling currents, which are expected to be important for barriers with thicknesses of 5 nm or less.

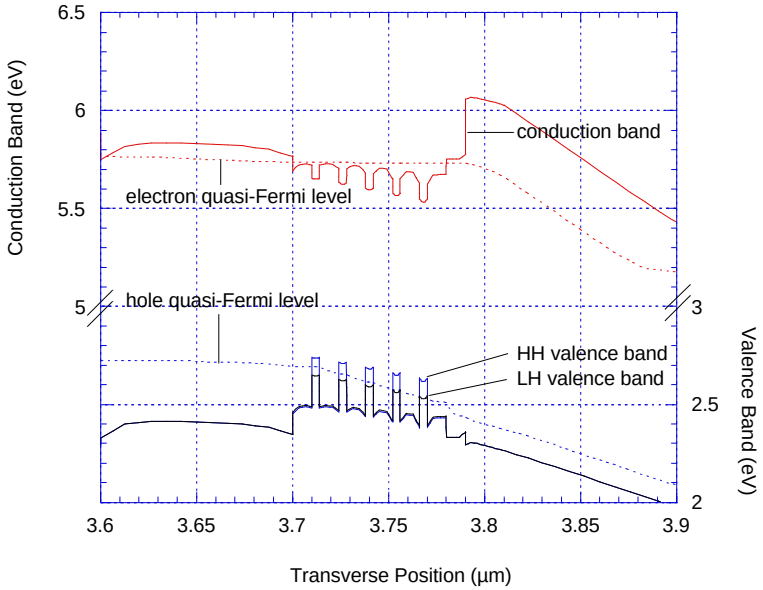

Figure 29. Band diagram at threshold for laser with a graded p-type AlGaN light guiding layer.

As shown in Figure 28, the electron barrier layer thickness can be varied without substantially changing the barrier to hole transport. One method for analyzing the effect of the barrier is to reduce the barrier and compare the results. To reduce the barrier to hole transport, the p-type GaN light-guiding region is replaced with a light guiding region that is linearly graded from p-type $Al_{0.2}Ga_{0.8}N$ to p-type GaN. By grading, the holes are injected more easily into the QW region. (Note that this does not remove the hole barrier completely, but this cannot be done in a realistic way without removing the electron barrier as well.) The effect of this graded layer is shown in Figures 29 and 30. Lasing threshold is actually slightly increased by the addition of the graded layer. This is likely due to reduced light guiding by introducing more AlGaN near the center of the lasing mode, which causes reduced optical confinement. The net effect is that the

grading has very little effect, which means that the hole flow is not being impaired significantly by the $Al_{0.2}Ga_{0.8}N$ barrier.

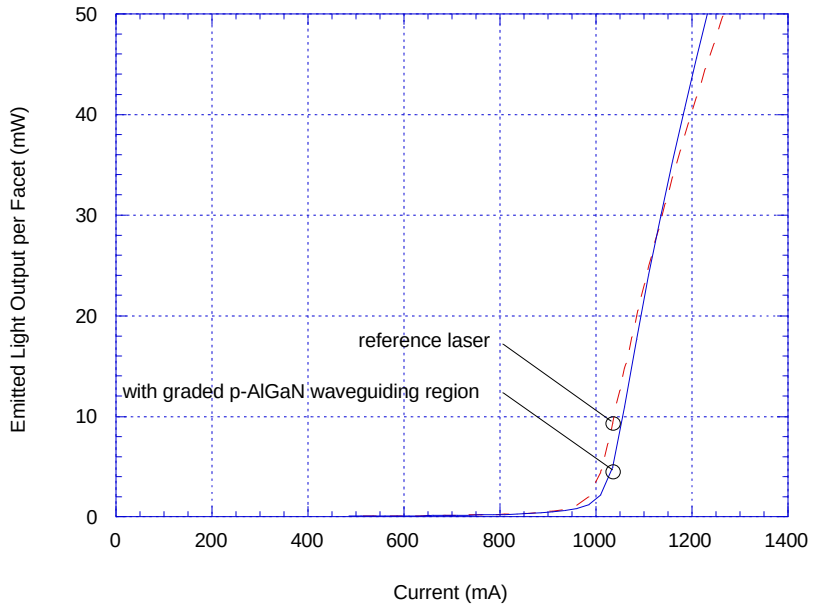

Figure 30. Laser light output for a laser with graded p-type AlGaN→p-type GaN light guiding layer is compared to the reference laser. The grading slightly increases lasing threshold (by 35 mA), but it does improve lasing efficiency. The increase in lasing threshold is believed to be due to reduced optical confinement.

3.4.3. Number of quantum wells

For all semiconductor material systems, there is a tradeoff between increasing the number of quantum wells so that there is more material to provide gain and reducing the number of quantum wells so that not as many wells need to be pumped to transparency or inversion. The optimum number of quantum wells depends on the material quality (modal loss), the cavity length (mirror loss), the waveguide design (confinement factor for high loss and high gain regions), the laser geometry (current confinement), the layer structure (carrier confinement), and many other design factors.

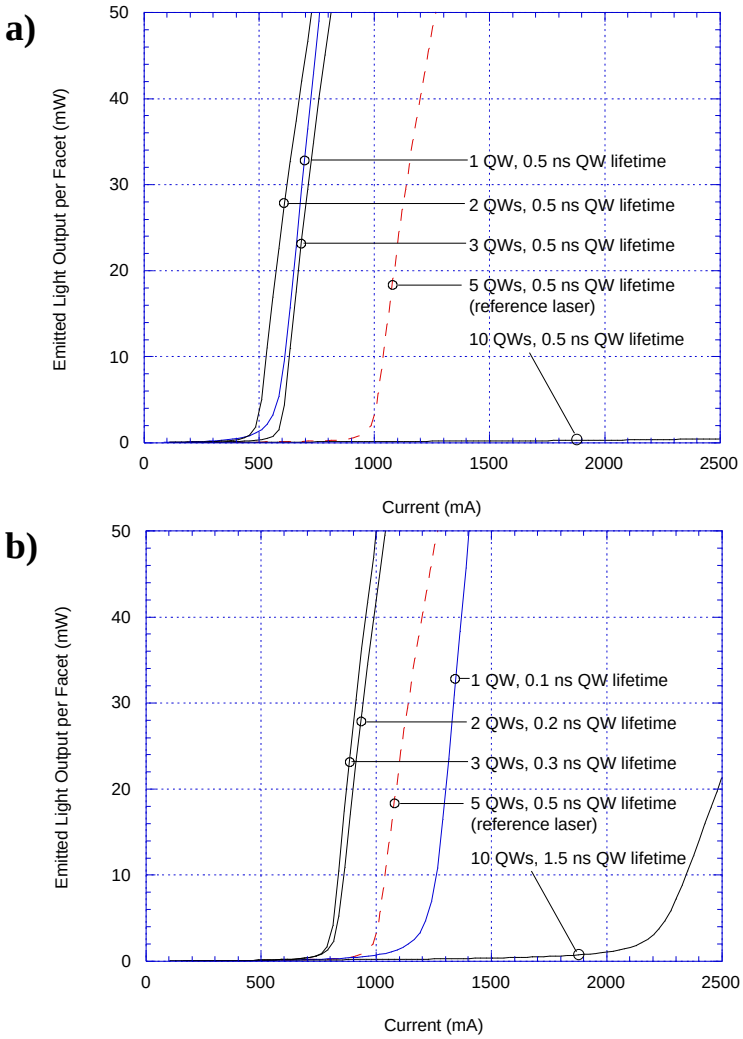

Figure 31. Laser light output is optimized for 2 or 3 quantum wells. The optimum number of QWs for a particular laser design will depend on factors such as facet reflectivity and carrier lifetime. (a) constant carrier lifetime of 0.5 ns for the MQW region (b) material quality dependent carrier lifetime of 0.1, 0.2, 0.3, 0.5, and 1.5 ns for the 1, 2, 3, 5, and 10 QW active regions [36].

For the laser described by the reference design, the optimum number of quantum wells is two or three, depending on the assumptions that are made for carrier lifetime. For fewer quantum wells, the gain begins to saturate before lasing is achieved. For more quantum wells, increased current is needed to pump the additional wells above transparency.

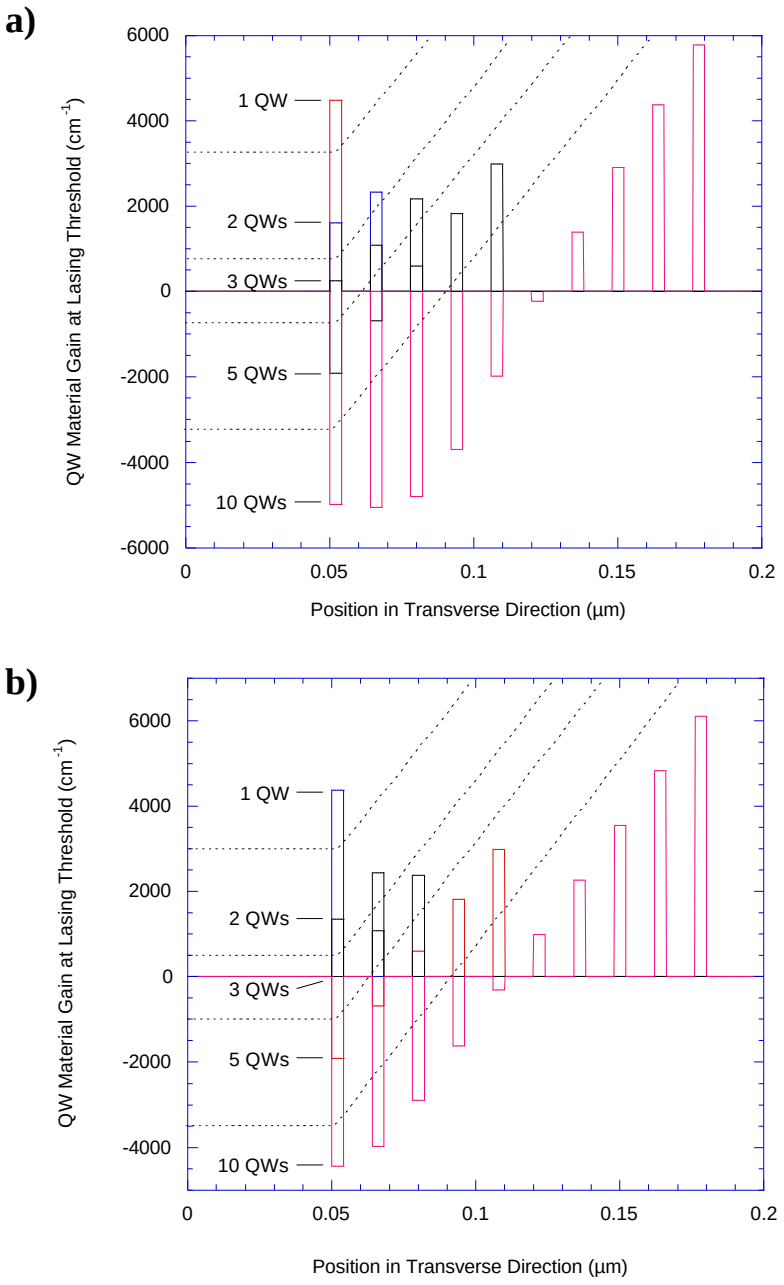

Figure 32. Peak MQW material gain at threshold. (a) constant carrier lifetime of 0.5 ns for MQW region (b) material quality dependent lifetime of 0.1, 0.2, 0.3, 0.5, and 1.5 ns for the 1, 2, 3, 5, and 10 QW active regions [36]. Dotted lines are used to separate the 1, 2, 3, 5, and 10 QW examples.

In addition to needing to pump more wells, laser structures with many quantum wells also suffer from inhomogeneity of the carrier density within the quantum wells. As shown in Figure 32, the asymmetry in the laser with 10 quantum wells is large enough that 5 of the quantum wells provide loss instead of gain at threshold. As the number of quantum wells is increased, the non-uniformity of carrier injection is increased.

3.4.4. Laser Designs A, B, and C

In addition to looking at trends within a design, the Lastip model can be used to compare laser geometries. Light output from laser Designs A, B, and C are compared in Figure 33.

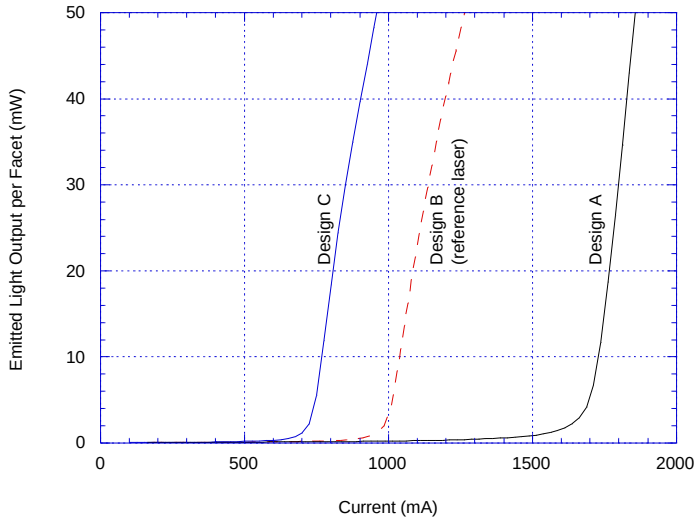

Figure 33. Light output for laser Designs A, B, and C.

Design A was modeled as different from the reference laser by removing the etched regions for the lateral waveguiding structure. The width of the ridge was effectively 25 μm. This is a good approximation of the actual laser geometry for Design A because most of the carrier and photon leakage occurs within the first 25 μm of ridge width. Unlike the real device, the electron barrier was not

removed from the modeled version of Design A. This was done so that the laser geometries could be compared more directly.

Design C is significantly different than Design B. This is because the structure is inverted and the ridge is etched in the n-type material instead of in the p-type material. For the model, it was assumed that the ridge stopped just above the MQW region. Thus, any lateral carrier currents in the MQW region will be included in this design. That makes a reasonable comparison to the Design B laser.

The conclusion from the Lastip model is that Design C is much better than Designs A and B. The lasing threshold for Design C is 650 mA, while Designs A and B have thresholds of 1700 and 940 mA, respectively. The differences between the laser designs are attributed to differences in lateral current flow, lateral optical confinement, and lateral carrier uniformity. Design A has significantly more lateral current than the other two designs. The waveguiding of the lateral modes is also reduced for this design due to the lack of an effective lateral waveguide. This design thus provides less optical confinement for the optical mode. Design B improves lateral leakage and lateral optical confinement, but there is still non-uniform carrier injection into the MQW active region. Figure 24 shows that the carriers are bunched to the right side of the waveguiding region for this laser geometry. This produces an optical beam that is skewed toward the right, due to absorption in the MQW region on the left side of the laser. Design C provides the improvements of Design B in lateral optical confinement, lateral carrier confinement, lateral current confinement, and carrier injection uniformity. In addition, Design C has virtually no lateral leakage current because the current is well confined in the n-type material and is only free to broaden in the highly resistive p-type material. In Design B, the lateral current confinement is in the p-type material, but significant broadening occurs within the n-type material. The other improvement for Design C is the uniformity of

carrier injection. The two contacts lie in a vertical line from each other, which means that there is not a bias pulling the carriers to the side of the ridge. This improves the uniformity of the lateral carrier distribution and reduces the lasing threshold.

The quantum efficiency is roughly the same for Designs B and C (~5% per facet), but is significantly better for Design A (~11% per facet).

Description of laser Geometry	Threshold (mA)	Quantum efficiency per facet (%)
reference laser 5 QWs, 0.5 ns lifetime, Design B	941	4.9
1 QW, 0.1 ns lifetime	1219	8.8
2 QWs, 0.2 ns lifetime	787	6.3
3 QWs, 0.3 ns lifetime	763	6.7
10 QWs, 1.5 ns lifetime	2198	2.3
1 QW, 0.5 ns lifetime	551	7.4
2 QWs, 0.5 ns lifetime	459	6.0
3 QWs, 0.5 ns lifetime	565	6.6
10 QWs, 0.5 ns lifetime	>2500	—
5 QWs Design A	1703	10.9
5 QWs Design C	653	5.0
5 QWs no lateral leakage	437	2.8
5 QWs no SRH recombination	354	6.0
5 QWs no electron barrier	>7000	—
5 QWs with graded p-AlGaN	975	6.2
5 QWs 5 nm p-AlGaN barrier	928	4.4
5 QWs 10 nm p-AlGaN barrier	936	4.6
5 QWs 50 nm p-AlGaN barrier	975	6.4

Table 4. Lasing thresholds and quantum efficiencies for laser designs presented in this section.

The lasing thresholds and quantum efficiencies were calculated by using linear least squares calculations to find the slope and intercept for the light output as a function of current. The threshold current is defined for these calculations as the intercept of the best linear fit with the x-axis (current axis). The quantum efficiency is calculated from the slope of this best linear fit.

3.5. Thermal modeling

The gain-guided geometry is electrically the worst of the three designs, but it is significantly better than the ridge waveguide geometry (Design B) for heat dissipation. For understanding the thermal dissipation advantages of the gain-guided laser, a simple intuitive picture is the most convincing model: In a tall ridge-waveguide laser, the thermal energy flows in the transverse direction until it reaches the bottom of the ridge. At this point, the heat can spread out and flow in both the lateral and vertical directions. However, for a gain-guided structure, the heat is free to spread out rapidly from the top of the structure in both the lateral and transverse directions. Design A was created to have as much area for heat spreading as possible. As mentioned in the last section, however, the large lateral resistance also introduces significant heating if the doping is not very high for the n-type GaN template region. So the structure would have been much better designed if the contact pad had been placed at one edge of the mesa instead of at the center. This also would have led to a reduction in current spreading in the active region.

To better understand the heat dissipation problem, it makes sense to first consider the thermal load of the devices. The best results to date for material from UCSB for threshold current density and voltage are approximately 10 kA/cm^2 and 25 V. This gives a threshold power density of 250 kW/cm^2. To calculate the temperature rise in the active region at threshold, the thermal impedance must be calculated for each structure.

The program ANSYS, which is used to calculate the thermal impedance of our devices, is a robust finite element analysis program that includes automated mesh generation and good statistical error analysis. This program was used to calculate the thermal impedance of the laser structures. Values for thermal conductivity for the laser materials are given in Table 5. The thermal resistances for Designs A, B, and C between the active region and the base of the laser

structure are 24.9, 60.5, and 25.3 degrees K/W. The thermal contour plots for these three cases are given in Figures 34-36.

	Thermal conductivity at room temperature (W/cm K)
sapphire	0.4
GaAs	0.45
GaN	1.3
Si	1.5
SiC	5
CVD diamond	12-18

Table 5. Thermal conductivity for materials used in GaN lasers.

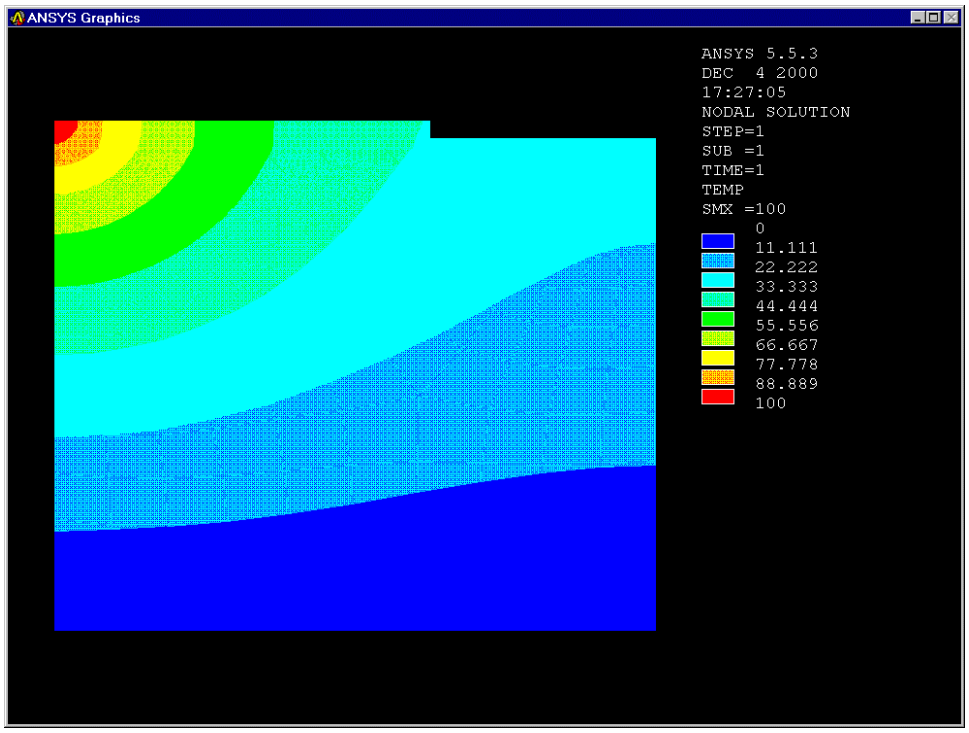

Figure 34. Thermal contour plots for gain-guided laser (Design A).

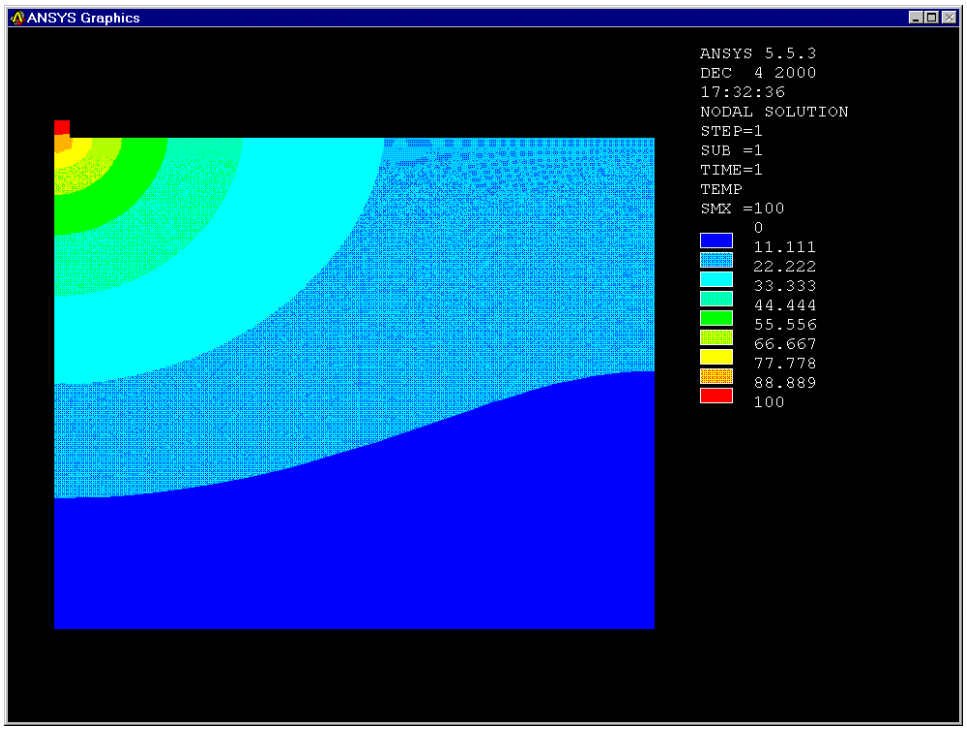

Figure 35. Thermal contour plots for ridge-waveguide laser (Design B).

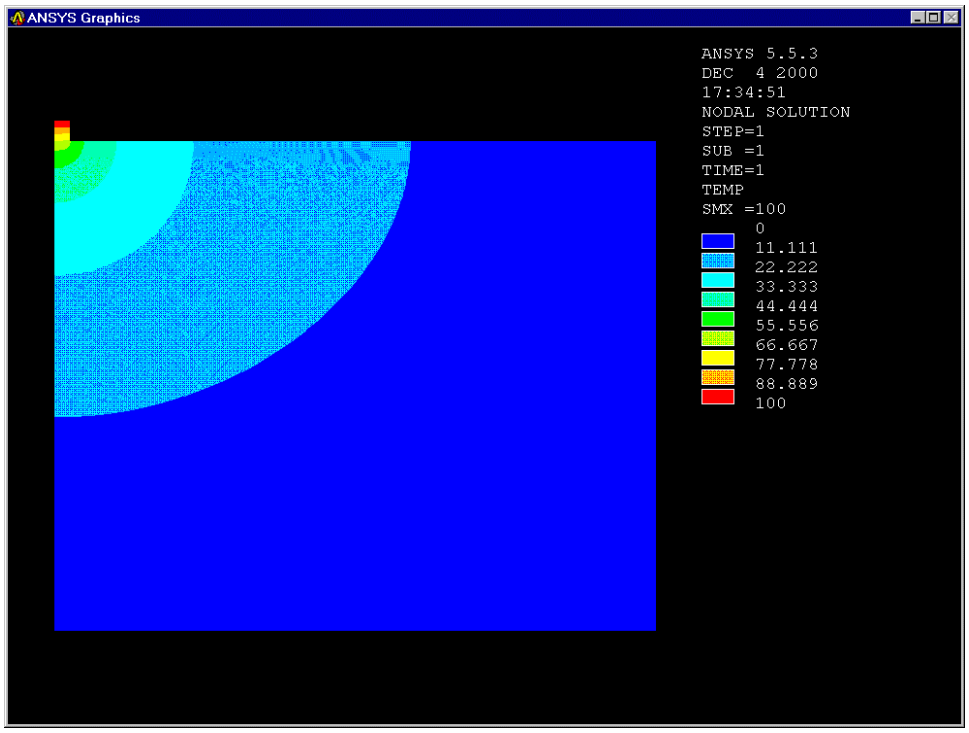

Figure 36. Thermal contour plots for gold-bonded laser when laser is bonded to a silicon substrate (Design C).

As seen by comparing Figures 35 and 34, the two-dimensional heat spreading offered by the gain guided device (Design A) offers a significant reduction in thermal impedance when compared to the comparable ridge-waveguide laser. Design C fabricated on a silicon substrate has better heat dissipation than Design B and comparable heat dissipation to Design A. If cleaved facets in the mounting substrate are not required, then a diamond and/or a copper mount can be used for even better thermal conductivity.

	Active region temperature increase (°C)
Gain guided laser (Design A)	620
Ridge-waveguide laser (Design B)	1500
Metal-bonded laser (Design C)	630

Table 6. Active region temperature for a heat load of (10 kA/cm^2)(25 V)(1 mm)(10 μm)=25 W per device for a laser with a 10 μm stripe width and a 1 mm cavity length.

Heat generation is not all bad in group-III nitride lasers. In fact, Mg activation of carriers is actually helped by heat generation. This effect can result in lower threshold voltages for CW operation over pulsed operation [37, 38]. However, threshold current is increased for higher temperature operation because of increased leakage current, increased non-radiative recombination current, and reduced gain. Therefore, steps should be taken to increase the ability of a structure to dissipate heat. Structures such as the gain-guided laser and the metal-bonded laser are superior in that respect to the ridge-waveguide laser.

3.6. Conclusions

This chapter has described the optical, electrical, and thermal properties of group-III nitride laser diodes. Extensive modeling has been performed to examine issues relevant to the design of both the epitaxial layer structure and the device geometry. Many of the models suffer from lack of accurate parameters. Nevertheless, these models have been used to gain valuable information about trends in nitride laser design.

The gain-guided laser geometry (Design A) was designed to have a wide area available for heat dissipation. However, the advantages of moving to a ridge waveguide or a metal-bonded laser seem to outweigh those of the improved heat dissipation of the gain-guided structure. For current confinement, the ridge-waveguide laser and the metal-bonded laser are expected to have similar

properties. However, the metal-bonded laser is expected to have lower thresholds than the ridge-waveguide laser due to more laterally uniform current injection, better heat dissipation, and higher quality cleaved facets.

3.7. References

[1] R. K. Sink, A. C. Abare, P. Kozodoy, M. P. Mack, S. Keller, L. A. Coldren, S. P. DenBaars, and J. E. Bowers, "Pulsed Operation of Cleaved-Facet InGaN Laser Diodes," presented at Materials Research Society Fall Meeting 1997, Boston, MA, 1997.

[2] M. P. Mack, A. C. Abare, M. Aizcorbe, P. Kozodoy, S. Keller, U. Mishra, L. A. Coldren, and S. P. DenBaars, "Room temperature pulsed operation of blue nitride laser diodes," presented at Second International Conference on Nitride Semiconductors, Tokushima, Japan, 1997.

[3] A. C. Abare, M. P. Mack, M. Hansen, R. K. Sink, P. Kozodoy, S. Keller, J. S. Speck, J. E. Bowers, U. K. Mishra, L. A. Coldren, and S. P. DenBaars, "Cleaved and Etched Facet Nitride Laser Diodes," *IEEE Journal of Selected Topics in Quantum Electronics*, vol. 4, pp. 505-509, 1998.

[4] S. P. DenBaars and S. Keller, "Metalorganic Chemical Vapor Deposition (MOCVD) of Group-III Nitrides," in *Semiconductors and Semimetals*, vol. 50: Academic Press, pp. 11-37, 1998.

[5] S. Nakamura, M. Senoh, S. I. Nagahama, N. Iwasa, T. Yamada, T. Matsushita, H. Kiyoku, Y. Sugimoto, T. Kozaki, H. Umemoto, M. Sano, and K. Chocho, "InGaN/GaN/AlGaN-based laser diodes with modulation-doped strained-layer superlattices grown on an epitaxially laterally overgrown GaN substrate," *Applied Physics Letters*, vol. 72, pp. 211-213, 1998.

[6] T. P. Pearsall, *Strain-Layer Superlattices: Physics* in *Semiconductors and Semimetals* vol. 32. New York, NY: Academic Press, 1990.

[7] P. Y. Yu and M. Cardona, *Fundamentals of Semiconductors: Physics and Material Properties*. Berlin, Germany: Springer-Verlag, 1996.

[8] W. W. Chow, S. W. Koch, and M. Sargent, *Semiconductor-Laser Physics*. Berlin: Springer-Verlag, 1994.

[9] S. Nakamura, "Characteristics of room temperature-CW operated InGaN multi-quantum-well-structure laser diodes," *MRS Internet Journal of Nitride Semiconductor Research*, vol. 2, pp. 5, 1997.

[10] D. Hofstetter, D. P. Bour, R. L. Thornton, and N. M. Johnson, January 31, 1997, personal communication.

[11] S. Nakamura, M. Senoh, S. I. Nagahama, N. Iwasa, T. Yamada, T. Matsushita, H. Kiyoku, Y. Sugimoto, T. Kozaki, H. Umemoto, M. Sano, and K. Chocho, "Violet InGaN/GaN/AlGaN-based laser diodes with an output power of 420 mW," *Japanese Journal of Applied Physics, Part 2 (Letters)*, vol. 37, pp. L627-629, 1998.

[12] D. K. Young, M. P. Mack, A. C. Abare, M. Hansen, L. A. Coldren, S. P. Denbaars, E. L. Hu, and D. D. Awschaloma, "Near-field scanning optical microscopy of indium gallium nitride multiple-quantum-well laser diodes," *Applied Physics Letters*, vol. 74, pp. 2349-2351, 1999.

[13] S. Nakamura, M. Senoh, S. I. Nagahama, N. Iwasa, T. Yamada, T. Matsushita, H. Kiyoku, Y. Sugimoto, T. Kozaki, I. Umemoto, M. Sano, and K. Chocho, "InGaN/GaN/AlGaN-based laser diodes grown on GaN substrates with a fundamental transverse mode," *Japanese Journal of Applied Physics, Part 2 (Letters)*, vol. 37, pp. L1020-1022, 1998.

[14] K. Domen, R. Soejima, A. Kuramata, and T. Tanahashi, "Electron overflow to the AlGaN p-cladding layer in InGaN/GaN/AlGaN MQW laser diodes," *MRS Internet Journal of Nitride Semiconductor Research*, vol. 3, pp. 2, 1998.

[15] K. Domen, R. Soejima, A. Kuramata, K. Horino, S. Kubota, and T. Tanahashi, "Interwell inhomogeneity of carrier injection in InGaN/GaN/AlGaN multiquantum well lasers," *Applied Physics Letters*, vol. 73, pp. 2775-2777, 1998.

[16] S. Li, "Lastip," v. 5.4.1 ed. Gloucester, Ontario, Canada: Crosslight Software, Inc., 2000.

[17] J. Piprek, R. K. Sink, M. A. Hansen, J. E. Bowers, and S. P. DenBaars, "Simulation and Optimzation of 420 nm InGaN/GaN Laser Diodes," presented at Physics and Simulation of Optoelectronic Devices VIII, 2000.

[18] S. L. Chuang and C. S. Chang, "A band-structure model of strained quantum-well wurtzite semiconductors," *Semiconductor Science and Technology*, vol. 12, pp. 252-263, 1997.

[19] Y. C. Yeo, T. C. Chong, and M. F. Li, "Electronic band structures and effective-mass parameters of wurtzite GaN and InN," *Journal of Applied Physics*, vol. 83, pp. 1429-1436, 1998.

[20] L. A. Coldren and S. W. Corzine, *Diode Lasers and Photonic Integrated Circuits*. New York, NY: John Wiley & Sons, 1995.

[21] M. Hansen, P. Fini, L. Zhao, A. V. Abare, L. A. Coldren, J. S. Speck, and S. P. DenBaars, "Improved characteristics of InGaN multiple-quantum-well laser diodes grown on laterally epitaxially overgrown GaN on sapphire," *Applied Physics Letters*, vol. 76, pp. 529-531, 2000.

[22] K. Domen, A. Kuramata, R. Soejima, K. Horino, S. Kubota, and T. Tanahashi, "Lasing mechanism of InGaN-GaN-AlGaN MQW laser diode grown on SiC by low-pressure metal-organic vapor phase epitaxy," *IEEE Journal of Selected Topics in Quantum Electronics*, vol. 4, pp. 490-497, 1998.

[23] C. Wetzel, T. Takeuchi, S. Yamaguchi, H. Katoh, H. Amano, and I. Akasaki, "Optical band gap in $Ga_{1-x}In_xN$ ($0<x<0.2$) on GaN by photoreflection spectroscopy," *Applied Physics Letters*, vol. 73, pp. 1994-1996, 1998.

[24] W. Gotz, N. M. Johnson, J. Walker, D. P. Bour, and R. A. Street, "Activation of acceptors in Mg-doped GaN grown by metalorganic chemical vapor deposition," *Applied Physics Letters*, vol. 68, pp. 667-669, 1996.

[25] D. P. Bour and P. S. Zory, "Visible Semiconductor Lasers (Short Course)," presented at Conference on Lasers and Electro-Optics, San Francisco, CA, 1998.

[26] J. H. Edgar, *Properties of Group-III Nitrides*. London, England: IEE/INSPEC, 1994.

[27] S. L. Chuang, "Optical gain of strained wurtzite GaN quantum-well lasers," *IEEE Journal of Quantum Electronics*, vol. 32, pp. 1791-1800, 1996.

[28] S. Strite and H. Morkoc, "GaN, AlN, and InN: A review," *Journal of Vacuum Science & Technology B (Microelectronics Processing and Phenomena)*, vol. 10, pp. 1237-1266, 1992.

[29] W. Fang and S. L. Chuang, "Theoretical prediction of GaN lasing and temperature sensitivity," *Applied Physics Letters*, vol. 67, pp. 751-753, 1995.

[30] L. H. Peng, C. W. Chuang, and L. H. Lou, "Piezoelectric effects in the optical properties of strained InGaN quantum wells," *Applied Physics Letters*, vol. 74, pp. 795-797, 1999.

[31] S.-H. Park and S.-L. Chuang, "Many-body optical gain of wurtzite GaN-based quantum-well lasers and comparison with experiment," *Applied Physics Letters*, vol. 72, pp. 287-289, 1998.

[32] G. Martin, S. Strite, A. Botchkarev, A. Agarwal, A. Rockett, H. Morkoc, W. R. L. Lambrecht, and B. Segall, "Valence-band discontinuity between GaN and AlN measured by X-ray photoemission spectroscopy," *Applied Physics Letters*, vol. 65, pp. 610-612, 1994.

[33] G. Martin, A. Botchkarev, A. Rockett, and H. Morkoc, "Valence-band discontinuities of wurtzite GaN, AlN, and InN heterojunctions measured by X-ray photoemission spectroscopy," *Applied Physics Letters*, vol. 68, pp. 2541-2543, 1996.

[34] J. Piprek, P. Abraham, and J. E. Bowers, "Carrier nonuniformity effects on the internal efficiency of multiquantum-well lasers," *Applied Physics Letters*, vol. 74, pp. 489-491, 1999.

[35] K. Domen, R. Soejima, A. Kuramata, and T. Tanahashi, "Electron overflow to the AlGaN p-cladding layer in InGaN/GaN/AlGaN MQW laser diodes," *MRS Internet Journal of Nitride Semiconductor Research*, vol. 3, 1998.

[36] M. S. Minsky, S. B. Fleischer, A. C. Abare, J. E. Bowers, E. L. Hu, S. Keller, and S. P. DenBaars, "Characterization of high-quality InGaN/GaN multiquantum wells

with time-resolved photoluminescence," *Applied Physics Letters*, vol. 72, pp. 1066-1068, 1998.

[37] S. Nakamura, "Progress of GaN-based blue/green LEDs and bluish-purple semiconductor LDs," *Transactions of the Institute of Electronics, Information and Communication Engineers C-II*, vol. J81C-II, pp. 89-96, 1998.

[38] R. Soejima, A. Kuramata, S. Kubota, K. Domen, K. Horino, and T. Tanahashi, "Continuous-Wave Operation at 250K of InGaN Multiple Quantum Well Laser Diodes Grown on 6H-SiC with Vertical Conducting Structure," *Japanese Journal of Applied Physics, part 2*, vol. 37, pp. L1205-1207, 1998.

Chapter 4

Nitride laser diodes on A-plane sapphire

Several research groups have fabricated nitride laser diodes as described in Chapter 1 [1-14]. Nakamura has demonstrated device lifetimes of 10,000 hours for CW lasers based on epitaxial lateral overgrowth (ELO) technology, which demonstrates that nitride lasers can be made robust enough to live up to commercial lifetime requirements [2]. Most of these lasers have etched facets that were formed by Cl_2 based reactive ion etching (RIE). However, cleaved facets are favored in commercial device manufacturing because of the reproducibility of the cleaving process and the independence from the processing parameters to which etched facets are subject [8]. Additionally, because the substrate facet is flush with the cleaved epitaxial layers unlike in etched-facet laser diodes, cleaved-facet laser diodes allow easy access to the facet for focusing into lenses that have high numerical apertures. Finally, cleaved-facet lasers do not suffer from the reflection of light from the substrate, which occurs in etched-facet lasers. This allows the potential for fundamental mode operation in the lateral and transverse directions. Unfortunately, however, sapphire is not as easy to cleave as many other III-V materials because there are many cleave planes within close angular proximity. Despite this difficulty, we confirm in this chapter that cleaving is a viable technology for nitride laser fabrication as was previously reported by Nakamura [9].

This chapter describes pulsed operation of cleaved-facet nitride laser diodes with lasing wavelengths ranging from 410 to 425 nm. This chapter describes the fabrication of blue-emitting nitride laser diodes on a-plane sapphire (11$\underline{2}$0). It describes many of the fabrication issues that are unique to the nitride material system, such as high temperature activation of p-type dopants. These lasers did not operate well, but with coating and improvements in material quality, the devices could be expected to obtain CW operation.

4.1. Processing

The laser fabrication process for nitride lasers grown on a-plane sapphire is shown in Figure 1. The process is similar to that for fabrication of broad area lasers in other material systems. There are a few differences due to the GaN etch chemistry and the sapphire substrate. These differences will be described in more detail in the sections that follow. This section outlines the basic fabrication process. Individual steps will be described in detail in the rest of the chapter.

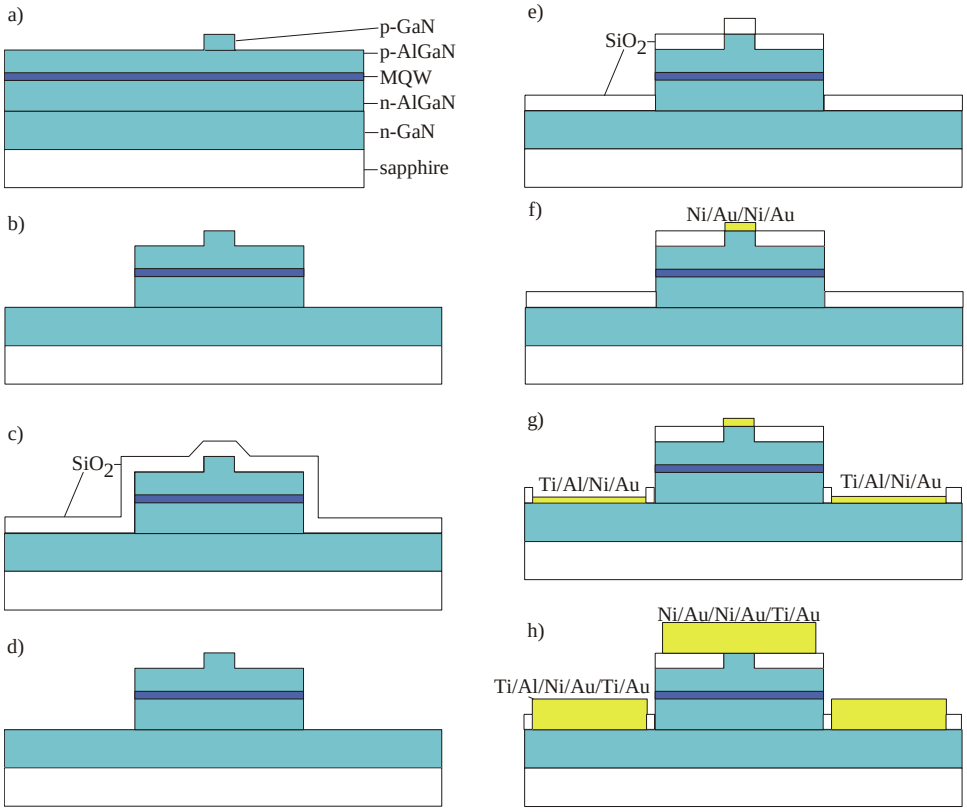

Figure 1. Summary of processing steps for fabrication of cleaved-facet laser diodes. The steps are described in more detail in the text.

The first step after MOCVD growth is to divide the wafer into smaller pieces for processing. The sample can then be divided into pieces using a dicing saw or using the scribe and break method. Due to the multiple cleave planes in sapphire,

the dicing saw method is recommended for critical work, although reasonably reliable results can be achieved by scribe and break with practice and a sharp scribe. The samples are then solvent cleaned to remove cleave dust and graphite particulates that remain from unloading the reactor.

Once the samples are clean, the p-type contact area is defined using a photoresist mask for an RIE etch (Figure 1a). This etch defines the current confinement region by patterning the p-GaN, which is much more conductive than the p-AlGaN. This etch is very shallow and extends only down through the top p-GaN contact layer (100 nm). The photoresist mask is then removed with hot 1165 (also called NMP).

A new photoresist mask is then patterned for RIE definition of the mesa (Figure 1b). The mesa is necessary in order to make contact to the n-type GaN material. Backside contacts are not possible because the sapphire substrate is an insulator. In the RIE conditions used, the unbaked photoresist is etched at approximately the same rate as the GaN. So for the 1.0-1.5 μm mesa etch, a photoresist mask that is 2 or 3 μm thick serves as a suitable mask.

Following the mesa etch, a 100 nm SiO_2 mask is deposited by PECVD as a cap for p-type dopant activation (Figure 1c). Rapid thermal annealing (RTA) at 950ºC for 3 minutes is used to activate dopants. After the activation, the SiO_2 mask is removed with buffered HF. This is more difficult than the standard SiO_2 removal because during the RTA the SiO_2 mask intermixes slightly with the GaN. For this reason, the removal of the oxide takes longer than usual. A long etch of at least 10 minutes in buffered HF is necessary to remove the SiO_2 mask and the GaN_xO_{1-x} that was formed during RTA (Figure 1d). This oxide removal step also serves to clean the surface of any contaminants, which is especially important for the formation of ohmic p-type contacts.

After this initial cleaning step, an additional 150 nm of SiO_2 is deposited by e-beam evaporation (Figure 1e). This layer serves two purposes: 1) it encapsulates

the p-type GaN and 2) it reduces the loss in the optical mode by pushing the mode away from the p-type metal contact. Encapsulation of the p-type GaN is also believed to reduce device degradation that occurs when hydrogen is readsorbed into the crystal structure. E-beam evaporation is used instead of PECVD because the PECVD process passivates the p-type dopants in GaN.

P-type contacts are then patterned and deposited as follows (Figure 1f). A PR mask is patterned for the p-type contact. Oxygen plasma is used to clean the surface by removing any residual photoresist. The SiO_2 in the mask opening is etched away with buffered HF diluted 1:10 with DI water. This solution etches SiO_2 at a rate of 100 nm/minute. A slight over etch is used to make sure that there is no residual oxide. This creates a slight undercut, but the undercut is very limited. Having the SiO_2 present while the photoresist mask is patterned helps to keep the GaN surface free of contaminants such as photoresist. The removal of the SiO_2 also helps to clean the surface by removing surface contaminants. P-type Ni/Au/Ni/Au (10/200/40/50 nm) contacts are deposited by e-beam evaporation and lifted off. Alternatively, the SiO_2 mask could be deposited after the deposition of the p-type contacts, but this leads to cracking of the SiO_2 film when it is deposited on top of metal contacts.

The n-type contacts are less sensitive to contamination than are the p-type contacts, but it is still important to keep the surface clean to create better adhesion of the contact metals. The n-type contact is prepared in the same way as the p-type contact: patterning of a photoresist mask, etching (buffered HF 1:10) of the SiO_2 mask, and lifting off of e-beam evaporated contacts (Figure 1g). The n-type contacts are Ti/Al/Ni/Au (8/200/40/50 nm).

A thick contact pad is desired since these devices are expected to have a large threshold current density. For this reason, thick Ti/Au (7/800 nm) contact pads are patterned for the p-type and n-type pads by liftoff (Figure 1h). As in other

material systems, the Ti layer is used to provide better adhesion for the deposited Au and the thick gold layer is deposited as the probe pad metal.

Samples are then complete except for the facet formation. In order to cleave reliably, the sapphire must be thinned to less than 80 μm. The preferred thickness is 50-60 μm. In order to thin the sapphire substrate this much, sample preparation is important and will be discussed in more detail below. Corners of the sample are rounded with 80 grit sandpaper to prevent chipping of the corners and the sample is polished using a series of diamond grit sizes—15, 6, 0.05 μm—on a cast iron lapping wheel. The wafer is then diced into 2 mm wide strips in order to create thinner strips for cleaving. The laser bars can then be cleaved using standard methods.

4.1.1. Material growth

The material growth is complicated and is not my area of expertise. Therefore, I will only describe the basics of material growth. More detailed information can be found in books, papers, and dissertations on GaN growth [1-3]. Specifically, reference [4] provides a good overview of many of the issues involved with GaN growth including growth chemistry, reactor design, precursors, and substrate choice.

The laser structure was grown on an a-plane ($11\underline{2}0$) sapphire substrate by metal-organic chemical-vapor deposition (MOCVD) at atmospheric and low pressures in a modified two-flow Thomas-Swan Ltd. horizontal reactor. The chemical precursors used were trimethylgallium (TMGa), trimethylindium (TMIn), trimethylaluminum (TMAl), ammonia (NH_3), disilane (Si_2H_6), and bis(cyclopentadienyl) magnesium (Cp_2Mg). More detail about the growth temperatures and pressures are given in Table 1.

Material	Growth Temperature	Growth Pressure	Group-III Source	Group-V Source(s)
GaN	1050-1100ºC	760 T	NH_3 (ammonia)	TMGa (trimethylgallium)
InGaN	800-850ºC	760 T	NH_3 (ammonia)	TMGa, TMIn (trimethylindium)
AlGaN	1050-1100ºC	300 T	NH_3 (ammonia)	TMGa, TMAl (trimethylaluminum)

Table 1. Source gases and growth conditions for the group-III nitrides.

One of the main issues for the growth of high quality group-III nitride epitaxial layers is reactor design. Proper flow to reduce prereaction of group III and group V precursors is one of the most difficult things to achieve because of the ease with which the ammonia (nitrogen source) reacts with the group V sources, especially TMAl and TMGa. This is only one of the issues and each particular alloy has its own problems for growth.

For InGaN growth, low temperatures are used because high temperatures increase the evaporation of indium from the surface and thus reduce the indium concentration of the film. In addition, higher temperatures lead to the film not wetting well. The result is large clumps of indium, which visibly darken the film and cause higher absorption for the lasing mode [5]. Indium segregation is also a problem for InGaN films with high indium content. Layers with high indium content and without indium droplets have been formed by growing InGaN/GaN superlattices. However, this method has not been widely adopted [5].

Cracking of the ammonia bonds does not occur very rapidly at the low temperatures used for InGaN growth. For this reason, smaller V/III ratios (i.e. a larger proportion of ammonia) are used in the growth of InGaN than for the growth of GaN and AlGaN [4].

AlGaN has a different set of problems. It does not suffer from aluminum segregation, but instead from cracks, from gas phase prereactions during growth, and from poor dopant incorporation. The lattice mismatch and thermal expansion

mismatch between AlGaN and GaN causes tensile strain which is much more difficult to handle than the compressive strain found in InGaN on GaN. For this reason, AlGaN is subject to cracking for relatively low concentrations of aluminum. Currently, we notice significant cracking in strained superlattices that are 0.5 μm thick with an average of aluminum composition of 10%. This growth limitation is heavily process dependent. Nakamura is able to grow a structure with a 1.2 μm n-type AlGaN SSL and a 0.6 μm p-type AlGaN SSL with an average aluminum composition of 7% [6]. This thick AlGaN layer allows significantly better optical confinement of the mode. Improvements in strain relief during the growth process will likely improve our ability to grow thick AlGaN cladding regions. One potential method for doing this is using epitaxial lateral overgrowth, which is believed to reduce the strain associated with thermal expansion differences between GaN and sapphire.

Another problem to be overcome with AlGaN is the reduction of parasitic prereactions of TMAl with ammonia. At the high growth temperatures used for growth of AlGaN, TMAl reacts easily with ammonia. The problem arises when this reaction occurs before the reactants reach the substrate surface. Since it is very difficult to control these reactions, low pressure (300 T) is used to reduce the frequency of these parasitic reactions.

A final problem with AlGaN growth is poor dopant incorporation. For n-type material, where the donor activation energy is relatively small, this is not as important because most of the donors that are incorporated generate carriers. However, for p-type AlGaN, where the acceptor activation energy is large, less than 1% of the Mg acceptors create carriers. Therefore, having a large incorporation of Mg atoms is crucial to obtaining low p-type resistivity.

As mentioned above, this is only a brief overview of a few of the encountered during nitride growth. Growth of GaN involves many more problems that stand in the way of creating high quality films uniformly and repeatably. The

fabrication and development of nitride lasers is still primarily limited by the growth technology. The primary problems that remain to be solved are increasing p-type doping in GaN and AlGaN, increasing AlGaN thicknesses, and reducing film defect densities.

Despite all of the problems, relatively good quality films have been produced. For our laser structure, growth was initiated on top of a low temperature 20 nm GaN buffer layer. A 3.0 μm GaN buffer layer was grown, which reduces the defect density in the film. A strain relief layer of 0.1 μm $In_{.05}Ga_{.95}N$ is grown below a 0.4 μm $Al_{.06}Ga_{.94}N$ cladding layer. The multi-quantum well (MQW) active region is composed of ten 3 nm $In_{.18}Ga_{.82}N$ quantum wells separated by 6 nm $In_{.06}Ga_{.94}N$ barriers. These MQW layers are capped with a low temperature growth of GaN to prevent deterioration of the quantum wells during subsequent high temperature growth steps. No AlGaN upper carrier confinement layer was used in this generation of devices. The top cladding layer is the same composition and thickness as the lower cladding. The final epitaxial layer is a highly doped p-GaN contact layer.

4.1.2. Etching

Once the layers are grown, the devices are patterned using dry etching. The most important use of etching in this laser process is to define the mesa and thus expose the n-GaN contact layers. In some other semiconductor material systems, this type of ridge waveguide etch is performed with an anisotropic wet etch. The wet etch can provide an edge with very small roughness and with significantly less damage to the semiconductor than the dry etch. Unfortunately, there is no useful wet etch for etching p-type material in the nitride system.

There have been some reports of development of photo-assisted wet etch processes in the nitrides. Vertical sidewalls can be created with photoelectrochemical (PEC) etching. Using this process, etch rates as high as 300

nm/min have been reported for intensities as low as 50 mW/cm^2 at 365 nm [7-12]. Unfortunately, this process is only useful in etching n-type material.

Another etching method, photo-thermal assisted etching, can be used for etching n-type or p-type material. This method uses a higher intensity of above bandgap light. This light is absorbed by the GaN and thus heats the sample locally. As mentioned earlier, heating GaN above 700ºC leads to desorption of nitrogen. After the nitrogen leaves the surface, the residual gallium can be easily etched in HCl. Laser assisted etching in HCl has been reported by several groups [13-16]. Since this process depends on absorption of light, however, this etching process depends strongly on material quality. It is, however, a robust technique for GaN material processing. In addition, this etching technique is the basis for the laser ablation process that can be used to remove the sapphire substrate [15]. Laser ablation will be discussed in more detail in the next chapter.

The photo-assisted processes are the best wet etches available for patterning the nitrides, but there are some wet etches with specific qualities that make them useful in nitride device fabrication. For example, there are several wet etches which etch the nitrides if the crystal quality is poor. AlN is found to etch in AZ400K developer if the crystal quality is poor [17]. However, more useful etches are ones that work for good quality material. GaN is found to etch crystalographically in several hot acids. These acids have been demonstrated to clean up rough sidewalls from RIE etch damage [18]. The etches described by Stocker, et al. are anisotropic, with one of the slow etch directions being the (0001) direction in GaN. This means that it is not useful for patterning GaN, but can be used for cleaning up edge roughness for ridge waveguides after using a dry etch for the initial patterning of the waveguide.

For the gain-guided structure described in this structure, the edge roughness and recombination at the surface are not significant due to the large separation between the lasing region and the sidewall. So dry etching is suitable without the

need for an additional sidewall cleanup. Even for very narrow waveguides, surface recombination is not expected to be a problem because the small carrier diffusion lengths in GaN limit the number of carriers that can diffuse to the surface for recombination. Edge roughness, on the other hand, could become an issue for ridge-waveguide lasers. In ridge-waveguide lasers, edge roughness will be more important because it causes scattering loss for the optical mode. So having a method for reducing the edge roughness of the waveguide could be important in that application.

The simplest method for patterning nitride epitaxy at this point is not the photo-assisted etching processes or the crystallographic wet etch but dry etching. Dry etching introduces damage, rough edges, and significant surface topology in comparison with a wet etch, but it provides a fast reproducible method for patterning. At UCSB, two different etch systems were compared. The first system was a commercial system sold by Plasma-Therm. The second system is a system built at UCSB by Allen Vawter. In both systems, Cl_2 is the reactive etch gas. Photoresist etches at approximately the same rate as the nitride. Similar etch rates have been achieved in both systems. Differences between the two systems arise in the chemistries that are used, the wafer cooling that is available, and the edge roughness of the resulting etch.

In the Plasma-Therm RIE system, very reasonable results are attained for etching of GaN. Currently, however, the He cooling does not work reliably on the system, which makes long etches less stable and makes it more difficult to remove photoresist masks after etching. Typical etch parameters consist of a flow of Cl_2 of 5 sccm, a chamber pressure of 2.5 mT, and an etch power of 250 W. The resulting etch conditions are (approximately) a bias of 450 V and an etch rate of 100 nm/min for GaN.

The second system was built at UCSB. It has a cooling system that works and also allows the addition of Ar. Significant characterization of this system has not

been performed, but initial results indicate that this system gives equally poor edge roughness. With characterization, however, the advantages of the improved cooling system, lower base pressure, and flexibility of gas chemistry should help to produce smoother etches. In addition, this system should give better and more consistent performance than the commercial system. For the devices presented in this chapter, however, etch roughness is not as important. As devices become more sophisticated, more careful characterization of the etch process may be warranted. It was found that the addition of small portions of Ar increased the etch rate slightly in this system. Typical etch parameters were 500 V bias (90 W), a chamber pressure of 3.4 mT, a Cl_2 flow of 7.5 sccm, and an Ar flow of 1 sccm. This yielded an etch rate of approximately 90 nm/minute.

Both systems have been used to etch the 125 μm mesas for the broad area devices and both have demonstrated suitable results. The Plasma-Therm is significantly easier to use and therefore is recommended for this type of non-critical etching. To take advantage of lateral index guiding and to reduce lateral resistance, however, narrower mesas will be employed in future devices. In this case, more thorough characterization of the UCSB RIE system may be warranted in order to optimize the etch characteristics. Alternatively, a dry etch can be used in combination with a crystallographic wet etch in order to create smooth, high quality sidewalls.

4.1.3. Activation of p-dopants

Once the mesas are etched, the p-type activation is performed. For this step, it is important to make sure the surface is clean. A thorough solvent clean is used and is followed by an oxygen plasma cleaning. As described in Chapter 2, hydrogen atoms passivate p-type GaN. Hydrogen is present during the growth of GaN because it is used as the carrier gas for ammonia. This hydrogen can be removed by using a thermal anneal of the p-type GaN. A larger percentage of the

hydrogen is removed for a higher temperature. In GaN, the maximum temperature of the activation is limited, however, because above 700ºC significant nitrogen desorption occurs from the GaN surface. Since the nitrogen vacancies act as shallow donors, nitrogen vacancies reduce the p-type carrier concentration. To prevent this nitrogen desorption, 100 nm SiO_2 is evaporated by PECVD to cap the GaN. This cap layer prevents nitrogen desorption. The p-dopants are then thermally activated using rapid thermal annealing at 950° C for 3 minutes in a nitrogen ambient. This is effective in activating the p-type GaN material to achieve p-type carrier concentrations of approximately $6 * 10^{17}$ cm^{-3}.

In addition to thermally activating the p-type dopants, the high temperature RTA process has several other effects on the GaN epilayers. Some of these are beneficial; others are not. Cole, et al. showed that the high temperature RTA actually improved the crystal quality [19]. They found that the defect density was actually decreased by 33% for an 800ºC 1 minute anneal in comparison to a 600ºC 1 minute anneal. This reduced defect density—and hence better material quality—is claimed to also significantly reduce the spiking of the metal contacts, which was correlated with the defected regions. The high temperature anneal also causes problems. The SiO_2 mask that is used as the cap for the nitride also acts as a diffusion source for oxygen. The formation energy for GaNO is very low. Therefore oxygen diffuses into GaN by exchanging positions with nitrogen lattice atoms. These oxygen contaminants act as non-radiative recombination centers and also compensate for p-type doping. SiN has been used as a mask by some researchers, and it does not show this effect [20]. High quality CVD SiN is much more difficult to remove from the surface than SiO_2, however, which makes SiO_2 a reasonable choice for a cap layer.

4.1.4. Contacts

Once the p-type material has been activated, the contacts should be deposited before additional processing steps contaminate the surface. The development of robust contact technology has been one of the limiting factors in the production of light emitting nitride devices. In particular, CW lasers have been difficult to fabricate. This is due in part to the large contact resistances for p-type GaN. In most semiconductors, high doping levels are used to fabricate ohmic contacts. The high doping means that even if a barrier exists, it can be easily tunneled through. This is difficult in GaN because the maximum p-type carrier levels are much lower than in other semiconductors. This increases the difficulty in making ohmic contacts and makes both contacts and material much more resistive.

As described in Chapter 3, fabrication of ohmic contacts in laser diodes is very important for achieving low threshold currents and CW operation. If ohmic contacts are not achieved then the extra voltage drop associated with the barrier for the contact directly affects the heat generation of the laser diode. Even for a small 0.1 V barrier, 1 A of current generates an additional 100 mW of thermal power in the device. This thermal power heats up the active region and thus decreases the gain of the active region. Reduced gain means that higher current densities are required to achieve the same modal gain. More current induces more heat, which in turn requires more current. The cycle continues until the active region cannot provide enough gain for lasing. In the case of GaN lasers, the primary sources of heat are the p-type material resistance and the p-type contact resistance.

Both of these problems are caused by the low carrier mobility and the low p-type carrier concentration in p-type GaN. The low carrier concentration is due to the large activation energy of the Mg acceptor. Improving either carrier concentration or carrier mobility in p-type GaN is a difficult process and only incremental progress has been made since the early publications of p-type

conductivity in GaN. Therefore, it is very difficult to reduce the heat generation that is caused by the p-type material resistance. The p-type contact, however, is sensitive to processing conditions and can be improved significantly. While the actual contact resistance depends heavily on the p-type doping of the contact layer, it is also sensitive to the contact preparation, annealing conditions, and metal structure.

For fabrication of p-type contacts, a clean surface is very important to improve the adhesion of the contacts to the surface since the Ni wetting layer is not as reactive with the GaN semiconductor as other metals used in other contact schemes, such as Ti. Also, contaminants on the surface create surface states that increase the contact resistance. Fortunately, GaN oxidizes much slower than other semiconductors; so thick oxide layers are not as much of a problem as in other systems, such as GaAs, which oxidize very rapidly. Removal of the oxidation layer is still required for the development of high quality ohmic contacts, however.

In the laser process described in this chapter, a SiO_2 cap layer is used for preventing nitrogen desorption during the activation of p-type carriers. Following this activation, a long BHF etch (>10 minutes) is used to remove the SiO_2 cap layer and any interfacial GaNO layer that has formed during the activation. It has also been found that a 30-60 second etch in HCl 1:1 is helpful to remove the last bit of GaNO after the buffered HF dip.

If material has been dry etched, the dry etching leaves a nitrogen-terminated surface even if the dry etch is followed by a wet etch. This nitrogen-terminated surface is n-type [21]. Therefore, if a p-type material is dry etched (or dry etched and followed by a wet etch), it is necessary to oxidize the surface using ozone and then remove the oxidized layer in order to restore the surface structure [22].

Ishikawa, et al. report that the contacts depend most importantly on the metal work function of the contact metal. Metals with higher work functions provide

lower contact resistance [23]. They conclude from this that the barrier height is not pinned by surface states due to contaminants and surface preparation techniques. It is still believed that it is important to remove contaminants and oxide from the surface. However, in the Ishikawa study, Ni/Au provided the lowest contact resistance for unannealed contacts and for contacts annealed at temperatures up to 500ºC. For comparison, the high work function Pt contacts were very close to or in some cases slightly better than the Ni/Au contacts, while Pd contacts were slightly worse. The Ta contacts mentioned in the next paragraph had 3 orders of magnitude higher contact resistances as deposited and well over 2 orders of magnitude higher contact resistance after annealing at 500ºC. The significant reduction in contact resistance reported for the Ta/Ti contact was not noticed until the annealing temperature was increased to 800ºC [24].

The most frequently referenced p-type contacts are Ni/Au, Pd/Au, and Cr/Au with Ni/Au being the most common. Above 400ºC, both Ni and Cr react with GaN to form an intermediate layer between the metal and semiconductor, but no reaction has been observed with Pd contacts [25]. This means that improved contacts can be formed by annealing Ni or Cr based contacts above 400ºC. Using Ni/Au, ohmic contacts have been created with a contact resistance of approximately $7 * 10^{-3}$ ohm cm^2 for p-type material with a hole concentration of $2 * 10^{17}$ cm^{-3} [24]. Taek, et al. report a one order of magnitude drop for contact resistance of Pd/Au contacts in comparison to Ni/Au contacts ($9 * 10^{-3}$ ohm cm^2 for p-type GaN with a hole concentration of $0.9 * 10^{17}$ cm^{-3}) [26]. Recently, Suzuki, et al. proposed using Ta/Ti as an alternative p-type contact [24]. They argue that the Ta and Ti both getter hydrogen; so these contacts should reduce the amount of residual hydrogen that remains in the p-type GaN after annealing. They report improved contact resistances of $3 * 10^{-5}$ ohm cm^2 to p-type GaN with a hole concentration of $7 * 10^{17}$ cm^{-3} [24]. Typical annealing conditions for

Ni/Au and Pd/Au contacts are 450-500ºC, while typical annealing conditions for the Ta/Ti contacts were 800ºC.

In deciding which p-type contact is best, it is difficult to separate the contact scheme from the more important differences in surface preparation and material quality. There does appear to be a slight improvement in p-type contact resistance for Pd/Au contacts over Ni/Au contacts, but the difference is slight. Other advantages of this contact such as the fact that it appears to be more durable for high temperature operation may make this contact better in the long run than Ni/Au contacts. Other experimentally presented contact structures such as the Ta/Ti structure presented by Suzuki, et al. have not had enough study to determine how they compare to Ni/Au and Pd/Au contacts, but could in the long term prove to be better contacts. All work presented in this dissertation has been performed using Ni/Au based p-type contacts.

P-type contacts are difficult to make. N-type contacts are relatively easy. In fact, n-type ohmic contacts can be formed using Al without removing the oxide layer if the sample has not been exposed to air for too many days. The almost universally used n-type contact metal for GaN is Al. For these contacts, Ti has been found to be a good sticking layer and the Al is usually capped with Ni/Au to provide a contact surface that does not oxidize and can be used for wire bonding. The first published report of this structure was by Tan, et al. who annealed at 900ºC for 30 seconds to obtain a contact resistivity of $1*10^{-7}$ ohm cm^2 for material with an n-type carrier concentration of $4 * 10^{17}$ cm^{-3}. [27]. In comparison to the best p-type contacts, the n-type contact has approximately two orders of magnitude lower contact resistance. For this reason, much more emphasis is placed on improving the p-type contact than on improving the n-type contact.

The contacts used for the laser process described in this chapter are deposited by e-beam evaporation and consist of the following: Ni/Au/Ni/Au (10/200/40/50

nm) and Ti/Al/Ni/Au (8/200/40/50 nm) for the p- and n-type contacts. For the p-type contact, the Ni acts as both the whetting layer and the contact layer. Some mixing with the Au layer does occur at elevated temperatures. A thicker Ni barrier layer is provided between the Au layer and the subsequent Au non-oxidizing contact layer. For the n-type contact, Ti acts as the whetting layer, while Al provides the actual contact. Again Ni serves as a barrier layer and Au is the non-oxidizing contact layer. An SiO_2 insulating layer was patterned on top of the mesa to limit the stripe width of the p-contact. A thick (7/800 nm) Ni/Au contact was then deposited. Our contacts were unannealed because little change in contact resistance was observed by annealing. For unannealed n-type contacts, thin 7-8 nm Ti layers are used. If contact annealing is performed, slightly thicker (10 nm) Ti layers can be used.

4.1.5. Polishing to prevent cracks

After patterning the contacts, the devices are finished except for cleaving the facets. The cleaving is much easier if the sapphire is reduced in thickness to less than 80 μm. Sapphire has a hardness of 9 mohs[4] or 1525-2000 Knoop. This makes it very difficult to lap. Several methods for polishing sapphire were tried. These methods are described in more detail in Appendix D. The advantages and disadvantages of each of these methods will be described in that Appendix.

4.1.6. Cleaving

After thinning the substrate, the laser bars are ready to be cleaved. I have found that cleaving a very wide bar is difficult; so I typically use the dicing saw (or a scribe and break tool) to break the laser sample into 2 mm strips, which are much easier to cleave because the cleave only has to propagate across 2 mm of material instead of across the entire sample.

[4] In this scale, 1 corresponds to the softest material—talc—and 10 corresponds to the hardest material—diamond.

The r-planes {1$\underline{1}$02} of the sapphire are used for cleaving vertical facets. Results of this process were discussed in Chapter 2 and a scanning electron microscope (SEM) image of the facet was shown in Chapter 2. The sapphire cleaves well, but the nitride epitaxial layers fracture due to a 2.4° misorientation between the sapphire r-plane (10$\underline{1}$2) and the GaN a-plane (11$\underline{2}$0). This mismatch occurs because the a-plane of the GaN orients along the c-plane of the sapphire during growth. The r-plane is 57.6° from the c-plane in sapphire, while the a-planes are distributed every 60° in GaN. The fractured a-plane appears to be very rough and this roughness is predicted to interfere with a coherent reflection from the facet.

A picture of completed laser bars is shown in Figure 2 and a picture of the cleaved facet was shown in Chapter 2 (Figure 8).

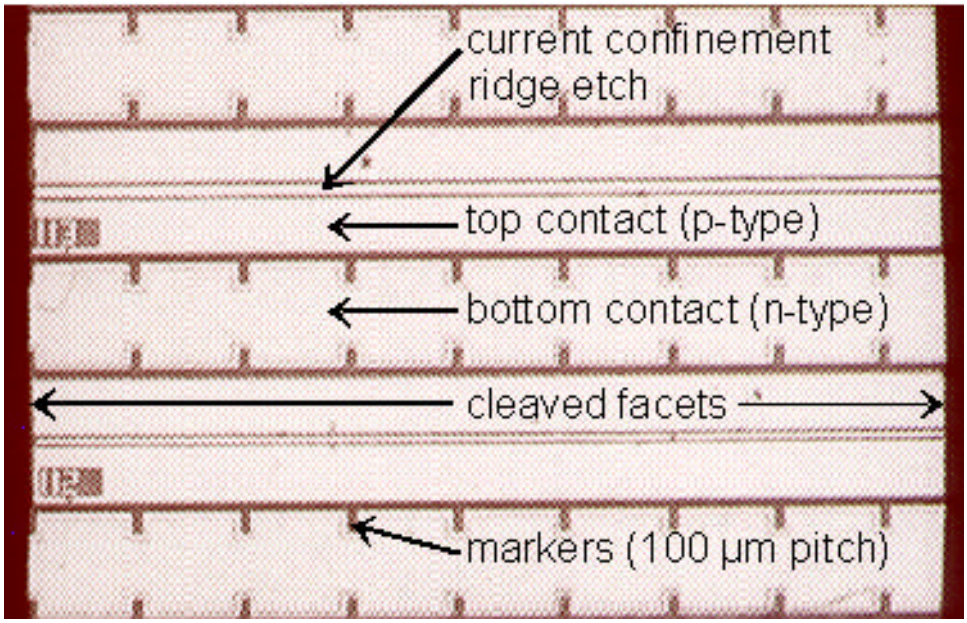

Figure 2. Pictures of completed laser bars on a-plane sapphire.

As discussed in Chapter 2, other methods do exist for forming cleaved facets in GaN. One of those methods is the use of c-plane sapphire substrates. If c-plane

sapphire is used, the cleave planes (a-planes) of sapphire line up with cleave planes of GaN. This means that the roughness of the facet will be reduced significantly in comparison with facets made using a-plane sapphire substrates. However, for c-plane sapphire, the r-planes of sapphire are not vertical. Therefore, it is much more difficult to force the cleave along the vertical a-planes and much more care must be taken because the sapphire must be thinned even more than for lasers made with a-plane sapphire substrates.

4.2. Results

Lasers have been fabricated according to the methods that were described in Section 4.1. The active region is composed of 10 $In_{.18}Ga_{.82}N$ quantum wells, which are grown by MOCVD. Diode wafers are thinned to less than 50 μm before they are cleaved along the sapphire r-plane ($1\underline{1}02$). After fabricating the laser diodes, typical tests are performed that indicated that the devices lase: Lasers show TE polarization, spectral line narrowing, and far-field interference patterns above the lasing threshold.

This section details the characteristics of these lasers and interprets the results. In summary, lasing wavelengths of 410-425 nm have been observed. Under pulsed operation at room temperature, the lowest observed threshold current density has been 13 kA/cm^2. Differential efficiencies are as high as 7% per facet with maximum output powers greater than 70 mW. Near and far-field mode patterns are presented. Structures are gain-guided devices with each device occupying a mesa with a width of 125 μm. Device widths range from 3 to 20 μm and device lengths vary from 300 to 1200 μm.

4.2.1. Light-voltage-current measurements

The V-I (voltage-current) and L-I (light power-current) curves for these laser diodes are shown in Figure 3. Due to variations in material characteristics and

cleave quality, measured values for threshold current density vary over a large range. The measured threshold current densities for a single wafer range from 15 kA/cm^2 to 90 kA/cm^2 for device lengths of 300 to 1200 μm. Device widths range from 3 to 20 μm. Device testing was performed with 50 ns pulses with a pulse repetition frequency of 5 kHz. This short pulse width made it difficult to accurately measure the threshold voltage due to the inductance in the probing circuitry. By measuring this inductance, this problem can be corrected numerically. This correction has been performed for the data presented in Figure 3. Corrected threshold voltages vary from 18 to 50 V.

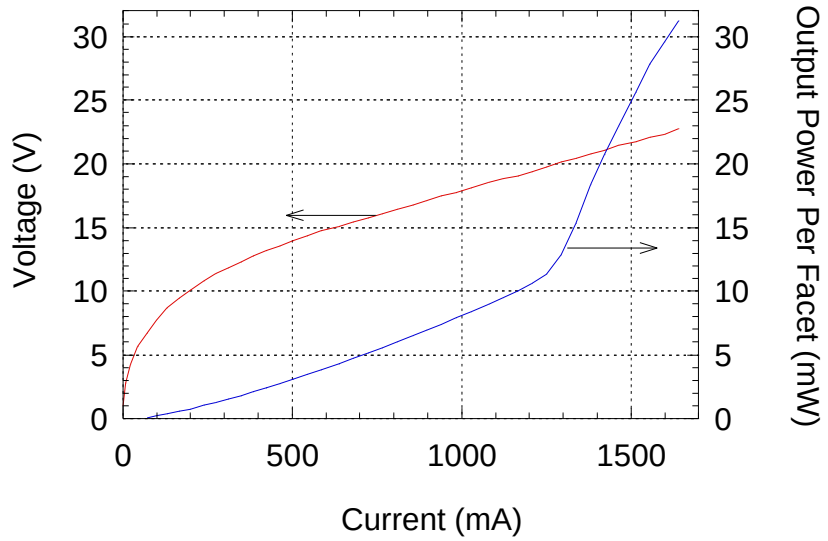

Figure 3. V-I (voltage-current) and L-I (light power-current) curves for a typical cleaved-facet laser diode. Maximum powers of >50 mW per facet have been measured and slope efficiencies range as high as 7% per facet.

4.2.2. Spectrum

The emission spectra of the laser bars narrow as expected (see Figure 4). The peak laser emission wavelength over a single wafer occurs in the range from 410-425 nm. The wavelength spectra shown in Figure 4 were measured with a 1 nm

resolution setting on an Ando 0.25 m spectrometer. As expected, the spectrum narrows as the laser current is increased to above threshold.

For a higher resolution scan (0.05 nm resolution), the laser is determined to have a FWHM of 0.6 nm and a peak wavelength of 413.0 nm for the device shown in Figure 4.

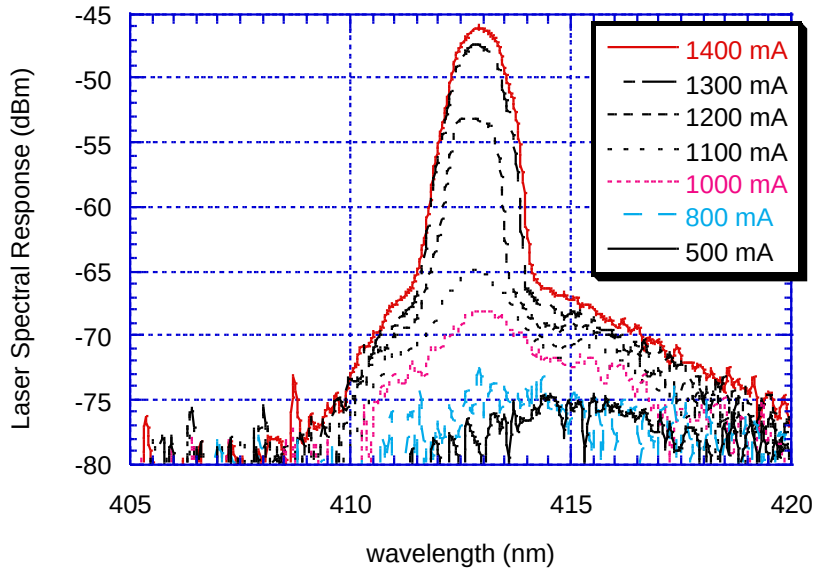

Figure 4. Laser emission spectra below and above lasing threshold. This scan was measured using a wavelength resolution of 1 nm. Laser threshold was approximately 1100 mA for this laser.

4.2.3. Far field

One of the advantages of cleaved-facet devices over etched-facet devices is the potential for fundamental transverse mode output, which is difficult to achieve in etched-facet devices due to a reflection from the substrate at the output of the etched facet. Due to the wide mesas that we have used in fabricating these devices and the non-optimized epitaxial laser structure, these lasers do not show fundamental mode operation in either the lateral or transverse directions. The far-field and near-field patterns are shown in Figures 5 and 6, respectively. The two-lobed nature of the far-field pattern shows a higher order transverse mode, which

has been predicted by Hofstetter et al for similar epitaxial layer structures [28] and was analyzed in the optical modeling section of Chapter 3. This can be contrasted with the three-lobed pattern that is visible from lasers with RIE etched facets that is believed to occur due to the reflection from the sapphire substrate [29]. The near field was imaged using a microscope objective with a numerical aperture of 0.4 to collimate the output beam onto a CCD array.

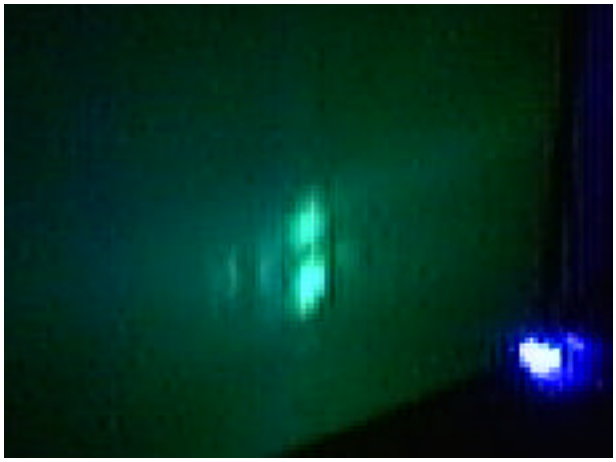

Figure 5. Far-field image of cleaved-facet laser operation just above threshold. The laser diode is shown in the lower right corner with the far-field image incident on a fluorescent card.

4.2.4. Near field

The laser nearfield is shown in Figure 6. All three pictures show the same laser on the same scale. Below threshold, light is emitted from a very wide aperture. The most plausible explanation for this wide emission below threshold is that the light is scattering from defects in the highly defected 0.5 μm of GaN at the GaN/sapphire interface. As the current is increased above threshold, the mode that lases is the one that has most of its power limited to the low defect region of the SCH. The lasing mode has less than 2% of its power in that region and, therefore, very little scattered light is visible above threshold.

Other possible sources of the wide emission pattern below threshold are current spreading and current injection through pinholes in the SiO_2 mask. Current spreading is expected to be significant for the n-type GaN and InGaN. The p-type material has significantly less current spreading as shown with the Lastip model in Chapter 3. The lateral hole current is slightly higher in the p-type GaN capping layer just above the quantum wells because this layer creates a slight potential well which allows the holes to move laterally more easily. This was shown in our paper based on the Lastip modeling (Chapter 3) in which lateral hole current was shown to be largest in this region [30]. The other possibility for the wide emission aperture below threshold is the possibility of current being injected through pinholes in the SiO_2. Only a single layer of SiO_2 was used as a mask for the p-type contact pad metal. Since GaN is heavily decorated with pits, chances of pinholes forming in SiO_2 are more likely in GaN than in other semiconductors. In addition, two layers of SiO_2 are often used in other material systems because of the possibility that a piece of dirt on the surface could provide a seed for a pinhole in the SiO_2 mask. Two layer masks of SiO_2 have not been tried yet. So it is unclear whether pinholes in the SiO_2 are the cause of the wide near field pattern below threshold.

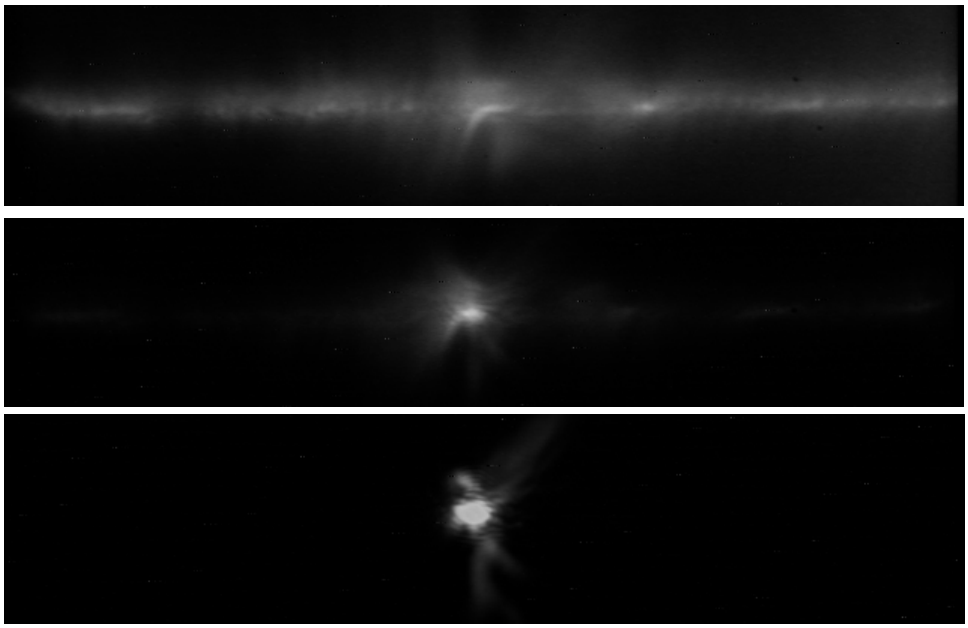

Figure 6. Near-field images of a cleaved-facet laser diode a) below threshold, b) just above threshold, and c) far above threshold.

Since a single microscope objective was used, I was not able to compensate for the astigmatism in the laser mode. Despite this, relatively clear images are produced of the near field, but resolution is limited due to the compromise in focal position. In addition, the lenses that were used were not antireflection coated for the lasing wavelength. This results in a slight flare being visible in each picture.

4.3. Conclusion

In summary, we have reported pulsed operation of cleaved-facet laser diodes based on a 10-well InGaN MQW active region and an a-plane sapphire substrate. Cleaving is performed along one of the r-planes of the sapphire substrate that is perpendicular to the wafer surface. Output powers of greater than 50 mW per facet are observed with differential quantum efficiencies as high as 7% per facet.

Threshold current densities as low as 13 kA/cm^2 are reported, but large variation in these values are observed due to facet quality and material nonuniformity. It is believed that by using c-plane sapphire substrates instead of a-plane sapphire substrates, the facet quality can be improved, although these facets are much more difficult to fabricate reliably. Near-field images show a strong tightening above threshold and far-field patterns show a double lobed interference pattern just above threshold.

4.4. References

[1] D. Kapolnek, "Selective Epitaxy of GaN and Related Materials by Metalorganic Chemical Vapor Deposition," Ph.D. Dissertation: Materials Department, University of California, Santa Barbara, 1999.

[2] S. Nakamura and G. Fasol, *The Blue Laser Diode*. Heidelberg, Germany: Springer, 1997.

[3] M. Mack, "Gallium nitride based semiconductor lasers," Ph.D. Dissertation: Materials Department, University of California, Santa Barbara, 1999.

[4] S. P. DenBaars and S. Keller, "Metalorganic Chemical Vapor Deposition (MOCVD) of Group-III Nitrides," in *Semiconductors and Semimetals*, vol. 50: Academic Press, pp. 11-37, 1998.

[5] M. Shimizu, K. Hiramatsu, and N. Sawaki, "Metalorganic vapor phase epitaxy growth of $(In_xGa_{1-x}N/GaN)^n$ layered structures and reduction of indium droplets," *Journal of Crystal Growth*, vol. 145, pp. 209-213, 1994.

[6] S. Nakamura, M. Senoh, S. I. Nagahama, N. Iwasa, T. Yamada, T. Matsushita, H. Kiyoku, Y. Sugimoto, T. Kozaki, H. Umemoto, M. Sano, and K. Chocho, "Violet InGaN/GaN/AlGaN-based laser diodes with an output power of 420 mW," *Japanese Journal of Applied Physics, Part 2 (Letters)*, vol. 37, pp. L627-629, 1998.

[7] C. Youtsey, I. Adesida, and G. Bulman, "Broad-area photoelectrochemical etching of GaN," *Electronics Letters*, vol. 33, pp. 245-246, 1997.

[8] L. Hongqiang, W. Ziming, and I. Bhat, "Photoassisted anodic etching of gallium nitride," *Journal of the Electrochemical Society*, vol. 144, pp. L8-11, 1997.

[9] C. Youtsey, I. Adesida, and G. Bulman, "Highly anisotropic photoenhanced wet etching of n-type GaN," *Applied Physics Letters*, vol. 71, pp. 2151-2153, 1997.

[10] S. Yoshida, "Electrochemical etching of a conductive GaN crystal for patterning," *Journal of Crystal Growth*, vol. 181, pp. 293-296, 1997.

[11] M. S. Minsky, A. M. White, and E. L. Hu, "Room-temperature photoenhanced wet etching of GaN," *Applied Physics Letters*, vol. 68, pp. 1531-1533, 1996.

[12] T. Rotter, D. Uffmann, J. Ackermann, J. Aderhold, J. Stemmer, and J. Graul, "Current controlled photoelectrochemical etching of GaN leaving smooth surfaces," presented at Nitride Semiconductors Symposium, Boston, MA, 1997.

[13] R. T. Leonard and S. M. Bedair, "Photoassisted dry etching of GaN," *Applied Physics Letters*, vol. 68, pp. 794-796, 1996.

[14] J. Zhang, K. Sugioka, S. Wada, H. Tashiro, and K. Midorikawa, "Study on high-speed deep etching of GaN film by UV laser ablation," presented at Second International Conference on Nitride Semiconductors, Tokushima, Japan, 1998.

[15] M. K. Kelly, O. Ambacher, R. Dimitrov, H. Angerer, R. Kandschuh, and M. Stutzmann, "Laser-processing for patterned and free-standing nitride films," presented at Nitride Semiconductors Symposium Nitride Semiconductors Symposium, Boston, MA, USA, 1998.

[16] H. Chen, R. D. Vispute, V. Talyansky, R. Enck, S. B. Ogale, T. Dahmas, S. Choopun, R. P. Sharma, T. Venkatesan, A. A. Iliadis, L. G. Salamanca-Riba, and K. A. Jones, "Pulsed laser etching of GaN and AlN films," presented at Nitride Semiconductors Symposium Nitride Semiconductors Symposium, Boston, MA, USA, 1998.

[17] J. R. Mileham, S. J. Pearton, C. R. Abernathy, J. D. MacKenzie, R. J. Shul, and S. P. Kilcoyne, "Wet chemical etching of AlN," *Applied Physics Letters*, vol. 67, pp. 1119-1121, 1995.

[18] D. A. Stocker, E. F. Schubert, and J. M. Redwing, "Crystallographic wet chemical etching of GaN," *Applied Physics Letters*, vol. 73, pp. 2654-2656, 1998.

[19] M. W. Cole, F. Ren, and S. J. Pearton, "Post growth rapid thermal annealing of GaN: the relationship between annealing temperature, GaN crystal quality, and contact-GaN interfacial structure," *Applied Physics Letters*, vol. 71, pp. 3004-3006, 1997.

[20] X. C. Wang, S. J. Xu, S. J. Chua, K. Li, X. H. Zhang, Z. H. Zhang, K. B. Chong, and X. Zhang, "Strong influence of SiO_2 thin film on properties of GaN epilayers," *Applied Physics Letters*, vol. 74, pp. 818-820, 1999.

[21] F. Ren, J. R. Lothian, S. J. Pearton, C. R. Abernahty, C. B. Vartuli, J. D. MacKenzie, R. G. Wilson, and R. F. Karlicek, "Effect of dry etching on surface properties of III-nitrides," presented at Low Energy Processes in Electronic Materials. Part of TMS Annual Meeting, Orlando, FL, 1997.

[22] S. J. Pearton, Feb. 18, 1999, personal communication.

[23] H. Ishikawa, S. Kobayashi, Y. Koide, S. Yamasaki, S. Nagai, J. Umezaki, M. Koike, and M. Murakami, "Effects of surface treatments and metal work functions

on electrical properties at p-GaN/metal interfaces," *Journal of Applied Physics*, vol. 81, pp. 1315-1322, 1997.

[24] M. Suzuki, T. Kawakami, T. Arai, S. Kobayashi, Y. Koide, T. Uemura, N. Shibata, and M. Murakami, "Low-resistance Ta/Ti Ohmic contacts for p-type GaN," *Applied Physics Letters*, vol. 74, pp. 275-277, 1999.

[25] J. T. Trexler, S. J. Pearton, P. H. Holloway, M. G. Mier, K. R. Evans, and R. F. Karlicek, "Comparison of Ni/Au, Pd/Au, and Cr/Au metallizations for ohmic contacts to p-GaN," presented at III-V Nitrides Symposium, Boston, MA, 1996.

[26] K. Taek, K. Jinseok, C. Suhee, and K. Tae-Il, "Low resistance contacts to p-type GaN," presented at Gallium Nitride and Related Materials II. Symposium Gallium Nitride and Related Materials II., San Francisco, CA, USA, 1997.

[27] Z. Fan, M. W. Kim, A. E. Botchkarev, K. Suzue, H. Morkoc, K. Duxstad, and E. E. Haller, "Ohmic contacts and Schottky barriers to n-GaN," presented at Symposium on Materials Science of Contacts, Metallization and Interconnects, Anaheim, CA, 1996.

[28] D. Hofstetter, R. L. Thornton, L. T. Romano, D. P. Bour, and N. M. Johnson, presented at Materials Research Society Fall '97 Meeting, Boston, MA, 1997.

[29] M. P. Mack, A. C. Abare, M. Aizcorbe, P. Kozodoy, S. Keller, U. Mishra, L. A. Coldren, and S. P. DenBaars, "Room temperature pulsed operation of blue nitride laser diodes," presented at Second International Conference on Nitride Semiconductors, Tokushima, Japan, 1997.

[30] J. Piprek, R. K. Sink, M. A. Hansen, J. E. Bowers, and S. P. DenBaars, "Simulation and Optimzation of 420 nm InGaN/GaN Laser Diodes," presented at Physics and Simulation of Optoelectronic Devices VIII, 2000.

Chapter 5

Gold-bonded laser diodes

The first chapter presented the current state of electrically pumped nitride laser diodes. The second chapter described the fabrication of cleaved facets for nitride lasers. Chapter 3 detailed methods for improving these structures and chapter 4 described the successful fabrication of cleaved-facet nitride lasers.

This chapter is a combination of the first four chapters. It starts with the cleaved-facet laser of Chapter 4 and demonstrates a method for implementing some of the improvements for the laser that were described in Chapter 3. The method used to form the facets was not described specifically in Chapter 2, but is closely related to the method based on wafer fusion that was described in that chapter.

The method described here is to use gold bonding to attach a GaN laser structure to another substrate. The sapphire substrate can be removed by laser ablation. Several other groups have used this method recently in order to remove the sapphire substrate from nitride epitaxial layers. A ridge-waveguide laser is then fabricated from this structure. Cleaved facets for the laser are formed using cleaved planes of the mount substrate.

5.1. Motivation

This new method offers a number of potential improvements over the cleaved-facet laser presented in the last chapter. These improvements include smoother cleaved facets, choice of substrate, better heat dissipation, and reduced electrical resistance. In addition, GaN devices can be integrated with other devices through this process.

The first advantage is the ability to obtain smoother cleaved facets. As described in Chapter 2, the cleave planes of a-plane sapphire are not parallel to those of c-plane GaN. The 2.4º misorientation between the cleave plane of the sapphire and the cleave plane of the GaN causes the GaN to fracture instead of

cleaving smoothly. This rough fracture significantly degrades the mirror quality and reduces the power reflected by the facet. Using the gold bonding technique, the cleave planes of the substrate can be lined up with the cleave planes of the GaN to make a much smoother cleave. Perfect alignment may be difficult, but by careful alignment, rotational accuracy of <0.2º should routinely be possible for the bonded wafers. This is close enough in alignment to allow the GaN to break along its crystal planes. The GaN is structurally separate from the substrate. This allows the substrate cleave plane to provide a direction for the GaN cleave, but not to force it to fracture along a non-cleave plane of the GaN as in the sapphire case. Note that this physical separation can also be a negative if the cleave does not propagate across the metal bonding layer. In my experience, the nitride layers did cleave well. Further details will be discussed later in this chapter.

The second advantage to the gold-bonded structure is that any choice of substrate can be made. The choice of substrate can be based on thermal conductivity, electrical conductivity, transparency, or thermal expansion. For high power electronic devices, heat dissipation is a huge problem. For such structures, the sapphire substrate can be removed and the device can conceivably be bonded between two separate heat spreading substrates to maximize the heat dissipation of the device. For the laser diode, p-side down mounting (mounted with the p-type material closest to the heat sink) yields a significant improvement in heat dissipation. Since most of the heat is generated in the p-type material and at the p-type contact, a device mounted p-side down has a reduced thermal resistance for the heat to flow out of the structure. This implies a lower operating temperature for the device. Alternatively, if a substrate with a low resistivity is chosen, then the total device resistance can be made very low. Reducing the device resistance reduces the heat generation in the device and therefore also reduces the operating temperature of the laser diode.

The third advantage is high-speed operation. With the proper design, high speed operation of these laser diodes can be achieved. This design has the advantage of making the ground plane very close to the top contact. This allows the design of a structure that is impedance matched to a 50Ω transmission line for improved injection of microwave power [1].

5.2. Device fabrication

The laser process that is used to fabricate laser diodes by this method is quite a bit different than the method described in Chapter 4. Most of the steps become easier for this process. In addition, there are 60% fewer mask steps (two compared to five) than for the cleaved-facet laser, but there are a few additional steps necessary for the gold bonding and laser ablation.

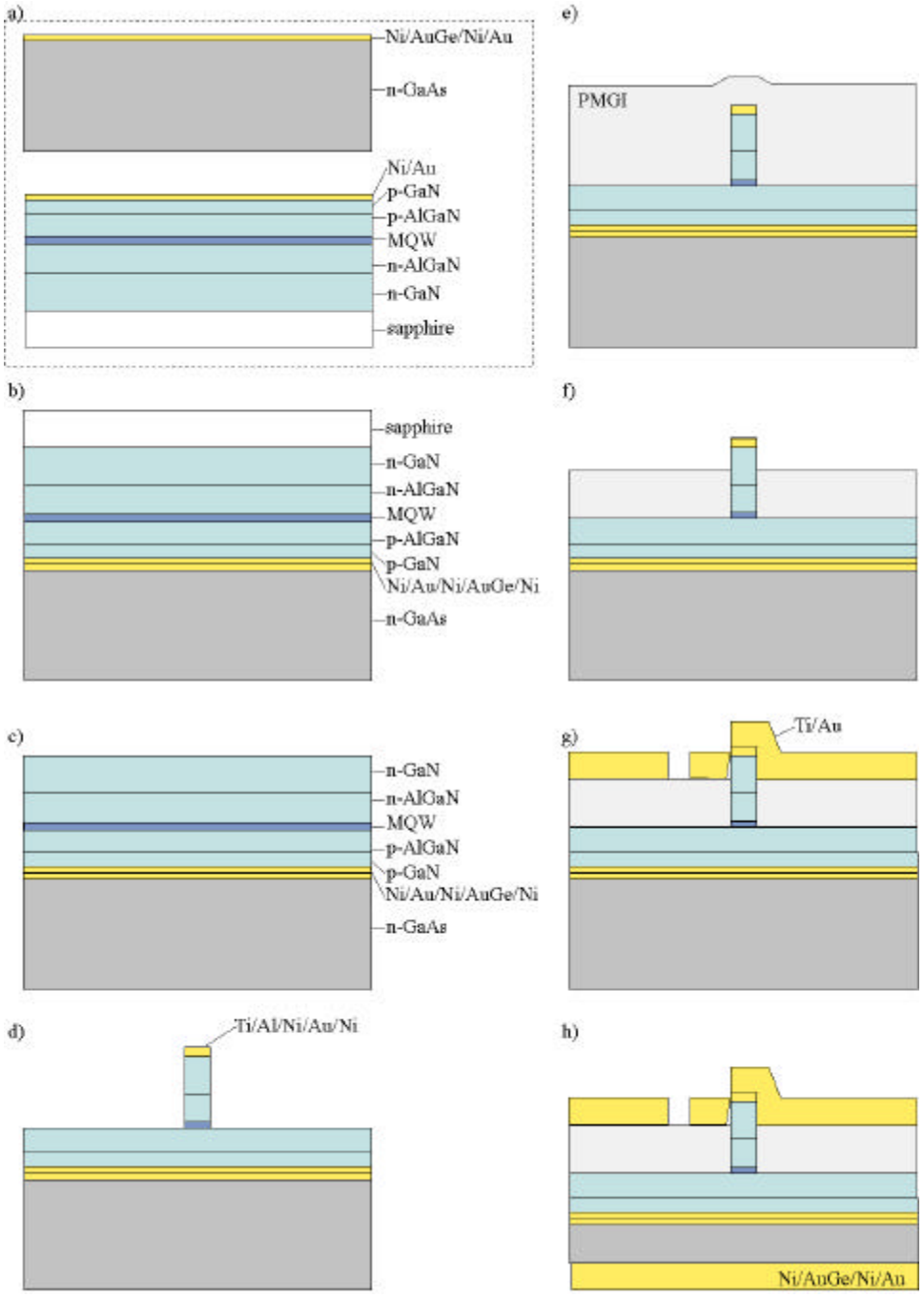

Figure 1. Processing schematic for fabricating a laser based on gold bonding of GaN to GaAs.

After MOCVD growth of the nitride laser structure, the laser structure and the n^+-GaAs substrate are diced into pieces 8x9 mm. Both the laser structure and the n^+-GaAs substrate are cleaned with solvents and oxygen plasma. The p-type GaN in the laser structure must be activated: 100 nm of SiO_2 is deposited by PECVD and the laser samples are annealed at 950ºC for 3 minutes. A 10-minute BHF etch and a 30-second HCl 1:1 etch are used to remove the SiO_2 and any GaNO that has formed at the SiO_2/GaN interface. The n^+-GaAs is etched for 30 seconds in HCl 1:1 to remove the native oxide. Thin contacts are deposited by e-beam evaporation onto each sample: Ni/Au (10/50 nm) for the p-GaN contact and Ni/AuGe/Ni/Au (5/100/20/40 nm) for the n^+-GaAs contact (Figure 1a). The samples are then bonded together under pressure for 90 minutes at 350ºC (Figure 1b). Care is taken to align the cleave planes of the two samples during bonding.

Once the samples are bonded, laser ablation is used to remove the sapphire substrate from the GaN laser structure (Figure 1c). Laser ablation will be discussed in more detail later in this chapter. The sample is then etched in HCl 1:3 for 1 minute to remove the gallium that remains on the laser ablated surface of the GaN. At this point, the GaN epitaxy has been transferred to the Au/GaAs substrate. It can now be patterned into a laser.

A short RIE etch is done to remove the highly defected layer of GaN. The substrate is patterned with photoresist and a Ti/Al/Ni/Au/Ni (7/200/20/200/250 nm) contact is deposited by e-beam evaporation. This contact is then used as the etch mask for RIE etching the ridge in the GaN (Figure 1d). The etching of the ridge is necessary to limit current spreading in the n-type GaN. It also provides beneficial index guiding for the optical laser mode.

The next step is to define the contact pads for the laser. An insulating layer of PMGI is spun onto the surface. An etch back process is used to expose the tops of the ridges and leaves the other regions covered with PMGI. A photoresist

mask is then used to lift off contact pad metal that is deposited at a slight angle by e-beam evaporation: Ti/Au (10/800 nm).

A simpler alternative to the PMGI pads was tried, but shorting of the final devices resulted. This alternative is presented here with the hope that the shorting problem will be solved by PEC etching, which is described in the next chapter. The alternative process is to angle evaporate a layer of SiO_2 over the top of the ridge. Two planarizing layers of 4330 photoresist can be spun onto the wafer and developed back until the tops of the ridges are exposed. At this point, BHF 1:10 can be used to etch the only SiO_2 on the tops of the mesas. The photoresist can be removed and the thick contact pads can be angle evaporated onto the structure (Figure 2). This process cannot be used with the PMGI process because the PMGI is too thick, which makes the effective shadow of the ridge too short to provide separation of the contacts when the contacts are angle evaporated. So for the PMGI process, an additional mask step is necessary for the patterning of the liftoff mask for the thick contact pads. Unfortunately, this process results in shorted contacts due to pinholes in the SiO_2. These pinholes are caused by depositing SiO_2 on RIE roughened GaN.

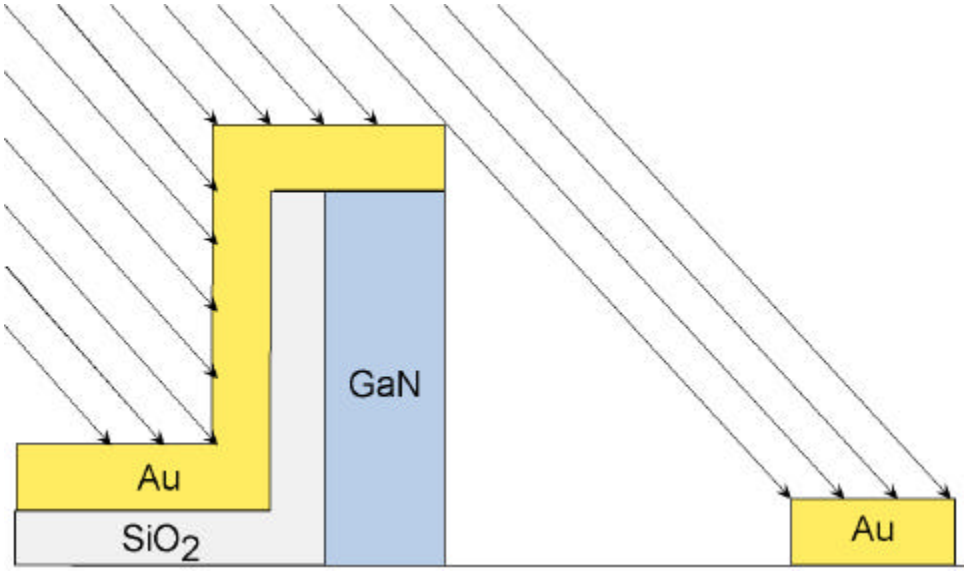

Figure 2. Angled evaporation over a ridge provides a physical separation for the contact metal on one side of the ridge from the metal on the other side of the ridge.

Using either the PMGI process or the SiO_2 process, the lasers are now done. The GaAs substrate can be thinned and the devices cleaved. Cleaving is performed by making a scribe mark on the GaN side of the wafer. This cleaving works much better than that of sapphire.

This process is slightly less complicated than the process used for the cleaved-facet lasers that was presented in Chapter 4: For this process, there is only a single etch step. The other process had two steps. Sapphire thinning is not necessary with this process. Instead, easy GaAs thinning is used. Cleaving is easier due to the use of GaAs cleave planes instead of sapphire cleave planes. Finally, only two mask steps are used in comparison with five mask steps for the previous process. (If the SiO_2 process is used, there is only one mask step.)

5.2.1. Dicing compared to scribe and break

For gold bonding, having two samples that are close in size is required and having the cleave planes oriented correctly is critical to being able to cleave

along the proper planes at the end of the process. Since the dicing saw is more accurate than scribe and break in both alignment and size, it is used to cut both the GaN and GaAs samples before bonding.

The problem with the dicing saw is that it leaves jagged, cracked edges that act as scribe marks when cleaving. The scribe and break method provides superior results if the sample is thin enough to have the break occur along the desired direction. In the case of the GaAs substrates, scribe and break is used to break the sample into smaller strips for final facet cleaving.

For the sapphire substrates used in Chapter 4, however, dicing was found to be more reliable. When roughness of the edges is important, as in the dicing of the final sapphire substrate in the cleaved-facet laser of Chapter 4, care is taken to choose the proper blade speed, blade type, and mounting conditions in order to get the smoothest edges. More details are given in Appendix E.

5.2.2. Gold bonding

Once the samples are diced, the p-type GaN contacts and n-type GaAs contacts are put down. These contacts serve as the glue for bonding the two wafers. Gold bonding is a simple process that involves putting two gold-coated samples together with heat and pressure. The fixture described in Chapter 2 that was used for wafer fusion is used for gold bonding [2, 3]. A commercial flip chip bonder has also been used, but the samples mated in the commercial bonder are only loosely held together after bonding. The maximum pressure that is available on this machine is not high enough for gold bonding.

Using the same type of fusion fixture, other published reports indicate that long bonding times at low temperatures are optimal for preventing metal spiking. Tauber published 300ºC bonding temperatures with 4 hour bonding times and 1ºC/minute cool down times [1]. Metal spiking into the GaAs is not important for this device. The temperature used for this process is somewhat higher than

300ºC. The temperature required for metal spiking in GaN is believed to be significantly higher than that required for spiking in GaAs due to the strong bond strength and high temperature stability of GaN.

The gold bonding process has been optimized experimentally and good adhesion is achieved with a slightly faster bonding cycle using the higher temperature: 350ºC with a bonding time of 90 minutes. Cooling rates as fast as 3ºC/minute do not result in reduced bonding strength. Faster cooling rates have not been tried, but may be suitable as well. If the cooling rate is too fast, then the difference in thermal expansion coefficients between the sapphire and the GaAs will break the gold bond during cooling. By cooling very slowly, the gold is given time to migrate to relieve the stress associated with the thermal expansion difference.

It is critically important to have a clean metal surface and to have smooth epitaxial growth of the GaN laser structure. Large surface topology in the metal or in the epitaxy will lead to poor bonding.

5.2.3. Laser ablation

Once the GaN and GaAs structures are bonded, the sapphire substrate can be removed by laser ablation. Attempts to remove the sapphire substrate without having a good gold bond resulted in flaking off of the GaN structure during the laser ablation process. For this reason, a strong gold bond is important.

Laser ablation for GaN was first presented as a technique for rapid etching of GaN. In 1996, Kelly, et al. showed that a laser above bandgap can be used to decompose GaN by heating the sample to induce the desorption of nitrogen from the surface [4]. The residual gallium is etched away by an HCl solution in which the sample was submerged. Etch rates as high as 70 nm/pulse are obtained with laser power densities of 0.4 J/cm^2 at 355 nm. Other groups have now demonstrated similar etching rates [5, 6].

Kelly, et al. have continued to develop their etching process to achieve etch rates as high as 330 nm/sec. They have also developed a process for removing small pieces of GaN from a sapphire substrate [7, 8]. Wong, et al. improved this process by bonding the GaN to a silicon wafer with epoxy, which has allowed them to separate GaN from sapphire on full 3x4 mm pieces of GaN using laser pulses power densities of 400-600 mJ/cm^2 [9]. When this laser ablation occurs the film changes from transparent (for visible light) to slightly reflective and gray in color. This indicates that the nitride layers have decomposed and that the sapphire substrate can be removed. Wong removed the substrate by heating the sample above the melting point of gallium and sliding the GaN/epoxy/Si stack off of the sapphire [9].

The gold bonding technique presented in this chapter is believed to be an improvement over the epoxy bonding process because it holds the GaN film more rigidly and prevents cracking of the GaN film as the laser beam is rastered over the surface of the GaN. This should allow larger samples to be removed.

A spot size of approximately 3x9 mm is created using a lens with a 500 mm focal length to reduce the beam size from a 248 nm KrF eximer laser. This lens is used in order to increase the peak power of the laser. Short 10 ns pulses were used with an experimentally optimized laser power of 110-140 mJ/pulse.

Optimization of the laser power density was performed by keeping the laser spot size the same and varying the pulse energy. The area that is ablated is dependant on the pulse energy. An example is illustrated in Figure 3. The ablated area for a 110 mJ pulse is approximately 2 mm^2 (Figure 3a) the ablated area for a 220 mJ pulse is approximately 8 mm^2 (Figure 3b). Using pulses with energies greater than 200 mJ/pulse have the advantage of decomposing a larger area of GaN, but these pulses have the disadvantage of creating a shock wave that breaks the gold bond in the surrounding area. This is not acceptable. So smaller pulse energies were chosen.

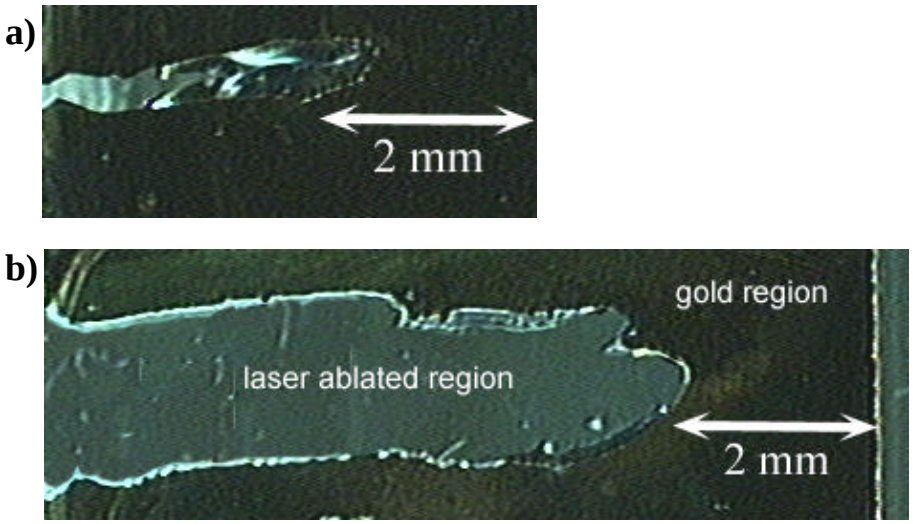

Figure 3. Area of GaN lifted off from a single pulse from an eximer laser a) for a pulse energy of 110 mJ and b) for a pulse energy of 220 mJ.

Thus, rastering of the laser beam using the lower power densities has been found to be the most effective technique for removing GaN from the sapphire substrate.

Note that pulses with energies less than 100 mJ did not ablate the material. However, defected material is removed for lower power densities. This is probably due to the fact that the absorption is higher for defected regions. In addition, defected regions do not bleach as rapidly because there are more electron states available for excitation and because the recombination lifetime is significantly shorter than the pulse width in these regions due to the non-radiative recombination paths available at defect sites.

5.2.4. Cleaving facets

After removing the sapphire substrate, the patterning of the devices is relatively easy and proceeds according to standard processing methods as described in the last chapter. Once the laser diodes have been fabricated, the cleaving process for the gold-bonded lasers is much easier than for the lasers on sapphire substrates.

Thinning GaAs to 100 μm is straightforward and the cleave planes of GaAs are easy to use. Also, since the GaAs and GaN are separated by a compliant metal layer, the GaAs cleave planes do not break through the GaN epitaxial layers. Instead the GaAs cleave plane provides a fulcrum around which the GaN is cleaved.

This physical separation can pose a problem for cleaving the GaN if proper care is not taken. Since the cleave does not propagate directly from the GaAs, it is important to not etch all the way through the GaN during the etching of the ridge waveguide. If the GaN ridge etch extends to the gold layer, then there will be isolated GaN mesas on the surface. Trying to cleave the isolated mesas results in many undesired cleaves instead of a single cleave plane for the entire laser bar. If at least 0.5 μm of GaN is left on the surface, the GaN cleaves easily across the entire length of the bar in the desired cleave plane.

This makes the RIE etch step a difficult step because the etch must stop within 0.3 μm of the active region for ideal performance, which is difficult after approximately 4 μm of etching. If the etch is too deep, the cleave will not be good because the remaining GaN is not thick enough to propagate the cleave. If the etch is not deep enough, then the low resistivity n-type material will induce significant current spreading in the laser. Ideally, the etch stops slightly below the active region. This will give better performance by eliminating current spreading in the n-type GaN and in the MQW region, while still providing a thick enough GaN layer for cleaving.

As mentioned above, the suitable etch depth is within 0.3 μm of the active region. The etch is made more difficult by the thickness variations in the GaN film. For a 5 μm film, these thickness variations can be significant. So even if the etch is done optimally on one side of the sample, the other side of the wafer may be significantly over or under etched. As a solution to this problem, the use of PEC etching will be described in the next chapter. This etch technique etches n-

type material selectively over p-type material and can be used to accurately etch down to the MQW region.

The cleaved facets of finished devices are presented in Figure 4. This figure shows the process with the SiO_2 mask for the top contact. Angled evaporation over the ridge was used to separate the contacts of the laser bars. A picture of a facet fabricated with the PMGI process is shown in the next section.

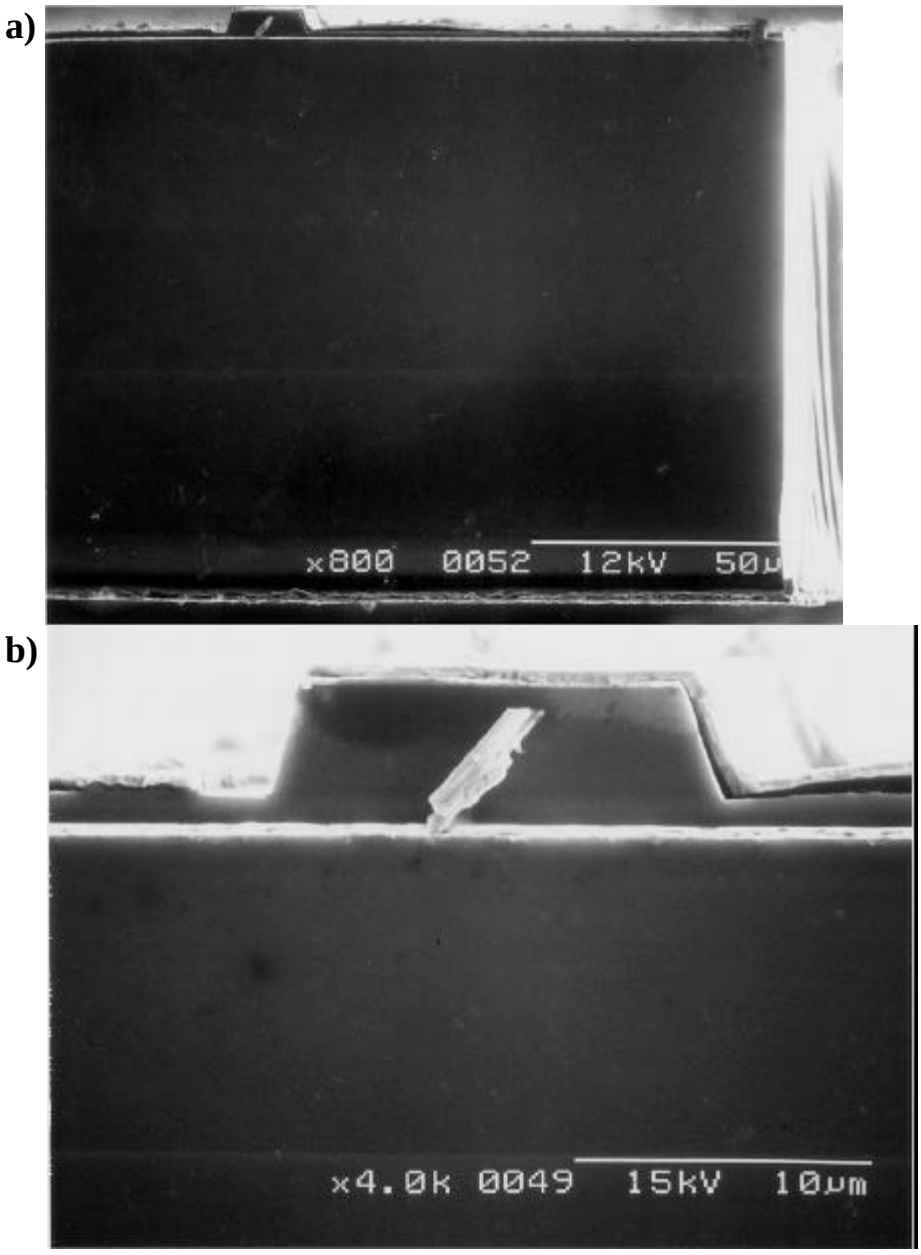

Figure 4. Cleaved facet formed in gold-bonded laser structure. a) GaAs and GaN facets cleave well. b) Close up of GaN facet.

5.3. Results

Several iterations of this process have been performed and many of the problems with the devices have been worked out. This section presents the results for some of these devices. The differences between the SiO_2 isolated devices and the PMGI isolated devices are discussed and IV curves for the fabricated devices are presented. Unfortunately, the active region appears to degrade during the laser ablation removal of the sapphire substrate. This results in very dim emission from the final laser diodes. The last part of this section describes two physical mechanisms that are likely causes of the active region degradation.

The first few iterations of these laser diodes used SiO_2 layers as the insulator for the contact pads, but these structures shorted very quickly when tested. The cause of this is believed to be that the GaN epitaxial layer was very rough after the 4 μm RIE etch. This meant that thin 100 nm SiO_2 had difficulty covering the entire surface. If the surface roughness has very sharp peaks, the non-conformal e-beam evaporation of SiO_2 over these regions would have coated these regions with only a very thin layer of SiO_2. These thin regions would short out quickly at the high voltages that are applied for the nitride lasers. Double-layer SiO_2 films were also tried with the hope that they would reduce the density of pinholes in the oxide, but similar results were obtained.

The PMGI based devices operate much better than the SiO_2 based devices. The SiO_2 devices shorted consistently, while very few of the PMGI based devices short at pulsed currents of up to 3 A. The PMGI based devices are not as easy to cleave, however, due to the thick amorphous structure of the PMGI. Most masks that are designed for use with PMGI that have cleaved facets leave gaps in the PMGI for cleaving the devices. The mask set for these devices does not have these gaps because it was designed for use with the SiO_2 process. So there is no separate mask for the PMGI process and hence no gap for cleaving. The cleaving

does still work for these devices, but it is not as easy as it was with the SiO_2 based structures.

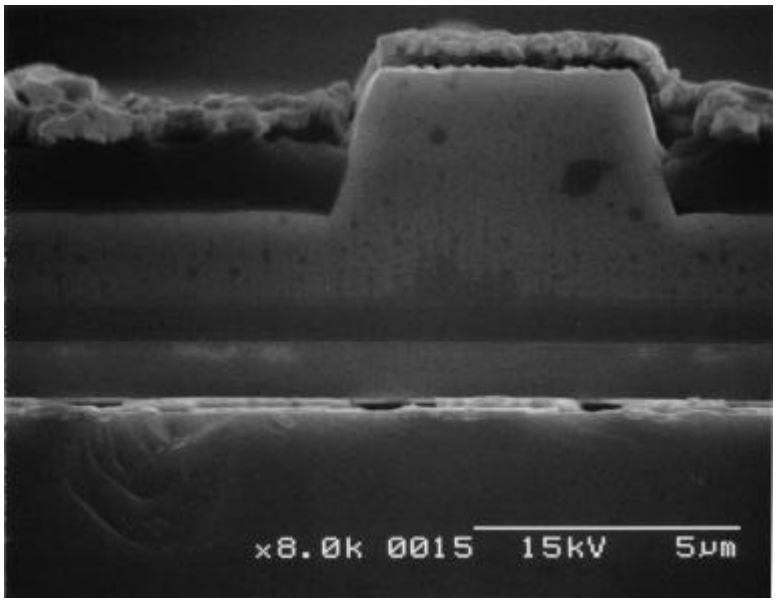

Figure 5. Cleaved facet in GaN formed with PMGI insulated contact pads.

As presented in Figures 4 and 5, cleaved-facet devices have been produced by both methods and these devices have been tested. Premature shorting occurs only for devices fabricated with the SiO_2 process or for devices fabricated on material with a large crack or high defect density. Typical devices fabricated with the PMGI process fail as open circuits when the contact metal burns around the edge of the mesa. This typically occurs for a current of 2.5 A at a voltage of 60 V.

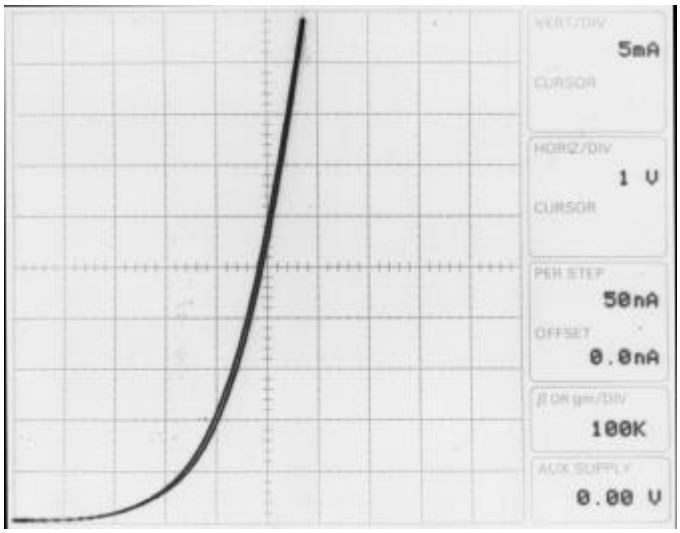

Figure 6. Current-voltage characteristics of nitride laser structure gold-bonded to n^+-GaAs substrate.

Unfortunately, even though the shorting problem with these devices has been solved, the light emission from these devices is still extremely dim. This is believed to be due to degradation of the active region. There are two likely causes for this degradation. The first possible degradation mechanism is cracking of the GaN film. The thick claddings used for the laser structure put the laser structure under large amounts of strain. For most growths of laser structures, cracks are seen in the epitaxy immediately after growth due to the large amount of strain in the thick AlGaN layers. When an explosive shock occurs in the crystal—such as that provided by the laser pulse used in laser ablation—the stress on the film may momentarily increase, resulting in cracking of the film. Qualitatively there does **not** appear to be a dramatic increase in visible crack density after the laser ablation. This is still a possibility as a degradation mechanism though. For higher power densities, significant cracking is observed. It is believed that for the power densities presented here, similar cracking is occurring, but only on a smaller scale. For small devices, such as LEDs or VCSELs, this cracking may be sparse enough that most devices survive the

ablation with little degradation. However, in plane lasers cover a large area. Therefore, many cracks can affect a single device. Even a small increase in the density of cracks causes a dramatic increase in lasing threshold by increasing scattering loss, by providing non-radiative recombination sites, or by providing leakage current paths.

The second potential degradation mechanism is heating. Since the laser pulse removes the substrate by heating the sample locally, the heat generated is large enough to decompose the material at the interface between sapphire and GaN. The thermal conductivity of GaN is much better than that of sapphire. Therefore, a large percentage of the thermal energy spreads first into the GaN before it has the chance to dissipate through the sapphire or GaAs substrates. This large thermal energy can cause 1) diffusion of the indium atoms, which reduces the quantum confinement in the quantum wells or 2) diffusion of the dopant atoms to move the pn junction out of the MQW gain region. For either of these two diffusion types, the lasing threshold is increased because the QWs no longer provide enough gain for the laser.

5.4. Conclusion

In summary, laser ablation has been used to successfully transfer GaN epitaxial layers from sapphire substrates to Au/GaAs substrates. These devices have respectable current-voltage response, but are much dimmer than the devices fabricated by the method described in Chapter 4. This dimness is believed to be caused by the degradation that occurs during the laser ablation. The most likely of the proposed degradation mechanism is believed to be diffusion of dopants during the laser ablation process. This moves the pn junction position out of the MQW layers and thus reduces the laser gain.

5.5. References

[1] D. Tauber, "Design And Performance Of InGaAsP/InP Semiconductor Microstrip Lasers," Ph.D. Dissertation: ECE Department, University of California, Santa Barbara, 1998.

[2] D. I. Babic, "Double-fused long-wavelength vertical-cavity lasers," Ph.D. Dissertation: ECE Department, University of California, Santa Barbara, 1995.

[3] N. Margalit, "High-temperature long-wavelength vertical-cavity lasers," Ph.D. Dissertation: ECE Department, University of California, Santa Barbara, 1998.

[4] M. K. Kelly, A. O. Ambacher, B. Dahlheimer, G. Groos, R. Dimitrov, H. Angerer, and M. Stutzmann, “Optical patterning of GaN films,” *Applied Physics Letters*, vol. 69, pp. 1749-1751, 1996.

[5] J. Zhang, K. Sugioka, S. Wada, H. Tashiro, K. Toyoda, and K. Midorikawa, “Precise microfabrication of wide band gap semiconductors (SiC and GaN) by VUV-UV multiwavelength laser ablation,” presented at Fourth International Conference on Laser Ablation, Monterey Bay, CA, USA, 1998.

[6] J. Zhang, K. Sugioka, S. Wada, H. Tashiro, and K. Midorikawa, “Study on high-speed deep etching of GaN film by UV laser ablation,” presented at Second International Conference on Nitride Semiconductors, Tokushima, Japan, 1998.

[7] M. K. Kelly, O. Ambacher, R. Dimitrov, H. Angerer, R. Kandschuh, and M. Stutzmann, “Laser-processing for patterned and free-standing nitride films,” presented at Nitride Semiconductors Symposium Nitride Semiconductors Symposium, Boston, MA, USA, 1998.

[8] M. K. Kelly, O. Ambacher, R. Dimitrov, R. Handschuh, and M. Stutzmann, “Optical process for liftoff of group III-nitride films,” *Physica Status Solidi A*, vol. 159, pp. R3-4, 1997.

[9] W. S. Wong, T. Sands, and N. W. Cheung, “Damage-free separation of GaN thin films from sapphire substrates,” *Applied Physics Letters*, vol. 72, pp. 599-601, 1998.

Chapter 6

Conclusions and future work

The research described by this dissertation has focused on the design and improvement of nitride laser diodes. The last two chapters have described two distinctly different processes for fabrication of in-plane nitride laser diodes. A successful demonstration of cleaved-facet laser diodes was presented in Chapter 4. Chapter 5 described an improved novel type of laser diode process based on gold bonding and laser ablation. This chapter will describe the methods by which the gold-bonded laser process can be improved and gives a critique of this process. The last section of this chapter gives suggestions for improving device operation and outlines the advantages of using GaN or SiC substrates instead of sapphire for the development of CW laser diodes.

6.1. Gold-bonded laser improvements

The gold-bonded laser process can be improved in several ways. This section describes two of those ways. The first way is by using photoelectrochemical (PEC) etching to improve the control of the ridge etch. The second improvement is to use a larger beam area for laser ablation in order to reduce the degradation of the active region material.

6.1.1. Photoelectrochemical (PEC) etching

The first improvement addresses the problem that the ridge etch, which is done by RIE is difficult to control due to the lack of a stop etch layer in the laser structure. As explained in the last chapter, this lack of control is a problem because the etch needs to stop within 0.3 μm of the active region. If the etch is too deep, then the laser bars are difficult to cleave well because the GaN layer is too thin to propagate the cleave across the entire length of the laser bar. If the etch is too shallow, the low resistance n-type material is not removed completely from the sides of the ridges and current spreading occurs in the n-type region above the active region.

PEC etching offers a solution to this problem. PEC etching is a selective etch that etches n-type GaN, but does not etch p-type GaN. This means that it can be used to accurately stop at the pn junction (active region).

There is one potential problem: the high defect density of GaN has been reported to cause non-uniform etching in n-type material and etching in defected regions of p-type material. Very low quality GaN can even be etched without light [1]. However, with an understanding of the etch chemistry, this problem can be reduced. Youtsey, et al. noticed that the defects in PEC etching can cause localized enhancement or reduction in the etch rate, but they also showed that smooth surfaces can be obtained by operating in the diffusion (reactant) limited regime (low etchant concentrations and high light intensities) [2].

A good overview of the chemistry involved is given in references [3] and [4]. The etching of GaN is believed to occur in two steps. The first is the formation of an oxide (ß-Ga_2O_3) and the second is the dissolving of that oxide in a strong base solution. The reaction is endothermic, meaning that it needs energy to occur. This energy is generated by the photoexcitation of electron/hole pairs at the surface of the semiconductor. (Instead of photogeneration of carriers, DC bias can also be used to provide the energy needed for the reaction [1].) P-type material is not etched because the holes are needed for the oxidation reaction to occur. For p-type material, "surface band bending" occurs at the semiconductor/electrolyte interface, which allows high energy holes to drift away from the surface of the semiconductor and making only low energy holes available for the oxidation reaction [5, 6]. Pt is used as the inactive cathode in the electrochemical cell [2].

Water is necessary for this reaction to take place. Experiments performed by Peng, et al. showed that if the solvent was switched to ethanol, the etching did not occur [4]. The authors propose that the oxygen used to form the oxide has its source in the free water molecules of the solution. Following the oxidation of the GaN, the oxide can be dissolved in either a strong acid or a strong base [4]. The

total etch rate is found to peak at pH values of 0.75 or 14.25. For stronger acids or bases, there are not enough free water molecules (ones that have not dissociated) available to oxidize the GaN film [4]. The photon provides energy to catalyze the oxidation reaction between the water molecule and the GaN film. The byproduct of this oxidation can then be etched away. KOH is most common etch solution because it gives the most rapid etch rates and the highest quality etches, although many solutions have been tried including HCl and H_3PO_4 [1-4, 6].

Smooth etches should be possible through optimization of the etch chemistry. Material quality is improving and should allow good selectivity for stopping on the p-type material. In addition, rapid etch rates can be achieved. Rates as high as 400 nm/minute have been reported [2]. Rapid etch rate, highly anisotropy in the <0001> direction, and p-type/n-type material selectivity make PEC etching a good choice for fabrication of the ridge-waveguide laser diode.

6.1.2. Laser ablation spot size increase

The second improvement that could be implemented for the gold-bonded laser process is to increase the laser ablation spot size so that the amount of material lifted off with each pulse was much larger than the area of a single laser diode.

As described in Chapter 5, the size of the area removed by a single pulse for the laser ablation process is approximately 0.5 x 4 mm. Degradation of the active region (reduced electroluminescence) was attributed to the laser ablation process. While localized heating is believed to be the primary cause of the degradation, the small spot size may also play a role. Since the sample is larger than this small spot size, the beam is rastered over the sample area to lift off the entire film. If the film is lifting off piece by piece, the strain caused as each of these pieces lifts off likely causes a large increase in the number of defects in the crystal. By increasing the area of the GaN that is removed by each pulse, some devices could

be fabricated that were in regions that do not experience a large increase in defect density.

The problem with this improvement is in trying to increase the power at the same rate as the area so that the power density stays the same. The typical maximum power for the laser is approximately four times the power that is currently used. Therefore, an increase in spot size from 0.5 x 4 mm to 1 x 8 mm could be expected by moving to maximum power using the same power densities that are presently used. This is not much of an improvement. Further improvement could come from improving the power density uniformity of the laser spot.

As described in Chapter 5, increasing the power density by a factor of two had more than a two-fold increase in the spot size. This also had the unfortunate side effect of breaking the gold bond for the surrounding GaN. Based on this experiment though, it does appear to be possible to liftoff a large area of GaN by using a larger power density in combination with a larger area. Further characterization is necessary to find the optimal laser parameters for ablating the largest area with a single pulse.

6.1.3. Outlook for the gold bonding process

After making these two improvements, will the lasers work? With more characterization of the laser ablation process and implementation of the two process improvements shown above, it probably would be possible to make a laser with this process. This type of laser process does have advantages over other types of lasers and may therefore be worth pursuing as an alternative to sapphire based nitride lasers. However, for this to be a viable process, the remaining problem of active region degradation must be addressed. Further characterization of the laser ablation process may be enough. This degradation is believed to be due to the heat generation near the active region. Optimization of

the laser ablation process would focus on developing a recipe to remove the most amount of material for the smallest increase in temperature.

I believe, however, that some degradation of the active region is inherent to the laser ablation process. The advantages that are gained by the gold bonding and substrate transfer will likely not be enough to overcome the substantial degradation in the electroluminescence. Researchers at Hewlett-Packard have been working with the Berkeley group to perform a similar laser ablation process for their LEDs. They have noticed similar degradation of the light output power. Other—better—options exist and will be discussed in the sections that follow.

6.2. Gold-bonded ELO GaN laser diodes

Since the gold bonding process offers a number of advantages over other sapphire based methods, it may be valuable to explore other options for removing the sapphire substrate. This section describes a similar gold bonding process that can be used for removing the sapphire substrate.

This method is based on the removal of ELO GaN by etching away the SiO_2 mask on which the ELO GaN wings rest and thereby freeing the substrate. To understand these methods, the growth of ELO GaN must be understood. The growth of ELO GaN is depicted in Figure 1.

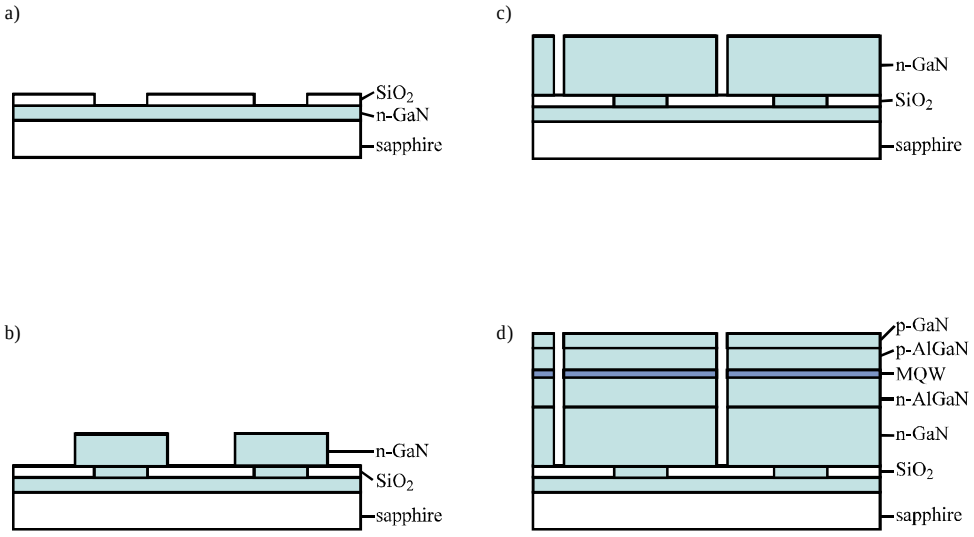

Figure 1. Growth process for epitaxial lateral overgrowth (ELO) of GaN.

An SiO_2 mask layer is patterned in stripes on top of a n-type GaN template layer (Figure 1a). Ga atoms have a low sticking coefficient to SiO_2. Therefore, most of the Ga atoms that are incident on the SiO_2 mask diffuse laterally until they reach the GaN. Nitrogen reacts with the Ga to for GaN. Thus, GaN grows up through the SiO_2 mask and then grows laterally along the top of the SiO_2 mask (Figures 1b and 1c). The remainder of the laser structure can then be grown (Figure 1d). ELO GaN has found many uses because it reduces the defect density in GaN by three or four orders of magnitude [7-10].

The ELO GaN structures can be gold bonded to another substrate as described in Chapter 5. Then the SiO_2 can be etched away to free the wings of the ELO from the sapphire substrate. However, this basic process must be modified to remove the ELO seed region, which lies in the SiO_2 mask openings. This GaN is still attached to the sapphire and is not undercut by removing the SiO_2. Therefore, some method of separating the ELO wing region from the ELO seed region must be developed. One such method is diagrammed in Figure 2. The first step of this method is to pattern the top of the mesa (Figure 2b) and etch through the entire

seed region until the SiO_2 mask is reached (Figure 2c). Following the etching, the ELO wings can be bonded to another substrate (Figure 2d) and then the SiO_2 mask can be etched away leaving the ELO wings bonded to the other substrate (Figure 2e). A photoresist mask can be etched back to expose the tops of the mesas (Figure 2f) for contact metallization and liftoff (Figure 2g).

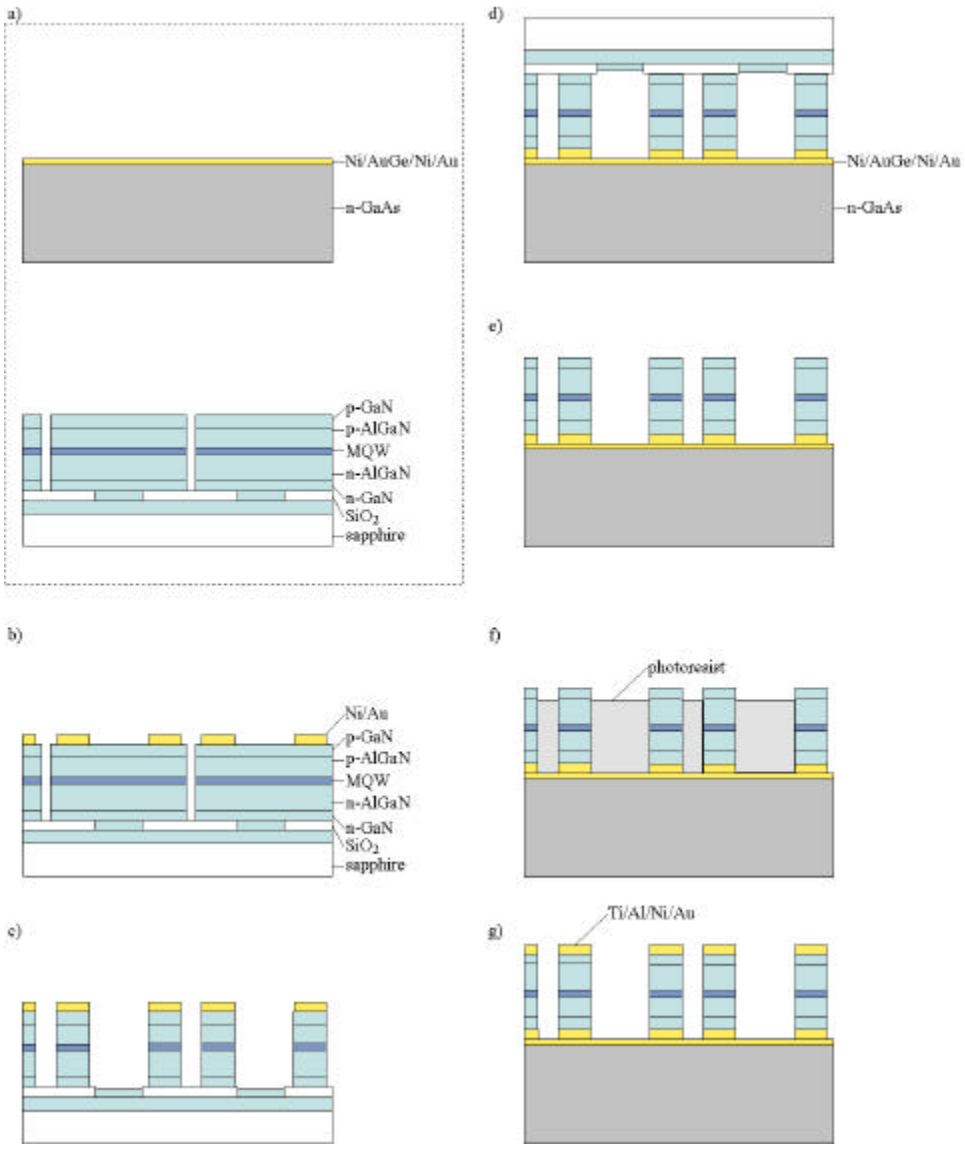

Figure 2. Process description for removing sapphire substrate for ELO GaN based laser structures.

There are two reasons that this method was not chosen originally. The first reason is that cleaving is difficult after the small ELO GaN wings are etched and lifted off. This difficulty is due to the metal layer that separates the GaN from the GaAs substrate. This limit can be worked around by using a very thin metal layer

on each side of the bonding surface or by using wafer fusion instead of gold bonding.

Another potential problem is the slope angle of the ELO GaN. When ELO GaN is grown, the c-axis of the wing material slopes away from the c-axis of the seed material by as much as 3º. This is a problem because at the end of a 15 μm wing, the ELO GaN is 0.8 μm below the top of the central portion of the ELO GaN. With careful control of the growth parameters, this slope has recently been reduced to less than 0.1º, which reduces the mismatch to 25 nm. This mismatch is small enough for gold bonding, but wafer bonding may still be difficult even at this reduced angle.

6.3. SiC substrates for nitride laser diodes

The gold-bonded laser is designed to have a number of advantages over other GaN lasers grown on sapphire substrates. These advantages include 1) easier formation of cleaved facets, 2) better heat dissipation, and 3) lower device resistance due to the bottom contacted structure in comparison to a laterally contacted structure. These advantages can also be obtained by growing GaN on SiC. SiC has cleave planes which are easy to use, are vertical, and are true cleave planes as opposed to fracture planes as described earlier for sapphire. SiC is an excellent heat spreader due to its high room temperature thermal conductivity (see Table 1). Also, with the introduction of a conductive buffer layer, bottom contacts can be used on SiC to reduce device resistance and make packaging easier.

	Thermal conductivity at 300 K (W/cm K)
sapphire	0.4
GaAs	0.45
GaN	1.3
Si	1.5
SiC	5
CVD diamond	12-18

Table 1. Thermal conductivity comparison for materials used in GaN lasers. Sapphire is a good thermal conductor at low temperatures, but is much worse at room temperature. The room temperature thermal conductivity of SiC is an order of magnitude larger than that of sapphire.

SiC has many technological advantages over sapphire as a substrate for MOCVD growth of GaN. However, there are only a handful of groups growing GaN on SiC substrates compared to several dozen growing GaN on sapphire substrates. The popularity of sapphire is due to several factors. The first is that initial growth quality on SiC was not as high quality as that on sapphire. Nakamura, a researcher at Nichia, said publicly that Nichia tried growing GaN on SiC and that the material quality was not as good. The second reason for the popularity of sapphire is that it is cheap: Polished 2"-6" sapphire wafers cost about $\$40/in^2$. For comparison, 2" wafers of good quality SiC are just becoming commercially available, but are approximately $\$500/in^2$. (The ideal substrate for GaN epitaxy would be GaN, but these are only available from laboratory HVPE reactors at this time. Sumitomo Electric has advertised that they will begin selling GaN substrates next year [11].)

Cree, Inc. fabricates SiC substrates and has been the leader in fabricating GaN lasers on SiC. High quality material has been demonstrated and GaN lasers operating in CW mode have been demonstrated on SiC [12]. With the introduction of a conductive buffer layer for SiC [13], most of the advantages of the gold-bonded laser process can be achieved with by growing the nitride lasers

on SiC. Nitride lasers on SiC can be gold bonded after fabrication onto diamond heat sinks to achieve even better thermal conductivity.

Nakamura is now growing very thick ELO GaN layers (80 μm) and is removing the sapphire substrates by lapping. With this process, Nakamura is able to arrive at many of the same advantages that are found in SiC substrates, such as cleaved facets, good thermal conductivity, good electrical conductivity, and conductive substrates [14-16].

There is one advantage that sapphire has over SiC. This is in strain relief incorporated in the ELO growth process. Effective strain relief has not been demonstrated on sapphire or SiC substrates. For that reason, ELO GaN (first introduced by Nakamura [17]) has been used to obtain low defect densities. The strain reduction that is obtained by ELO allows Nakamura to grow thick AlGaN cladding regions, which are important for low loss structures [10]. If SiC is chosen as the substrate for GaN lasers, the important question of how to increase the cladding region thickness without introducing cracks is still a significant problem to solve. There is no reason why ELO cannot be used on SiC as well. So this should not pose a significant problem in the long term.

In summary, SiC offers many advantages over sapphire for making nitride laser diodes. These advantages have not made SiC the popular choice for GaN epitaxy, however. This lack of enthusiasm for SiC stems from initial reports of poorer material quality for GaN on SiC, an order of magnitude higher substrate cost for SiC over sapphire, and a relatively low volume production of SiC worldwide. Transferring ELO technology to SiC may create the strain relief needed for growth of high quality GaN and thick AlGaN cladding regions. Despite its slow start, SiC has proven to be a viable option for fabrication of nitride laser diodes. CW operation has been demonstrated on SiC substrates and substrate prices continue to fall as larger volumes of SiC become available from Cree, Inc.

6.4. Achieving CW operation of nitride lasers

To achieve CW operation of nitride laser diodes at UCSB, focused improvement in several areas needs to occur. 1) Strain relief or strain compensation needs to be incorporated so that thicker AlGaN cladding regions can be grown. This will reduce the modal loss significantly. 2) Heat dissipation needs to be improved by flip chip bonding to diamond heat spreaders or fabrication of laser diodes on a substrate with better thermal conductivity such as GaN or SiC. This will reduce the active region temperature significantly. 3) Loss mechanisms need to be identified and their effects reduced. For example, loss due to free carrier absorption in the n-type GaN template region has not been explored, but may be significant. Reducing the doping levels in this region may cause a significant reduction in loss. This doping reduction will cause a slight increase in resistance for side-contacted structures like that laser grown on a-plane sapphire that was described in Chapter 4. However, for conductive substrates, such as SiC or GaN, the conduction path will be vertical, which means that the conductivity of this layer will not be as important. 4) High quality cleaved-facet mirrors need to be fabricated. SiC and GaN substrates both have vertical cleave planes that can be used effectively. Alternatively, dry etched mirrors can be fabricated and then cleaned up with a crystallographic etch as described in Chapter 4 [18]. 5) Decreasing p-type material resistivity and reducing p-type contact resistance will reduce the operating voltages of these devices and allow for much lower operating temperatures. Based on all of the required improvements, growth on SiC or GaN substrates is recommended for fabrication of a nitride laser diode operating in CW mode.

6.5. References

[1] S. Yoshida, "Electrochemical etching of a conductive GaN crystal for patterning," *Journal of Crystal Growth*, vol. 181, pp. 293-296, 1997.

[2] C. Youtsey, I. Adesida, L. T. Romano, and G. Bulman, "Smooth n-type GaN surfaces by photoenhanced wet etching," *Applied Physics Letters*, vol. 72, pp. 560-562, 1998.

[3] L.-H. Peng, C. W. Chuang, Y. C. Hsu, J. K. Ho, C. N. Huang, and C. Y. Chen, "Hydration effects in the photoassisted wet chemical etching of gallium nitride," *IEEE Journal of Selected Topics in Quantum Electronics*, vol. 4, pp. 564-569, 1998.

[4] L. H. Peng, C. W. Chuang, J. K. Ho, C. N. Huang, and C. Y. Chen, "Deep ultraviolet enhanced wet chemical etching of gallium nitride," *Applied Physics Letters*, vol. 72, pp. 939-941, 1998.

[5] C. Youtsey, I. Adesida, and G. Bulman, "Broad-area photoelectrochemical etching of GaN," *Electronics Letters*, vol. 33, pp. 245-246, 1997.

[6] M. S. Minsky, A. M. White, and E. L. Hu, "Room-temperature photoenhanced wet etching of GaN," *Applied Physics Letters*, vol. 68, pp. 1531-1533, 1996.

[7] O. H. Nam, T. S. Zheleva, M. D. Bremser, D. B. Thomson, and R. F. Davis, "Organometallic vapor phase lateral epitaxy of low defect density GaN layers," presented at Nitride Semiconductors Symposium Nitride Semiconductors Symposium, Boston, MA, 1997.

[8] A. Sakai, H. Sunakawa, and A. Usui, "Defect structure in selectively grown GaN films with low threading dislocation density," *Applied Physics Letters*, vol. 71, pp. 2259-2261, 1997.

[9] S. Nakamura, "InGaN/GaN/AlGaN-based laser diodes with an estimated lifetime of longer than 10000 hours," presented at Material Research Society Fall '97 Meeting, Boston, MA, 1997.

[10] S. Nakamura, M. Senoh, S. I. Nagahama, N. Iwasa, T. Yamada, T. Matsushita, H. Kiyoku, Y. Sugimoto, T. Kozaki, H. Umemoto, M. Sano, and K. Chocho, "Violet InGaN/GaN/AlGaN-based laser diodes with an output power of 420 mW," *Japanese Journal of Applied Physics, Part 2 (Letters)*, vol. 37, pp. L627-629, 1998.

[11] "Sumitomo to Offer GaN Single Crystal Products," *Compound Semiconductor*, vol. 6, 2000.

[12] J. A. Edmond, H. Kong, M. T. Leonard, K. Doverspike, G. E. Bulman, W. Weeks, K. G. Irvine, and V. A. Dmitriev, "Nitride-based emitters on SiC substrates," presented at Second International Conference on Nitride Semiconductors, Tokushima, Japan, 1997.

[13] K. Doverspike, G. E. Bulman, S. T. Sheppard, H. S. Kong, M. T. Leonard, H. Dieringer, J. A. Edmond, K. L. More, Y. K. Song, M. Kuball, and A. V. Nurmikko,

"InGaN/GaN lasers grown on SiC," presented at In-Plane Semiconductor Lasers: from Ultraviolet to Mid-Infrared II, San Jose, CA, 1998.

[14] S. Nakamura, M. Senoh, S. Nagahama, N. Iwasa, T. Matsushita, and T. Mukai, "InGaN/GaN/AlGaN-based violet laser diodes with a lifetime of more than 10,000 hours," presented at Blue Laser and Light Emitting Diodes II Proceedings of 2nd International Symposium on Blue Laser and Light Emitting Diodes, Chiba, Japan, 1998.

[15] S. Nakamura, M. Senoh, S. I. Nagahama, N. Iwasa, T. Yamada, T. Matsushita, H. Kiyoku, Y. Sugimoto, T. Kozaki, I. Umemoto, M. Sano, and K. Chocho, "InGaN/GaN/AlGaN-based laser diodes grown on GaN substrates with a fundamental transverse mode," *Japanese Journal of Applied Physics, Part 2 (Letters)*, vol. 37, pp. L1020-1022, 1998.

[16] S. Nakamura, M. Senoh, S. Nagahama, N. Iwasa, T. Yamada, T. Matsushita, H. Kiyoku, Y. Sugimoto, T. Kozaki, H. Umemoto, M. Sano, and K. Chocho, "InGaN/GaN/AlGaN-based laser diodes with cleaved facets grown on GaN substrates," *Applied Physics Letters*, vol. 73, pp. 832-834, 1998.

[17] S. Nakamura, M. Senoh, S. I. Nagahama, N. Iwasa, T. Yamada, T. Matsushita, H. Kiyoku, Y. Sugimoto, T. Kozaki, H. Umemoto, M. Sano, and K. Chocho, "Present status of InGaN/GaN/AlGaN-based laser diodes," presented at Second International Conference on Nitride Semiconductors, Tokushima, Japan, 1998.

[18] D. A. Stocker, E. F. Schubert, and J. M. Redwing, "Crystallographic wet chemical etching of GaN," *Applied Physics Letters*, vol. 73, pp. 2654-2656, 1998.

Appendix A

Wafer fusion

As mentioned in chapter 2, wafer fusion can be useful for the creation of cleaved facets in GaN optoelectronic devices. In addition, wafer fusion of GaN to InP or GaAs has other applications such as capping GaN for the activation of p-type dopants and for providing an improved p-type injection contact.

A.1. Activation of p-type dopants in GaN

P-type GaN material provides the limiting resistance in many GaN device structures. There are two main reasons for this. First, Mg atoms have a high activation energy in GaN. Second, Mg atoms are passivated by hydrogen during the growth of GaN.

The high activation energy of Mg atoms cannot be changed. Other dopants, such as Zn, have been explored, but their activation energies are significantly higher than the activation energy for Mg (see Table 1). Mg incorporates on the Ga substitutional site to act as a p-type dopant and has an activation energy of 170 meV. For comparison, the activation energy of p-type dopants in other light emitting III-V materials are much lower as shown in Table 1. GaAs, for example, has a low acceptor activation energy of 26 meV for carbon. This means that to achieve the same concentration of holes, GaN must have almost 200 times more dopant atoms than GaAs.

III-V material	Acceptor	Acceptor activation energy	Carriers per acceptor
GaN	Mg	170 meV [1]	$1.4\ 10^{-3}$
	Zn	340 meV [2]	$2.1\ 10^{-6}$
GaAs	C	26 meV [3]	0.27
	Be	28 meV [3]	0.25
	Mg	28 meV [3]	0.25
	Zn	31 meV [3]	0.23

Table 1. Acceptor activation energy for GaAs and GaN. The acceptor activation energy in GaN is much higher in comparison. This means that a smaller percentage of the dopants will produce carriers. The number of carriers per acceptor assumes $E_F = E_v$ and the temperature is 300 K.

During the growth of p-type GaN (or AlGaN), hydrogen carrier gas is often used because this results in a more efficient incorporation of the Mg dopants. However, some of these hydrogen molecules (H_2) crack apart at the high growth temperatures and become incorporated into the GaN lattice. As described in Chapter 1, hydrogen passivates the p-type dopants in Mg-doped GaN by neutralizing the vacant bond site between the Mg and N atoms [4]. To achieve suitable p-type doping, the hydrogen passivation must be removed.

Two methods for activating the p-type dopants have been developed. The first to be developed was the use of low-energy electron beam irradiation (LEEBI) by Amano et. al. in 1989 [5]. After such treatment, Amano was able to create a pn junction in material that was n-type as grown. The second method to be developed was the thermal activation of the dopants. In 1992, Nakamura et. al. fabricated a pn junction by heating the Mg doped GaN to 700ºC in a nitrogen ambient for 20 minutes. Heating the GaN allows hydrogen atoms to leave these passivation sites, thus allowing the p-type Mg dopant to be activated. Nakamura's study of annealing temperature as a function of p-type dopant activation temperature revealed that heating GaN did indeed improve Mg activation in GaN for annealing temperatures 500-700°C [6]. Above 700°C, nitrogen begins to

leave its lattice site. The nitrogen vacancies formed in this way act as n-type dopants and therefore compensate for the increased activation of the p-type dopant. The trend as temperature is increased above 700°C is that the net p-type carrier concentration is reduced. Therefore, the optimum activation temperature was initially thought to be just below 700ºC [6].

To increase this optimal temperature, methods for inhibiting nitrogen desorption were explored. One solution to this problem is to use proximity activation. Proximity activation has been performed in many semiconductor systems. This involves placing one wafer on top of another so that their surfaces are in close proximity. If these wafers are of similar composition (i.e. both GaAs), then as the wafer is heated, gas will be desorbed from both samples. In theory, this gas will be held between the two samples, thus creating a high overpressure of the desorbing gas and reducing the desorption rate from the two samples. However, in many cases, the overpressure is not enough to prevent desorption or decomposition of the surface.

An even better solution for GaN is to cap GaN with another material to prevent the desorption of nitrogen from the surface and at the same time allow desorption of hydrogen from the Mg-H-N formations. Amorphous SiO_2 is frequently used because it can be removed easily with a wet etch (10-15 minutes in 49% HF) after thermal activation. However, this is a three-step process and can potentially result in additional doping through the diffusion of silicon or oxygen into the GaN:Mg. Both silicon and oxygen act as donors in GaN, thus negating the advantage of thermally activating the material.

Wafer bonding provides a potentially better way: Wafer bonding allows a cap layer to be used that otherwise could not be deposited on GaN. Sink, et. al. have proposed that p-type activation can be performed by wafer bonding to another material [7]. GaAs, InP, GaP, SiN, or SiO_2 can potentially be fused to GaN:Mg as a cap layer. These materials can be monocrystalline, polycrystalline, or

amorphous, depending on the characteristics desired. In many cases, thermal and electrical conductivity will be improved by choosing monocrystalline structures. One could use a compound that contains both nitrogen and magnesium in order to increase the dopant concentration and limit the desorption of nitrogen. In addition, the high temperatures and long times used for wafer fusion will also be helpful for the thermal activation of GaN:Mg. Thus, the wafer fusion and the p-type activation could be performed in a single step. Exploring other materials as the cap material for thermal activation of p-type GaN potentially allows much higher temperatures to be used without the problem of diffusion of n-type dopants such as silicon and oxygen into (p-type) GaN:Mg.

A.2. Fabrication of p-type contacts to GaN

A second potentially significant application of fusion is the fabrication of improved p-type contacts to GaN. One possible material choice is epitaxial p-InP/p-InGaAs grown on InP. This structure can be fused to p-GaN. In this case, the p-InP serves as a fusion layer to p-GaN. The InP substrate can then be removed by wet etching in order to make contact to the p-InGaAs. Making metal contacts on p-InGaAs is relatively easy and produces low contact resistances. This procedure is not limited to p-InP/p-InGaAs: Other material structures such as p-GaAs/p-AlGaAs could be used. Also, the p-InP fusion layer may be unnecessary and may be eliminated from the structure in the future. If the p-InP layer were removed, the p-InGaAs could act as both the fusion layer and the contact layer.

Each of these applications can be used independently or they can be combined to fabricate an in-plane laser. One advantage of wafer fusion over classical growth techniques is flexibility in material choice. The restrictions of material choices due to thermal expansion and lattice mismatch are less stringent for fused

interfaces than for heterojunctions grown by MOCVD or MBE. For both VCSELs and in-plane lasers, these relaxed restrictions will give device designers increased flexibility to choose materials based on desired thermal or electrical properties. Therefore, many of the problems that have prevented an adequate transfer of technology from existing laser material systems to the nitrides could likely be addressed by the development of wafer fusion technology.

A.3. References

[1] W. Gotz, N. M. Johnson, J. Walker, D. P. Bour, and R. A. Street, "Activation of acceptors in Mg-doped GaN grown by metalorganic chemical vapor deposition," *Applied Physics Letters*, vol. 68, pp. 667-669, 1996.

[2] S. Strite and H. Morkoc, "GaN, AlN, and InN: A review," *Journal of Vacuum Science & Technology B (Microelectronics Processing and Phenomena)*, vol. 10, pp. 1237-1266, 1992.

[3] S. M. Sze, *Physics of Semiconductor Devices*, 2nd ed. New York: John Wiley & Sons, 1981.

[4] Y. Okamoto, M. Saito, and A. Oshiyama, "First-principles calculations on Mg impurity and Mg-H complex in GaN.," *Japanese Journal of Applied Physics, Part 2 (Letters)*, vol. 35, pp. L807-809, 1996.

[5] H. Amano, M. Kito, K. Hiramatsu, and I. Akasaki, *Japanese Journal of Applied Physics*, vol. 28, pp. L2112, 1989.

[6] S. Nakamura, T. Mukai, M. Senoh, and N. Iwasa, "Thermal annealing effects on p-type Mg-doped GaN films," *Japanese Journal of Applied Physics, Part 2 (Letters)*, vol. 31, pp. L139-142, 1992.

[7] R. K. Sink, S. Keller, B. P. Keller, D. I. Babic, A. L. Holmes, D. Kapolnek, S. P. DenBaars, J. E. Bowers, X. H. Wu, and J. S. Speck, "Cleaved GaN facets by wafer fusion of GaN to InP," *Applied Physics Letters*, vol. 68, pp. 2147-2149, 1996.

Appendix B

Calculation of complex index of refraction in nitride alloys

In Chapter 3, the basic design of the edge emitting laser diode was described. To model the optical characteristics of this device, the complex index of refraction for each of the materials is needed. This Appendix describes the method used to calculate the index values used in Chapter 3. First, the large variety of bowing parameters for use with Vegard's Law is discussed. After choosing a set of bowing parameters, the alloy bandgaps are calculated and used to describe the index of refraction for varying alloy compositions. Once the index is known for each of the layers in the epitaxial structure, 1-dimensional optical modeling can be performed as described in Chapter 3.

B.1. Calculation of material band gap

Accurate calculation of the band gap of nitride alloys is necessary for accurate electrical and optical models. Vegard's Law describes a linear interpolation of bandgap as a function of alloy composition. In some cases, such as for AlGaN alloys, this approximation is reasonably accurate. However, in other cases, such as for InGaN alloys, substantial non-linearity — band bowing — is observed and a quadratic term is added to Vegard's Law as shown in Equation 1.

$$E_g(Ga_xIn_{1-x}N) = E_g(GaN) * x + E_g(InN) * (1-x) - b * x * (1-x) \quad (1)$$

The amount of band bending in InGaN alloys was reported by Nakamura, who claimed that the InGaN system had a band bending parameter of b=1.0 eV [1]. With more accurate measurement and interpretation of the x-ray diffraction data and with better quality material, estimates for the bowing parameter in InGaN alloys have been revised. For alloy compositions of $x<0.20$, b=3.2 eV is a commonly used number for band bending in InGaN [2]. This value includes the influence of strain. So it is not a true band bending parameter, but since all material that we will consider is strained, this value is the one that is relevant. For

indium compositions higher than x=0.20, higher order bowing parameters are necessary to accurately model the shape of the bowing.

	Band bowing parameter—b (eV)	**Applicable compositions**
InGaN	3.2 (strained)	x<0.20
AlGaN	0.25 (strained)	x<0.25
InGaN	3.8 (unstrained)	x<0.20

Table 1. Band bowing parameters for AlGaN and InGaN, from reference [2].

Early reports for bowing in the AlGaN system were also widely scattered: These reports claimed band bending parameters for AlGaN from -1.0 eV to +1.0 eV [3-6]. The best measurements of the band bending indicate that the band bending is b=0.25 eV for AlGaN alloy compositions of x<0.25 [2]. As for InGaN, this bowing parameter value also includes the effect of strain.

B.2. Calculation of refractive indices

The index of GaN is 2.5067 at room temperature for a wavelength of 420 nm as measured by several researchers using spectroscopic ellipsometry [7-9]. However, the index of refraction for the group-III nitride alloys (InGaN and AlGaN) are still not well established. As groups focus on CW operation of laser diodes, optical modeling of waveguide modes is becoming a more important topic. There have been a large number of papers that have been published in the last year that model the index of refraction of GaN and its alloys as a function of wavelength [7, 9-13]. Unfortunately, the more difficult task of systematically measuring the index for a broad range of different alloy compositions has not been published.

Surface roughness, variations in material quality, and different interpretations of alloy composition have led to a variety of differing reports and extrapolations.

This has led to different models for how the index varies with composition [7]. The model presented here is based on work by Zhang, et al. who measured the refractive index of GaN using a waveguide configuration [14]. This data was fit to a theoretical model to give an analytic expression for the index as a function of wavelength as shown in Equation 2. This curve is then shifted in energy space by the energy difference between the alloy and GaN. The value of the index of refraction for the alloy can then be estimated [14].

$$n_o = \sqrt{b_1 - \frac{b_2}{b_3+\lambda^2} + \frac{b_4}{b_5+\lambda^2} - b_6*\lambda^2} \qquad (2)$$

$$b_1 = 7.2757576$$

$$b_2 = 3.1884011\ \mu m^2$$

$$b_3 = 1.0577376\ \mu m^2$$

$$b_4 = 0.3028841\ \mu m^2$$

$$b_5 = 0.219\ 10^{-6}\ \mu m^2$$

$$b_6 = 0.7133304\ \mu m^{-2}$$

For calculation of the index of refraction for InGaN and AlGaN, this model assumes that the variation of index with photon energy is the same for GaN, InGaN, and AlGaN [14]. By making an accurate measure of the index of refraction as a function of photon energy for GaN, the indices of refraction for the alloys can then be calculated by shifting the index of refraction curve by the change in bandgap between the alloy and the GaN. This simple method works well for getting a reasonably accurate measure of the index for small alloy compositions, where deviation from the shape of the GaN curve is expected to be small. The bowing parameters from the last section are used to calculate the bandgaps for InGaN and AlGaN alloys. Calculated values of index for AlGaN and InGaN at 420 nm are presented in Table 2 and in Figure 1.

Appendix B. Calculation of complex index of refraction in nitride alloys

x	$Al_xGa_{1-x}N$	$In_xGa_{1-x}N$
0.0	2.5067	2.5067
0.01	2.5014	2.5160
0.02	2.4963	2.5255
0.03	2.4911	2.5349
0.04	2.4861	2.5444
0.05	2.4810	2.5539
0.06	2.4761	2.5634
0.07	2.4712	2.5730
0.08	2.4663	2.5825
0.09	2.4615	2.5920
0.10	2.4568	2.6014
0.11	2.4521	2.6109
0.12	2.4475	2.6203
0.13	2.4430	2.6296
0.14	2.4385	2.6389
0.15	2.4341	2.6481
0.16	2.4298	2.6573
0.17	2.4255	2.6664
0.18	2.4213	2.6754
0.19	2.4172	2.6843
0.20	2.4131	2.6932
0.21	2.4091	2.7019
0.22	2.4052	2.7105
0.23	2.4014	2.7191
0.24	2.3976	2.7275
0.25	2.3940	2.7358

Table 2. Calculated indices of refraction as a function of alloy composition for 420 nm light.

Appendix B. Calculation of complex index of refraction in nitride alloys

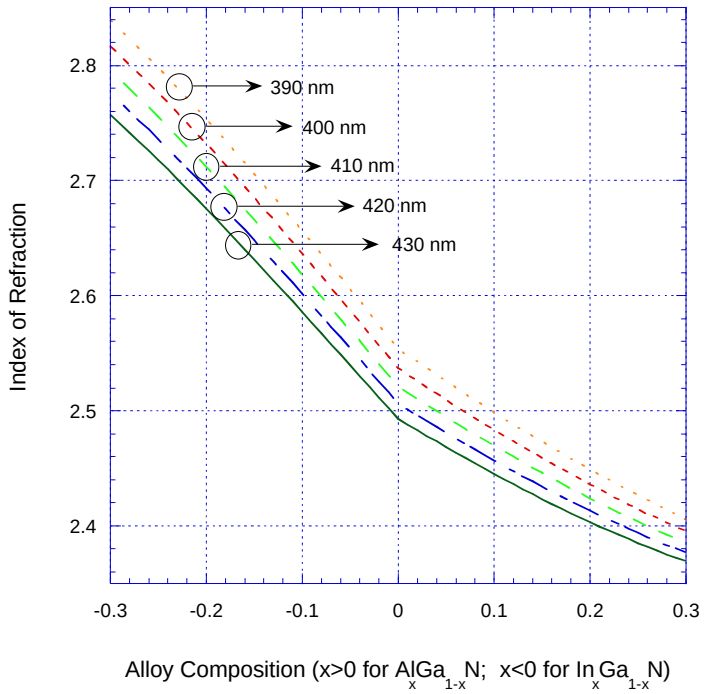

Figure 1. The index of refraction for InGaN and AlGaN alloys for wavelengths of interest. $Al_xGa_{1-x}N$ alloys are shown as positive x values, while $In_xGa_{1-x}N$ alloys represented with negative x values.

Using this method, dispersion curves for each alloy are also easily calculated. These are presented in Figure 2.

Appendix B. Calculation of complex index of refraction in nitride alloys

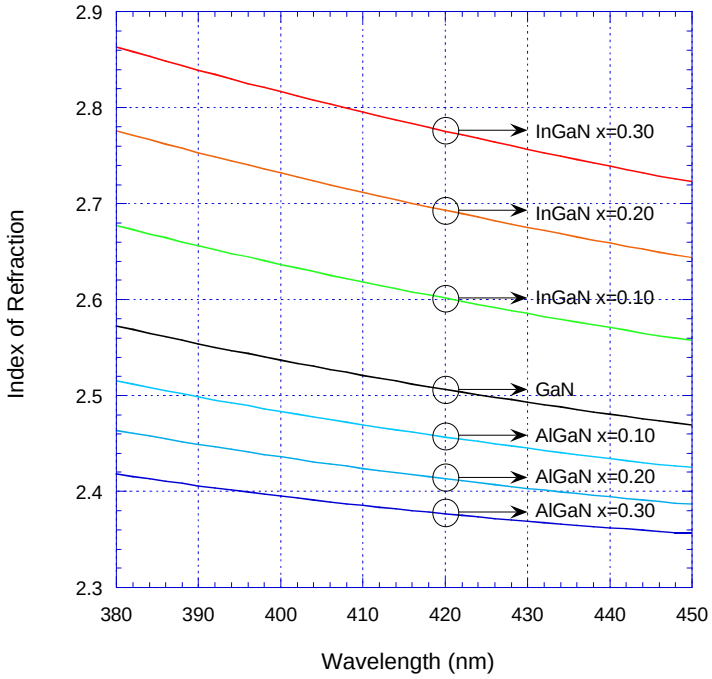

Figure 2. Dispersion curves for group-III nitride alloys calculated from Equation 2.

Other choices can be made for a description of the dispersion curve for GaN. Yang, et al. [7] present a slightly different fit for the experimentally measured index of GaN that is valid for photons with wavelength longer than 420nm. This fit is shown in Equation 3 and gives a slightly different dispersion curve than the one described above [7].

$$n(\lambda) = A + \frac{B}{\lambda^2} + \frac{C}{\lambda^4} \qquad (3)\ [7]$$

$$A = 2.2796 \pm 0.00064$$

$$B = 0.011750 \pm 0.000375\ \mu m^2$$

$$C = 0.0044175 \pm 5.18\ e\text{-}5\ \mu m^4$$

It is unclear which dispersion curve is more accurate. The model presented by Equation 3 was not chosen because of the limited accuracy of the model for wavelengths close to the bandgap wavelength.

Ultimately, what is important is that a consistent set of data be measured. The method of approximating alloy indices based on GaN dispersion curves works relatively well because what is important is not so much the absolute magnitude of the index, but instead the relative magnitude of the indices of adjacent layers. For example, waveguides with indices of 2.4 and 2.5 have very similar if their cladding regions are 2.0 and 2.1. So even though the absolute accuracy of this method may not be as good as some other methods, it still yields suitable results because it calculates relative magnitudes reasonably well.

One other thing that could be considered in optical modeling is that GaN is birefringent with an index difference of approximately 0.038 between n_o and n_e [14]. Since the modes that we are interested in are TE modes, only n_o is considered in this chapter.

B.3. Loss mechanisms

In addition to index of refraction, loss and gain values for each layer are necessary if a useful model is to be made. Unfortunately, accurate measurements for these values have not yet been reported. Values for modal gain have been reported in isolated instances. For example, for his early lasers Nakamura published a modal loss value of 43 cm^{-1}, which he measured by plotting the threshold current density as a function of laser cavity length [15, 16]. Xerox PARC researchers have estimated modal loss values of approximately 200 cm^{-1} [17]. However, actual measurements of gain and loss for each layer have not been reported.

One of the reasons for this lack of information is that the values of loss still vary significantly with material quality. Defects are responsible for absorption and readmission of a yellow band of light as evidenced by photoluminescence measurements [18]. Scattering loss from defects is significant. For material that

has a high defect concentration, such as GaN (defect density 10^8 - 10^{10} defects/cm^3 for non-ELO material), the defects are believed to produce significant scattering loss. For this reason, universal numbers for loss are difficult to report and numbers for loss for defect free material are not useful for modeling the current generation of devices.

In the waveguide model presented here, the template layer is broken up into three layers to better simulate the changing defect density as thicker material is grown. The layer closest to the sapphire is highly defected and is attributed a very high loss value of 5000 cm^{-1}. This highly defected region in the model is limited to the lowest 0.5 μm of GaN material, which matches the physical layer structure. The next layer is approximately 1.0 μm thick and represents the region where the GaN defects terminate as the GaN is grown thicker. The remainder of the template layer represents a region with fewer defects, but the remaining defects are threading dislocations, which do not terminate as the material is grown thicker.

In addition to scattering loss from defects, there are other loss mechanisms that must be considered. Among these are free carrier absorption, scattering loss from cracks (see Figure 3) or ridge roughness, scattering from index variations due to indium segregation, absorption at defects, and absorption in unpumped regions of the device. For the template region, both defect scattering and free carrier absorption are believed to be problems for highly doped n-type GaN. By reducing the amount of optical power in this region, the doping can be increased to optimal levels based on electrical and morphological requirements without incurring a penalty due to increased free carrier absorption.

Appendix B. Calculation of complex index of refraction in nitride alloys

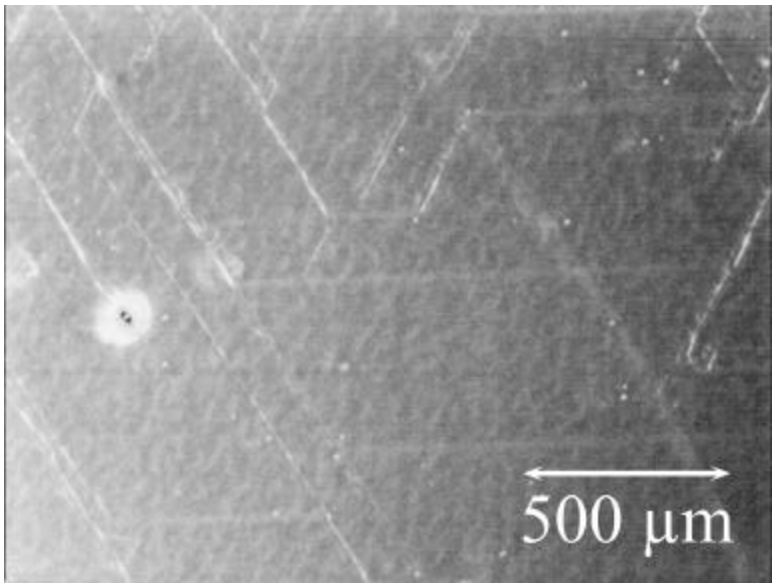

Figure 3. Cracks and defects in a sample with two 0.5 µm thick $Al_{.20}Ga_{.80}N$/GaN SSL cladding layers.

Despite the lack of available numbers for loss, estimates can be made for the loss in each layer by a combination of 1) intuition from other material systems and 2) matching to modal loss values like the ones given above.

For the metals and substrates used in nitride laser structures, the parameters for index and loss are somewhat easier to find in the literature. These values are given in Table 3.

Material	Index of refraction	Loss (cm^{-1})	Reference
Gold	1.626	$5.83\ 10^5$	[19, 20]
Aluminum	0.542	$15.29\ 10^5$	[19]
Titanium	1.61	$6.55\ 10^5$	[19]
Nickel	1.615	$7.42\ 10^5$	[20]
Palladium	1.34	$9.30\ 10^5$	[21]
Sapphire	1.766	0	

Table 3. Loss and index values at a wavelength of 420 nm.

B.4. Gain measurements

There are only a few reports of quantitative gain measurements. Using optical pumping, modal gain values of up to 650 cm^{-1} were measured for optical pumping intensities of 20 MW/cm^2 [22] and 100 cm^{-1} at 20 mJ/cm^{-2} [23]. Nakamura has reported modal gain values as high as approximately 100 cm^{-1} corresponding to a material gain of approximately 5200 cm^{-1}, a threshold current density of 8.8 kA/cm^2, and a threshold carrier density of $2\ 10^{20}$ cm^{-3} [16]. Nakamura's value for confinement factor is off by a factor of two, which makes his QW gain only 2600 cm^{-1} in reality. Theoretical models place material gain as high as 6000 cm^{-1} per QW for carrier concentrations of $4\ 10^{19}$ cm^{-3} [24].

Of course, gain depends on carrier density. For multiple quantum wells, non-uniformity in pumping of the wells is a problem (see Chapter 3). This means that the net gain for the MQW stack will be lower than if all wells were pumped uniformly. For the optical model presented here, a value of 2,600 cm^{-1} (corrected value from Nakamura's experimental result) was used as the net gain for the MQW stack in the laser structure.

B.5. References

[1] S. Nakamura and T. Mukai, *Journal of Vacuum Science and Technology A*, vol. 13, pp. 705, 1995.

[2] T. Takeuchi, H. Takeuchi, S. Sota, H. Sakai, H. Amano, and I. Akasaki, "Optical properties of strained AlGaN and GaInN on GaN," *Japanese Journal of Applied Physics, Part 2 (Letters)*, vol. 36, pp. L177-179, 1997.

[3] S. Yoshida, S. Misawa, and S. Gonda, *Journal of Applied Physics*, vol. 53, pp. 6844, 1982.

[4] D. K. Wickenden, C. B. Bargeron, W. A. Bryden, J. Miragliova, and T. J. Kistenmacher, *Applied Physics Letters*, vol. 65, pp. 2024, 1994.

[5] K. Osamura, K. Nakajima, Y. Murakami, P. H. Shingu, and A. Otsuki, *Solid State Communications*, vol. 11, pp. 617, 1972.

[6] Y. Koide, H. Itoh, M.R.H.Khan, K. Hiramatsu, N. Sawaki, and I. Akasaki, *Journal of Applied Physics*, vol. 61, pp. 4540, 1987.

[7] T. Yang, S. Goto, M. Kawata, K. Uchida, A. Niwa, and J. Gotoh, "Optical properties of GaN thin films on sapphire substrates characterized by variable-angle spectroscopic ellipsometry," *Japanese Journal of Applied Physics, Part 2 (Letters)*, vol. 37, pp. L1105-1108, 1998.

[8] T. Kawashima, H. Yoshikawa, S. Adachi, S. Fuke, and K. Ohtsuka, "Optical properties of hexagonal GaN," *Journal of Applied Physics*, vol. 82, pp. 3528-3535, 1997.

[9] G. Yu, H. Ishikawa, M. Umeno, T. Egawa, J. Watanabe, T. Jimbo, and T. Soga, "Optical properties of $Al_xGa_{1-x}N$/GaN heterostructures on sapphire by spectroscopic ellipsometry," *Applied Physics Letters*, vol. 72, pp. 2202-2204, 1998.

[10] A. B. Djurisic and E. H. Li, "Modeling the optical properties of hexagonal GaN," *Applied Physics Letters*, vol. 73, pp. 868-870, 1998.

[11] A. B. Djurisic and E. H. Li, "Modeling the optical constants of hexagonal GaN, InN, and AlN," *Journal of Applied Physics*, vol. 85, pp. 2848-2853, 1999.

[12] J. Wagner, A. Ramakrishnan, D. Behr, H. Obloh, M. Kunzer, and K. H. Bachen, "Spectroscopic ellipsometry characterization of (InGa)N on GaN," *Applied Physics Letters*, vol. 73, pp. 1715-1717, 1998.

[13] M. M. Y. Leung, A. B. Djurisic, and E. H. Li, "Refractive index of InGaN/GaN quantum well," *Journal of Applied Physics*, vol. 84, pp. 6312-6317, 1998.

[14] H. Y. Zhang, X. H. He, Y. H. Shih, M. Schurman, Z. C. Feng, and R. A. Stall, "Waveguide study and refractive indices of GaN:Mg epitaxial film," *Optics Letters*, vol. 21, pp. 1529-1531, 1996.

[15] L. A. Coldren and S. W. Corzine, *Diode Lasers and Photonic Integrated Circuits*. New York, NY: John Wiley & Sons, 1995.

[16] S. Nakamura, "Characteristics of room temperature-CW operated InGaN multi-quantum-well-structure laser diodes," *MRS Internet Journal of Nitride Semiconductor Research*, vol. 2, pp. 5, 1997.

[17] D. Hofstetter, D. P. Bour, R. L. Thornton, and N. M. Johnson, January 31, 1997, personal communication.

[18] T. Ogino and M. Aoki, *Japanese Journal of Applied Physics*, vol. 19, pp. 2395, 1980.

[19] D. R. Lide, *CRC Handbook of Chemistry and Physics*, 71 ed. Boca Raton: CRC Press, 1990.

[20] E. D. Palik, *Handbook of optical constants of solids I*. Orlando, FL: Academic Press, 1985.

[21] E. D. Palik, *Handbook of optical constants of solids II*. San Diego, CA: Academic Press, 1991.

[22] G. Mohs, T. Aoki, M. Nagai, R. Shimano, M. Kuwata-Gonokami, and S. Nakamura, "Failure of the modal gain model in a GaN based laser diode," *Solid State Communications*, vol. 104, pp. 643-648, 1997.

[23] R. Klann, O. Brandt, H. Yang, H. T. Grahn, and K. H. Ploog, "Optical gain in optically pumped cubic GaN at room temperature," *Applied Physics Letters*, vol. 70, pp. 1076-1077, 1997.

[24] Y. C. Yeo, T. C. Chong, and L. Ming-Fu, "Uniaxial strain effect on the electronic and optical properties of wurtzite GaN-AlGaN quantum-well lasers," *IEEE Journal of Quantum Electronics*, vol. 34, pp. 2224-2232, 1998.

Appendix C

Waveguide modeling program: ModeSolver

The index values calculated in Appendix B are used to calculate the transverse optical mode for the lasers that were presented in Chapter 3. The optical mode calculations are based on well-known methods, which will be described briefly in this Appendix. To implement these methods and to calculate characteristics of the optical mode, I have written a C++ program called ModeSolver. The characteristics of the optical mode that are calculated by ModeSolver include the optical field profile, the modal index of refraction, the modal gain, and the optical far field pattern. The program allows looping of variable thicknesses so that layer thicknesses can be optimized. This Appendix describes the program.

C.1. TE and TM optical modes

ModeSolver can be used to calculate the eigenstate for an optical TE-polarized mode, the eigenstate for an optical TM-polarized mode, or the eigenstate for a particle confined in a quantum well. The equations presented here are for TE optical modes. The QW case is mathematically equivalent to the TE case. The TM optical mode case is very similar. The boundary conditions for TE modes are presented in Equation 7. An overview of the derivation of these equations is presented in Equations 1-5. More detailed derivations can be found in textbooks on optical waveguides and quantum mechanics [1-4].

The first boundary condition is straightforward: By definition, a guided optical beam and a confined eigenstate for a quantum well have the boundary condition that as x approaches positive or negative infinity, the electric field (or wavefunction for the QW case) must approach zero.

Propagation of a plane wave is described by Equation 1.

$$\mu\varepsilon \frac{d^2}{dt^2}\mathbf{E} = \nabla^2\mathbf{E} \qquad (1)$$

This equation can be simplified for a plane wave described by the equation $\mathbf{E} = \mathbf{E_0}\, e^{-j(wt-\mathbf{k(r)}\bullet\mathbf{r})}$. First, the gradient can be described using its Cartesian coordinate representation. Second, for a plane wave in a slab waveguide, there is no variation of the electric field in the **y** direction, which means that $k_y = 0$.

$$\nabla^2\mathbf{E} = \frac{d^2\mathbf{E}}{dx^2} + \frac{d^2\mathbf{E}}{dy^2} + \frac{d^2\mathbf{E}}{dz^2} = \frac{d^2\mathbf{E}}{dx^2} + 0 + (-k_z^2)\,\mathbf{E} \qquad (2)$$

$$\mu\varepsilon \frac{d^2}{dt^2}\mathbf{E} + k_z^2\,\mathbf{E} = \frac{d^2\mathbf{E}}{dx^2} \qquad (3)$$

$$\mu\varepsilon \frac{d^2}{dt^2}\mathbf{E} = \mu\varepsilon(\mathbf{r})\,\omega^2\,\mathbf{E} = -|\mathbf{k}(\mathbf{r})|^2\,\mathbf{E} = -n^2(\mathbf{r})\,k_0^2\,\mathbf{E} \qquad (4)$$

In these equations, $\mathbf{E}(\mathbf{r})$ is the electric field profile, k_z is the eigenvalue for the mode, $n(\mathbf{r})$ is the index as a function of position, and $\mathbf{k}(\mathbf{r})$ is the wave function. The modal index is calculated as $\bar{n} = k_z/k_0$, where $k_0 = 2\pi/\lambda$.

For uniform propagation in the **z** direction, we want to describe the mode shape in the x direction. **k** is proportional to the index of refraction in each section and so it varies across the waveguide. For a single mode, k_z remains the same across the entire waveguide. For this reason, the second derivative of E with respect to x position must change to compensate for the change in index in each layer of the waveguide.

$$\frac{d^2\mathbf{E}}{dx^2} = -(n^2(\mathbf{r})\,k_0^2 - k_z^2)\,\mathbf{E} \qquad (5)$$

For the TE and TM cases, Maxwell's equations require that the transverse electric and magnetic field be continuous across a dielectric boundary. The requirements of Maxwell's equations on the TE mode yield boundary conditions at an index step. Equation 7 describes the boundary conditions for the TE mode.

$$E_1 = E_2 \text{ and } \frac{dE_1}{dx} = \frac{dE_2}{dx} \qquad (6)$$

C.2. Implementation

The program implements two methods for solving the eigenmodes of the system. The first method starts with discrete approximations to the differentials in Maxwell's equations. These approximations describe a system of linear equations that can be solved to find the eigenvalues (modal index) and eigenvectors (optical mode profile) of the eigensystem. The approximations are chosen such that the matrix is tridiagonal, which makes it relatively straightforward to solve using published library files [5-7].

The second method for the eigenmodes and eigenvalues of the optical system is the transfer matrix method. The transfer matrix method is described by numerous sources in great detail. This method is popular because it requires very little effort to implement for most geometries and is much less computation intensive than the tridiagonal matrix method. This method is described for the case of quantum well eigenstates by Kromer [2] and for the optical case by Coldren and by Schelerth and Tacke [1, 8]. Their explanations are concise and straightforward. So I will not repeat them here.

The tridiagonal matrix method approximates the continuous boundary conditions (Equation 7) using discrete boundary conditions.

$$\frac{d^2E}{dx^2} = \frac{d}{dx}\left(\frac{E_{n+1}-E_n}{\Delta x_n} + \frac{E_n-E_{n-1}}{\Delta x_{n-1}}\right)\frac{1}{2}$$

$$= 2\,\frac{(E_{n+1}-E_n)\,\Delta x_{n-1} + (E_{n-1}-E_n)\,\Delta x_n}{(1/2)\,\Delta x_n\,\Delta x_{n-1}\,(\Delta x_n + \Delta x_{n-1})} \qquad (7)$$

This equation can easily be put into a tridiagonal matrix and solved to calculate the eigenvalues (k_z) and the eigenvectors (E(x)). This works relatively well as long as the differences Δx_n-Δx_{n-1} and Δx_{n+1}-Δx_n are relatively small and approximately equal. Otherwise the approximation for the derivative is not very accurate.

These approximations yield a system of linear equations. The eigenvalues for this system can be found by standard methods. For an accurate calculation, the size of the matrix can easily be 100x100 or even 1000x1000. To solve the eigenvalue of a general matrix of this size would take more memory than is available in a typical computer. However, by using a tridiagonal matrix, even large matrices are easily solved. The system can be arranged into a tridiagonal matrix as shown in Equation 8.

$$\begin{bmatrix} A & B & 0 & 0 & 0 \\ B & A & B & 0 & 0 \\ 0 & B & A & B & 0 \\ 0 & 0 & B & A & B \\ 0 & 0 & 0 & B & A \end{bmatrix} \bullet \begin{bmatrix} x_1 \\ x_2 \\ x_3 \\ x_4 \\ x_5 \end{bmatrix} = \begin{bmatrix} \lambda_1 \\ \lambda_2 \\ \lambda_3 \\ \lambda_4 \\ \lambda_5 \end{bmatrix} \tag{8}$$

A represents the value of the electric field at the point x_i itself and the values of B are used to represent the discrete approximations of the derivatives as described in Equation 8. The eigenvalues for tridiagonal matrices are much simpler to calculate than are the eigenvalues for the same size generalized matrix.

The disadvantage of this approach is that for good accuracy, many steps are needed, which takes more processing time. The other method—the transfer matrix method—is significantly faster. The transfer matrix method, described by Kromer, represents each boundary using a 2x2 matrix. By multiplying these matrices together, it is relatively simple to calculate the eigenvalues of the system. Unfortunately, this method only returns one of the eigenvalues. The eigenvalue that it picks is based on the starting guess for the eigenvalue that is chosen. Since the eigenvalue spacing is originally unknown, another method must be found for picking the initial eigenvalue guesses. For this, the tridiagonal

matrix method is used, but with a relatively coarse resolution so that little processing time is used. I believe that this hybrid approach produces a relatively fast calculation time and allows looping of thicknesses relatively easily.

For the case of the TE and TM optical modes, the mode profile that results is the near field. From this near field, the far field is calculated by taking a fast Fourier transform of the near field, and applying appropriate scaling factors [1]. This far field can be described in two slightly different ways: angular distribution relative to the peak of the mode and positional distribution at a plane some distance away from the laser facet. The difference between these two approaches is small for small divergence angles.

The optical modes and index profile are saved to a text file for plotting. The farfield is stored in another text file for plotting. If looping is done, multiple modes can be plotted to a single output file so that they can be plotted on the same graph, or they can be plotted in separate files to reduce the overall file size. Output for modal index and modal gain are output to a single file during looping runs so that trends can be analyzed. Examples of the output from looping runs are shown in Chapter 3.

Thanks to Dr. Radha Nagarajan who let me use his source code for the tridiagonal matrix method solver. While I did not use his code directly, I did get many ideas from it for features and implementation. The ModeSolver program has been successfully used to calculate mode profiles for other laser structures described in the Ph.D. dissertations of Abare and Mack [9].

C.3. References

[1] L. A. Coldren and S. W. Corzine, *Diode Lasers and Photonic Integrated Circuits*. New York, NY: John Wiley & Sons, 1995.

[2] H. Kroemer, *Quantum Mechanics: For engineering, material science, and applied physics*. Englewood Cliffs, NJ: Prentice Hall, 1994.

[3] L. C. Shen and J. A. Kong, *Applied Electromagnetism*, 2nd ed. Boston, MA: PWS Engineering, 1987.

[4] R. F. Harrington, *Time-harmonic electromagnetic fields*. New York, NY: McGraw-Hill, Inc., 1961.

[5] A. R. Gourlay and G. A. Watson, *Computational Methods for Matrix Eigenproblems*. London: John Wiley & Sons, 1973.

[6] J. H. Wilkinson and C. Reinsch, *Handbook for Automatic Computation*, vol. II. Berlin: Springer-Verlag, 1971.

[7] B. T. Smith, J. M. Boyle, B. S. Garbow, Y. Ikebe, V. C. Klema, and C. B. Moler, *Lecture notes in computer science: Matrix eigensystem routines - EISPACK guide*. Berlin: Springer-Verlag, 1974.

[8] K. H. Schlereth and M. Tacke, "The complex propagation constant of multilayer waveguides: An algorithm for a personal computer," *IEEE Journal of Quantum Electronics*, vol. 26, pp. 627-630, 1990.

[9] M. Mack, "Gallium nitride based semiconductor lasers," Ph.D. Dissertation: Materials Department, University of California, Santa Barbara, 1999.

Appendix D

Thinning sapphire

The last step of the laser fabrication process is cleaving to form reflective laser facets. This step requires that the substrate be thinned. For GaN lasers on sapphire, the cleaving is much easier if the sapphire is thinned to less than 80 μm. Sapphire has a hardness of 9 mohs[5] (1525-2000 Knoop). This makes it very difficult to lap. Several methods for lapping sapphire were tried. These methods are described in this Appendix.

For each method, the sample is mounted using crystal bond onto a metal wafer chuck that has been prepared to a desired planarity and parallelism so that the sample will be held parallel to the lapping surface and uniform pressure can be applied to the sample.

Cracking of the sapphire in GaN laser structures occurs primarily because the material is hard and brittle. For GaAs, small chips do not crack the polished surface because the GaAs chips are quickly broken up as they are crushed by the lapping fixture. The sapphire chips are much more robust and are not broken up as quickly by the lapping fixture. This means that large chips can remain in the lapping mixture. Due to their large size, these particles can scratch the surface deeply. These scratches act as scribe marks in the sapphire and result in the sapphire falling apart as soon as it is removed from the metal chuck. Therefore, it is important 1) to prevent chips from being created along the edges and corners of the sapphire substrate and 2) to reduce the chance of these chips from contacting the sapphire surface if they are created.

To reduce the chance of forming chips in the first place, sample preparation is important. For our processes, we use small rectangular samples. As the sample is thinned, the sharp corners are easily broken. Smaller samples are more difficult to polish because flatness is more difficult to maintain over the surface of the wafer. If one edge or corner is significantly thinner than the other sides, it is more likely to chip as the wafer is thinned.

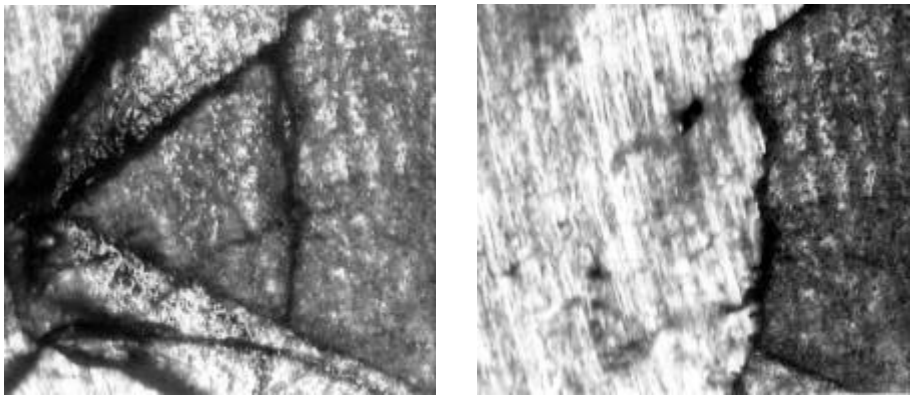

Figure 1. Sharp corners are more likely to crack and chip when lapping because as they get thin, the material is not as well supported by the rest of the sapphire wafer. The left figure shows a sharp corner after it has cracked. The right figure is after the corner (and the surrounding wax) has been removed. To prevent this cracking, it is important to round all corners prior to lapping.

In GaAs and InP, it is desirable to remove all crystal bond surrounding the sample during the lapping process. For sapphire, this is not the case. InP and GaAs are relatively soft materials, which lap very easily. The crystal bond used for mounting is significantly more difficult to remove by lapping. So if wax remains around the outside of the semiconductor, the discontinuity in lapping rates is significant enough to cause significantly slower lapping and to gum up the abrasive. For sapphire, the difference in lapping rates between the crystal bond and the sapphire is much less and the sapphire is even more difficult to remove than the crystal bond. The crystal bond does make the lapping proceed more slowly for equivalent weight applied to the fixture, but for similar applied pressures (pressure = weight / total exposed area), the lapping rate is roughly equivalent. For sapphire, the crystal bond actually has the beneficial effect of providing an intermediate rigidity surface between air and sapphire. This process helps to reduce cracking of the sapphire by reducing the edge chipping of the sapphire.

[5] In this scale, 1 corresponds to talc (soft) and 10 corresponds to diamond (hard).

Another important sample preparation consideration is that the sample must be mounted parallel to the wafer chuck. This allows even pressure to be applied to the substrate during lapping and prevents one side from becoming significantly thinner than another side during lapping. Using the South Bay Technologies and the UCSB polishing jigs, the angle of the sample is limited by how accurately the sample can be leveled as it is put on the crystal bond. Improvement of the alignment can be made only by reheating the crystal bond and repositioning the sample. This trial and error process for alignment produces reasonable results with practice, but is far from ideal. The polishing jig on the Malvern polishing machine has a more sophisticated method for quickly adjusting alignment: A screw allows the sample angle to be adjusted accurately and adjustments can be made as soon as polishing is started if it is seen that one edge is polishing preferentially. An autocollimator is also available for use with the Malvern, if desired. For all of the mounts, larger samples are easier to polish because they are easier to make flat. For this reason, the small 1 cm^2 samples, which are common for GaN laser samples, are more difficult to align properly than are larger samples.

Once the sample is mounted on the chuck, there are several methods that can be used for lapping the sapphire. The first method was to use a rotating glass wheel. A film impregnated with diamond grit was placed on the wheel[6]. Water was used as the lubricant to allow the sample to slide easily on the diamond grit. Grit size of 30 μm down to 0.25 μm were used in order to get a very smooth polish. This process works well and quickly for polishing vertical or angled facets. The large grit sizes are necessary to form the initial shape of the facet. Incrementally smaller grit sizes are used to polish out the roughness created by the larger grits. If the decrease in grit size is made too rapidly, the polishing takes

[6] Diamond paste cannot be used directly on this wheel because this wheel has been designated for use with the diamond-impregnated films only.

much longer than necessary. A typical polishing sequence is 30 µm, 15 µm, 6 µm, 3 µm, 1µm, 0.25 µm. Reducing the number of grit sizes will still work, but the polishing takes longer overall. For example, it takes much longer to remove trenches cut with 30 µm grit using 0.25 µm grit than it is with 15 µm grit. This method is useful for polishing facets and for angle thinning corners for TEM samples. However, using this method for thinning larger samples wears out the diamond impregnated films very rapidly. Additionally, the thinning takes much longer than some of the other methods described below.

A second method that was used for thinning sapphire was to use an x-y oscillating lapping machine. This machine consists of a glass lapping plate that is held up by its four corners and these corners are connected to motors, which spin the corners synchronously. The lapping fixture sits on the plate and the inertia of the lapping fixture provides the relative motion between the lapping fixture and the plate. Pressure is applied solely by the weight of the fixture. Paste with a high concentration of diamond grit was used with an oil base. Both of these are available from South Bay Technology. This method worked well for thinning the sapphire substrates and was used to demonstrate the work on the formation of cleaved facets that was described in Chapter 2.

There are two problems with this method. First, it is very difficult to thin the sapphire less than 100 µm. Any small chips from the sapphire substrate remain on the surface of the glass lapping plate. When the sample next passes over these bits of sapphire, very large scratches are created. These scratches act as scribe marks in the sapphire and result in the sapphire falling apart as soon as it is removed from the metal chuck. For this reason, an alternate machine with a cast iron lapping plate is preferred.

Thinning of the sapphire is performed using diamond paste with 15 µm particulates and a cast iron lapping wheel. Some diamond gets impregnated in the wheel, but chips from sapphire do not stick into the wheel. This makes it a

suitable material for the thinning stage. Copper on the other hand is very soft and allows any chipped particles to stick into the lapping surface and scratch the surface of the sapphire. These chips are not easily removed from the copper; so once they are embedded in the copper, the empty polishing fixture must be passed over the wheel for several hours until the particles are worked out of the wheel.

The roughness of the cast iron lapping plate makes it unsuitable for polishing with finer grits. Using a copper lap provides a better surface for polishing sapphire, but as mentioned above, the particles which are removed from sapphire become embedded in the copper and thus damage the wheel. A glass wheel represents a compromise between the roughness of the cast iron lap and the softness of the copper lap. The sapphire particles will not stick into a glass wheel, but at the same time the wheel can be smooth enough to produce a finer polish. A glass lap therefore provides a good surface for intermediate polishing.

The final polishing step can be performed on a copper lap or on a polishing pad. The copper lap is unsuitable for lapping in my opinion because it is too easily damaged. Instead, a disposable polishing pad with adhesive backing can be attached to a flat stainless steel plate. For the rough thinning stages described in the previous two paragraphs, the process is primarily abrasive and the chemical composition of the slurry is not as important. For final polishing of other III-V materials, a chemical component is often added to the mix. Sapphire, however, is known for its chemical inertness. So in this case, the polishing slurry that is used is designed to act primarily by abrasive means. The slurry, Nalco 2360, is sold by Rodel, Inc. A Nalco:water ratio of 1:5 is recommended for sapphire polishing and works well. It is important to keep the polishing surface wet. Unlike the thinning stage, this process requires constant attention because the automatic drip mechanism cannot be used because the Nalco solution clogs the drip tubes. Different polishing slurries for other materials are available with chemical

components to aid in the polishing. For example, in GaAs polishing NaOCl can be used as chemical polishing additive to abrasive colloidal silica polishing slurry [1].

There are a number of parameters that control the lapping rate and the lapping results. These include oil flow rate, sample pressure, wheel rotation speed, grit composition, and wheel material. Typical wheel rotation rates are 30-40 rpm. Lapping rates of approximately 4 μm/min yield the best results for sapphire lapping. Faster lapping is more abrasive and more likely to form chips or thickness variations across the wafer.

Pressure is also important for controlled lapping. For the start of the sample polishing very little pressure is applied. If the sample is slightly off angle, this gives the sample the chance to polish the raised side slowly. After the sample is polishing evenly over the entire surface, the pressure is increased every couple of minutes until the desired final pressure is achieved. For a 1-2 cm^2 sample, approximately 1 kg is applied to the top of the fixture. This provides slightly less than 1 N of force to the sample because a small amount of the force from the weights goes into pushing against a spring which lifts the sample above the lapping plate if no force is applied. For sample with an area of 2 cm^2 and wax with an additional area of 2 cm^2, this provides a pressure on the sample of $\frac{1\ N}{4 * 10^{-4}\ m^2} \approx 2.5$ kPa.

One or two drops of blue oil per minute are sufficient to lubricate the surface of the lapping wheel. Too much oil makes the diamond grit wear off very quickly. Too little oil makes the sample more likely to bind. Very little oil is actually needed, however, and reducing the oil below one drop per minute is preferable to increasing the oil flow. Optimized commercial systems use a larger flow rate of oil. These systems not only circulate the oil, but also diamond particles.

In summary, the Malvern lapping fixture and a cast iron lapping wheel can be used to reliably thin sapphire to less than 80 μm, even for small 1 cm^2 samples. To polish the sample, the grit size is reduced for one or two intermediate lapping stages on the cast iron wheel. A glass wheel should be ordered if well-polished substrates are desired. The final polish is performed with a polishing slurry on a polishing pad to provide a very smooth finish.

D.1. References

[1] H. Zheng, J. Bu, H. He, R. Wu, F. Cao, Y. Bai, and F. Hui, "[Analyses of sub-surface damages in SI-GaAs wafers caused by chemomechanical polishing]," *Research & Progress of SSE*, vol. 19, pp. 111-115, 1999.

Appendix E

Dicing sapphire

Sapphire is very hard and is therefore difficult to saw. Blades wear out much more rapidly when cutting sapphire than when cutting softer materials such as GaAs and InP. However, with proper care and technique, blades can make many cuts in sapphire before wearing out. For extending blade life and for making a smooth cut, heat generation should be minimized during cutting. To do this, blade speed should be slower for cutting sapphire than for cutting other materials. For sapphire, 15-18 krpm is recommended (typical dicing saw speed is 30 krpm for softer materials). The slower blade speed means that the blade will heat up less and therefore have less chance to break. In addition, the cutting speed should be rapid so that the blade does not create more friction than necessary by dwelling in a region longer than necessary. Fast cut speeds as high as 3 mm/sec can be used with sapphire to provide good results. Finally, the amount of wax used in mounting the sample should be minimized. Excess wax (either under the sample or around the sample) will create a significant amount of friction on the blade. Using too much wax is one of the primary reasons for blades breaking prematurely.

The recommended blade choice for sapphire is one that has an exposure that is less than 7 times the blade width and has 1/2 to 2/3 of the exposure buried in the GaN cut. Thinner blades cause less damage to the surface because they have to cut less of the material. For the 52 mm blades, there is 0.8 mm of blade exposure (0.032”), which means that the blade should be 0.005” or thicker. (Typical blades used at UCSB are 0.008” thick.) Another important parameter is diamond grit size. Large diamond grit is used because it cuts through sapphire more easily than small grit. 40-65 μm grit size should be used. A higher concentration of grit in the blade makes the blade last longer, but it also increases the roughness of the cut. For smooth cuts, Thermocarbon blade 2.050-5B-40RU7-1 is recommended. This blade is 0.005” wide and has low concentration of 40 μm grit in the blade. For longer blade life, Thermocarbon blade 2.050-8B-

54RU7-3 is recommended. This blade is 0.008” wide and has a high concentration of 54 µm diamond grit in the blade [1]. If these suggestions are followed, relatively smooth edges can be created and/or blade life can be extended.

E.1. References

[1] M. Reeves, 1997, personal communication.

Index